



**INSTITUTE OF BIOORGANIC CHEMISTRY**

**Polish Academy of Sciences**

Department of Molecular Probes and Prodrugs

&

Centre for Chemical Biology ERIC (Laboratory of Medicinal Chemistry)

**Masroor Ahmed Khan**

Doctoral Thesis

**Synthesis of bioluminogenic substrates  
of firefly and NanoLuc® luciferases and  
validation of their response to analytes  
involved in redox homeostasis**

**PhD advisor:** Dr. Hab. Jacek L. Kolanowski

**Auxiliary PhD advisor:** Dr. Dorota Jakubczyk

Poznań 2024

*The work described in this thesis has been carried out at the Institute of Bioorganic Chemistry, Polish Academy of Sciences in Poznań in the Department of Molecular Probes and Prodrugs and the Centre for Chemical Biology (Laboratory of Medicinal Chemistry) under the supervision of Dr. Hab. Jacek L. Kolanowski and auxiliary supervision of Dr. Dorota Jakubczyk. This work was supported by SONATA grant no. 2017/26/D/NZ1/01234 of the National Science Centre of Poland (NCN).*



NATIONAL SCIENCE CENTRE  
POLAND

بِسْمِ اللَّهِ الرَّحْمَنِ الرَّحِيمِ

*In the name of God, the Gracious, The Merciful*

*This PhD thesis is dedicated to my two most beloved and dearest to me:*

*My Ammi (mom) and Abajee (dad)*

*For always praying for me*

*For your unwavering love and support*

*For always believing in me and pushing me to be my best*

*And for shaping me into the person that I am today*

*This milestone would not have been possible without you both*

## **Acknowledgements**

*My deepest gratitude goes to my PhD advisor **dr. hab. Jacek Kolanowski**, for giving me the opportunity to do a PhD in his group. Your kindness, enthusiasm, insightful feedback, encouragement, deep discussions and unwavering belief in my potential have been a constant source of motivation for me. Your vast and broad expertise in organic chemistry and chemical biology has also been instrumental in shaping my knowledge. With all these qualities, you created the perfect and collaborative group atmosphere, you were always open to ideas and made me reflect deeper about my work. I sincerely thank you for making me the scientist that I am today. Thank you for being a dedicated mentor and for creating a this nice research environment. I am truly fortunate to have had you as my PhD supervisor.*

*My sincerest gratitude to my auxiliary PhD advisor **dr. Dorota Jakubczyk**, head of the Laboratory of Medicinal Chemistry, for allowing me to do my work in her lab, for aiding me in setting up my HPLC experiments, and also teaching me her know-how regarding HPLC and MS. Your knowledge and experiences helped me greatly during my journey and above all else, thank you for creating a nice, friendly atmosphere, inside the lab, but also outside the lab during our lab social gatherings.*

*I would also like to thank each and every person at IBCH PAS during my PhD journey. The culmination of this work is the result of all the combined efforts, and could not have been done without you. Special thanks go to:*

*Members of the Laboratory of Molecular Assays and Imaging: **Dr. Dorota Kwiatek**, for giving advice on experiments and for the nice atmosphere in lab 102 back when I started as PhD student. **Dr. Michał Gładysz**, for being the best and funniest lab manager, for being a wonderful person, for helping me out in admin-related stuff, and for also being a fellow adventurer together with me in trying out new (unhealthy) food places together. **Dr. Michał Jakubczyk**, for the deep insightful discussions on organic chemistry, and for his valuable advice on certain reactions. **Dr. Krzysiek, Dr. Asia, Monika and Natalia** for being awesome people and for the nice atmosphere at the Wielkopolska Center of Advanced Technologies. **Dr. Volodymyr** and **dr. Mariia** for the wonderful time and conversations we have had in lab 102 on certain topics. **Adrian**, for being a great collaborator in the furimazine project and our interesting (scientific) discussions. And my fellow PhD students **Francesca** and **Ania**, in being part of my doctoral journey, I thoroughly enjoyed working with you both and enjoyed sharing these and experiences (and struggles) together.*

Furthermore, I also want to thank **dr. Tomasz Ostrowski**, **dr. Grzegorz Framski** and **dr. Maurycy Szlenkier**, for the time spent together at the Wielkopolska Center of Advanced Technologies in the beginning of my PhD journey and for helping me in my synthetic endeavors. I also want to thank **Wiktoria Nitka** who worked on the split-luciferin project.

I want to thank the members of the Department of Biomolecular NMR and the Laboratory of NMR. **Dr. Witold Andrałojc** for giving nice and interesting lectures regarding NMR spectroscopy, in aiding me when I had trouble with NMR spectrometer and also teaching me the intricacies of NMR spectrometer. **Dr. Karol Pasternak** and **Ania Teubeurt** for teaching me how to perform NMR, for setting up overnight carbon spectras and in helping me trouble-shoot NMR problems.

**Dr. Łukasz Marczak** of the Laboratory of Mass Spectrometry for performing HR-MS of my compounds.

I also would like to show my sincere gratitude to my collaborators **Dr. Natalia Rozwadowska**, **dr. Iwona Ziółkowska-Suchanek** and **Michalina Krakowiak** (Department of Molecular Pathology, Institute of Human Genetics, Polish Academy of Sciences) for their work in testing out my probes in cells.

I would like to thank **Prof. Jacek Stawiński** and **Prof. Adam Kraszewski** for the interesting lectures and seminars organized for chemists at our Institute.

Lastly, I want to thank the members of my family. My Ammi and Abajee for their continuous support, love and prayer during my PhD. I want to thank my brothers and my nephews for being a part of my PhD journey, for all of your endless love and support, and for your prayers. A special shout-out goes to my sister-in-law Bashi, who has helped since my childhood in my academics since primary all the way to middle school, and as a result this achievement today would not have been possible without her. Thank you for the continuous support and prayers. Finally, I want to thank my fiancée Alisha for her continued support and kind words during the last month of my PhD. This work would not have been possible without all of you.

# Table of Contents

|  |           |
|--|-----------|
| <b>Abstract</b> .....  | <b>9</b>  |
| <b>Streszczenie</b> .....  | <b>12</b> |
| <b>1. Abbreviations</b> .....  | <b>15</b> |
| <b>2. Introduction</b> .....   | <b>18</b> |
| 2.1. Bioluminescence .....   | 18        |
| 2.2. Luciferin-Luciferase Systems .....  | 18        |
| 2.2.1. D-Luciferin and Firefly Luciferase .....  | 18        |
| 2.2.2. Imidazopyrazinone-based Systems (Coelenterazine and Furimazine)                               | 19        |
| 2.3. Mechanisms of Bioluminescence Reactions .....   | 20        |
| 2.3.1. D-luciferin mechanism .....   | 20        |
| 2.3.2. Imidazopyrazinone-based mechanism .....   | 20        |
| 2.4. Applications of Bioluminescence in Biological Research.....                                     | 23        |
| 2.4.1. Challenges and limitations of bioluminescence imaging .....                                   | 24        |
| 2.4.2. <i>In vivo</i> bioluminescence imaging considerations.....                                    | 24        |
| 2.5. Design Strategies For Responsive Bioluminogenic Probes .....                                    | 25        |
| 2.6. Redox Homeostasis as Target for Bioluminescent Sensing .....                                    | 31        |
| 2.6.1. Overview of redox homeostasis .....   | 31        |
| 2.6.2. Key analytes in redox homeostasis .....   | 32        |
| <b>3. Objectives</b> .....   | <b>34</b> |
| <b>4. Results and Discussion</b> .....   | <b>35</b> |
| 4.1. Iron(II) responsive bioluminogenic substrate for detection by split<br>luciferin strategy ..... | 35        |
| 4.1.1. Synthesis .....   | 36        |
| 4.1.2. Response to iron(II) .....  | 39        |
| 4.1.3. Probe's performance in biologically-relevant conditions .....                                 | 42        |
| 4.1.4. Metal ion-dependent signal interference.....  | 46        |
| 4.1.5. Summary of discussion .....   | 52        |

|           |  |           |
|-----------|--|-----------|
| 4.2.      | NTR Responsive Bioluminogenic Substrates (Single Analyte) .....                                | 53        |
| 4.2.1.    | NTR-responsive OH-CBT for use in the split-luciferin strategy .....                            | 53        |
| 4.2.2.    | NTR-responsive D-Cys for use in the split-luciferin strategy .....                             | 55        |
| 4.2.3.    | Summary of split-luciferin-based probes for NTR detection .....                                | 61        |
| 4.3.      | NTR-responsive furimazine .....  | 62        |
| 4.3.1.    | Synthesis .....  | 62        |
| 4.3.2.    | Response to NTR .....  | 69        |
| 4.3.3.    | Summary of NTR-responsive furimazine .....   | 71        |
| 4.4.      | Dual-analyte NTR-GGT probes .....  | 72        |
| 4.4.1.    | Dual-analyte NTR-GGT based on D-aminoluciferin .....   | 72        |
| 4.4.2.    | Dual-analyte NTR-GGT analyte based on D-luciferin .....  | 84        |
| 4.4.3.    | Summary of dual-analyte probes for NTR and GGT based on D-aminoluciferin and D-luciferin ..... | 89        |
| <b>5.</b> | <b>Conclusions and Perspectives .....</b>  | <b>90</b> |
| <b>6.</b> | <b>Materials and Methods .....</b>   | <b>92</b> |
| 6.1.      | Materials .....  | 92        |
| 6.2.      | Instruments .....  | 93        |
| 6.3.      | Chemistry .....  | 94        |
| 6.3.1.    | Synthesis of 4 .....   | 94        |
| 6.3.2.    | Synthesis of 8 .....   | 98        |
| 6.3.3.    | Synthesis of 10 .....  | 99        |
| 6.3.4.    | Synthesis of 19 .....  | 101       |
| 6.3.5.    | Synthesis of 29 .....  | 108       |
| 6.3.6.    | Synthesis of 34 .....  | 113       |
| 6.4.      | <i>In vitro</i> bioluminescence studies .....  | 118       |
| 6.4.1.    | <i>In vitro</i> procedure for 4 .....  | 118       |
| 6.4.2.    | <i>In vitro</i> procedure for 10 .....   | 118       |
| 6.4.3.    | <i>In vitro</i> procedure for 19 .....   | 119       |

|   |            |
|---|------------|
| 6.4.4. <i>In vitro</i> procedure for 29 .....           | 119        |
| 6.5. HPLC .....   | 120        |
| 6.5.1. Kinetic study of 10 and NTR.....                 | 120        |
| 6.6. Biology.....                                       | 121        |
| 6.6.1. Cell culture .....                               | 121        |
| 6.6.2. Cell lysate preparation .....                    | 121        |
| 6.6.3. Probe testing in lysates.....                    | 121        |
| 6.6.4. Probe testing in live cells.....                 | 122        |
| 6.6.5. Bioluminescence recording of cell samples: ..... | 122        |
| <b>7. Bibliography.....</b>                             | <b>123</b> |
| <b>8. Supplementary Information .....</b>               | <b>133</b> |
| <b>9. List of Publications.....</b>                     | <b>190</b> |



# Abstract

Bioluminescence is a phenomenon that relies on the emission of light resulting from the oxidation of the light-emitting molecule luciferin by its corresponding luciferase enzyme. It is pivotal in biological research due to its high sensitivity, non-invasive nature, and ability to enable real-time monitoring. One application of bioluminescence is the detection of physiologically and pathologically-relevant analytes in through the use of activity-based probes. These bioluminescent probes are engineered to sense specific analytes by masking the functional groups of luciferin with an analyte-targeting moiety, which prevents its reaction with luciferase. When the target analyte is encountered, the masking group is cleaved, freeing the luciferin that can then react with luciferase to generate photons, thereby allowing the quantification of the analyte's presence and activity through the emitted light.

Many diseases involve complex interactions between multiple analytes. Understanding these interactions can inform more effective therapeutic approaches. This requires a simultaneous monitoring of multiple analytes but this approach has been rarely explored for bioluminescent probes. It can be achieved by the use of two separate single-analyte probes, ideally with the same luciferase system to avoid doubling up on the need of introducing two enzymes to the system. Split-luciferin strategy is well suited for that purpose as two separate halves can be caged independently and upon uncaging, undergo a bio-orthogonal reaction at physiological pH to form active D-luciferin. Another way of simultaneous analytes' monitoring is a use of the so-called dual-analyte bioluminescent probes, with each containing two analyte-responsive groups. This eliminates as challenges of the use of two single-analyte probes that can suffer from differences in their pharmacokinetics and co-localization complicating signal interpretation. Nevertheless, up to date, very few such bioluminescent probes have been reported.

The aim of this work was to synthesize and characterise several bioluminescent probes to expand the palette of bioluminescent tools for simultaneous detection of multiple analytes. The primary scaffolds utilized in this research are based on firefly luciferin and furimazine, a substrate for the small luciferase NanoLuc®.

NanoLuc® offers advantages such as brighter luminescence, smaller size, and greater stability compared to traditional luciferases, and it does not require cofactors like ATP or  $Mg^{2+}$ , which are needed for firefly luciferase. This work targets analytes related to redox homeostasis, specifically iron, gamma-glutamyltransferase (GGT), and nitroreductase (NTR), as the importance of their interplay in diseases such as cancer is vital and still not fully understood.

First, a split luciferin strategy-compatible probe was developed for the detection of ferrous ions. This probe exhibited responsiveness when tested in vitro and in cell lysates. However, while the expected response could be observed in live cell studies, low intensity and high complexity of response posed challenges in reliable interpretation of the results. Further investigations revealed that certain metal ions, including Fe(II) have the ability to biologically inhibit luciferases, with firefly luciferase being particularly susceptible to this inhibition. This work has therefore contributed to the understanding of challenges associated with the reliable use split luciferin design in real-life detection of analytes in biology and provided tools to ensure their robust validation.

Next, three different nitroreductase-responsive (NTR) probes were developed, compatible with split luciferin as well as NanoLuc systems. In particular, two variants were developed based on 2-cyano-6-hydroxybenzothiazole and D-cysteine. The novel D-cysteine probe, in particular, demonstrated significant activity in vitro, which was validated through spectroscopic and high-performance liquid chromatography (HPLC) kinetic studies. Additionally, the first furimazine-based bioluminescent probe was created that enables potentially more reliable NTR detection taking advantage of the cofactor-independent functionality of the NanoLuc® luciferase. This probe also exhibited a robust response, even at low concentrations of NTR.

Finally, a dual-analyte probe was synthesized based on the aminoluciferin scaffold, which was capable of detecting simultaneous presence of nitroreductase (NTR) and gamma-glutamyltransferase (GGT). This validated the feasibility of using a single molecular probe to monitor multiple analytes simultaneously. Additionally, a D-luciferin variant of this dual-analyte probe was developed, featuring a dual-analyte responsive motif for NTR and GGT as intermediate that can be conjugated

to other fluorophores or bioluminophores. These results expand the available molecular toolset of multi-target bioluminescent probes.

In conclusion, this thesis represents advancements in the field of bioluminescent probes, generating novel tools for the concurrent investigation of multiple analytes within biological systems and shading the light on advantages and limitations of variable probe designs. These probes, therefore, inform future use of such tools in cellular and in vivo applications with higher reliability, which is critical for disease understanding and ultimately development of enhanced therapeutic approaches.

# Streszczenie

## **Synteza bioluminogenych substratów lucyferaz świetlika i NanoLuc® oraz walidacja ich odpowiedzi na anality zaangażowane w homeostazę redoks.**

Bioluminescencja to zjawisko polegające na emisji światła w wyniku utlenienia cząsteczki lucyferyny przez odpowiadający jej enzym lucyferazę. Metoda ta ma kluczowe znaczenie w badaniach biologicznych ze względu na wysoką czułość, nieinwazyjność i możliwość monitorowania w czasie rzeczywistym. Jednym z zastosowań bioluminescencji jest wykrywanie analitów zaangażowanych w procesy fizjologiczne i patologiczne za pomocą sond opartych na reakcji chemicznej z analitem (tzw. activity-based probes). Takie sondy bioluminescencyjne projektuje się, aby wykrywały określone anality poprzez maskowanie grup funkcyjnych lucyferyny za pomocą odpowiednich grup ochronnych o aktywności ukierunkowanej na analit, co zapobiega jej reakcji z lucyferazą. Po napotkaniu docelowego analitu grupa maskująca zostaje chemicznie usunięta, uwalniając lucyferynę, która może następnie reagować z lucyferazą generując fotony. Umożliwia to ilościowe określenie obecności i aktywności analitu na podstawie emitowanego światła.

Wiele chorób obejmuje złożone interakcje pomiędzy wieloma analitami. Zrozumienie tych interakcji może przyczynić się do opracowania skuteczniejszych metod terapeutycznych. Wymaga to jednoczesnego monitorowania wielu analitów, jednak podejście to było rzadko eksplorowane w przypadku sond bioluminescencyjnych. Jest to możliwe poprzez zastosowanie dwóch oddzielnych sond jednoanalitowych, najlepiej z tym samym systemem lucyferazy, aby uniknąć konieczności wprowadzania dwóch enzymów do układu. Strategia „rozszczerzonej lucyferyny” (tzw. split luciferin) jest dobrze dopasowana do tego celu, ponieważ dwie oddzielne połowy mogą być niezależnie maskowane i po aktywacji ulegają bio-ortogonalnej reakcji w fizjologicznym pH, tworząc aktywną D-lucyferynę. Innym sposobem jednoczesnego monitorowania analitów jest zastosowanie tzw. bioluminescencyjnych sond dwuanalitowych, z których każda zawiera dwie grupy reagujące na analit. Eliminuje to wyzwania związane z użyciem dwóch sond jednoanalitowych, które są szczególnie skomplikowane z powodu różnic w ich farmakokinetyce i kolokalizacji, co komplikuje interpretację sygnału. Niemniej

jednak, do tej pory opublikowano bardzo niewiele takich sond bioluminescencyjnych.

Celem mojej pracy była synteza i scharakteryzowanie sond bioluminescencyjnych z zamiarem rozszerzenia palety narzędzi bioluminescencyjnych do jednoczesnego wykrywania wielu analitów. Główne struktury wykorzystane w tym badaniu oparte są na lucyferynie świetlika i furimazynie, substracie dla małej lucyferazy NanoLuc®. NanoLuc® posiada takie zalety jak, jaśniejsza luminescencja, mniejszy rozmiar i większa stabilność w porównaniu do tradycyjnych lucyferaz, a także nie wymaga kofaktorów takich jak ATP czy  $Mg^{2+}$ , które są potrzebne dla lucyferazy świetlika (ang. firefly luciferase). Niniejsza praca skupia się na analitach związanych z homeostazą redoks, w szczególności żelazie, gamma-glutamylotransferazie (GGT) i nitroreduktazie (NTR), ponieważ znaczenie ich wzajemnego oddziaływania w chorobach takich jak nowotwory jest kluczowe i wciąż nie w pełni zrozumiane.

W pierwszym etapie badań opracowano sondę kompatybilną ze strategią rozszczepionej lucyferyny do wykrywania jonów żelaza(II). Sonda ta wykazywała odpowiedź w testach *in vitro* i w lizatach komórkowych. Mimo, że oczekiwana odpowiedź była obserwowana w badaniach na żywych komórkach, niska intensywność i wysoka złożoność odpowiedzi stanowiły wyzwanie w wiarygodnej interpretacji wyników. Dalsze badania ujawniły, że niektóre jony metali, w tym Fe(II), mają zdolność do biologicznego inhibowania lucyferaz, przy czym lucyferaza świetlika jest szczególnie podatna na tę inhibicję. Zatem omawiane badania przyczyniły się do zrozumienia wyzwań związanych z wiarygodnym wykorzystaniem strategii rozszczepionej lucyferyny w rzeczywistym wykrywaniu analitów w biologii i dostarczyła narzędzi do zapewnienia ich solidnej walidacji.

Następnie opracowano trzy różne sondy reagujące na nitroreduktazę (NTR), kompatybilne zarówno z systemem rozszczepionej lucyferyny, jak i NanoLuc®. W szczególności opracowano dwa warianty oparte na 2-cyjano-6-hydroksybenzotiazolu i D-cysteinie. Nowa sonda na bazie D-cysteiny wykazała znaczącą aktywność *in vitro*, co zostało potwierdzone w spektroskopowych badaniach kinetycznych jak i z wykorzystaniem wysokosprawnej chromatografii cieczowej (HPLC). Dodatkowo, stworzono pierwszą bioluminescencyjną sondę opartą na furimazynie, która umożliwia potencjalnie bardziej wiarygodne

wykrywanie NTR, wykorzystując niezależną od kofaktora funkcjonalność lucyferazy NanoLuc®. Sonda ta również wykazała znaczną odpowiedź nawet przy niskich stężeniach NTR.

Finalnie zsyntetyzowano sondę dwuanalitową opartą na szkielecie aminolucyferyny, która była zdolna do wykrywania jednoczesnej obecności nitroreduktazy (NTR) i gamma-glutamylotransferazy (GGT). Potwierdziło to możliwość wykorzystania pojedynczej sondy molekularnej do jednoczesnego monitorowania wielu analitów. Dodatkowo opracowano wariant D-lucyferyny tej sondy dwuanalitowej, zawierający motyw responsywny na dwa anality - NTR i GGT, jako związek pośredni, który może być sprzężony z innymi fluoroforami lub bioluminoforami. Te wyniki poszerzają dostępny zestaw narzędzi molekularnych z grupy wieloanalitowych sond bioluminescencyjnych.

Podsumowując, niniejsza praca doktorska przedstawia osiągnięcia i postęp w dziedzinie sond bioluminescencyjnych, generując nowe narzędzia do jednoczesnego badania wielu analitów w systemach biologicznych oraz rzucając światło na zalety i ograniczenia różnych konstrukcji sond. Opracowane sondy dostarczają istotnych informacji dla przyszłego wiarygodnego wykorzystania takich narzędzi w zastosowaniach komórkowych i in vivo, co jest kluczowe dla zrozumienia przyczyn i przebiegu chorób i ostatecznie opracowania skuteczniejszych metod terapii.

# **1. Abbreviations**

**$\alpha$ -CT:** alfa-chymotrypsin

**ABS:** activity-based sensing

**Ac:** acetyl

**ALP:** alkaline phosphatase

**AMP:** adenosine monophosphate

**ATP:** adenosine triphosphate

**BLI:** bioluminescence imaging

**CBT:** cyanobenzothiazole

**COSY:** correlated spectroscopy

**CTSC:** cathepsin C

**CTSL:** cathepsin L

**Cys:** cysteine

**DABCO:** 1,4-diazabicyclo[2.2.2]octane

**DCM:** dichloromethane

**DIPEA:** N,N-Diisopropylethylamine

**DMAP:** 4-Dimethylaminopyridine

**DMF:** *N,N*-Dimethylformamide

**DMSO:** dimethyl sulfoxide

**EDTA:** ethylenediaminetetraacetic acid

**ESI:** electrospray ionization

**EtOAc:** ethyl acetate

**FAAH:** fatty-acid amide hydrolase

**FAS:** ferrous ammonium sulfate

**FLuc:** firefly luciferase

**GGT:** gamma-glutamyl transferase

**GLuc:** *Gaussia* luciferase

**GSH:** glutathione

**GST:** Glutathione S-transferases

**GUSB:**  $\beta$ -Glucuronidase

**HATU:** hexafluorophosphate azabenzotriazole tetramethyl uronium

**HEPES:** 4-(2-hydroxyethyl)-1-piperazineethanesulfonic acid

**HOAt:** 1-hydroxy-7-azabenzotriazole

**HPLC:** high-performance liquid chromatography

**HRMS:** high resolution mass spectrometry

**HTS:** high-throughput screening

**IBCF:** isobutyl chloroformate

**IC50:** half-maximal inhibitory concentration

**MAO:** mono-amine oxidase

**MeOH:** methanol

**MS:** mass spectrometry

**NADH:** nicotinamide adenine dinucleotide (reduced form)

**NBS:** N-bromosuccinimide

**NLuc:** NanoLuc®

**NMR:** nuclear magnetic resonance

**NTR:** nitroreductase

**ONOO<sup>-</sup>:** peroxynitrite

**PABA:** 4-aminobenzyl alcohol

**PBS:** phosphate buffered saline



**PLC:** preparative layer chromatography

**RCF:** relative centrifugal force

**Ref.:** reference

**Rf:** retention factor

**RLuc:** *Renilla* luciferase

**RLU:** relative luminescence units

**ROS:** reactive oxygen species

**RP:** reverse-phase silica (C18-derivatised)

**RT:** room temperature

**SC:** screening conditions

**t-Bu (or tBu):** tert-butyl

**TCEP.HCl:** tris(2-carboxyethyl)phosphine hydrochloride

**Temp.:** temperature

**TFA:** trifluoroacetic acid

**THF:** tetrahydrofuran

**TLC:** thin layer chromatography

**TMS:** trimethylsilyl

**TRIS:** tris(hydroxymethyl)aminomethane

**Ts:** tosyl

**TYR:** tyrosinase

**UV:** ultraviolet

## **2. Introduction**

### **2.1. Bioluminescence**

Bioluminescence is a phenomenon that refers to the emission of light by living organisms. It is a type of chemiluminescence, which is the emission of light resulting from a chemical reaction. Bioluminescence occurs as a result of a reaction between a light-emitting molecule, known as luciferin, and its enzyme, known as luciferase.<sup>1</sup> Examples of organisms that exhibit bioluminescence include bacteria, insects, and marine organisms. Some examples of terrestrial bioluminescent organisms include fireflies, click beetles, glow worms, and certain species of mushrooms. These organisms employ bioluminescence for a range of purposes, such as camouflage, attracting mates, communication, and repulsion.<sup>2,3</sup>

### **2.2. Luciferin-Luciferase Systems**

#### **2.2.1. D-Luciferin and Firefly Luciferase**

Firefly luciferase, the first discovered luciferase, is a 61 kDa protein that uses D-luciferin as its substrate and emits light at an emission wavelength of 558 nm after oxidation of D-luciferin.<sup>1,4</sup> Firefly (*Photinus*) and click beetle (*Pyrophorus*) luciferases utilize D-luciferin (also known as firefly luciferin) as their substrate, and require oxygen, magnesium ions and ATP as cofactors. D-luciferin is oxidized to oxyluciferin (**table 2.1**) in an excited electron state, which decays back to its ground state and emits a photon.<sup>4</sup> All of these insect luciferases use D-luciferin as their substrate, but they have different light emission spectra. The exact emission wavelength is determined by both the substrate molecule and the enzyme's internal microenvironment at the active site.<sup>4,5</sup>

The ATP necessary for D-luciferin/firefly luciferase system grants distinct advantages. For instance, D-luciferin's required activation through adenylation enhances its stability and reduces auto-oxidation in solution, leading to lower background chemiluminescence. The ATP dependence of the D-luciferin/FLuc assay enables sensitive detection of ATP in the nanomolar range, applicable to quality control, hygiene assessment, and bacterial contamination evaluation. Furthermore, D-luciferin boasts superior aqueous solubility and lower toxicity compared to other luciferins such as coelenterazine. Moreover, D-luciferin exhibits

the highest quantum yield and longest emission wavelength amongst known luciferin/luciferase pairs, making it ideal for imaging applications involving blood due to its reduced absorption by hemoglobin and tissues.<sup>4</sup>

There are several limitations associated with the D-luciferin/firefly luciferase pair. D-luciferin is sensitive to light, oxygen, and in solid form also to moisture. Therefore, it is important to minimize the exposure of the solid form and solution to direct light.<sup>6</sup> The poor pharmacokinetic properties of D-luciferin, such as it not being freely permeable across the cell membrane and blood-brain barrier, can have implication for imaging *in vivo*.<sup>7,8</sup> Moreover, the use of FLuc and D-luciferin provides a single imaging signal, limiting studies to a single molecular event or a single population of cells. Lastly, the large size of FLuc may result in steric hindrance when used as a recombinant protein.<sup>9</sup>

Several synthetic analogues have been synthesized and reported in literature regarding the D-luciferin scaffold. The main objective of these modifications is to yield more red-shifted analogues, as the photons generated by D-luciferin bioluminescence is 558 nm, which is not highly penetrable in deep tissues. By creating red-shifted luciferin analogues, it allows for better detection sensitivity of targets in deep tissues *in vivo*.<sup>10-12</sup> One analogue used in this work is D-aminoluciferin, wherein the 6'-hydroxyl group of D-luciferin is replaced with a 6'-amino group. This leads to a red-shifted light emission (emission wavelength: 590 nm)<sup>13</sup> with a higher affinity (approximately 10-fold) for luciferase compared to D-luciferin.<sup>14</sup> The use of D-aminoluciferin enables for interesting probe designs, for example in detecting certain proteases.<sup>10</sup>

### **2.2.2. Imidazopyrazinone-based Systems (Coelenterazine and Furimazine)**

Luciferases found in marine organisms, such as *Renilla* or *Gaussia*, use coelenterazine as their substrate (**table 2.1**). In the presence of molecular oxygen, bioluminescent light is emitted, with a wavelength of 460-480 nm, upon the luciferase-catalyzed oxidation of coelenterazine to coelenteramide. RLuc is a 36 kDa protein derived from a marine organism (sea pens, *Renilla*) and utilizes coelenterazine as its substrate. No additional cofactors are required, besides oxygen, when using RLuc, making it well-suited for extracellular applications.<sup>1,15</sup>

NLuc, one of the smallest luciferases in existence (19 kDa), is derived from the luciferase enzyme of the deep-sea shrimp *Oplophorus gracilirostris* through directed evolution and optimization by Promega. NLuc emits a glow-type luminescence upon reaction with its substrate, furimazine, producing light with higher intensity and a longer half-life compared to other commonly used luciferases like Renilla luciferase (RLuc) or firefly luciferase (FLuc).<sup>16,17</sup> The disadvantage of using BLI based on RLuc or NLuc is the chemical instability of their respective substrates, which degrade in presence of air or in aqueous environment.<sup>18</sup>

### **2.3. Mechanisms of Bioluminescence Reactions**

#### **2.3.1. D-luciferin mechanism**

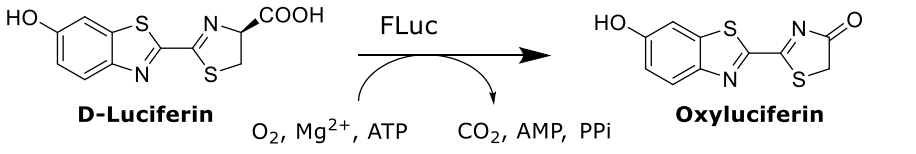
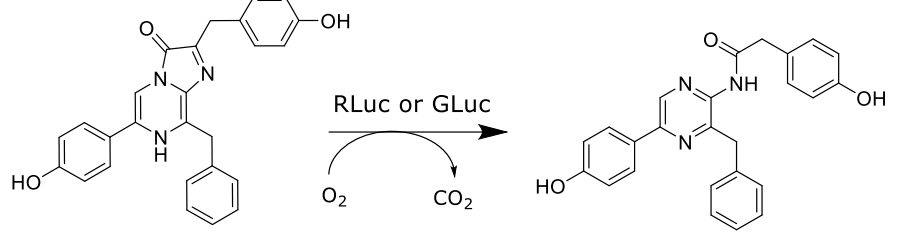
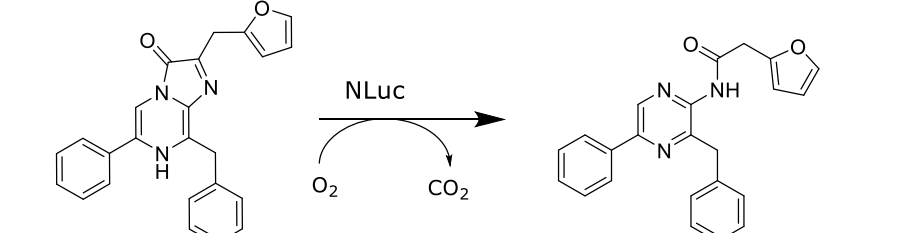
The mechanism of action for bioluminescence is shown in **scheme 2.2** for D-luciferin. The first step is an adenylation of the 4-COOH group in the enzymatic site. This AMP substituent increases the acidity of the C4 hydrogen, resulting in the formation of a carbanion intermediate, which can perform a nucleophilic attack on molecular oxygen. After AMP release, a luciferin dioxetanone is formed, which consists of a four-membered strained ring. This dioxetanone can rearrange to release CO<sub>2</sub> and yielding the excited singlet state of oxyluciferin. Finally, the luminescent light is produced with a peak intensity of approximately 560 nm (at pH 7.6) upon relaxation to the ground state.<sup>19,20</sup> The emission wavelength is dependent on a number of factors, such as the pH and temperature.<sup>21</sup>

#### **2.3.2. Imidazopyrazinone-based mechanism**

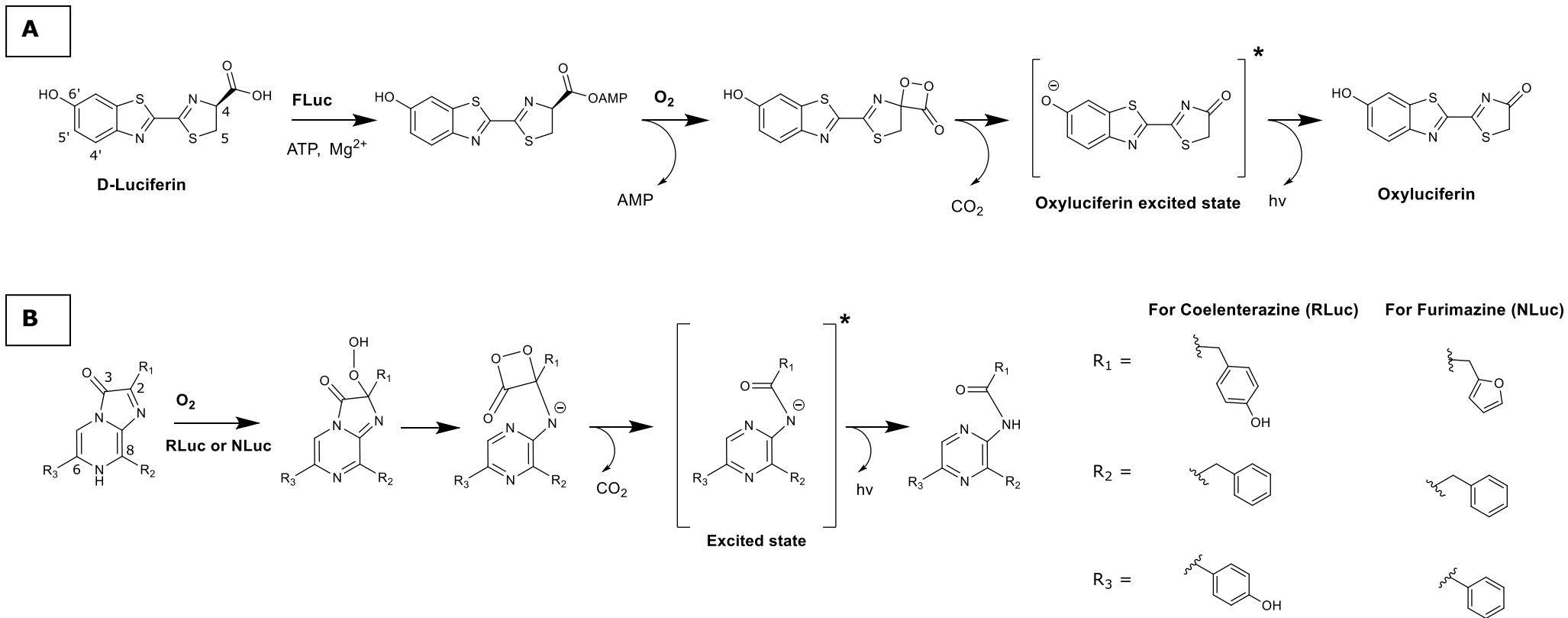
For imidazopyrazinone-based luciferins, the reaction proceeds without any cofactors, as seen in **scheme 2.2**. After addition of oxygen at C2, an intramolecular attack occurs at C3, yielding a dioxetanone, an intermediate also formed in the reaction mechanism of D-luciferin bioluminescence. After release of CO<sub>2</sub>, an excited state coelenteramide or furimamide is formed, which can relax to the ground state after emission of a photon.<sup>15</sup>

## Chapter 2: Introduction

**Table 2.1:** Examples of reactions shown for some luciferin/luciferase pairs. Only the final oxidation product is shown. For a detailed reaction mechanism, see **scheme 2.2**.

| Luciferase    | Enzymatic reaction   | Ref. |
|---------------|--|------|
| FLuc          |  <p style="text-align: center;"> <chem>CC(=O)O[C@@H]1CN2C(=N1)c3ccc(O)cc3S2</chem> <math>\xrightarrow[\text{O}_2, \text{Mg}^{2+}, \text{ATP}]{\text{FLuc}}</math> <chem>O=C1CN2C(=N1)c3ccc(O)cc3S2</chem> </p> <p style="text-align: center;"> <b>D-Luciferin</b> <span style="margin-left: 150px;"></span> <b>Oxyluciferin</b><br/> <math>\text{CO}_2, \text{AMP}, \text{PPi}</math> </p> | 1    |
| RLuc and GLuc |  <p style="text-align: center;"> <chem>CC(=O)O[C@@H]1CN2C(=N1)c3ccc(O)cc3N2</chem> <math>\xrightarrow[\text{O}_2]{\text{RLuc or GLuc}}</math> <chem>O=C1NC2=C(N1)c3ccc(O)cc3N2</chem> </p> <p style="text-align: center;"> <b>Coelenterazine</b> <span style="margin-left: 150px;"></span> <b>Coelenteramide</b><br/> <math>\text{CO}_2</math> </p>  | 1,15 |
| NLuc          |  <p style="text-align: center;"> <chem>CC(=O)O[C@@H]1CN2C(=N1)c3ccoc3N2</chem> <math>\xrightarrow[\text{O}_2]{\text{NLuc}}</math> <chem>O=C1NC2=C(N1)c3ccoc3N2</chem> </p> <p style="text-align: center;"> <b>Furimazine</b> <span style="margin-left: 150px;"></span> <b>Furimamide</b><br/> <math>\text{CO}_2</math> </p>   | 1,15 |

## Chapter 2: Introduction



**Scheme 2.2:** Molecular mechanism of action of bioluminescence for:

A) D-luciferin in the presence of O<sub>2</sub> via FLuc (with ATP and Mg<sup>2+</sup> as cofactors)

B) Imidazopyrazinone-based compounds in the presence of O<sub>2</sub> via RLuc (coelenterazine) or NLuc (furimazine).

The carbon atoms of importance have been numbered for D-luciferin and imidazopyrazinone-based compounds.

## **2.4. Applications of Bioluminescence in Biological Research**

Bioluminescence has found extensive applications in biological research due to its numerous advantages. It exhibits a high signal-to-noise ratio, as the background luminescence is negligible compared to the signal generated by the bioluminescent reaction. Furthermore, bioluminescence does not require external excitation light sources, unlike fluorescence, thus eliminating the risks of photobleaching and phototoxicity. Consequently, bioluminescent signals can be monitored over prolonged periods without adversely affecting reporter molecules or cells, making them well-suited for live-cell imaging. The non-invasive nature of bioluminescence enables it to be a highly specific and sensitive technique in biology. Bioluminescence sensing facilitates the longitudinal monitoring and quantification of biological processes at the cellular and molecular levels within living organisms, such as animal models of disease. This approach is extensively utilized in preclinical oncology research and drug development, for instance, in the assessment of tumor growth, metastasis, gene expression, and protein-protein interactions.<sup>4,20,22,23</sup>

Since its initial identification, FLuc has been widely employed as a biosensor through recombination with other proteins of interest, as well as an ATP sensor, taking advantage of its ATP-dependency.<sup>4</sup> There are also several activity-based probes based on D-luciferin, which will be described in subchapter 2.5, to detect a wide variety of analytes of interest. The gene encoding the luciferase of interest can be introduced into mammalian cells, bacteria, fungi, protozoa, and viruses, which can be used to track their proliferation and for imaging.<sup>4</sup> D-luciferin, along with D-luciferin-based probes, can be used in a variety of *in vitro* analytical assays for the detection of certain analytes in biomedical research<sup>20</sup> and in high-throughput screening campaigns in drug discovery research.<sup>24</sup> Of all natural luciferin/luciferase pairs, the D-luciferin/firefly luciferase pair from *Photinus pyralis* remains the most common choice for *in vivo* imaging.<sup>4</sup>

Several examples involving the use of RLuc include protein-protein interactions and conformational rearrangements in live cells, for non-invasive bioimaging, and as probes for biological sensing.<sup>15,18,25,26</sup> Some examples of NLuc usage include as a reporter gene in molecular biology and biotechnology applications, such as protein-protein interaction assays, cellular imaging, and high-throughput

screening assays. Its small size, high solubility, and superior luminescent properties make it a great tool for various research purposes.<sup>9,16,17,27</sup>

#### **2.4.1. Challenges and limitations of bioluminescence imaging**

While bioluminescence-based imaging has been successfully employed in various applications to obtain semi-quantitative insights into biological processes in living organisms, several important considerations must be taken into account when utilizing this technology. The intensity of bioluminescence is fundamentally limited by the availability of substrate molecules that can be catalyzed by the luciferase enzyme. Moreover, the quantification of light emission alone may not accurately reflect the underlying biological effects being studied. This is because the luciferase reaction involves a complex interplay of multiple molecules, including ATP, oxygen, and luciferin. If any of these essential components are not abundantly present, the observed light emission may not faithfully represent the true luciferase activity.<sup>12,28</sup>

Additionally, the limited and wavelength-dependent transmission of light through animal tissues poses a significant challenge. As a general principle, there is approximately a 10-fold decrease in photon intensity for every centimeter of tissue depth traversed. Furthermore, the surface-weighted nature of BLI images means that light sources closer to the tissue surface appear brighter than deeper sources, due to the attenuating properties of the intervening tissues. Dynamic changes in the geometry and/or optical properties of tissues can also affect light scattering, absorption, and the ultimately detected bioluminescence. Consequently, while BLI offers a unique and powerful methodological approach, the quantitative analysis of such data must be undertaken with caution, and validation for each specific application is necessary.<sup>12,28,29</sup>

#### **2.4.2. *In vivo* bioluminescence imaging considerations**

When performing *in vivo* bioluminescence imaging, it is important to note that mammalian tissues are not transparent and thus reduce the strength of optical signals by both absorbing and scattering light. The shifts in the refractive index between tissue boundaries, cell membranes, or organelles cause light scattering in living organisms. The absorption of photons varies based on the type of tissue and endogenous chromophores such as hemoglobin, which primarily absorbs in the blue-green region (460-570 nm) of the visible spectrum. This makes it difficult



to detect signals from deep tissues. In the red and near-infrared spectrum (> 600 nm), the absorption of hemoglobin is lower, enabling red light to penetrate tissue up to a depth of a few centimeters.<sup>30-32</sup> *Renilla*, *Gaussia*, and NLuc emit light in the region of 460-480 nm, resulting in lower tissue penetration, making them less suitable for *in vivo* studies compared to the FLuc/D-luciferin pair, which produces a more red-shifted light. Nevertheless, the lack of dependence on cofactors (ATP and magnesium ions) for RLuc or NLuc makes them advantageous for *in vitro* applications, as they can effectively monitor both intracellular and extracellular environments. Moreover, combining multiple luciferase/luciferin pairs with different emission wavelengths can be used simultaneously for multicolor imaging. This allows monitoring multiple processes simultaneously by recording different wavelengths of light emission.<sup>33</sup>

### **2.5. Design Strategies For Responsive Bioluminogenic Probes**

Bioluminescent substrates can be transformed into probes for activity-based sensing (ABS) of various analytes. These ABS probes utilize a masking strategy, where luciferins are "caged" by attaching a reactive group sensitive to the target analyte (e.g. enzyme or small molecule) at specific positions on the luciferin molecule. In this "caged" state, the reactive group hinders interaction between luciferin and luciferase, preventing light emission. These caging groups can be attached at the 6'-OH or 6'-NH<sub>2</sub> for respectively D-luciferin or D-aminoluciferin, and at the 4-COOH position. When the target analyte interacts with and cleaves the reactive group, free luciferin is released, which will generate a bioluminescent signal. The intensity of this signal is proportional to the amount of uncaging and thus serves as a functional indicator of the target analyte's activity.<sup>20,34</sup>

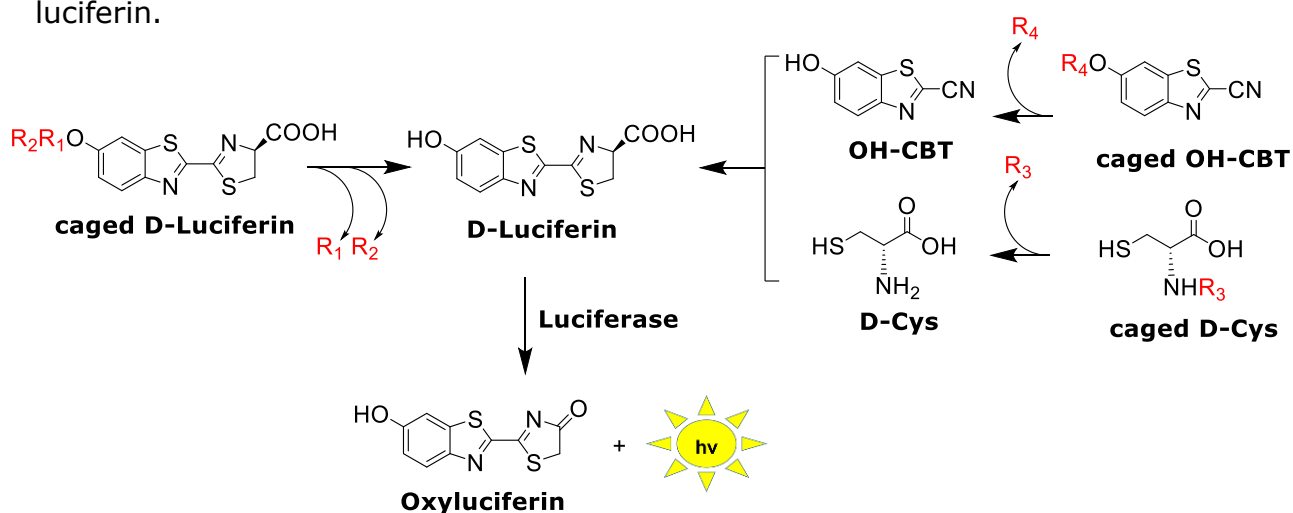
While single-analyte probes are useful, the concurrent detection of multiple analytes is crucial for understanding complex biological processes and disease states. Dual-analyte bioluminescent probes, which can simultaneously detect two target compounds within the same environment, offer a promising approach to this challenge. Although using two separate single-analyte probes is possible, this strategy may be complicated by differences in their pharmacokinetic properties, potentially obscuring the true relationship between the analyzed species. An ideal dual-analyte bioluminescent probe would exhibit high specificity toward the two target analytes when they are present together, enabling a clear and unified

assessment of their interplay within the system. Several attempts for developing such probes but based on fluorescent readout have been described and summarized before<sup>35,36</sup> and their numbers are rapidly increasing in the last years.

In order to transfer these designs to bioluminescent-based sensing systems, two main strategies can be used to develop dual-analyte probes for FLuc:

- Attaching two caging groups to D-(amino)luciferin<sup>37</sup>, or
- Using the “split-luciferin” approach, in which D-(amino)luciferin is formed *in situ* by the reaction of a 2-cyanobenzothiazole derivative and D-Cys at physiological pH, after uncaging of both derivatives.<sup>38</sup>

**Scheme 2.3** illustrates the above-mentioned dual-analyte methods for D-luciferin.



**Scheme 2.3:** Design strategies for dual-analyte sensing using FLuc.

In the first strategy, a potential method for creating dual-analyte bioluminescent probes would be to attach the first analyte-targeting group to the 6'-OH or 6'-NH<sub>2</sub> of respectively D-luciferin or D-aminoluciferin, while the second analyte-targeting moiety can be attached to 4-COOH position, in the form of an amide or hydrazide<sup>10</sup>. An exception could be made for esters, as it is usually not a good and common approach for analyte-targeting groups, due to susceptibility of ester hydrolysis by esterases *in vivo*.

## Chapter 2: Introduction

The split-luciferin approach employs two inactive fragments; a D-cysteine derivative (D-Cys-X) and a hydroxy/amino-cyanobenzothiazole (OH-CBT/NH<sub>2</sub>-CBT). The CBT derivatives lack the crucial carboxylate group essential for recognition by the luciferase enzyme, while D-Cys possesses the missing carboxylate group but lacks the remaining structural components of D-luciferin. These fragments are both caged and independently delivered to the target location and remain biologically inactive until a specific target analyte is present. This trigger (an enzyme or a biomolecule) cleaves the caging groups connected to the D-Cys fragment and the CBT fragment, releasing free D-Cys and CBT.<sup>38,39</sup>

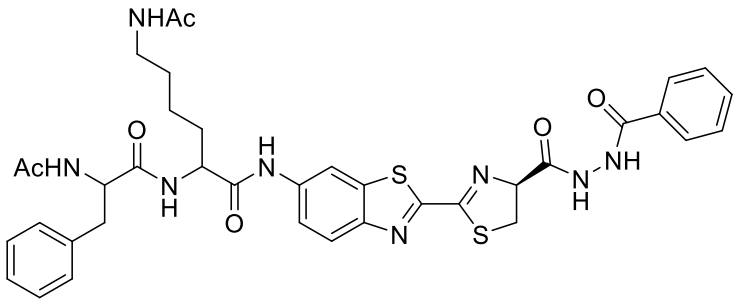
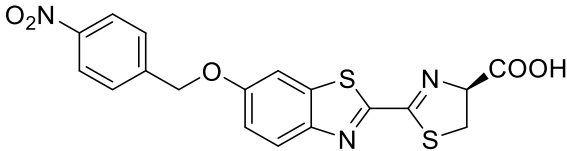
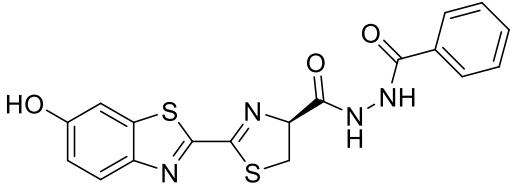
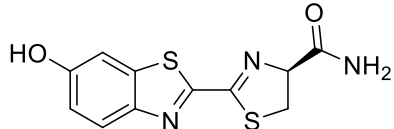
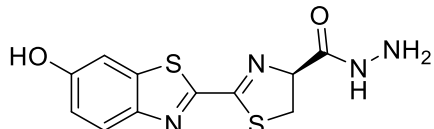
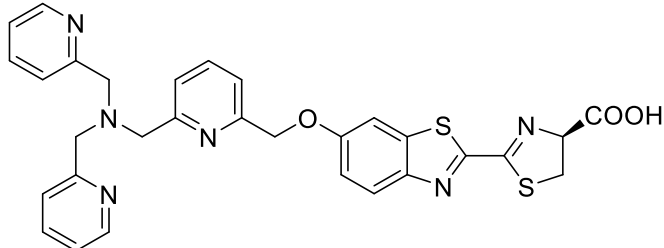
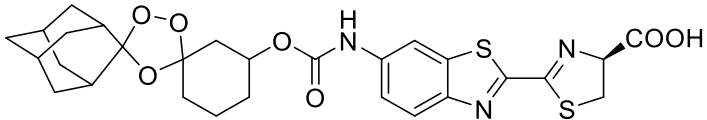
Upon trigger-mediated release, D-Cys undergoes a selective, bio-orthogonal reaction with the OH-CBT/NH<sub>2</sub>-CBT fragment at physiological pH, resulting in the formation of a functional D-(amino)luciferin. This newly formed luciferin can then be recognized and utilized by luciferase for bioluminescence generation. The intensity of the emitted light is proportional to the amount of luciferin formed, reflecting the activity of the trigger.<sup>38</sup>

The condensation reaction between CBT and 1,2-aminothiols is particularly attractive for bioconjugation applications. This is because the reaction can be carried out at room temperature under aqueous, physiological conditions and exhibits a high selectivity for aminothiols over other biological nucleophiles.<sup>38,39</sup> Additionally, the reaction kinetics are highly rapid, with a second-order rate constant of  $9.19 \text{ M}^{-1}\text{s}^{-1}$  for the reaction between L-cysteine and 2-cyano-6-aminobenzothiazole, yielding L-aminoluciferin, which is bioluminogenically inactive (also true for L-luciferin).<sup>40</sup> It is important to note that this condensation reaction between CBT-derivatives and 1,2-aminothiols only occurs at neutral or basic pH conditions. This is because the thiazolidine ring formation of D-(amino)luciferin does not occur at acidic pH.<sup>39</sup>

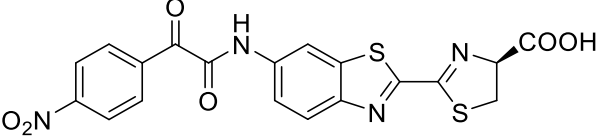
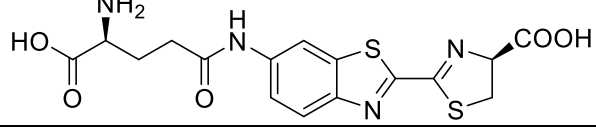
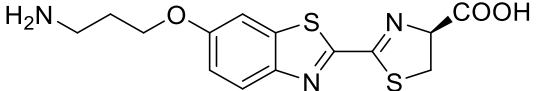
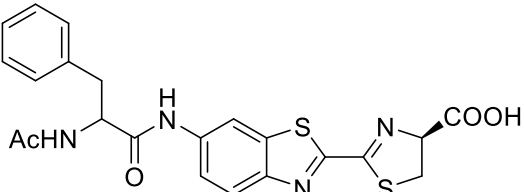
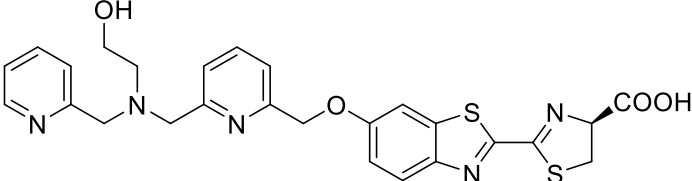
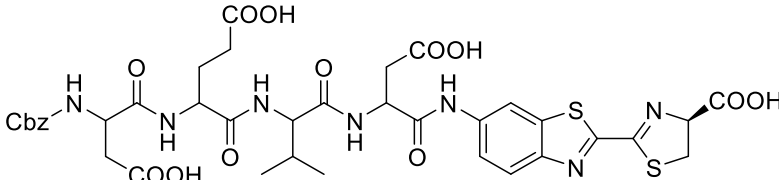
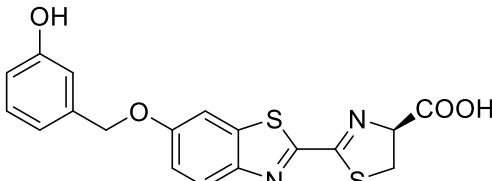
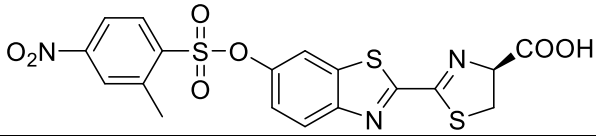
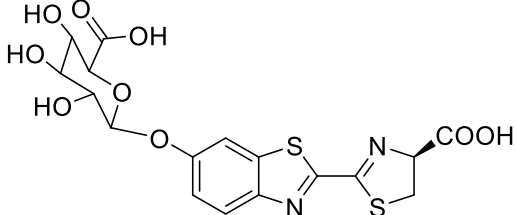
Compared to traditional bioluminescence imaging methods, the split-luciferin approach offers enhanced background reduction. This is achieved because the luciferin fragments are inactive until triggered, minimizing unspecific background luminescence arising from non-specifically released luciferin. This leads to a higher signal-to-noise ratio, enhancing the sensitivity and specificity of the imaging technique.<sup>38,39</sup>

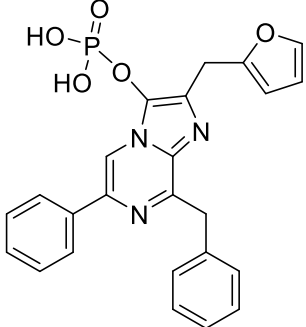
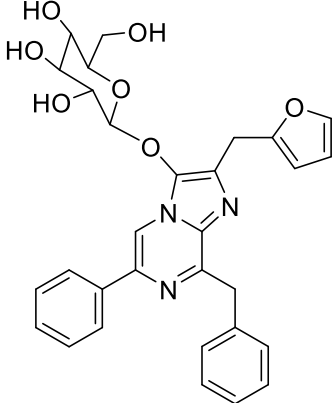
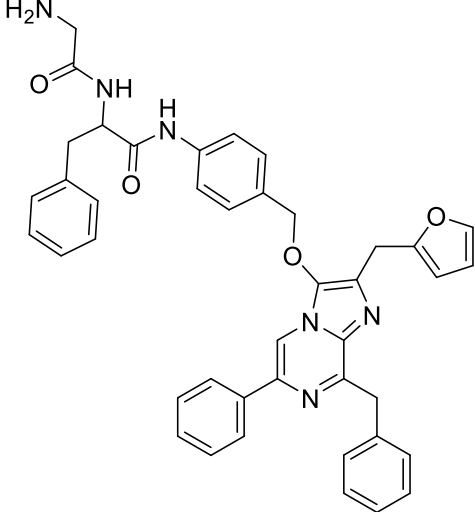
**Table 2.4** shows a select amount of published single-analyte probes based on D-luciferin or furimazine. At the time of writing, only one other dual-analyte probe based on the D-luciferin scaffold was published, targeting  $\text{ClO}^-$  and CTSL.

**Table 2.4:** Select examples of published designs for bioluminescent probes for FLuc and NLuc.

| FLuc probe  | Analyte                 | Ref.               |
|---|-------------------------|--------------------|
|    | $\text{ClO}^-$ and CTSL | Ref. <sup>37</sup> |
|   | NTR                     | Ref. <sup>41</sup> |
|  | $\text{ClO}^-$          | Ref. <sup>42</sup> |
|  | FAAH                    | Ref. <sup>43</sup> |
|  | Cu(II)                  | Ref. <sup>44</sup> |
|  | Cu(I)                   | Ref. <sup>45</sup> |
|  | Fe(II)                  | Ref. <sup>46</sup> |

## Chapter 2: Introduction

| FLuc probe  | Analyte           | Ref.               |
|---|-------------------|--------------------|
|    | ONOO <sup>-</sup> | Ref. <sup>47</sup> |
|    | GGT               | Ref. <sup>48</sup> |
|    | MAO               | Ref. <sup>49</sup> |
|    | α-CT              | Ref. <sup>50</sup> |
|   | Co(II)            | Ref. <sup>51</sup> |
|  | Cas 3/7           | Ref. <sup>52</sup> |
|  | TYR               | Ref. <sup>53</sup> |
|  | GST               | Ref. <sup>54</sup> |
|  | GUSB              | Ref. <sup>55</sup> |

| NLuc probe  | Analyte     | Ref.               |
|---|-------------|--------------------|
|    | ALP         | Ref. <sup>56</sup> |
|   | Glucosidase | Ref. <sup>56</sup> |
|  | CTSC        | Ref. <sup>56</sup> |

## **2.6. Redox Homeostasis as Target for Bioluminescent Sensing**

### **2.6.1. Overview of redox homeostasis**

Redox homeostasis is a critical aspect of cellular function, maintaining the delicate balance between oxidative and reductive states within the cell. This dynamic equilibrium is essential for the proper functioning of various cellular processes, from energy production to cellular signaling and stress response. At the core of redox homeostasis are reactive oxygen species (ROS), which are generated as byproducts of cellular metabolism, particularly in the mitochondria. When produced in controlled amounts, these reactive species can serve as important signaling molecules, regulating crucial cellular activities. However, an imbalance in the production and clearance of these reactive species can lead to a state of oxidative stress. This imbalance can lead to severe consequences, including damage to cellular macromolecules such as lipids, proteins, and nucleic acids, as well as the activation of programmed cell death pathways. Imbalances in cellular redox homeostasis have been associated with the pathogenesis of various chronic diseases, such as cancer, type 2 diabetes, and cardiovascular diseases.<sup>57-59</sup>

The primary factors contributing to cellular redox homeostasis include the generation of reactive oxygen species (ROS) as byproducts of cellular metabolism, particularly through mitochondrial respiration, as well as the intricate network of antioxidant systems that work to neutralize these reactive species. Antioxidant enzymes such as catalase<sup>60</sup> and glutathione peroxidase<sup>61</sup> play a vital role in this process, converting potentially harmful hydrogen peroxide and superoxide anions into more benign molecules. Additionally, non-enzymatic antioxidants, such as glutathione and ascorbic acid, also contribute to the maintenance of redox balance. When this critical balance is disrupted, either due to excessive ROS production or a depletion of antioxidant defenses, a state of oxidative stress ensues.<sup>59,62</sup>

### **2.6.2. Key analytes in redox homeostasis**

Three key analytes involved in redox homeostasis - ferrous ions, nitroreductase (NTR), and gamma-glutamyl transferase (GGT) – were selected as targets for the development of bioluminescent probes in this work, given the critical importance of cellular redox balance.<sup>63-65</sup>

Ferrous ions are essential for various cellular processes, including electron transfer reactions, gene regulation, and the regulation of cell differentiation and growth. Ferrous ions are particularly important for the activity of enzymes involved in the production of reactive oxygen species (ROS) and nitric oxide, which are important for immune function and pathogen defense. The ability of ferrous ions to readily donate electrons makes them a valuable component of many cellular enzymes and protein complexes, such as those involved in photosynthesis, respiration, and other vital processes. However, this same property also makes ferrous ions potentially harmful, as they can participate in the generation of highly reactive hydroxyl radicals through Fenton reactions. To mitigate this risk, eukaryotic cells have evolved complex mechanisms to carefully regulate the levels of free ferrous ions, ensuring that they are efficiently scavenged from the environment and delivered to the appropriate cellular compartments and enzymes. This regulation involves a variety of transport proteins, chaperones, and chelating agents, such as glutathione and metallothionein, which work together to maintain the appropriate balance of ferrous ions in the cell. Disruption of this homeostasis can lead to oxidative stress, cellular damage, highlighting the critical importance of ferrous ion regulation in eukaryotic cells.<sup>64,66</sup>

Hypoxia, a state of low oxygen availability, and nitroreductase enzymes, which metabolize nitroaromatic compounds, can both significantly impact cellular redox homeostasis. Hypoxic conditions can lead to mitochondrial dysfunction and increased generation of superoxide and other reactive oxygen species, contributing to oxidative stress. Nitroreductases, on the other hand, can generate reactive nitrogen species, such as peroxynitrite, which can also disrupt the delicate redox balance.<sup>41,65</sup>



## Chapter 2: Introduction

Gamma-glutamyl transferase is responsible for the catabolism of glutathione, breaking down this tripeptide into its constituent amino acids. This process is essential for the recycling of cysteine, a key component of glutathione and a critical substrate for the de novo synthesis of this antioxidant. Glutathione is a biothiol that protects cellular components from oxidative damage of ROS, such as hydrogen peroxide and organic peroxides via GSH peroxidases, and also aids in detoxification of electrophilic metabolites and xenobiotics. Deficiency of GGT results in oxidative stress and cellular susceptibility to oxidant injury, while elevated serum GGT appears to be implicated in certain types of cancers. This suggests that the maintenance of proper gamma-glutamyl transferase function is critical for preserving cellular redox homeostasis and, consequently, overall cellular health and function. <sup>61,63,67,68</sup>

## 3. Objectives

The overarching aim of this research is to develop a palette of bioluminescent probes for the simultaneous detection of multiple analytes implicated in redox homeostasis.

To achieve this aim, the following objectives were established:

1. Design and synthesize a series of novel bioluminescent probe systems through multi-step organic strategies, attaching target responsive moieties to various bioluminescent scaffolds:
  - a. Develop split-luciferin probes containing D-Cysteine and 6-hydroxy-2-cyanobenzothiazole (OH-CBT) for the detection of nitroreductase (NTR) and ferrous ions,
  - b. Create dual-analyte probes based on D-luciferin and D-aminoluciferin for the simultaneous detection of NTR and  $\gamma$ -glutamyl transpeptidase (GGT), and
  - c. Explore the potential of furimazine as a scaffold for creating activatable bioluminescent substrate probes, specifically for NTR detection.
2. Conduct comprehensive characterization of all synthesized probes and intermediates and evaluate their bioluminescent response to analytes through *in vitro* testing, assessing their efficacy and specificity in detecting the target analytes and identify advantages and challenges associated with different designs.

This synthetic and biochemical research intended to contribute to the understanding and optimization of the design, synthesis and validation workflows for the development of bioluminogenic substrates as tools for simultaneous detection of multiple biochemical analytes. In particular, it aspires also to give experimental evidence and insights into the advantages and limitations of variable multianalyte detection approaches. These are to inform future development and practical *in cellulo* and *in vivo* applications of multi-analyte bioluminescent probes for the simultaneous detection of key biochemical factors, potentially leading to more comprehensive insights into cellular processes and disease mechanisms.

## 4. Results and Discussion

### 4.1. Iron(II) responsive bioluminogenic substrate for detection by split luciferin strategy

In order to expand the palette of bioluminogenic substrates suitable for multianalyte detection of redox-involved analytes, a split-luciferin variant of the probe was made for sensing Fe(II) using the OH-CBT moiety. The D-luciferin version of this probe is already described in the literature<sup>69</sup>, but unlike in that probe, with a split-luciferin design, the CBT version of the probe can be multiplexed with protected cysteine to enable dual-analyte detection system<sup>39</sup>. The published full luciferin probe's mechanism of action is based on a biomimetic oxidation reaction (**figure 4.1**). It proceeds first via the chelation of Fe(II) by an iron(II)-specific multidentate ligand (red on **figure 4.1**), followed by iron(II)-catalyzed oxidative cleavage of the bond between phenolic oxygen and benzylic carbon by a molecular oxygen, to release D-luciferin in this case. Our design of **4** is also based on this approach, in which OH-CBT should be released after reaction with Fe(II). A similar mechanism of action is also present in human mono-oxygenases, e.g. for the metabolization of xenobiotics.<sup>70</sup>

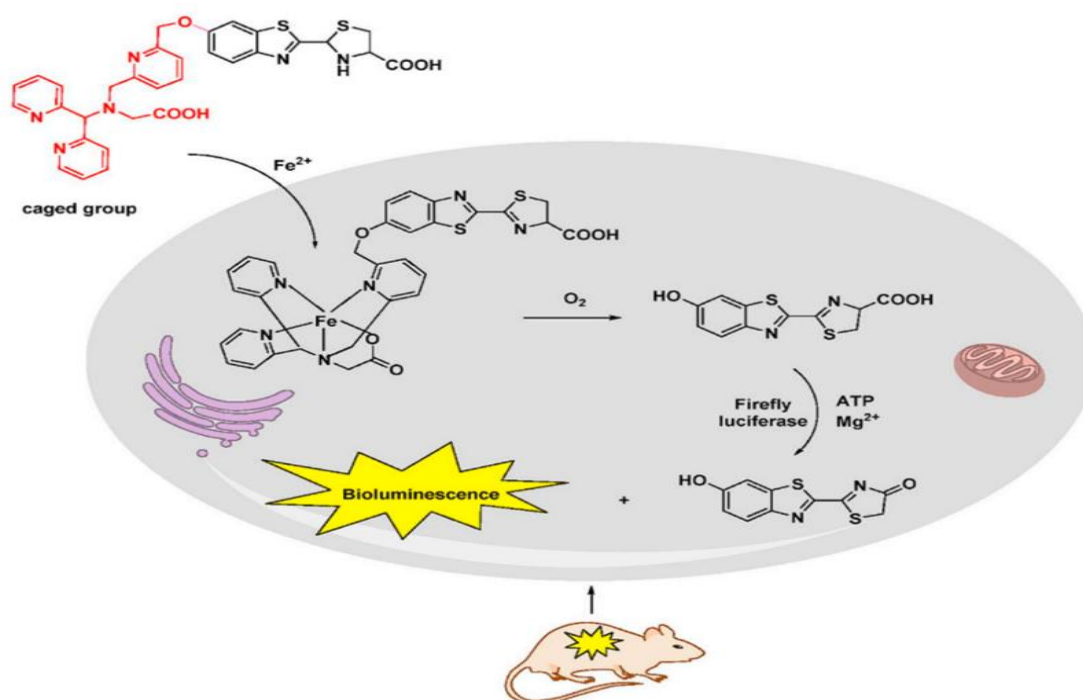
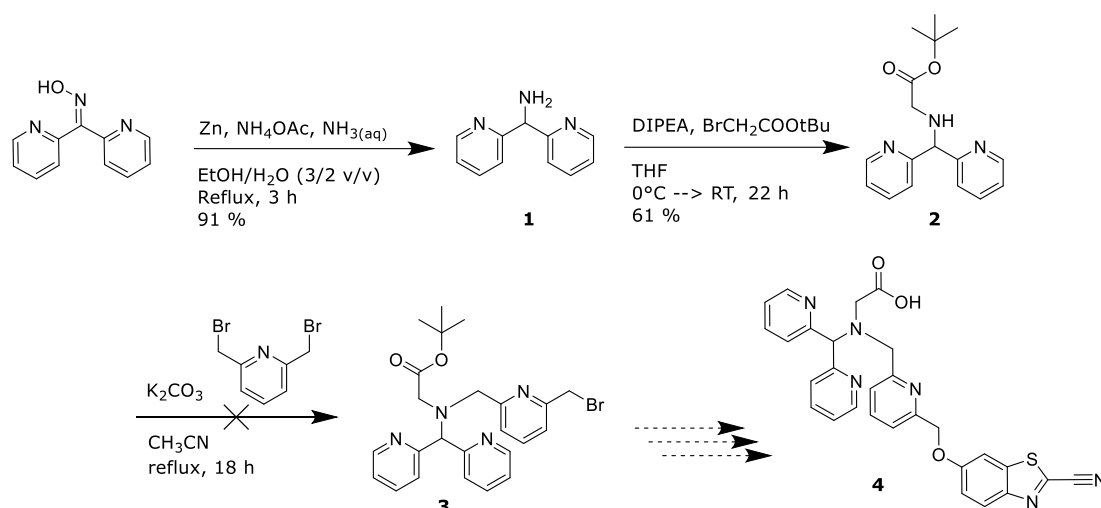


**Figure 4.1:** Mechanism of action for a D-luciferin-based Fe(II) probe. Image adopted from ref.<sup>69</sup>

#### 4.1.1. Synthesis

The synthesis of **4** was first attempted according to the previously reported<sup>69</sup> synthetic pathway presented on **scheme 4.2**. In this procedure, a chelating moiety **3** is synthesized first in a form of a benzylic bromide suitable for a nucleophilic substitution reaction by OH-CBT. The synthesis begins with the reduction of the ketoxime with zinc metal to yield **1**, according to the reported procedure<sup>71</sup>. Afterwards, a nucleophilic substitution reaction of **1** with tert-butyl bromoacetate, in the presence of DIPEA and anhydrous THF was performed. When pure tert-butyl bromoacetate was added dropwise to a solution of **1** in ice bath, increasingly more di-substitution was noted. To ensure predominantly mono-substitution, a diluted solution of tert-butyl bromoacetate in THF was added instead that indeed lowered di-substitution significantly. The challenging part was also to purify this compound via silica gel column chromatography. Since polar amines can interact strongly with the acidic silanol groups, one of the approaches is to use a different stationary phase (e.g. basic alumina) or to add a small amount of competing base in the mobile phase, such as triethylamine or  $\text{NH}_{3(\text{aq})}$ . In my work, a purification with silica gel was performed using an eluent system of EtOAc/MeOH/25%  $\text{NH}_{3(\text{aq})}$  97/2/1 v/v/v, compared to the original procedure which used DCM/MeOH 100/3 v/v. The reason for changing the eluent system is due to the high polarity of compound **2**, and by using silica gel column chromatography without the addition of a competing base, will assuredly give trouble in purification. Although the reported mobile phase (DCM/MeOH 100/3 v/v) was not tested with a competing base, the eluent system of EtOAc/MeOH/25%  $\text{NH}_{3(\text{aq})}$  97/2/1 v/v/v was chosen due the higher polarity of EtOAc compared to DCM, along with the addition of water, which will aid in purifying **2** via silica gel column chromatography. Another reason is that EtOAc can dissolve very small amounts of water, around 3% at room temperature, compared to DCM, which can only dissolve 0.24%, which could pose a problem, since small percentages of water dissolved in an eluent can be useful in purifying highly polar compounds. This gave a good separation between disubstituted impurity and **2**, with an isolated yield of 62%. Afterwards, a nucleophilic substitution reaction was carried out using 2,6-bisbromomethyl pyridine to yield chelator moiety **3** as previously reported<sup>69</sup>. On TLC, a new spot was formed after reacting overnight, however the product of this reaction proved to be difficult to purify, due to its high polarity that is a typical

challenge for the preparation of an amine/nitrogen rich multidentate ligands. The purification could not be replicated by using the author's solvent phase of DCM/MeOH 99/1 v/v in silica gel column chromatography, and a repeat of this reaction using neutral alumina as a stationary phase gave the same result of an impure mixture being isolated. One of the possible reasons for this could be a presence of multiple nitrogen-rich and therefore polar byproducts caused by the presence of two electrophilic sites on the bisbromomethyl pyridine reagent.

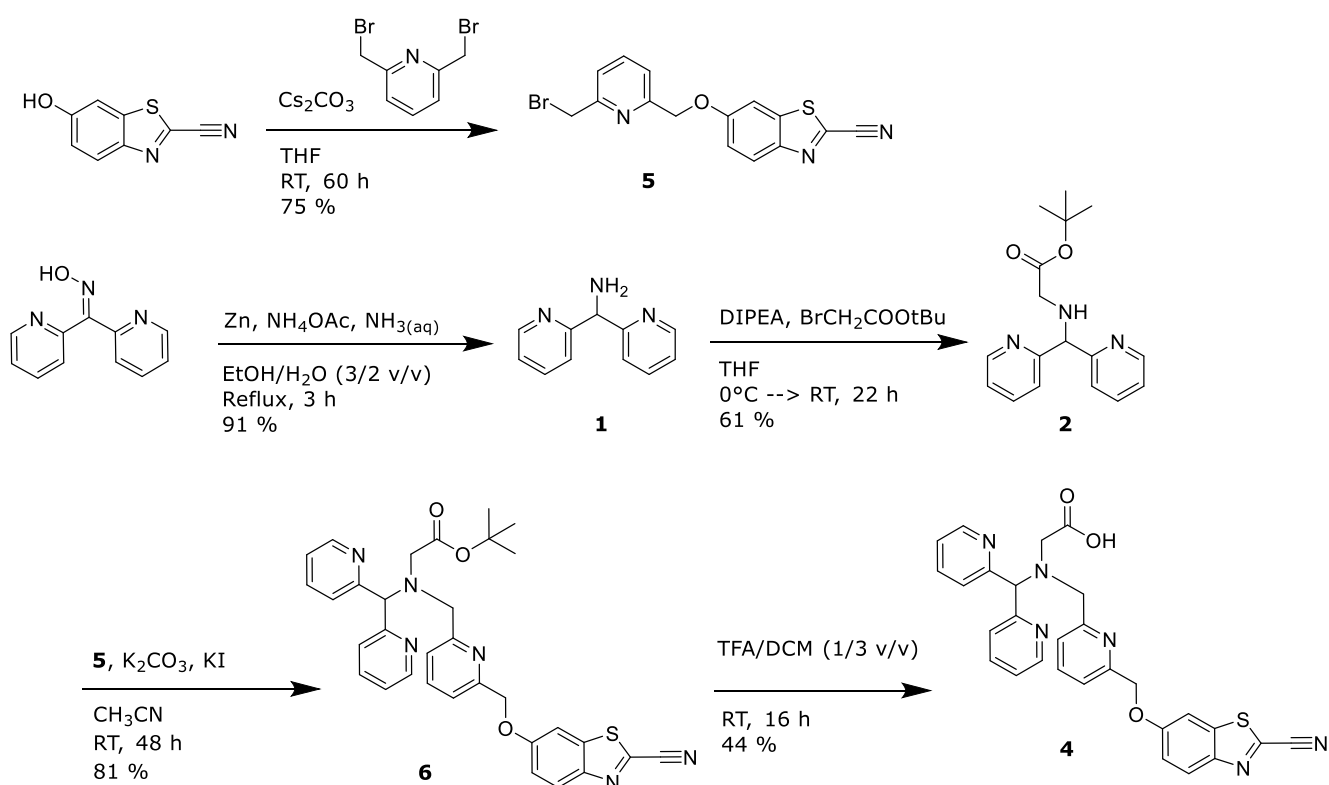


**Scheme 4.2:** Synthetic scheme for **4** (based on a previously reported method<sup>69</sup>), via the synthesis of chelator functionality **3**.

Due to the failure of the first route caused by a presence of a difficult to separate impurity, a new method (**scheme 4.3**) was developed that avoided a formation of a full nitrogen-rich chelator. Instead, part of the chelator has been constructed on the OH-CBT moiety before condensing it with a remaining part of the chelating motif. In particular, at first a nucleophilic substitution, was carried out by reacting OH-CBT and 2,6-bisbromomethyl pyridine in THF at room temperature utilizing  $\text{Cs}_2\text{CO}_3$  as the base over weekend (60 h), using a modified method previously reported<sup>72</sup>, giving product **5** with 75% yield. In the original procedure, this reaction was performed for 15 h at 50 °C for 15 h, giving **5** in 69% yield. The modification of stirring for longer time at room temperature gave a slight yield increase compared to the original procedure. Afterwards, **5** was then coupled to mono-amine **2** in  $\text{CH}_3\text{CN}$  using  $\text{K}_2\text{CO}_3$  as the base over two days stirring at room temperature. This product was able to be purified with silica gel column chromatography using isocratic elution with 0.5%  $\text{Et}_3\text{N}$  in  $\text{EtOAc}$ , yielding tBu-

## Chapter 4: Results and Discussion

ester protected **6**. The final step involved a TFA deprotection in DCM to yield **4**. After evaporation of TFA, residual amounts of TFA can potentially stick to the product potentially in a form of a salt that is harder to purify via silica stationary phase. Several attempts at purification with silica TLC were made, but to no avail. Therefore, in the attempt to alleviate the problem, TFA was neutralized after reaction with Et<sub>3</sub>N. This was then diluted with DCM, the organic layer was washed once with water and brine, then the organic layer was evaporated and purified via silica TLC. Purification via silica TLC was successful and analysis of <sup>1</sup>H NMR indicated the formation of product **4**, with all aromatic hydrogens visible, and slight aliphatic impurities. The advantage of this route is that two smaller building blocks are coupled together, while also skipping the synthetic step of the chelator core **3**, thus making purification easier.



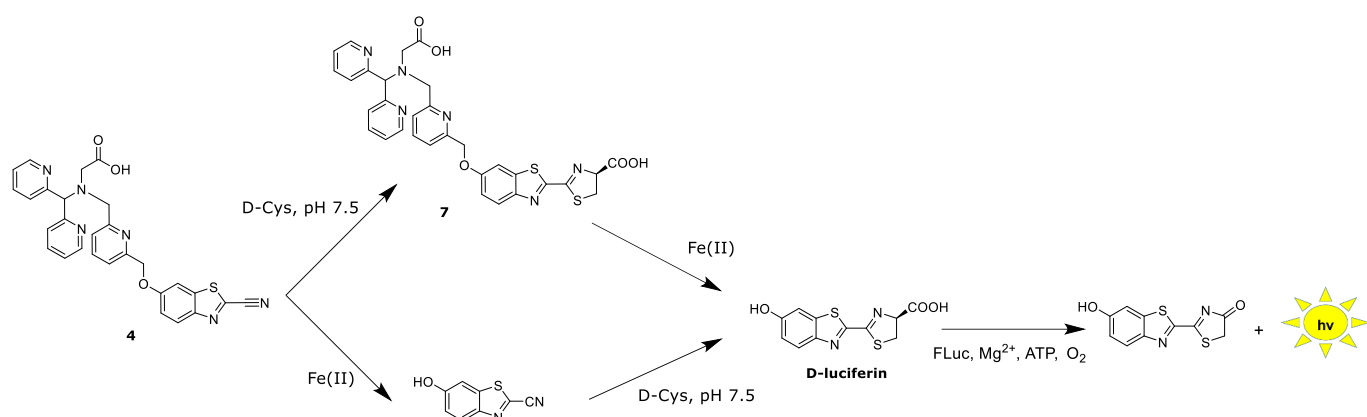
**Scheme 4.3:** Synthetic scheme for **4**, skipping the synthesis of chelator functionality **3**.

#### 4.1.2. Response to iron(II)

Following a successful synthesis and separation **4**, the bioluminescent response to the presence of iron(II) was investigated. The detailed sequence of reactions expected to take place in the presence of iron are presented on **scheme 4.4**. Ferrous ions can first react with **4** to yield OH-CBT, that then reacts with D-Cys to form D-luciferin. Another possibility is that **4** can react first with D-Cys to form the D-luciferin-based probe **7**, described previously<sup>69</sup>, and then form pure D-luciferin after reaction with ferrous ions.

To appropriately interpret the results observed, it is therefore also important to clarify that the bioluminescent signal that was recorded for the experiments discussed below is generated in an irreversible reaction between luciferase enzyme and D-luciferin. Since our probe is based on OH-CBT instead, an addition of D-cysteine to the assay (we have used equimolar quantities with the probe) is indispensable for the formation of D-luciferin scaffold (via OH-CBT and D-Cys condensation) and subsequent signal generation. Bioluminescence is then in fact a direct measure of luciferase activity (a direct measure of the rate of reaction), that in turn is positively correlated with the concentration of D-luciferin, given the reaction conditions and concentrations of other reagents and reactants (luciferase, oxygen, ATP, Mg<sup>2+</sup>) are constant or in sufficient excess to appear constant over the period of experiment.

With that in mind, a series of bioluminescent analytical experiments were performed in bioluminescence-compatible white 96-well plates. TRIS-HCl buffer was utilized as previously reported for these types of assays and at 50 mM concentration to ensure robust pH stabilization. The *in vitro* experiment was carried out by first mixing 50 mM TRIS-HCl pH 7.5, containing 10 mM MgCl<sub>2</sub> and 0.1 mM EDTA, together with **4**, then adding the solutions in the following order: firefly luciferase, ATP, D-Cys and FAS. Once the additions are completed, bioluminescence intensity was immediately measured for 30 min. at 37 °C.



**Scheme 4.4:** Split-luciferin reaction of **4**, showcasing the many reaction kinetics that are important in the final bioluminescent signal.

Firstly, a control experiment with D-Cys and OH-CBT (unmasked version of the probe) led to the rapid, near-linear increase of bioluminescent signal in the first 10-15 min. (change from 0 to 800 000 RLU – see insert in **figure 4.5**, dark blue), followed by a gradual decrease in the signal afterwards (from approx. 800 000 RLU at 12 min. to approx. 700 000 at 30 min.). Through experimental conditions chosen (see above & methodology, i.e. enzyme concentration constant, oxygen and ATP at least 100x excess throughout the experiment), the bioluminescent signal is proportional to the concentration of the D-luciferin as the rate-limiting reagent. Therefore, the observed signal modulation indicates that the initial kinetic of formation of D-luciferin in these experimental conditions is faster than the depletion of D-luciferin via a bioluminescence-generating reaction of this substrate with luciferase enzyme. In turn, it leads to the gradual accumulation of D-luciferin in the first 10-15 min. of the reaction after which the rate of the formation of luciferin is lower than the rate of the bioluminescent reaction, leading to gradual depletion of effective luciferin concentration available for luciferase.



## Chapter 4: Results and Discussion

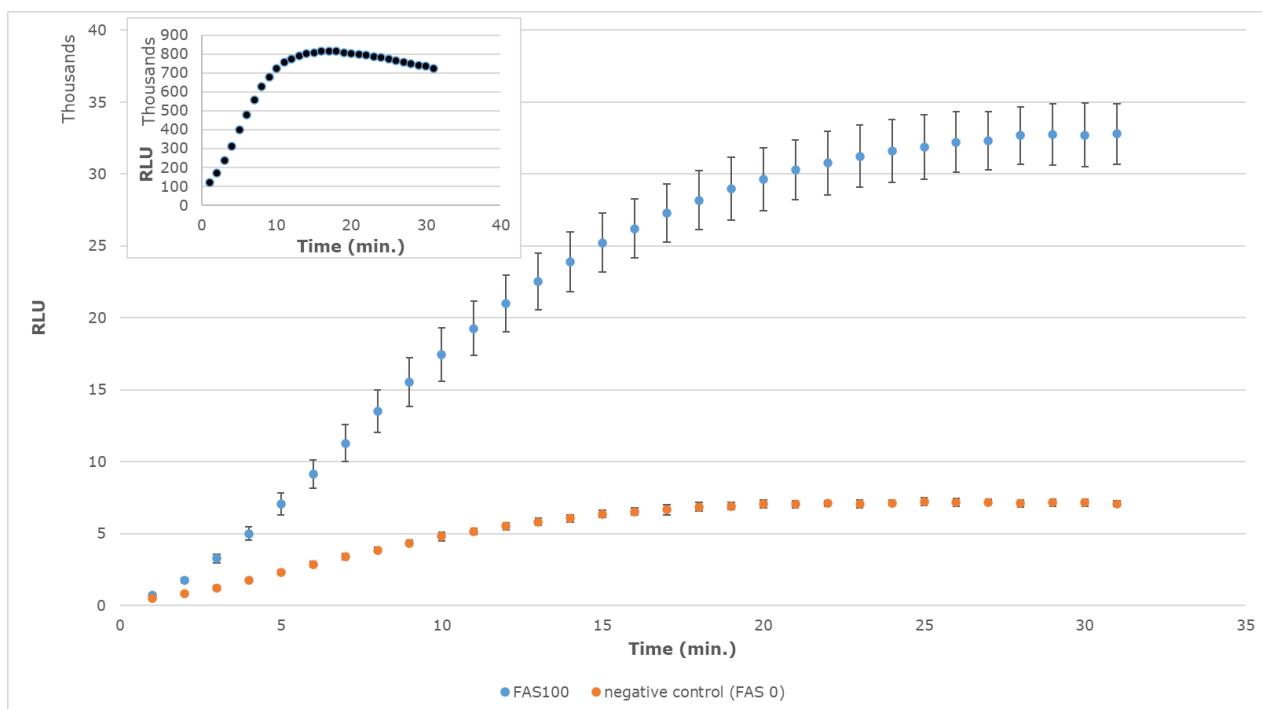


**Figure 4.5:** Average bioluminescent response (expressed in RLU) of positive control (OH-CBT + D-Cys, dark blue, insert), **4** with D-Cys in the presence of 100  $\mu\text{M}$  FAS (light blue) or no FAS as negative control (orange). Final concentrations were used for the following components: 20  $\mu\text{M}$  for **4** and OH-CBT, 2 mM ATP, 20  $\mu\text{M}$  D-Cys and 20  $\mu\text{g}/\text{mL}$  for FLuc. The buffer used here is TRIS-HCl (50 mM, pH 7.4) containing 10 mM  $\text{MgCl}_2$  and 0.1 mM EDTA. Result shown for **4** with D-Cys in the presence of 100  $\mu\text{M}$  FAS is the average of 10 values, for negative control the average of 4 values, for positive control the average of 2 values. Experiments were performed for 30 min. at 37  $^\circ\text{C}$ , with an integration time equal to 1 second and an interval time of 1 min., using the following order of addition: OH-CBT or **4**, buffer, FLuc, ATP, D-Cys and FAS.

When analyzing the bioluminescent signal modulation for probe **4** in the presence and absence of Fe(II), it can be noted that the initial rate of luciferase reaction (i.e. bioluminescent signal generation) is significantly lower (approximately 26 times) than in the case of the positive control OH-CBT. Additionally, the maximal signal intensity (and so the highest attainable rate) is also significantly lower and is reached only at min 30. This all points, as expected, at lower effective concentration of D-luciferin at any given time than in the case of OH-CBT+D-Cys control, that in turn is a consequence of the fact that additional iron(II)-catalyzed cleavage of the chelator moiety of probe **4** is required to enable D-luciferin generation. Importantly, however, the signal in the presence of Fe(II) is significantly higher than in its absence (up to 6 times), confirming the responsiveness of the probe to this analyte.

#### 4.1.3. Probe's performance in biologically-relevant conditions

To confirm the reproducibility of the response, similar experiments, but using alternative instrumentation, were repeated in collaboration with the team of prof. Natalia Rozwadowska (including dr. hab. Iwona Ziółkowska-Suchanek and Michalina Krakowiak) from the Institute of Human Genetics, Poznan, Poland (**figure 4.6**). For these experiments, to compare the effects, a pure water or lysates of H1299 LUC cells, which are cell lines derived from human non-small cell lung carcinoma expressing FLuc, were used (lysed with commercially available Cell Lysis Buffer – Promega). Afterwards, to a black 96-well plate with a transparent, flat bottom was then added 25 mM TRIS-HCl pH 7.5 buffer, containing MgSO<sub>4</sub> and EDTA as additives. In the following order, cell lysate (or pure water), D-Cys, FAS, firefly luciferase, ATP and **4** were added. As positive control, OH-CBT was used instead of the probe and for negative control, FAS was omitted.

As observed in the case of our *in vitro* studies, in water samples (no lysates), an addition of 100 µM of Fe(II) led to a parabolic increase in bioluminescent signal over 30 min. to approx. 2.5 million RLU (violet trace on **figure 4.6**) while the signal was significantly lower in the absence of Fe(II) (blue trace on **figure 4.6**). In particular, the ratio of the signal with and without iron in pure water changed from 3 at 5 min. to approx. 13 at 25 min when it was the highest, with the baseline signal with no iron changing marginally over time. This confirms the gradual accumulation of D-luciferin over time in the presence of iron(II) validating the mechanism of response of the probe as discussed above.

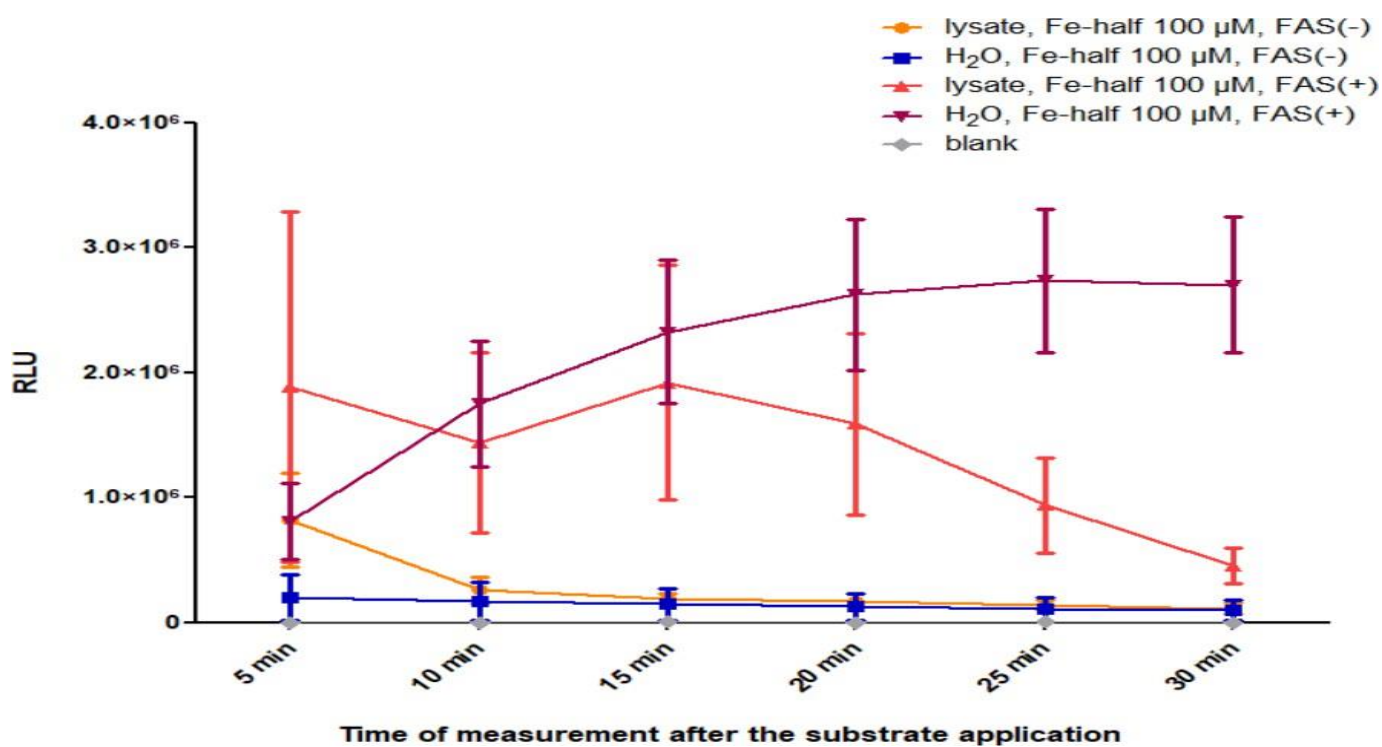


**Figure 4.6:** "The bioluminescence signal measured on H1299 LUC cell lysate samples, after Fe-half probe application (100 μM final concentration). FAS (ferrous ammonium sulfate) final concentration – 100 μM; luciferin final concentration – 20 μg/ml; cell lysate – 20 μl (=50 000 cells). Measurement conditions: 5 min exposure, 6 measurements, no breaks. FAS(-) – sample without FAS addition; FAS(+) – sample with FAS addition. Considering 100 μM concentration of the Fe-half probe, after 10 min from the substrate application, the signal from both FAS(+) samples is higher than the signal detected in FAS(-) samples."

Image and description adopted from MSc. Thesis of Michalina Krakowiak.

Interestingly, however, the lysate samples exhibited the highest rate of bioluminescence reaction (i.e. highest bioluminescent signal) at 5 min time point (near-to-initial rate), with a rapid decrease to background levels for experiment with no extra iron (orange trace in **figure 4.6**) and a plateau until 20 min, followed by gradual drop after that for iron-spiked conditions (red trace in **figure 4.6**). Importantly, when compared the initial reaction rates at 5 min for all conditions, the highest one is observed for lysate spiked with Fe(II), followed by relatively equal rates (signal intensities) for lysate with no extra iron and pure water with iron, and finally with the lowest (near-background) rate for no iron in pure water.

One of the potential explanations of this result is the fact that iron(II) is present in the lysate and the possibility of measuring that signal means that the probe is sensitive enough to pick endogenous levels of iron(II). However, the signal quickly drops, possibly due to a relatively lower endogenous Fe(II) concentration. When comparing samples with exogenously added Fe(II) for both lysate and water, an initially high rate of reaction for lysate might suggest either a presence of additional endogenous iron(II) (and therefore effectively higher concentration) or compromised stability of the probe in lysates vs water. Additionally, a large variability of bioluminescent signal intensity of technical repeats for lysate-based samples further suggests a cellular media-dependent effects are in play.

*In cellulo* experiments were also performed by the group of prof. Rozwadowska from the Institute of Human Genetics, Poznan, Poland. H1299 LUC cells were cultured for 24 h, and then seeded on a black 96-well plate, followed by incubation with 100 or 200  $\mu$ M FAS for either 1 h or 24 h. Then, a subsequent incubation for 30 min. was performed with D-Cys and 25 mM TRIS-HCl pH 7.5. The measurement was started immediately after addition of OH-CBT or **4**. Results show that initially, the rate of reaction for Fe(II) preincubated cells is higher than with no iron or no probe, confirming the observation from the lysates with no additional iron(II), i.e. that the probe can actually detect endogenous levels of iron. Unfortunately, the sensitivity of **4** is low in H1299 LUC cells (**figure 4.7**) and the signal drops within 10 minutes. **4** also suffers from a large variability of response in lysates hindering any quantification and compromising the robustness of the readout. The insufficient reliability of the response could be attributed to poor pharmacokinetics of **4**, such as low cellular uptake due to the high polarity of **4**, slow diffusion or low metabolic stability inside the cells. Another reason could be the spatial

## Chapter 4: Results and Discussion

heterogeneity, which is to say the effective local concentration of different reactants inside the cell.

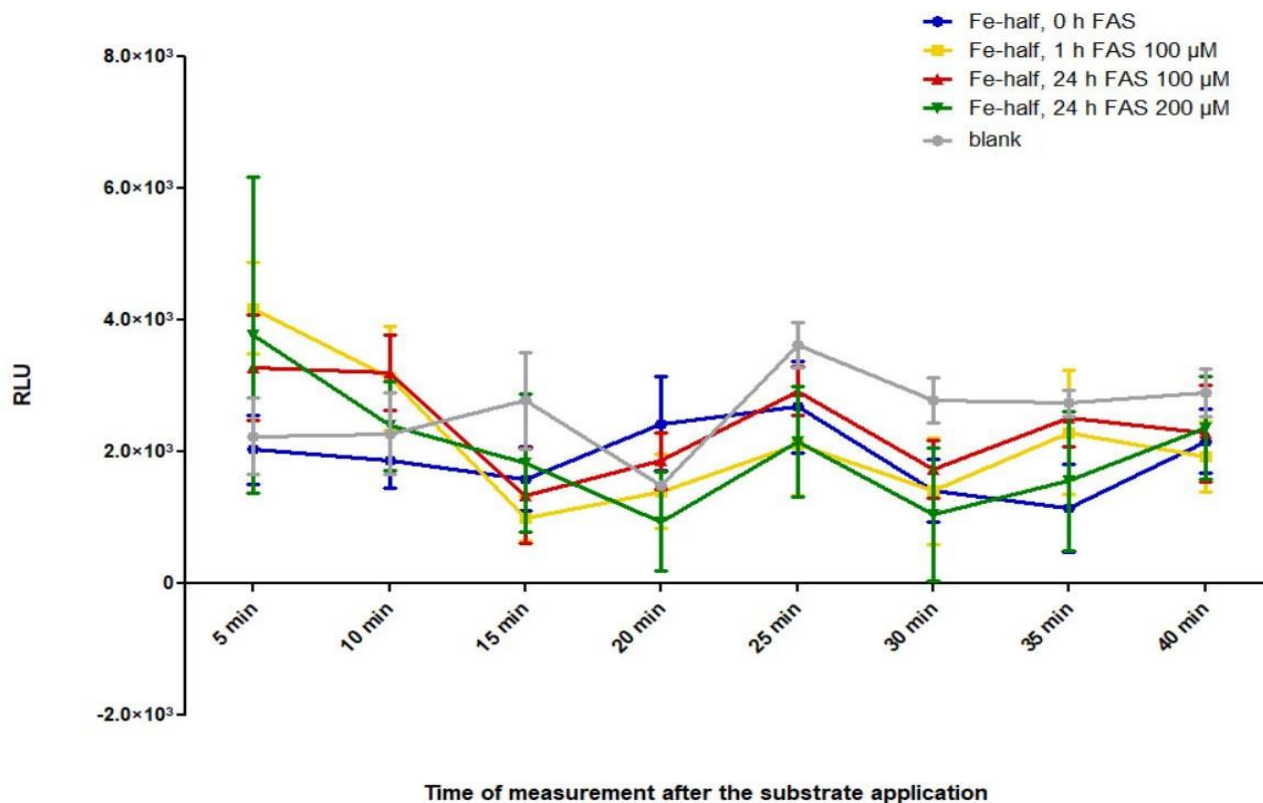


**Figure 4.7:** "The bioluminescence signal measured on H1299 LUC cells, after Fe-half probe application (100  $\mu$ M final concentration). Cells were incubated 0 h, 1 h (100  $\mu$ M final concentration) or 24 h (100  $\mu$ M or 200  $\mu$ M final concentration) with FAS (ferrous ammonium sulfate). Control sample - 0 h FAS, meaning no supplementation with FAS. Measurement conditions: 5 min exposure, 8 measurements, no breaks. RLU - relative luminescence units."

Image and description adopted from MSc. Thesis of Michalina Krakowiak.

#### 4.1.4. Metal ion-dependent signal interference

An interesting observation has also been made when investigating iron concentration-dependence of the bioluminescent signal generation by **4**. **Figure 4.8** shows the relative change of bioluminescent signal generated by luciferase system in the presence of 20  $\mu\text{M}$  **4** with different concentrations of FAS, ranging from 25  $\mu\text{M}$  to 200  $\mu\text{M}$ .

It is important to note that RLU is a representation of kinetics at a given time. A steeper increase in reaction rate in **figure 4.8** (top panel), correlates with an increased amount of D-luciferin formed at a given time. This corresponds to a relative rate of oxyluciferin oxidation, which is proportional to D-luciferin formed and therefore its concentration. Although **figure 4.8** (top panel) shows a large variability for 50, 100 and 200  $\mu\text{M}$  FAS without statistical significance, a semi-quantitative trend can be observed, with higher ferrous ion concentrations leading to a quicker turn-over for D-luciferin formation. Thus, for a given day, the highest concentration of FAS gives a higher reaction rate. The relative trend of increase in the ratio of bioluminescent signal between iron(II) and control experiments is observed for increasing Fe(II) concentration (**figure 4.8**, bottom panel) but the differences are not statistically significant due to a large day-to-day variability. This is particularly severe for the highest Fe(II) concentration tested (200  $\mu\text{M}$ ), that when averaged suggests that at this concentration, the bioluminescent signal is quenched (blue bar in **figure 4.8**, bottom panel).

## Chapter 4: Results and Discussion

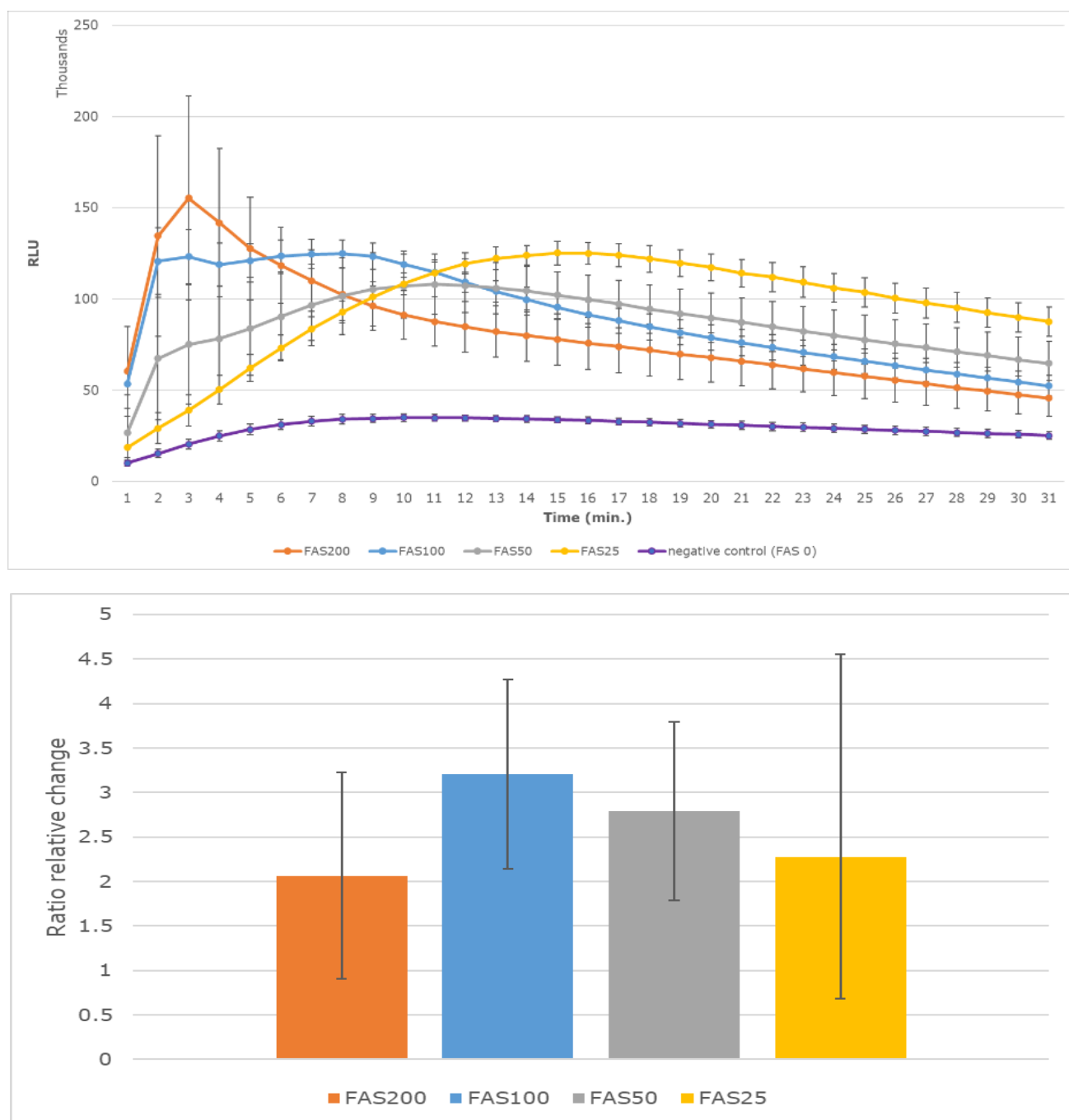


**Figure 4.8:** **Top:** RLU of **4** in the presence of 25 (yellow), 50 (grey), 100 (blue) and 200 (orange)  $\mu\text{M}$  FAS, with negative control (purple, no FAS). Results are average of 5 values. Final concentrations used for the following components: 20  $\mu\text{M}$  for **4**, 2 mM ATP, 20  $\mu\text{M}$  D-Cys and 20  $\mu\text{g}/\text{mL}$  FLuc. The buffer used here is TRIS-HCl (50 mM, pH 7.5) containing 10 mM  $\text{MgCl}_2$  and 0.1 mM EDTA. Experiments were performed for 30 min. at 37  $^\circ\text{C}$ , with an integration time equal to 1 second and an interval time of 1 min., using the following order of addition (all mixed together immediately): **4**, buffer, FLuc, ATP, D-Cys and FAS. **Bottom:** Average ratio of relative change, obtained by taking the averaged sum of responses over 20 min. of **4** (tested in a given FAS concentration) divided by averaged sum of responses over 20 min. of negative control. Standard deviations calculated for 16 values (200), 15 values (100), 7 values (50) and 4 values (25).

Inspired by this observation and following the results of the Fe(II) detection in cell lysates and in live cells, we have investigated the potential interference of metal ions on firefly luciferase system in more details to better understand the challenges and limitations of the design and use of bioluminescence-based responsive probes. In particular, the experimental results above indicating lower bioluminescent signal at high iron(II) concentrations despite the presence of iron(II) responsive bioluminogenic probe and the variability of the responses to Fe(II) in cell lysates and live cells, prompted us to investigate the effects of Fe(II) further regarding the impact on bioluminescence, along with a set of other biologically relevant metal ions.

Indeed, early studies showed that certain metal ions can have an impact on the final bioluminescence output<sup>73</sup>. In our study, performed in collaboration with Francesca Canyelles Font, Krzysztof Żukowski, Dorota Kwiatek and Jacek L. Kolanowski (manuscript under revision), we investigated the effects of selected metal ions of biological relevance on the bioluminescence of FLuc, NLuc and RLuc. A panel of 21 biologically relevant metal ions was screened (**figure 4.9**) in a robust HTS assay conditions ("SC" assays) with the readout of luminescence of FLuc, RLuc, and NLuc luciferases (note: only data for FLuc is shown). We also developed an optimised HEPES buffer variants ("H" assays) for direct luciferases' comparison for FLuc, NLuc and RLuc. Interference in bioluminescent signal generation was quantified by calculating IC<sub>50</sub> values from concentration-dependent experiments for selected highly active and relevant metal ions. Finally, we also probed metal ion inhibition mechanisms by variations in specific reagents, EDTA, GSH, and the sequence of addition and buffer composition.

In our experiments, we determined that the IC<sub>50</sub> for FAS in SC conditions and H conditions for FLuc, which was 180.67  $\mu$ M and 23.76  $\mu$ M respectively. We observed that all metal ions at a concentration of 1 mM inhibited to some extent firefly bioluminescence in both SC and H conditions (**figure 4.9**). The main difference between SC and H conditions is the buffer composition (**table 4.10**). The buffer for SC condition has a lower buffering capacity, which was evident when the effect of the metal ions on pH was studied, along with the presence of additional chelating agents like glycine. The pH after addition of 5 mM (**table 4.11**) metal changed for many metals, including FAS (Fe(II)-1), indicating that HEPES has better buffering capacity as expected from its higher concentration. This shows



the importance of choosing a good buffer with high buffering capacity, and that the inhibition by metal ions of FLuc independent of pH effect.

The observed inhibitory effects of metal ions may stem from various mechanisms, including direct interactions with the luciferase enzyme, interference with substrate binding or turnover, sequestration of substrates and reactants, or alterations to the chemical environment necessary for the bioluminescent reaction. As these processes are broadly dependent on the affinities of metal ions to various ligands, such as amino acid residues on enzymes, chelating motifs on substrates and reactants, or buffer components, discerning the precise mechanisms remains challenging. However, the diverse experimental approaches discussed have allowed for quantification of these effects and provided insights into the role of reactants and buffer components in metal-mediated interference with luciferase-driven bioluminescent signal generation. TRIS buffer also shares the quality of a good buffering capacity, similar to HEPES. However, there is some indication that TRIS also has chelating properties<sup>74</sup>. A possible quenching effect of FAS in firefly bioluminescence could be the reason for the low response of **4**. Additionally, a presence of EDTA in the assay can lead to an increased chelation of iron(II) making it less available for a reaction with probe **4**, even though a ligand on **4** is designed to effectively compete (stronger binding constants) for Fe(II) with oxygen-based ligands like EDTA.

Another potentially significant reason for a compromised Fe(II) readout in cells with the use of the probe is a susceptibility of Fe(II) to oxidation on air. EDTA, in fact, as an oxygen-rich ligand, stabilizes harder Fe(III) ions better than Fe(II) promoting Fe(II) oxidation. The rate of oxidation of iron(II) is also increased by a higher pH as reported previously<sup>75</sup> and is higher in HEPES than in TRIS-HCl.<sup>76</sup> Indeed, in the *in vitro* experiments with **4**, a color change from colorless to yellow was observed, suggesting Fe<sup>3+</sup> formation.

All of the evidence gathered in this thesis and supported by the literature clearly demonstrate a big challenge in the detection of iron(II) by D-luciferin-based probes due to a high susceptibility to assay conditions as well as buffer and media composition. This becomes even more complex in a more diverse environments like cell lysates or live cells, that contain multitude of potential interferents of the bioluminescent signal.

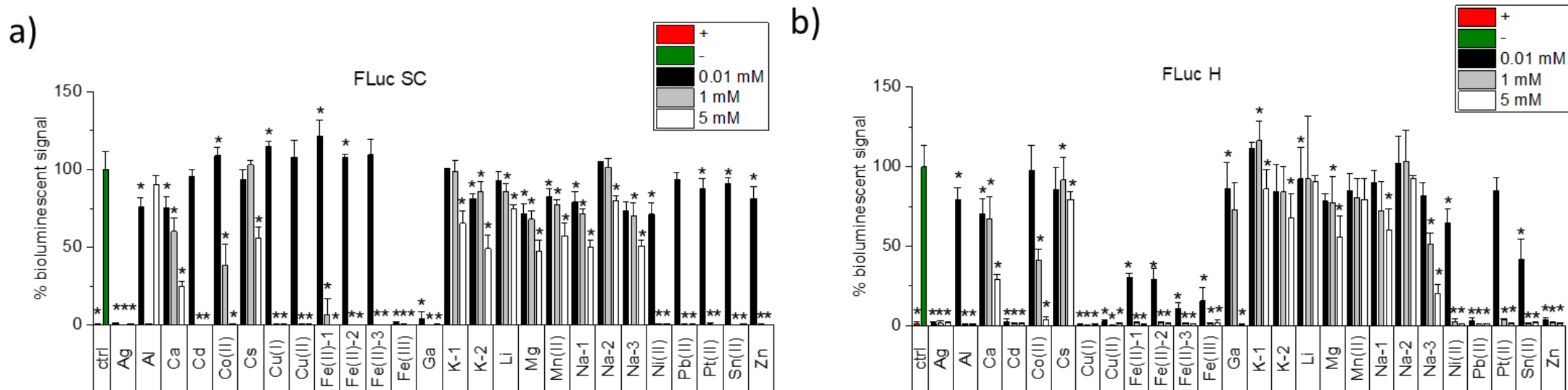


**Figure 4.9:** Normalized bioluminescent signal for Fluc in the presence of three different concentrations (0.01. mM, black; 1 mM, light grey; 5 mM, white) of metal ion salts.

**Table 4.10:** comparison of conditions for FLuc bioluminescence used for SC, H and in vitro assay conditions for 4.

| Enzyme | Substrate   | Final buffer conditions   |   |   |
|--------|-------------|---|---|---|
|        |             | Screening conditions (SC)   | HEPES conditions (H)                                      | Conditions used for 4 in vitro                                |
| FLuc   | D-luciferin | 0.5 mM Trizma base, 0.05 M glycine, 0.5 mM EDTA, 5 mM MgSO <sub>4</sub> , 10 μM ATP, pH 7.6 | 100 mM HEPES, 5 mM, MgSO <sub>4</sub> , 10 μM ATP, pH 7.5 | 50 mM TRIS-HCl, 10 mM MgCl <sub>2</sub> , 0.1 mM EDTA, pH 7.5 |

## Chapter 4: Results and Discussion

**Table 4.11: Top table:** Concentrations (mM) of each metal ion at their respective addition steps (x, x1, x2, x3, see **bottom table** for exact final concentration at addition step, in mM) in FLuc buffer conditions for SC or H. Concentration of metal ions before addition was 0 mM and after a final addition it was 5 mM for all metal ions and buffers. Note: Fe(II)-1 is FAS, Fe(II)-2 is FeCl<sub>2</sub>.

|                    | C [mM]    | Ag          | Cu(II)      | Fe(II)-1    | Fe(II)-2    | Fe(III)     | Zn          |
|--------------------|-----------|-------------|-------------|-------------|-------------|-------------|-------------|
| <b>FLuc<br/>SC</b> | <b>0</b>  | 6.95 ± 0.03 | 6.94 ± 0.10 | 6.94 ± 0.06 | 6.92 ± 0.07 | 6.88 ± 0.09 | 6.89 ± 0.08 |
|                    | <b>x</b>  | 6.92 ± 0.03 | 6.90 ± 0.06 | 6.93 ± 0.03 | 6.96 ± 0.05 | 6.64 ± 0.05 | 5.39 ± 0.06 |
|                    | <b>5</b>  | 5.97 ± 0.18 | 3.53 ± 0.07 | 5.75 ± 0.02 | 5.79 ± 0.11 | 3.29 ± 0.08 | 5.05 ± 0.05 |
| <b>H</b>           | <b>0</b>  | 7.32 ± 0.03 | 7.18 ± 0.03 | 7.19 ± 0.06 | 7.19 ± 0.04 | 7.23 ± 0.03 | 7.27 ± 0.02 |
|                    | <b>x1</b> | 7.27 ± 0.01 | 7.16 ± 0.01 | 7.16 ± 0.03 | 7.17 ± 0.02 | 7.19 ± 0.03 | 7.22 ± 0.02 |
|                    | <b>x2</b> | 7.26 ± 0.02 | 7.15 ± 0.01 | 7.16 ± 0.02 | 7.15 ± 0.01 | 7.15 ± 0.03 | 7.19 ± 0.02 |
|                    | <b>x3</b> | 7.25 ± 0.02 | 7.15 ± 0.01 | 7.14 ± 0.02 | -           | 7.02 ± 0.03 | 7.18 ± 0.02 |
|                    | <b>5</b>  | 7.06 ± 0.05 | 6.92 ± 0.04 | 7.13 ± 0.03 | 7.13 ± 0.04 | 6.86 ± 0.04 | 7.17 ± 0.01 |

| Buffer     | variable | Ag     | Cu(II) | Fe(II)-1 | Fe(II)-2 | Fe(III) | Zn    |
|------------|----------|--------|--------|----------|----------|---------|-------|
| SC<br>FLuc | x        | 0.0005 | 0.2    | 1        | 0.02     | 0.5     | 2.5   |
| HEPES      | x1       | 0.0001 | 0.0001 | 0.1      | 0.025    | 0.1     | 0.025 |
| HEPES      | x2       | 0.025  | 0.025  | 0.5      | 0.5      | 1       | 1     |
| HEPES      | x3       | 0.1    | 0.1    | 2.5      | n/a      | 2.5     | 2.5   |

#### 4.1.5. Summary of discussion

**Scheme 4.4** highlights the intricate network of reactions influencing the bioluminescent signal generated by probe **4** for Fe<sup>2+</sup> detection. While *in vitro* responses may be higher, five different transformations needed for signal generation (as it is the case for split-luciferin strategy) with their individual and different rate constants contribute to the final output, introducing complexity. The cellular environment, with its chemical and spatial heterogeneity, further complicates matters as various elements can potentially hinder any of these reactions, possibly by interacting with probe **4**, D-cysteine, or firefly luciferase. Furthermore, the low bioluminescent response observed both *in vitro* and in cell lysates suggests a limited sensitivity of the probe for Fe(II).

In conclusion, probe **4** exhibited a clear iron(II) response *in vitro* and was able to qualitatively detect even endogenous levels of iron(II) in cell lysates and live cells. However, a high variability of that response, caused by the multitude of factors and interferences, exacerbated by the split-luciferin design that multiplies the complexity of transformations leading to signal generation, all compromise its cellular applicability. These findings however, emphasize the critical importance of thoroughly validating split-luciferin probes *in vitro* with a robust bioluminescent response before cellular experimentation to ensure reliable readouts and what is critical, they provide a methodology and a set of assays to perform these validations.

## **4.2. NTR Responsive Bioluminogenic Substrates (Single Analyte)**

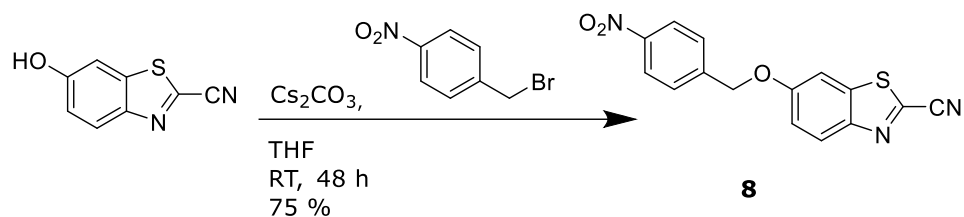
### **4.2.1. NTR-responsive OH-CBT for use in the split-luciferin strategy**

#### **4.2.1.1. Synthesis**

Following the same strategy as the one for Fe(II) probe compatible with split-luciferin system and therefore enabling multiplexing, an analogous version of the probe was prepared, but with NTR-responsive motif instead. In designing NTR-based probes, a common strategy used is to attach a 4-nitrobenzyl group on a phenolic OH group. Many examples of NTR-sensing fluorescent probes have used this strategy with success for imaging hypoxic cells<sup>77,78</sup>. The same synthetic strategy has also been applied by before<sup>41</sup> to design a bioluminescent probe for NTR, by attaching a 4-nitrobenzyl group at the 6'-oxygen of D-luciferin that is, however, not compatible with split luciferin-enabled multiplexing.

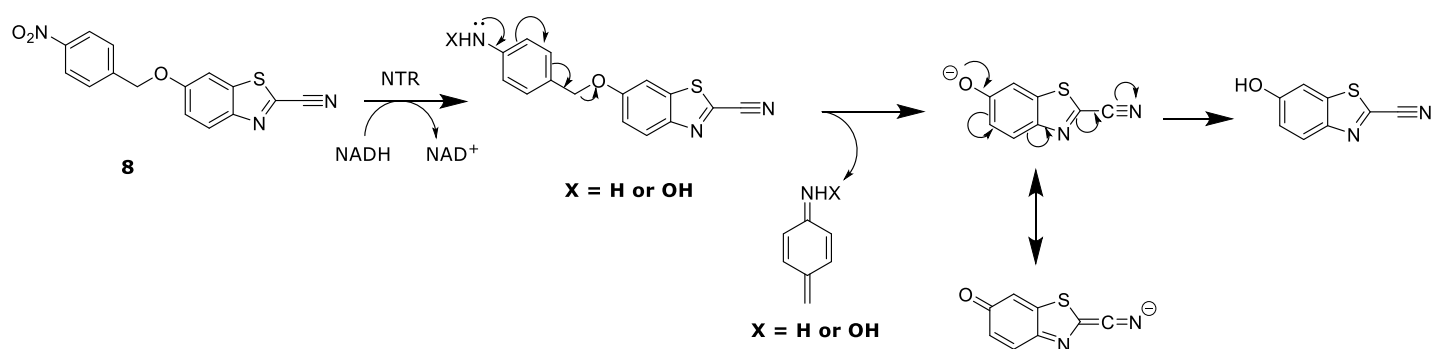
Our goal was to design a NTR-based OH-CBT probe, which could be used in a split-luciferin reaction to sense NTR. The synthesis of compound **8** was performed in a 1-step reaction by a slight modification of the previously reported procedure<sup>41</sup>, depicted in **scheme 4.12**. The starting material, 2-cyano-6-hydroxybenzothiazole (OH-CBT) was reacted with 4-nitrobenzyl bromide, with Cs<sub>2</sub>CO<sub>3</sub> as the base, to yield the final product **8**. A plausible explanation for the reaction is that a phenolate can be formed, due to the acidity of the 6'-OH group of OH-CBT, which then performs a nucleophilic attack on the benzylic carbon, giving the substituted product **8**. Compared to the original procedure, which used DMF as a solvent and was performed for 5 hours at 50 °C, it was opted to run this reaction for 48 h over weekend in THF at room temperature, which also gave a good yield of 75%. By substituting DMF with THF, both of them aprotic polar solvents, it allowed for easier purification and gave better yield compared to the original procedure (60%), when stirred at room temperature.

## Chapter 4: Results and Discussion



**Scheme 4.12:** synthesis of **8**.

The mechanism of a response of probe **8** to NTR is depicted in **scheme 4.13**: in short, NTR in hypoxic conditions would reduce the aromatic 4-nitro group to a 4-amino group, which then undergoes a spontaneous 1,6-elimination reaction to yield an iminoquinone methide and a free OH-CBT. An important note is that OH-CBT is a good leaving group in this mechanism, because the negative charge on the 6'-oxygen is stabilized by resonance due to the mesomeric withdrawing effect of the cyano group.



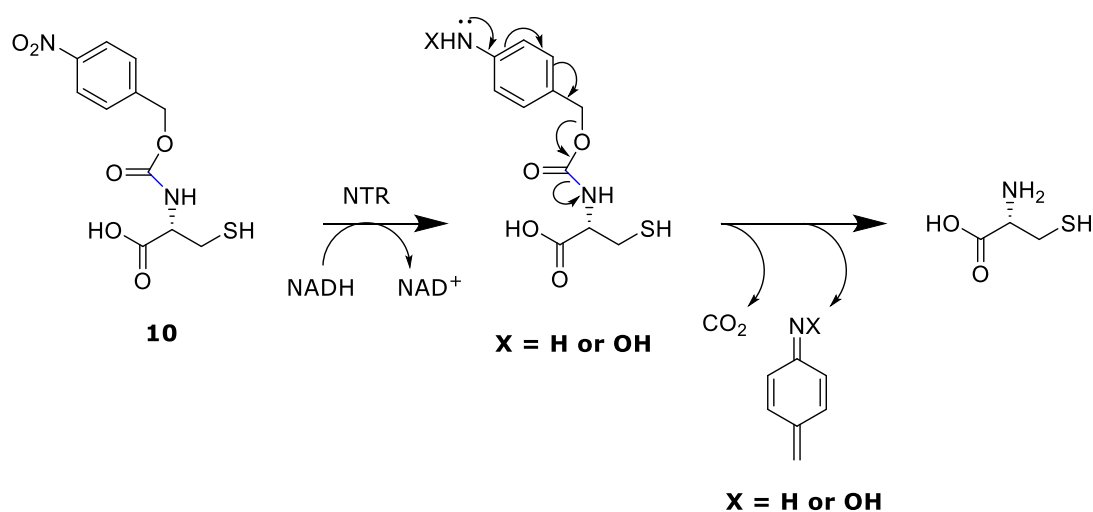
**Scheme 4.13:** Mechanism of action for **8** when reacting with NTR.

## 4.2.2. NTR-responsive D-Cys for use in the split-luciferin strategy

### 4.2.2.1. Synthesis

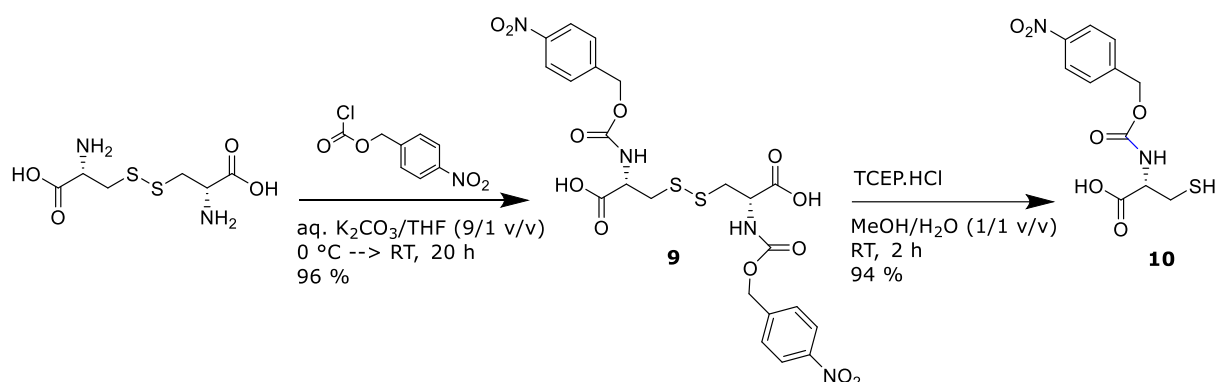
To enable a multiplexing with OH-CBT probes, we have prepared also an NTR-responsive version of the probe but based on D-cysteine (D-Cys) – a second half of the split luciferin strategy. As described in the introduction, by protecting one of the functional groups on D-Cys with analyte responsive moiety, the analyte presence is required to liberate D-Cys that can then spontaneously condense with the nitrile group of CBT (cyanobenzothiazole) in aqueous & biological conditions to yield D-luciferin, a bioluminogenic luciferase substrate.<sup>39</sup>

When designing a D-Cys-based probe for NTR sensing in the split-luciferin reaction, the strategy changes slightly, due to the presence of the NH<sub>2</sub> group on D-Cys instead of the OH group on CBT. Thus, 4-nitrobenzyl linker cannot be used here. Inspired by the design strategies used in several fluorescent probes for NTR, the aliphatic primary amine-like NH<sub>2</sub> group is decorated with a NTR-cleavable 4-nitrobenzyl carbamate functionality.<sup>79,80</sup> The proposed mechanism of the response of the desired probe **3** to NTR activity is shown in **scheme 4.14**: it is analogous to the mechanism described for compound **8**, but with the slight difference that CO<sub>2</sub> is also eliminated in the process that drives the reaction. A carbamate moiety that links the responsive group and D-cysteine is generally relatively stable in biological media and has been used in the past to create robust responsive probes for biological applications.<sup>35,38–40,81</sup>



**Scheme 4.14:** Mechanism of action for **3** when reacting with NTR.

Compound **10** can be synthesized according to **scheme 4.15** in two steps using D-cystine, oxidized derivative of D-Cys, as the starting material that masks the otherwise potentially highly nucleophilic and interfering SH group of D-Cys with a disulfide bond. At the last step of the synthesis, a mild reduction can be performed to transform the S-S bond into an SH group. Prior literature work<sup>82</sup> has shown that 4-nitrobenzyl chloroformate can be reacted with L-cystine in water to yield the corresponding carbamate, using sodium bicarbonate as the base.



**Scheme 4.15:** Synthesis of **10**.

This condition provided a good foundation for designing a synthetic route leading to **10**. However, due to the poor aqueous solubility of 4-nitrobenzyl chloroformate, a small amount of organic co-solvent, miscible with water, was to be added to promote the partial solubilization of the electrophile. It was seen that THF could solubilize the chloroformate separately, which can then be added dropwise to the ice cold aqueous solution of D-cystine and  $K_2CO_3$ . When this reaction was performed overnight in melting ice bath, TLC showed formation of **9**. The chloroformate will react preferentially with the amine, due to the higher nucleophilicity than the carboxylate, which is a weaker nucleophile in protic solvents. Even if the reaction happens at the COOH group, it will yield an anhydride, which will subsequently be hydrolyzed so no COOH-centred addition should be observed. The chosen method for purification was via liquid-liquid extraction. First, the aqueous layer was washed with EtOAc to remove unreacted starting chloroformate and other by-products. Because the initial reaction conditions used an excess of  $K_2CO_3$ , the product was expected to partition preferentially into the basic aqueous layer, in the form of a carboxylate salt.



Secondly, acidification with 3 M HCl<sub>(aq)</sub> of the aqueous layer should protonate the carboxylic acid and push compound **9** to the organic layer, while unreacted D-cystine will stay in the acidic aqueous layer as a hydrochloride salt. NMR and MS analysis showed that compound **9** was synthesized successfully and in a pure isolated form. To obtain the final working compound **10**, the disulfide bond needs to be reduced to a thiol group. Previously used protocol<sup>82</sup> utilized NaBH<sub>4</sub> in CHCl<sub>3</sub>/EtOH. However, for the synthesis of **10**, an alternative reducing reagent was used instead: TCEP.HCl. This water-soluble, mild reducing reagent is commonly applied in protein biochemistry for the reduction of disulfide bonds, and provides a safer alternative to NaBH<sub>4</sub>. To test this reagent out, **9** was dissolved in methanol, followed by the addition of an aqueous solution of TCEP.HCl, yielding a clear, colorless solution. The reaction occurs with TCEP getting oxidized into a phosphine oxide, while the disulfide bond gets reduced to a thiol to form two equivalents of **10**. Analysis of silica TLC showed that after 2 hours of stirring at room temperature, the reaction was completed, with very little traces of starting material. The idea for purification was to employ a liquid-liquid extraction to remove excess TCEP.HCl and the corresponding phosphine oxide by-product. After evaporating methanol, the reaction was diluted with DCM and water, and the organic layer was separated. By washing the aqueous layer three times with DCM, and after drying and evaporating the organic layer, compound **10** was made in a very good yield, confirmed by NMR and MS analysis. HPLC analysis showed a purity of 98%.

#### 4.2.2.2. Response to NTR

Following synthesis of **10**, *in vitro* studies were carried out for activity against NTR in a split-luciferin assay employing OH-CBT. When **10** was used without NTR, no response was observed (**figure 4.16**), but a luminescent response was observed when **10** was present with NTR and OH-CBT, indicating the formation of D-Cys that afterwards needed to react with OH-CBT to yield D-luciferin required for bioluminescent reaction with firefly luciferase and bioluminescent signal generation. The maximal signal for **10** + OH-CBT + NTR was however approximately 5 times lower than the positive control (using OH-CBT and D-Cys in the presence of 5 µg/mL NTR), which could be explained due to the necessity of the occurrence of multiple transformations to acquire a bioluminescent signal from **10**: conversion of the nitro group by NTR, followed by 1,6-elimination reaction, and then reacting with OH-CBT to form D-luciferin, and finally reacting with firefly luciferase to yield a bioluminescent signal (the two latter are the same for a control with D-Cys and OH-CBT). Overall, it was observed that **10** showed a response *in vitro* to NTR, owing to the difference between negative control (**10** + OH-CBT with no NTR) and the response of **10** with NTR and OH-CBT.

The above-mentioned sequence of transformations was partially confirmed also by HPLC kinetic studies (**figure 4.17**). These showed that when NTR is incubated with **10**, formation of an intermediate was observed after 1 hour (**figure 4.17B**), and complete consumption of the substrate is seen after 4 hours (**figure 4.17C**). Although the signal for D-Cys is not visible on HPLC, due to the usage of a UV-VIS detector at 254 nm wavelength, it can be reasonable hypothesized that **10** does form D-Cys, due to the complete disappearance of **10** on the chromatogram, along with the *in vitro* data shown in **figure 4.17**, in which a bioluminescent response can be seen. Thus, both *in vitro* and HPLC experiments show that **10** is usable in the split-luciferin approach for sensing NTR.

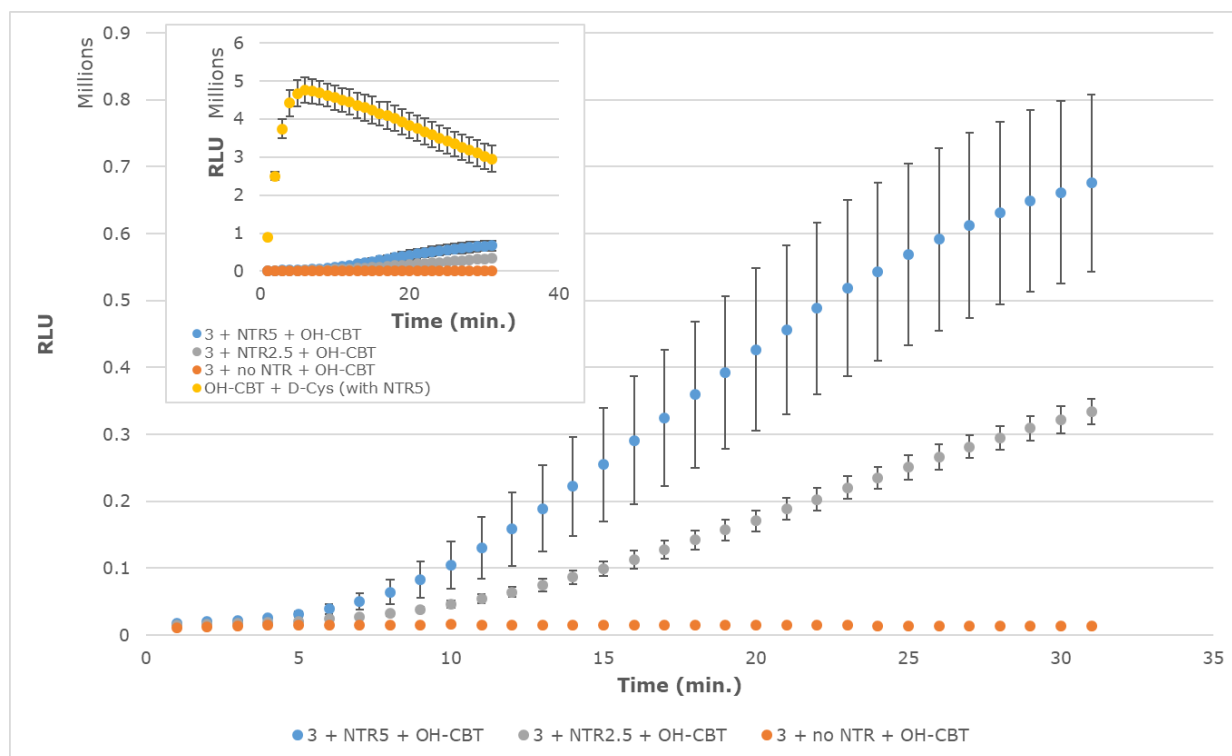


**Figure 4.16:** Average bioluminescent response (expressed in RLU) of positive control (OH-CBT + D-Cys in the presence of 5  $\mu\text{g/mL}$  NTR, yellow), **10** with OH-CBT in the presence of 5  $\mu\text{g/mL}$  NTR (blue), 2.5  $\mu\text{g/mL}$  NTR (gray) or no NTR as negative control (orange). For reactions containing NTR, the concentration of NADH was kept at 0.5 mM. Final concentrations were used for the following components: 20  $\mu\text{M}$  for **10**, 20  $\mu\text{M}$  OH-CBT, 2 mM ATP and 20  $\mu\text{g/mL}$  FLuc. The buffer used here is TRIS-HCl (50 mM, pH 7.5) containing 10 mM  $\text{MgCl}_2$  and 0.1 mM EDTA. All results are average of 3 values. Experiments were performed for 30 min. at 37  $^\circ\text{C}$ , with an integration time equal to 1 s and an interval time of 1 min. The order of addition was: **10**, buffer, FLuc, NTR, NADH, ATP, and finally OH-CBT.

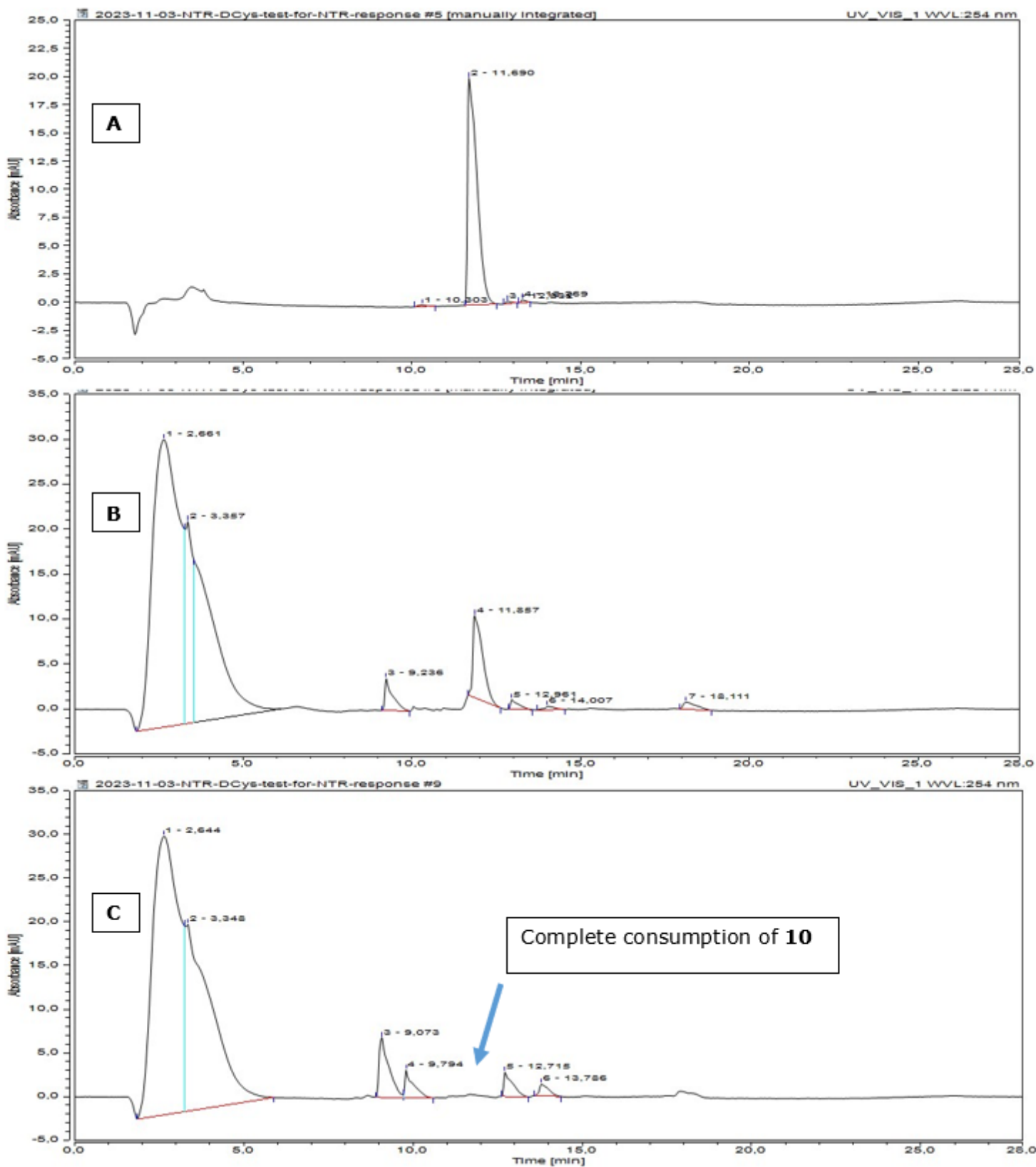


**Figure 4.17:** Chromatogram of

A) 0.2 mM **10**

B) 0.1 mM **10** + 5 µg/mL NTR + 0.5 mM NADH, 1 h, 35 °C

C) 0.1 mM **10** + 5 µg/mL NTR + 0.5 mM NADH, 4 h, 35 °C

### 4.2.3. Summary of split-luciferin-based probes for NTR detection

Chapter 4.2 described the design and synthesis of split-luciferin probes responsive to NTR, compounds **8** (based on OH-CBT) and **10** (based on D-Cys). Compound **8** was synthesized in one step, while **10** is a novel split-luciferin probe, synthesized in two steps. It was observed that **10** was able to detect NTR activity *in vitro* using a split-luciferin bioluminescence assay in conjunction with OH-CBT. Building on prior knowledge of analogous derivatives, a synthetic route was developed, and compound **10** was successfully prepared in two steps with an overall yield of 90%. Compared to other NTR-responsive compounds, such as compound **8**, the key difference is the usage of a carbamate moiety. Through *in vitro* assays and HPLC kinetic studies, it has been clearly demonstrated that **10** can serve as a viable tool for sensing NTR in a split-luciferin reaction *in vitro*. Relative to the negative control, compound **10** exhibited a 50-fold increase in bioluminescence signal at 5 µg/mL NTR concentration, highlighting its utility for NTR sensing. The response with 2.5 µg/mL NTR was observed to be a 25-fold increase compared to the negative control (linearly dependent on concentration). HPLC studies have also provided clear evidence that the signal of compound **10** decreases over time on the chromatogram, and after 4 hours, no traces of compound **10** were detectable on HPLC with a UV-VIS detector at 254 nm wavelength.

Compound **10** demonstrated a clear and specific response to NTR activity in the split-luciferin assay. This work introduces a new design strategy for NTR-responsive probes, utilizing a 4-nitrobenzyl carbamate functionality linked to the D-cysteine moiety. The resulting probe is novel and readily incorporated into a split-luciferin bioluminescence assay, and can be potentially used in combination with a caged OH-CBT derivative to enable dual-analyte sensing. The simple synthesis and NTR specificity make this probe an attractive tool for studying NTR activity in various biological contexts, with potential utility for multiparametric detection.

In summary, by developing a novel NTR-responsive split-luciferin probe and characterizing its performance in an *in vitro* split-luciferin bioluminescence assay, we have increased the toolbox of available probes for studying simultaneously redox activity and virtually any other analyte of interest.

### **4.3. NTR-responsive furimazine**

#### **4.3.1. Synthesis**

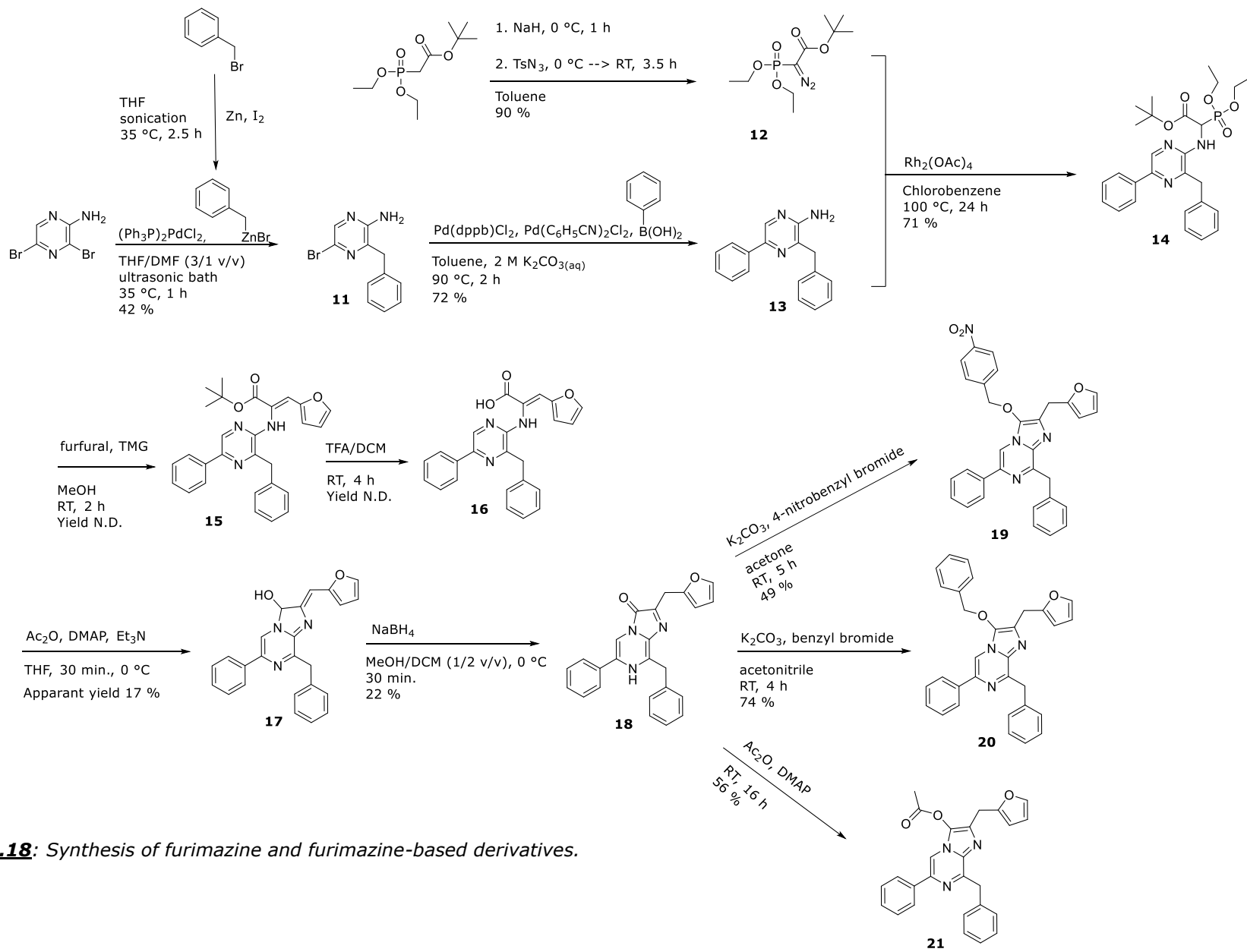
This work was performed in collaboration with dr. Grzegorz Framski and Adrian Rufli. My role was to perform synthesis and purifications, leading to furimazine. A synthetic route for the preparation of furimazine was inspired by prior work<sup>83</sup> done, shown in **scheme 4.18**. An important intermediate in this route is 2-amino-3-benzyl-5-phenylpyrazine (**13**). This can be synthesized by first performing a Negishi coupling<sup>84</sup>, utilizing 2-amino-3,5-dibromopyrazine, benzylzinc bromide and bis(triphenylphosphine)palladium dichloride as the catalyst. This enables the formation of a carbon-carbon bond to yield **13**. Considerable amounts of optimizations were required to get a decent yield, since the reaction did not occur using 1.5 equivalents of commercial benzylzinc bromide solution in THF. When using 3 equivalents of the same solution, a small amount reacted in very low yield (around 20%). This proved that the commercial reagent did not work as intended, possibly due to degradation. Thus, a decision was made to synthesize benzylzinc bromide separately, via the reaction of benzyl bromide (BnBr) and zinc metal, in the presence of iodine, to activate the zinc surface, using dry THF as the solvent. Many conditions were tested in the synthesis of compound **11** using in situ preparation of benzylzinc bromide. The variables tested, were among many:

- Sonication vs. regular stirring (time: 1 – 2 h)
- Equivalents of benzyl bromide: 1 eq., 1.5 eq. or 3 eq.

## Chapter 4: Results and Discussion

The most optimal condition was sonication for 1 h and using 1.5 eq., which gave a decent yield of mono-substituted product. An important note is that anhydrous conditions were maintained in all trials, and all reagents and glassware were dried prior to use. Compound **11** was successfully synthesized and matches the  $^1\text{H}$  NMR spectrum according to literature.<sup>84</sup> A Suzuki coupling<sup>85</sup> was then performed afterwards to yield **13**, which proceeded without any complication. In this reaction, it was not necessary to use strict anhydrous conditions. Afterwards, diazo compound **12** was made according to previously reported protocol for this type of transformation<sup>86</sup>. Since the referenced literature procedure used solid tosyl azide, which is dangerous to handle (danger on explosion), a commercially available solution in toluene was used instead. The crude product was then used in a rhodium-catalyzed C-N insertion reaction to yield **14**, and then subjected to a Horner-Wadsworth-Emmons-olefination to install the furan core. Following the work-up of **15**, it underwent tBu-ester cleavage in the presence of TFA to yield crude material **16**.

## Chapter 4: Results and Discussion

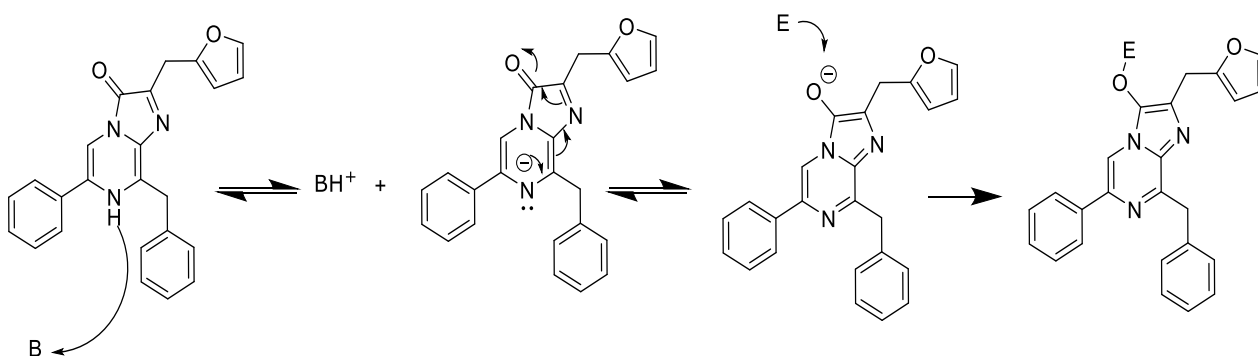


**Scheme 4.18:** Synthesis of furimazine and furimazine-based derivatives.



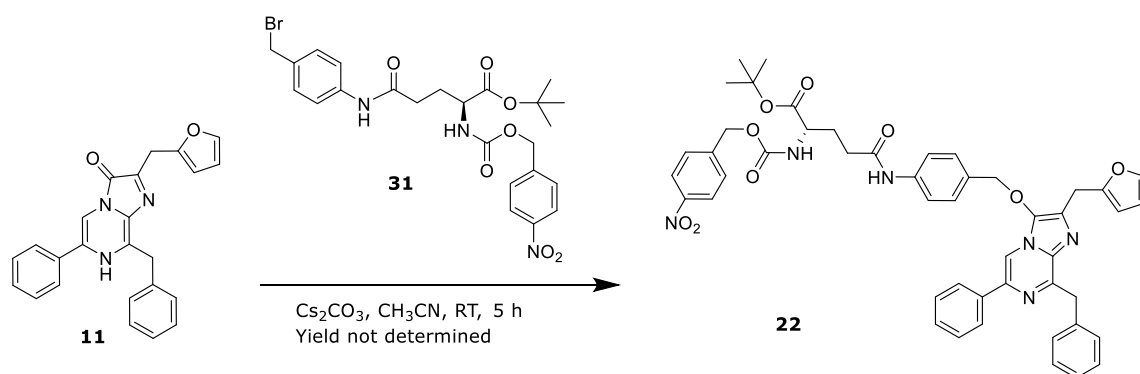
The overall yield for this route was 1% over 8 steps. The biggest yield losses come from the final two steps: the cyclization reaction to yield **17**, followed by the immediate reduction to yield final furimazine (**18**). An alternative synthetic approach to furimazine is reported<sup>87</sup>, which has an overall yield of 10% over 7 steps. To get sufficient amounts of furimazine to perform further experiments, it was necessary to use at least gram amounts of crude product **16**, which gave working amounts of furimazine (~ 100 mg) that could then be alkylated in basic conditions to yield furimazine derivatives. In this work, benzylfurimazine (**20**) was synthesized as a negative control for *in cellulo* studies in the future, and acetylfurimazine (**21**) was made as a more shelf-stable, easy to back-convert and a pharmacokinetically better version of furimazine, with higher bio-availability. These advantages allow acetylfurimazine to be used in bioluminescence imaging over a longer time period, according to previous report.<sup>17</sup>

Once the structure of furimazine was confirmed via NMR, it was then subjected to further alkylation, drawing inspiration from prior work<sup>88</sup> on similar derivatives, with benzyl bromide or 4-nitrobenzyl bromide to yield **20** or **19** respectively. The general reactivity of furimazine towards electrophiles is shown in **scheme 4.19**. The first step involves a keto-enol tautomerization in the presence of a base B, which will cause delocalization of electrons to yield an enolate, which can then react with an electrophile E, to generate O-substituted furimazine derivatives.



**Scheme 4.19:** Schematic overview of reactivity of furimazine towards electrophiles.

Finally, we also checked whether alkylation could occur using a sophisticated electrophile. Developing a method of furimazine alkylation that can withstand a wide range of functional groups and sophisticated pendent arms is a key to enable a swift access to a wide range of probes in the future. For this reaction, shown in **scheme 4.20**, compound **31** was chosen (see subchapter 4.4.2 for synthesis). Using CH<sub>3</sub>CN at room temperature and Cs<sub>2</sub>CO<sub>3</sub> as the base, furimazine was consumed (according to TLC) and formed compound **22**. This compound could prove to be a functional and useful dual-analyte probe based on furimazine for sensing NTR and GGT, after removal of the tBu-ester using TFA/DCM.



**Scheme 4.20:** Reaction of furimazine with electrophile **25**.

Proof of its identity and its formation is provided by HRMS and <sup>1</sup>H NMR of the crude mixture. The reaction described above was shown to form **22**, however it could not be purified successfully with silica gel chromatography. The mass spectrum (**figure 4.21**) shows the m/z peak at 851.3322, corresponding to the [M+H]<sup>+</sup> peak with 9 ppm difference (calc. [M+H]<sup>+</sup> for C<sub>48</sub>H<sub>46</sub>N<sub>6</sub>O<sub>9</sub>: 851.33987), proving that the product was formed with high likelihood.

Additionally, <sup>1</sup>H NMR analysis (**figure 4.22**) showed peaks at 1.43, 2.01, 2.26 and 2.42 ppm pointing to the presence of aliphatic protons of the glutamic acid moiety. The aromatic region starting from 7.00 – 8.10 ppm are also showing extra aromatic hydrogens, thus demonstrating the substitution reaction being successful. While impurities are also present in the aromatic region, we can conclude with a degree of confidence that the product was formed based on HRMS and <sup>1</sup>H NMR analysis. This in turn provides the scientific community with the evidence of the possibility of decorating furimazine scaffold with even highly elaborate structures in a single step.

## Chapter 4: Results and Discussion

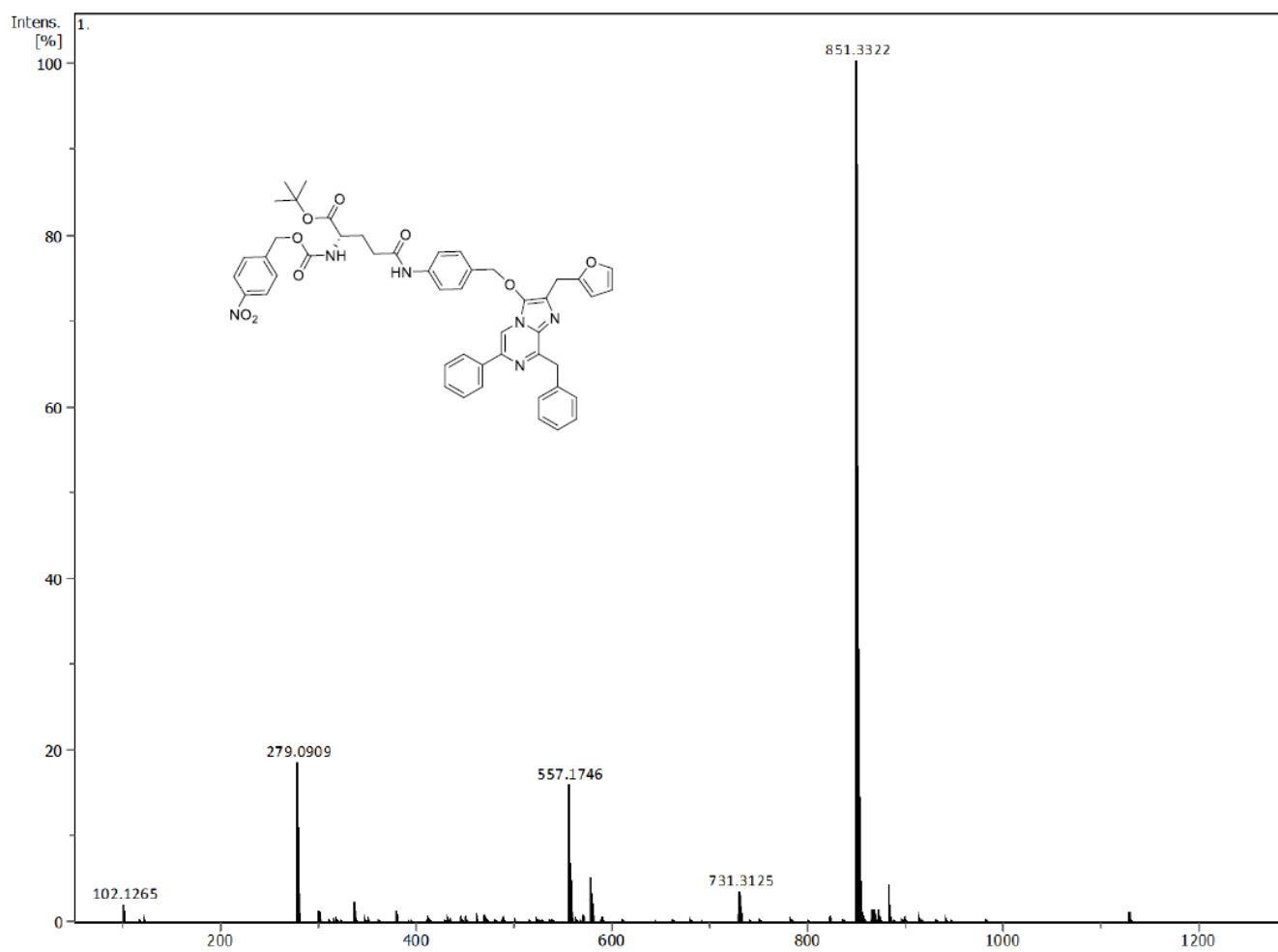


**Figure 4.21:** Mass spectrum of compound 22.

Chapter 4: Results and Discussion

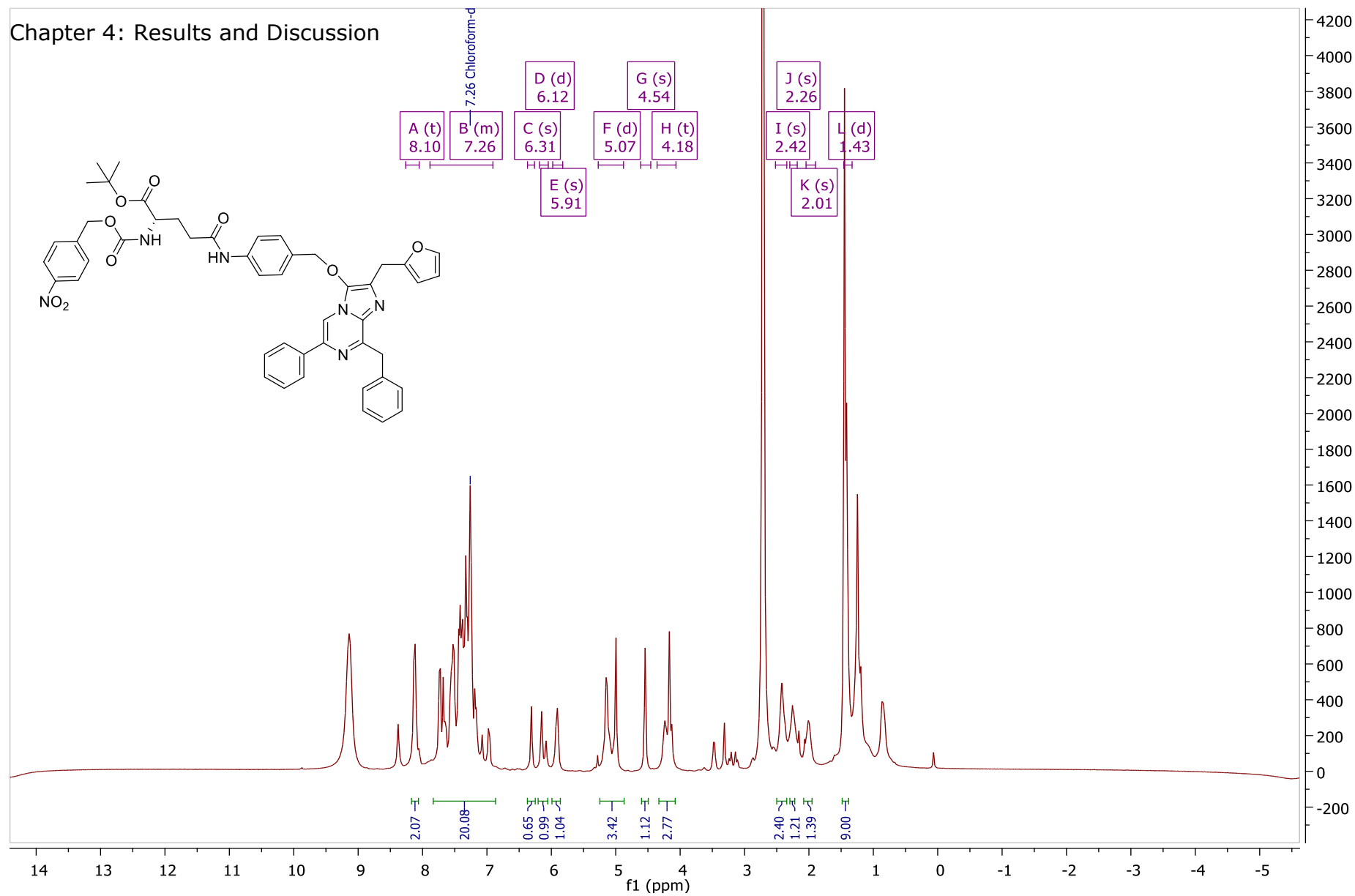


**Figure 4.22:** NMR of compound 22.

### 4.3.2. Response to NTR

The mechanism of response is analogous as previously described for **8**, wherein furimazine is released after reaction of **19** with NTR, and then reacting with NanoLuc® to yield a bioluminescent response. An initial increase in bioluminescent signal, which is directly correlatable with the rate of reaction, suggests that indeed in the first part of the response there is a gradual accumulation of the furimazine, as seen in **figure 4.23** (so initially NTR-dependent cleavage is faster than luciferase-furimazine reaction). At approximately 10 min. though, the rate increases its maximum followed by a gradual decrease that can be explained by a decrease in the concentration of free furimazine available for a bioluminogenic reaction. In other words at that point, the initial levels of the probe are depleted in time leading to a drop of the rate of conversion of the probe to furimazine. This leads to a flash-type luminescence a largely seen also for other probes for NTR described in this thesis but this fact is dependent on the initial relative concentrations of the probe, luciferase and NTR enzymes.

The work described above was performed in years 2020-2022 and as such it was a first instance of the responsive furimazine-based probe. However, as of 2024, **19** was published in February 2024 by another group.<sup>89</sup> Importantly though, all spectroscopic characterizations of the molecule **19** published by this other team correlated with our data, proving that the same compound has been synthesized.

## Chapter 4: Results and Discussion

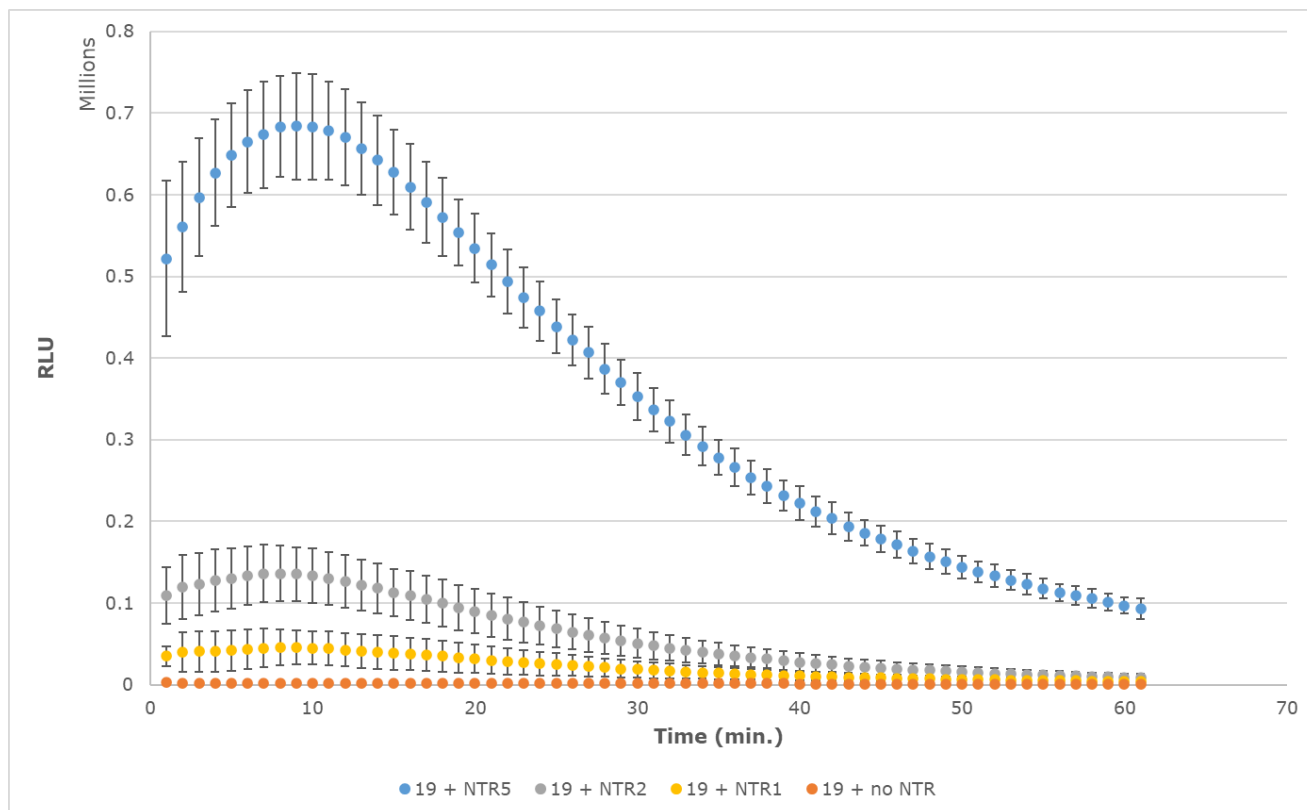


**Figure 4.23:** Average bioluminescent response (expressed in RLU) of **19** in the presence of 5  $\mu\text{g}/\text{mL}$  NTR (blue), 2  $\mu\text{g}/\text{mL}$  NTR (gray), 1  $\mu\text{g}/\text{mL}$  NTR (yellow) or no NTR (orange) as negative control. For reactions containing NTR, the concentration of NADH was kept at 0.5 mM. Final concentrations were used for the following components: 20  $\mu\text{M}$  **19** and 0.4  $\mu\text{g}/\text{mL}$  NanoLuc®. The buffer used here is PBS pH 7.4. Results are average of 4 values. Experiments were performed for 60 min. at 37 °C, with an integration time equal to 1 second and an interval time of 1 min. Order of addition: **19**, buffer, NLuc, NADH, NTR.

### 4.3.3. Summary of NTR-responsive furimazine

Furimazine was synthesized according to a modified procedure in 9 steps, with a very low overall yield (1%). This was then reacted successfully to yield compound **19**, the first furimazine-based probe for NTR. Two derivatives **20** and **21** were synthesized as a negative control and as a lipophilic version of furimazine with improved pharmacokinetics respectively. Compound **19** was then tested *in vitro* successfully and showed a concentration-dependent response to the presence of NTR concentrations, that was also significantly different from the background. In this thesis it was shown that in fact even only 1 µg/mL concentration of NTR could be effectively and robustly detected *in vitro* with the use of the probe.

Compared to other literature designs for NTR-responsive probes, **19** has the advantage of generating a very high luminescence. The lack of a need of additional reagents, like in the case of firefly luciferase systems, makes this probe also an interesting alternative. The particular advantage comes from the fact that unlike in the case of firefly luciferase probes, NanoLuc® furimazine-based probe **19** is ATP independent and so it is compatible with the applications where ATP is unknown/low. One of such applications is detection of hypoxia in cancer – the very state previously reported D-luciferin-based probes were designed to sense but have limited practical use due to the fact that in hypoxic regions of the tumor ATP is low (due to a lot of cells undergoing near-apoptotic death) and so significantly altering the bioluminescent signal for D-luciferin-based probes. While the synthesis of furimazine-based derivatives is more complex than that of traditional D-luciferin-based probes, owing to the multiple steps required to produce furimazine, the advantages and versatility that NanoLuc®-based probes offer compensate for these drawbacks.

## **4.4. Dual-analyte NTR-GGT probes**

### **4.4.1. Dual-analyte NTR-GGT based on D-aminoluciferin**

#### **4.4.1.1. Synthesis**

Previous chapters have reported on the single-analyte probes that can be multiplexed using split-luciferin strategy for multianalyte detection as well as the first at the time furimazine-based responsive probe based on NTR. In the final work of this thesis, we have aimed at synthesizing and validating also another design of dual-analyte bioluminescent detection but in a single molecule.

To design such dual-analyte probes using a single D-aminoluciferin molecule as the signaling motif, two enzyme-cleavable, analyte-targeting moieties are required that are attached to two functional groups on the bioluminophore, in this case to the 6'-NH<sub>2</sub> and 4-COOH (refer to **scheme 2.2** for numbering). Only one probe has been described in the literature using a dual-analyte design using D-aminoluciferin, described in chapter 2.5. In there, the analyte-targeting moieties are placed on two different sides of the molecule (two different functional groups).

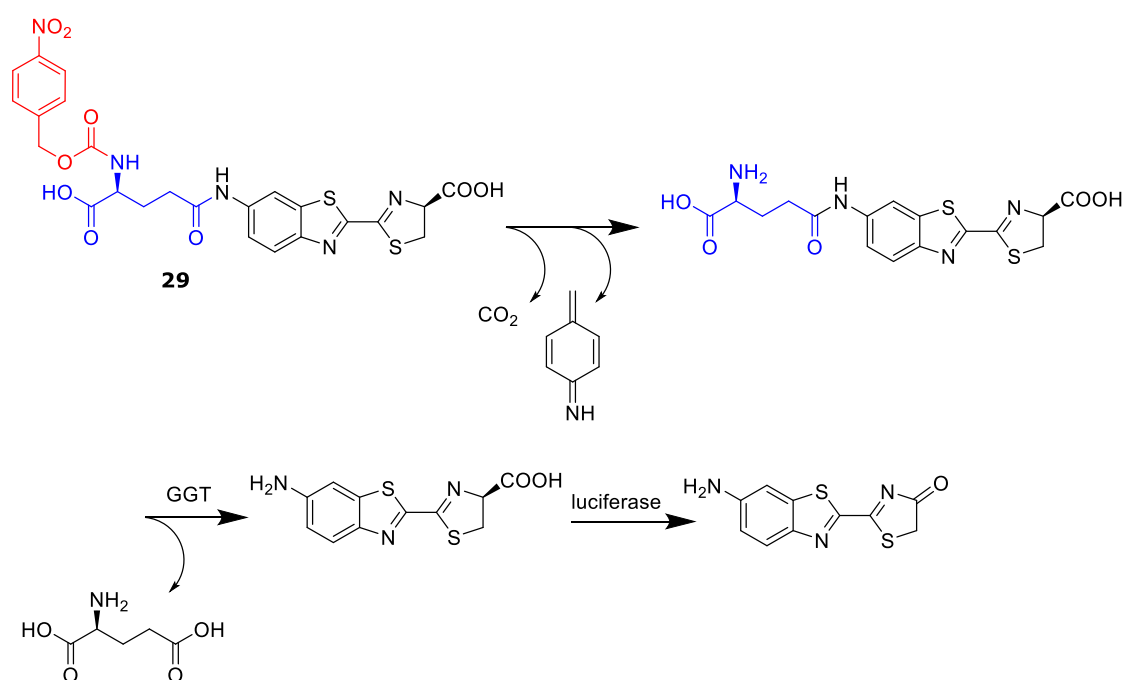
A strategy that was executed successfully here, and not described prior in the literature, was attaching one analyte-targeting moiety to the 6'-NH<sub>2</sub> of D-aminoluciferin, and then attaching the second analyte-targeting moiety to a functional group present on the first analyte-targeting moiety. However, to use this strategy successfully, this heavily depends on the functional groups that are present on the first analyte-targeting moiety which allow it to be used as an "anchor". This has been inspired by a similar approach in the development of fluorescently-responsive probes for two enzymatic activities published before<sup>35</sup>.

The two enzymes targeted in our design were NTR, that we have targeted in the previous chapters, and gamma-glutamyltransferase. Both NTR and GGT are implicated and elevated in many types of cancers. Notably, NTR is predominantly associated with hypoxic tumors, which are linked to tumorigenesis, malignant progression, tumor metastasis, and resistance to therapies.<sup>41,65,78</sup> Conversely, high levels of GGT is primarily related to the occurrence and progression of cancer.<sup>63,67,68,90</sup> In the design of NTR-GGT aminoluciferin (compound **29**), a gamma glutamyl moiety was attached to the 6'-NH<sub>2</sub> of D-aminoluciferin. Then, the alfa-amine on the gamma-glutamoyl moiety was transformed into a 4-nitrobenzyl



carbamate, which makes it responsive to NTR, in a similar fashion described for **10**.

A literature study done on the GGT enzyme showed a structure-activity relation of the  $\alpha$ -NH<sub>2</sub> and the  $\alpha$ -COOH groups in a gamma-glutamoyl peptide model.<sup>91</sup> They showed that the  $\alpha$ -amine and the  $\alpha$ -COOH were important for its recognition inside the active site of GGT. Introducing a small methyl substituent on the  $\alpha$ -COOH moiety led to a 50% decrease in activity, while a substituent on the  $\alpha$ -amine group completely abolished the activity. This described observation gave us a plausible hypothesis that **29** could also function as such: by capping the  $\alpha$ -amine with an analyte-responsive group to NTR, it could prevent reaction with GGT and allow it to react with NTR first. Thus, after a sequential reaction with first NTR, followed by GGT, a bioluminescent signal could be obtained. A proposed mechanism of reaction is shown in **scheme 4.24**.



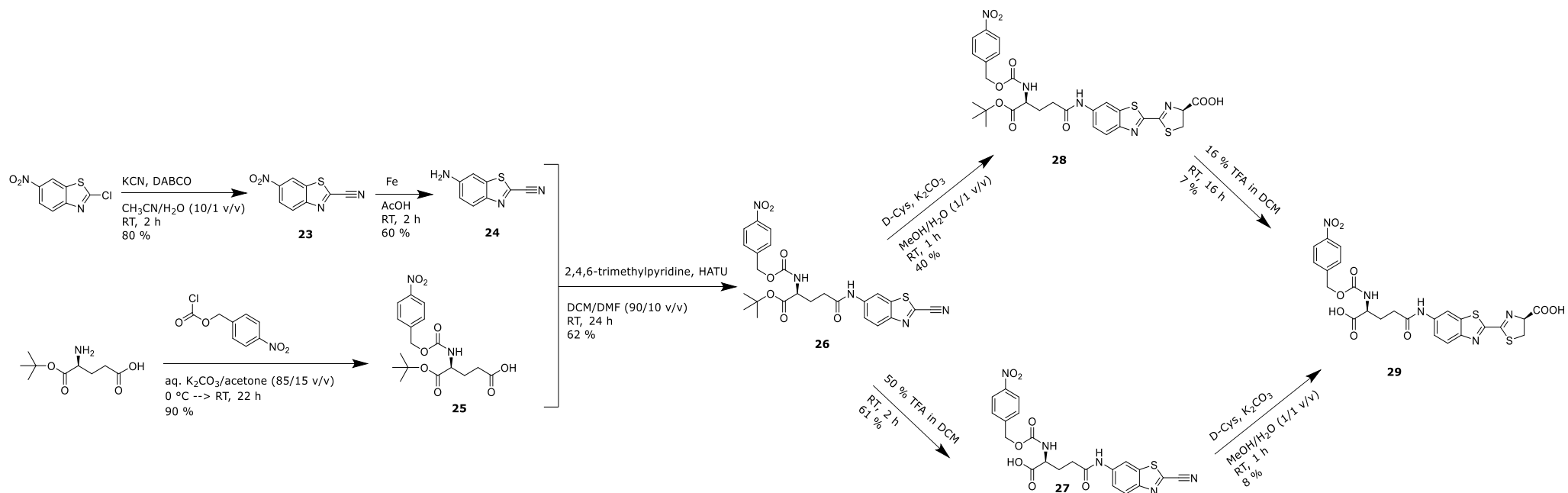
**Scheme 4.24:** Proposed mechanism of action for probe **29**. Colored in red is the analyte-responsive group for NTR and in blue for GGT.

The synthesis, depicted in **scheme 4.25** starts out with the reaction of H-Glu-OtBu with 4-nitrobenzylchloroformate in aqueous  $K_2CO_3$ /acetone to yield **25**. This reaction was inspired by prior work done to synthesize **9**. The initial conditions for synthesizing **25** involved using THF as a co-solvent, which gave 79% yield. In an effort to increase the yield, acetone was also tried as a co-solvent, which showed a better result with 90% yield. The proportion of water/acetone was also changed slightly, from 90/10 v/v to 85/15 v/v. Afterwards, the synthesis of 2-cyano-6-aminobenzothiazole (**24**) was performed. There are two methods<sup>92,93</sup> described in literature that were tried out in this work.

In the first route<sup>92</sup>, the initial step involves the reduction of 2-chloro-6-nitrobenzothiazole using refluxing ethanol, hydrochloric acid, and tin(II) chloride, resulting in the formation of 2-chloro-6-aminobenzothiazole with a 54% yield, which is comparable to the reported literature value (58%). Subsequently, a cyanation reaction is carried out using potassium cyanide in DMSO at 130 °C, yielding the final product **24** with a 33% yield, a slightly better yield compared to the referenced procedure (25%). However, this synthetic route has several drawbacks, including a poor overall yield, the use of an expensive metal for the reduction step, and the requirement of DMSO as a solvent, which can complicate the purification process. Furthermore, the toxicity of potassium cyanide and the ability of DMSO to enhance the dermal absorption of salts necessitate extreme caution when handling this reaction. The combination of these unfavourable factors has resulted in the utilization of the second approach.

The second route for synthesizing **24** (depicted in **scheme 4.25**), that I have also attempted, starts in reverse, by first reacting the same starting material used in the first route, namely 2-chloro-6-nitrobenzothiazole, with KCN and catalytic amounts of DABCO in  $CH_3CN/H_2O$  90/10 v/v. A proposed mechanism is that DABCO acts as a nucleophilic catalyst by displacing the 2-chloro group to form a transition state, which allows the nucleophilic cyanide anion to attack to form **23**. The authors have also seen that when reacting DABCO with 2-chloro-6-aminobenzothiazole, no reaction was observed. They propose that the electron deficient system, created by the 6-nitro group, is necessary for reaction to take place.

## Chapter 4: Results and Discussion



**Scheme 4.25:** Synthesis of a dual-analyte probe for NTR and GGT based on aminoluciferin scaffold.

A TLC analysis showed that all starting material was consumed in 2 hours, while the original reported procedure<sup>93</sup> stirred for 24 hours at room temperature. The yield of the shortened reaction was 80%, almost similar to the yield in the referenced procedure. Afterwards, a reduction was carried out with iron powder in acetic acid. The great advantage of this method is that iron powder is very cheap. This reaction was also shortened to two hours according to TLC analysis, compared to overnight stirring in the original procedure<sup>93</sup>. Compound **24** was obtained in 60% yield, giving an overall yield of 48% over two steps, much higher than the 18% overall yield (over two steps) obtained with the first method.

Following the synthesis of **24**, it was then subjected to an amide coupling. The first coupling agent tried was isobutyl chloroformate (IBCF) with DIPEA as the base and dry THF as the solvent, gave **26** in a rather poor yield (~20%). A possible reason for this low yield could be that the reaction was done with non-anhydrous DIPEA, and that the commercial anhydrous THF over time may potentially have become slightly wet with atmospheric water. Also, glass ware and solids were not dried maximally, which could explain the low yield.

In the second attempt, it was decided to try HATU as the coupling agent, with DCM/DMF 90/10 v/v as the solvent system, due to the bad solubility of **24** in DCM, and DIPEA as the base. HATU generates active esters *in situ* derived from 1-hydroxy-7-azabenzotriazole (HOAt). Compared to other coupling agents, HATU is shown to be a very good coupling agent with high coupling efficiencies and fast reaction rates. A yield of ~40% was obtained in this amide coupling reaction. In an attempt to improve the yield, the base was changed from DIPEA to 2,4,6-trimethylpyridine. This increased the yield to 60%, but it is not clearly understood why this increase happened, since the pKa of DIPEA is higher than 2,4,6-trimethylpyridine (11 vs. 7.4).

After obtaining compound **26**, two possible methods were possible for further continuation:

- 1) Deprotection in TFA/DCM (1/1 v/v) to remove the tert-butyl ester to yield **27**, followed by a condensation reaction with D-Cys to yield final probe **29**.
- 2) Synthesize the D-aminoluciferin core by reacting first with D-Cys to yield **28**, followed by a deprotection reaction with TFA/DCM (1/6 v/v) to yield **29**.

In the first method, a yield of 61% was obtained in the deprotection reaction with TFA (see **figure 4.26**). The disappearance of the tBu peak at 1.47 ppm is a strong indication towards deprotection. Afterwards, reaction with D-Cys in methanol/water, with  $K_2CO_3$  as the base, gave **29** in 8% yield after purification with TLC. NMR and MS showed that compound **29** was synthesized successfully. However, this reaction was not reproducible in our hands, and therefore it was decided to use the second method. In here, the reaction order is reversed, starting first with the condensation reaction with D-Cys to yield the functional D-aminoluciferin core and then TFA-mediated tBu ester deprotection. The volume percentage of TFA is reduced to 16% prevent any possible side reactions. When synthesizing D-(amino)luciferin-based probes, deprotection reactions usually occur last, as is seen in the following examples.<sup>90,94</sup> In this case, I was able to obtain **29** with 7% yield, purified via preparative silica TLC, a similar yield as in the first method.

Chapter 4: Results and Discussion

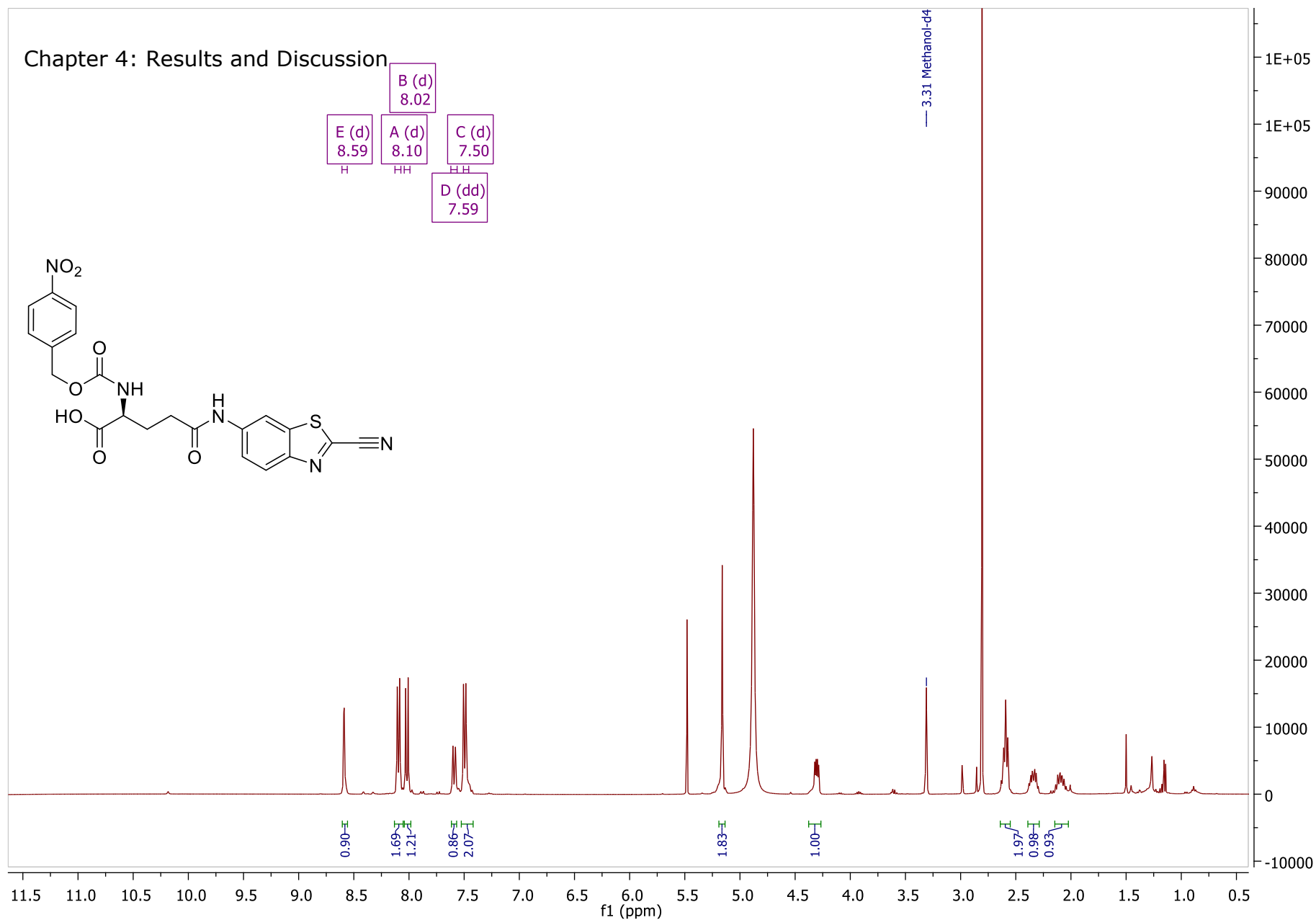
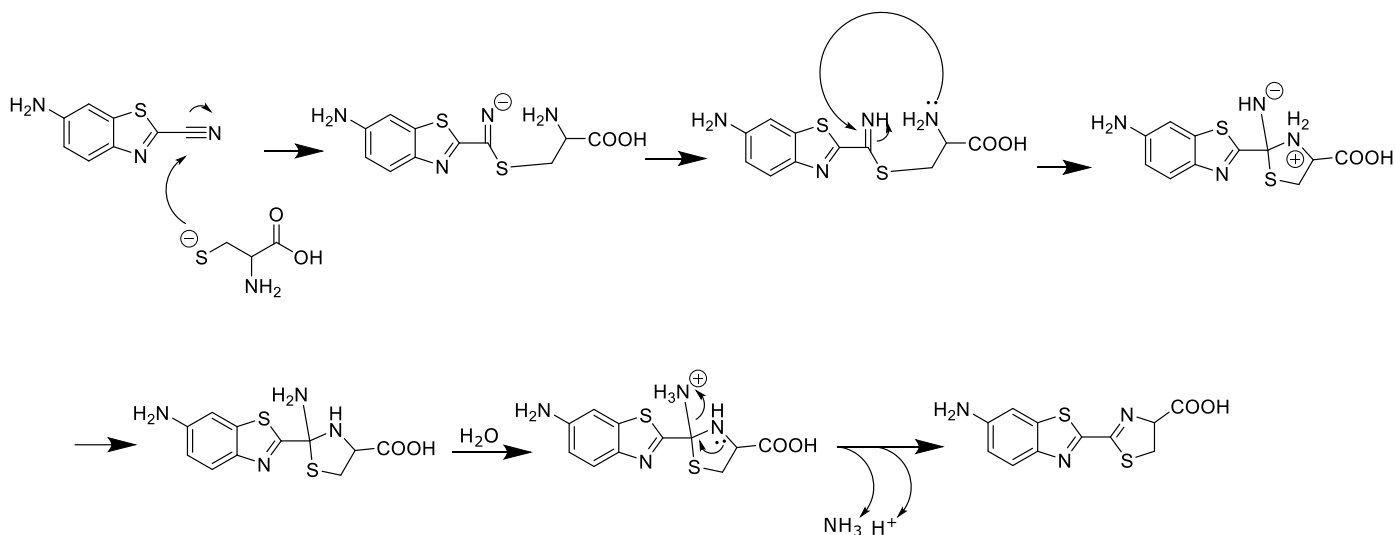


**Figure 4.26:** NMR of deprotected 27.

## Chapter 4: Results and Discussion

The mechanism for the condensation reaction of Cys and 2-cyano-6-aminobenzothiazole is shown in **scheme 4.27**.<sup>95</sup> A thiolate will attack the cyano group, which is then followed by attack of the alpha-amine of Cys on the imine carbon. After ring closure and subsequent elimination of  $\text{NH}_3(\text{g})$ , the thiazoline core is synthesized, yielding aminoluciferin. A previous study has demonstrated that certain aryl cyanides can undergo similar reactions with cysteine, as well as other 1,2-aminothiols.<sup>96</sup>



**Scheme 4.27:** Reaction mechanism showcasing the formation of the thiazoline ring, using Cys and **24**.

A COSY analysis was performed on **29** (**figure 4.28**). This analysis tells us which proton is coupled to another neighbouring proton. In a COSY analysis, observations of couplings are seen mainly between hydrogens on carbons across 3 bonds, and up to 4 bonds. In **figure 4.28**, three regions of interest are encircled in different colors: red, green and black. In the red region, we can observe a coupling between the benzylic hydrogens and the meta-hydrogens of the 4-nitrobenzylcarbamate system. The green region shows couplings between the alfa-hydrogen, the beta hydrogen and the gamma hydrogen in the glutamic acid moiety. Finally, the black region shows clear indication of a coupling between the hydrogens present in the thiazoline ring.



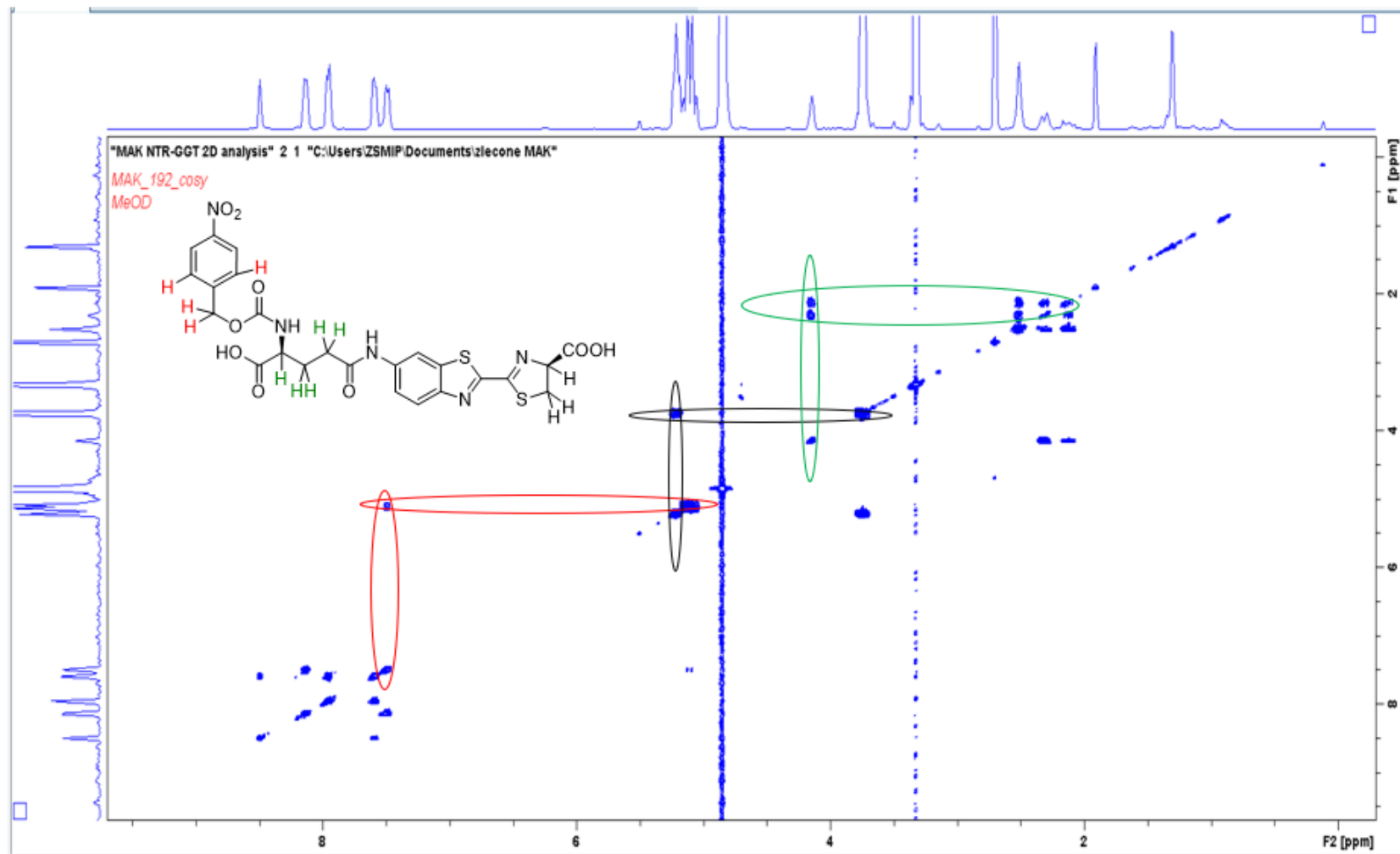


**Figure 4.28:** COSY spectrum of **29**. Certain hydrogens of **29** are colored in a specific way that correlates to a specific coupling seen on the COSY spectrum, which is encircled in the same color.

#### 4.4.1.2. Response to NTR and GGT

Initial *in vitro* studies have shown that **23** shows a bioluminescent response only in the presence of both enzymes, but no response when none or only one of either enzyme is present (**figure 4.29**). Thus, **23** has been shown to work as a functional dual-analyte probe for NTR and GGT as a true AND gate by the definitions of molecular logic gates.

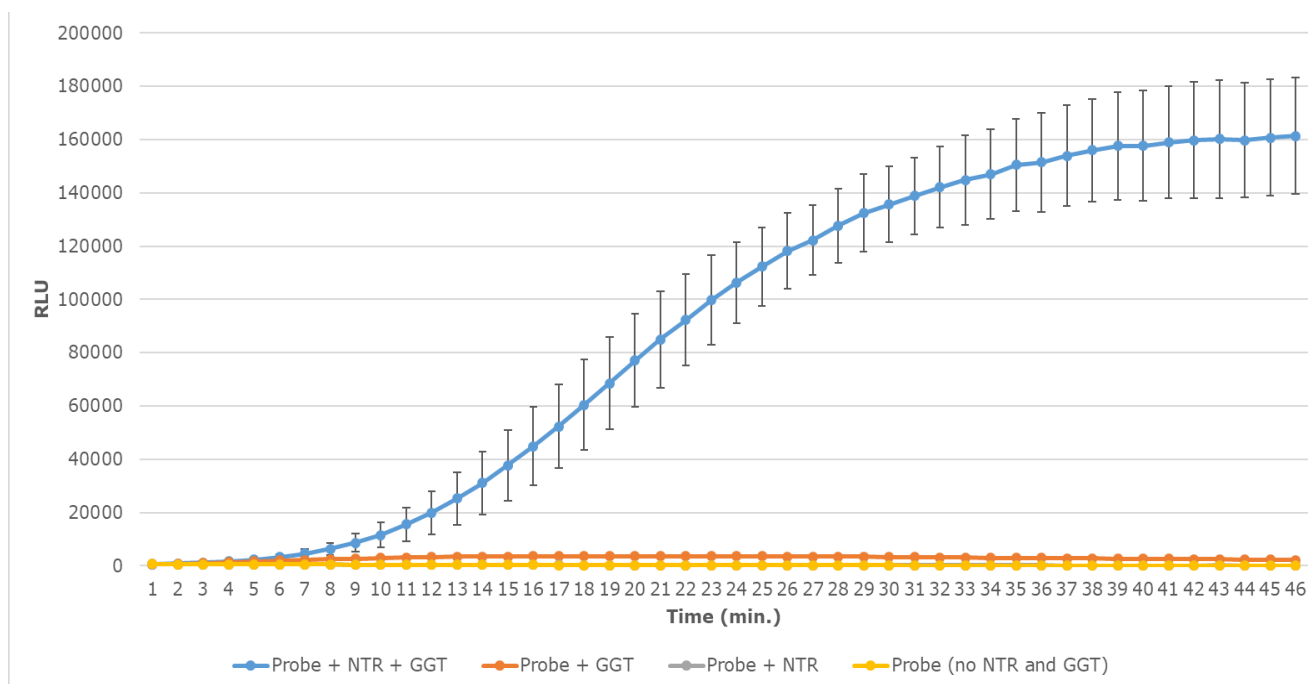


**Figure 4.29:** Average bioluminescent response (expressed in RLU) of **29** in the presence of 5  $\mu\text{g/mL}$  and 50 U/L GGT (blue), 50 U/L GGT only (orange), 5  $\mu\text{g/mL}$  NTR (gray) or no NTR and GGT (yellow). For reactions containing NTR, the concentration of NADH was kept at 0.5 mM. Final concentrations were used for the following components: 20  $\mu\text{M}$  **29**, 20  $\mu\text{g/mL}$  FLuc, 50 U/L GGT, 5  $\mu\text{g/mL}$  NTR and 2 mM ATP. The buffer used here is TRIS-HCl (50 mM, pH 7.5) containing 10 mM  $\text{MgCl}_2$  and 0.1 mM EDTA. Results are average of 4 values. Experiments were performed for 45 min. at 37  $^\circ\text{C}$ , with an integration time equal to 1 second and an interval time of 1 min. Order of addition is: **29**, buffer, FLuc, GGT, NADH, ATP and NTR.

## Chapter 4: Results and Discussion

Afterwards, it was also demonstrated how changes in the concentration of each of the analytes influence the signal generation (**figure 4.30**). In particular, our experimental conditions (details in the legend of the figure) doubling the concentration of NTR with keeping GGT constant indeed lead approximately to doubling the rate of reaction and the signal intensity (light blue vs grey, orange vs yellow). On the other hand, doubling the concentration of the GGT lead to a less pronounced increase in rate and the signal intensity (light blue vs orange and grey vs. yellow, **figure 4.30**). This may suggest that in these experimental conditions (at these concentrations of substrate, ATP and luciferase), NTR cleavage, which is the first in the sequence of responses, might be the rate-determining step in the whole chain of reaction.

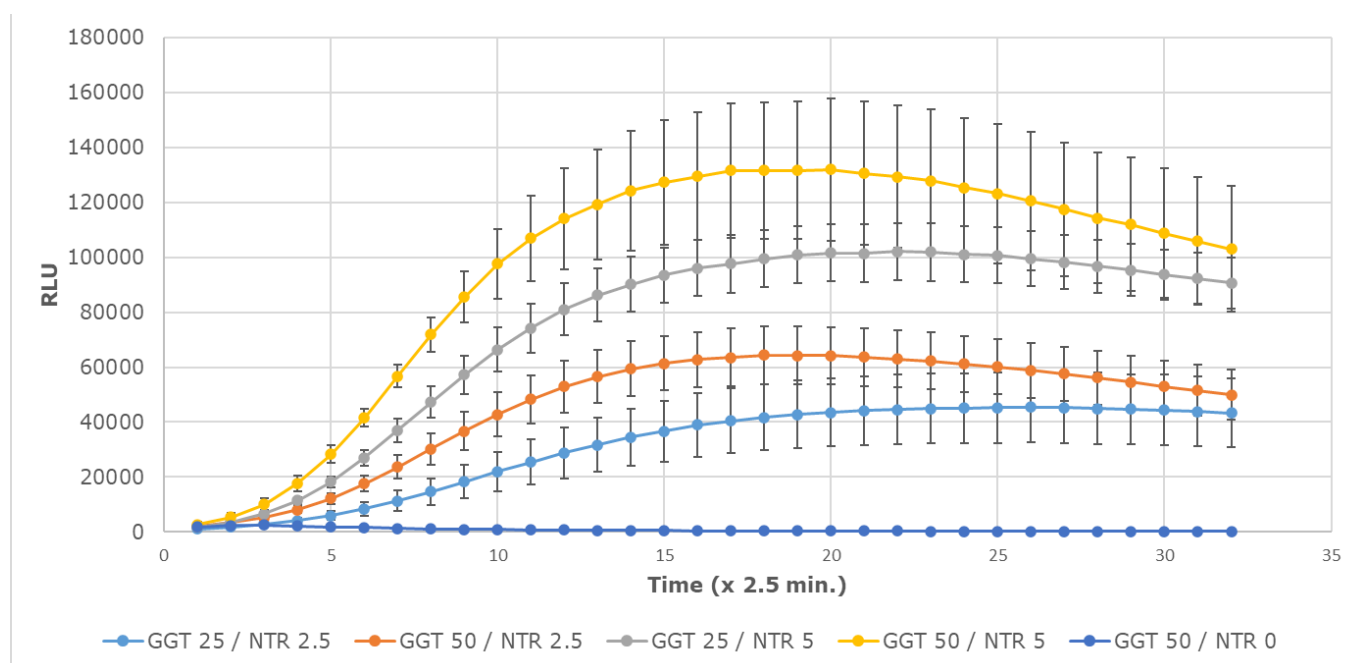


**Figure 4.30:** Average bioluminescent response (expressed in RLU) of **29**. For reactions containing NTR, the concentration of NADH was kept at 0.5 mM. Final concentrations were used for the following components: 20  $\mu\text{M}$  **29**, 20  $\mu\text{g/mL}$  FLuc and 2 mM ATP. The buffer used here is TRIS-HCl (50 mM, pH 7.5) containing 10 mM  $\text{MgCl}_2$  and 0.1 mM EDTA. Results are average of 4 values. Experiments were performed for 80 min. at 37  $^\circ\text{C}$ , with an integration time equal to 1 second and an interval time of 2.5 min. Order of addition is: **29**, buffer, FLuc, GGT, NADH, ATP and NTR.

The following enzyme concentrations were tested:

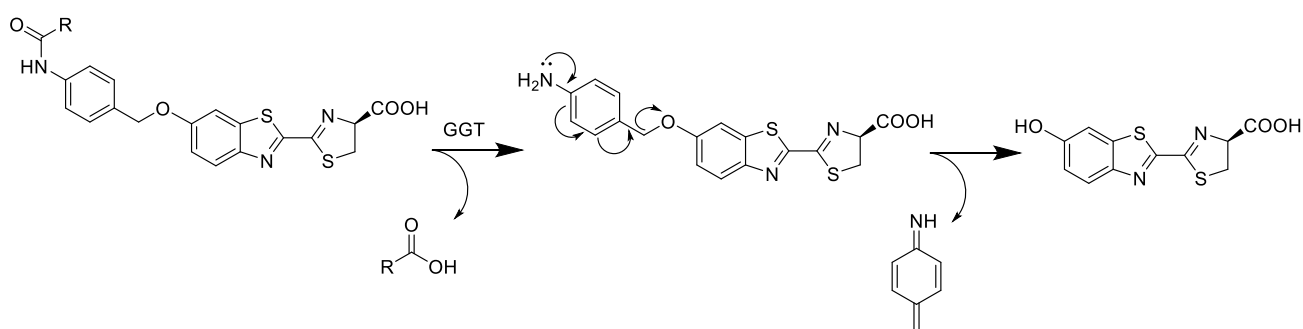
- 25 U/L GGT and 2.5  $\mu\text{g/mL}$  NTR (light blue)
- 25 U/L GGT and 5  $\mu\text{g/mL}$  NTR (grey)
- 50 U/L GGT and 2.5  $\mu\text{g/mL}$  NTR (orange)
- 50 U/L GGT and 5  $\mu\text{g/mL}$  NTR (yellow)
- 50 U/L GGT and no NTR as negative control (dark blue)

### 4.4.2. Dual-analyte NTR-GGT analyte based on D-luciferin

#### 4.4.2.1. Synthesis

To create a functional dual-analyte probe for NTR and GGT based on D-luciferin instead of amino-luciferin, a different approach is needed. A necessary requirement here is the 4-aminobenzyl group (or para-aminobenzyl, PABA), which links the NTR-GGT analyte-targeting groups and the D-luciferin core. This 4-aminobenzyl linker is a widely known self-immolative spacer or linker. A self-immolative spacer is a degradable chemical connector that is used for creating prodrugs, pro-fluorophores and pro-bioluminophores. Upon activation (i.e. enzymatically or chemically), self-immolative linkers will undergo degradation via intramolecular reactions, driven by a positive reaction entropy. These intramolecular interactions cause an electronic cascade in aromatic or  $\pi$ -extended systems (as is the case for PABA, via a 1,6-elimination) and release the free active product (in this example: D-luciferin).<sup>41,97</sup> There are also other types of self-immolative spacers described in the literature, which can undergo intramolecular cyclization after activation.<sup>98</sup> A lot of work has been done on self-immolative spacers, but since it is outside the scope of this work to discuss this in detail, the readers are given some references for further reading.<sup>97,99,100</sup>

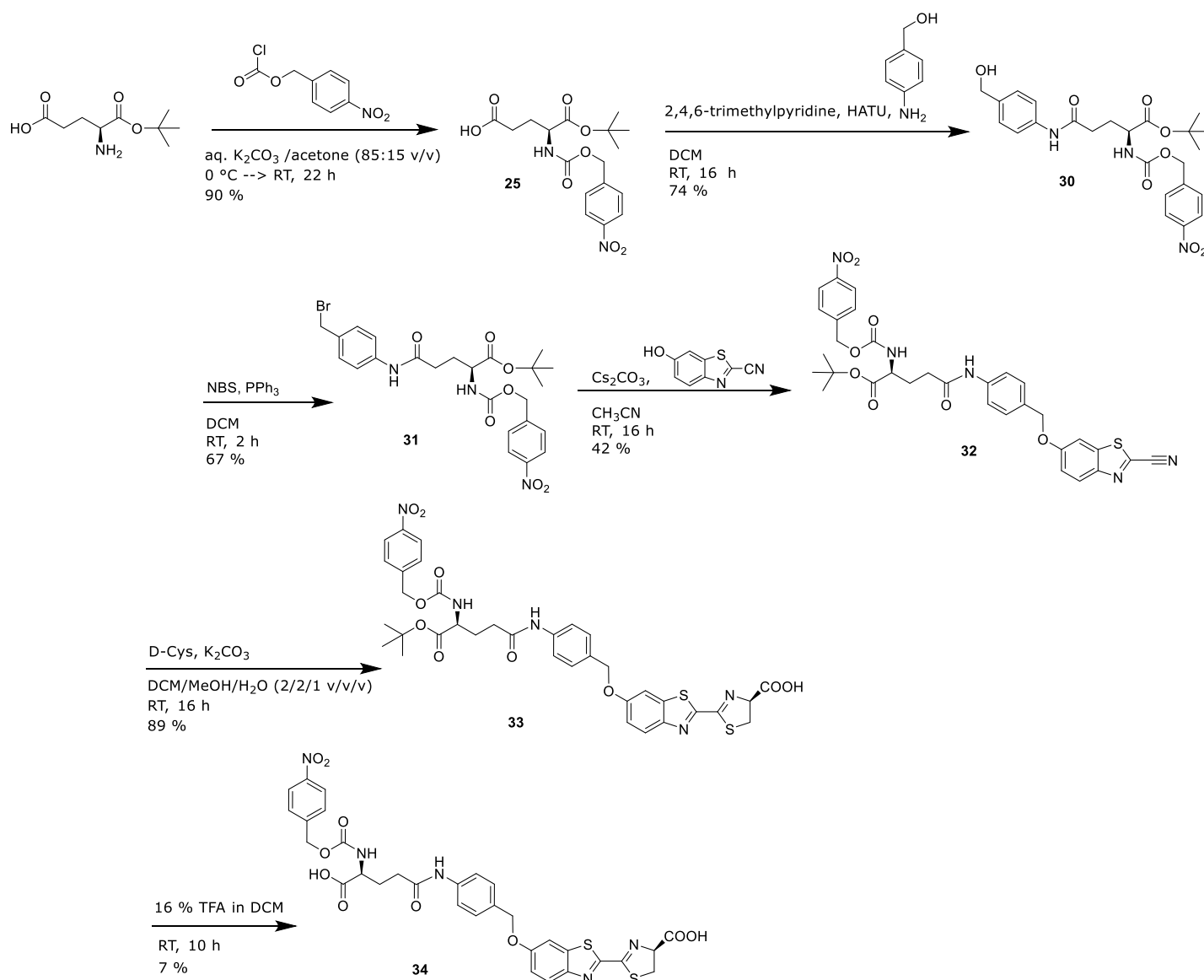
**Scheme 4.31** illustrates a proposed mechanism of response to the analytes for compound **34**: after reacting with NTR, followed by GGT, a 4-aminobenzyl moiety is left, which undergoes a 1,6-elimination reaction (like in **scheme 4.14**), to yield free D-luciferin.



**Scheme 4.31:** Proposed mechanism of action for **34**.

## Chapter 4: Results and Discussion

By incorporating a self-immolative linker, the synthesis will also change slightly compared to **29**. The synthesis is shown in **scheme 4.32**. An amide coupling is performed between **25** and 4-aminobenzyl alcohol, using HATU and DCM/DMF 90/10 v/v as the solvent system, similar to the conditions described for **26**. This yielded the synthesis of **30** in 74% yield.

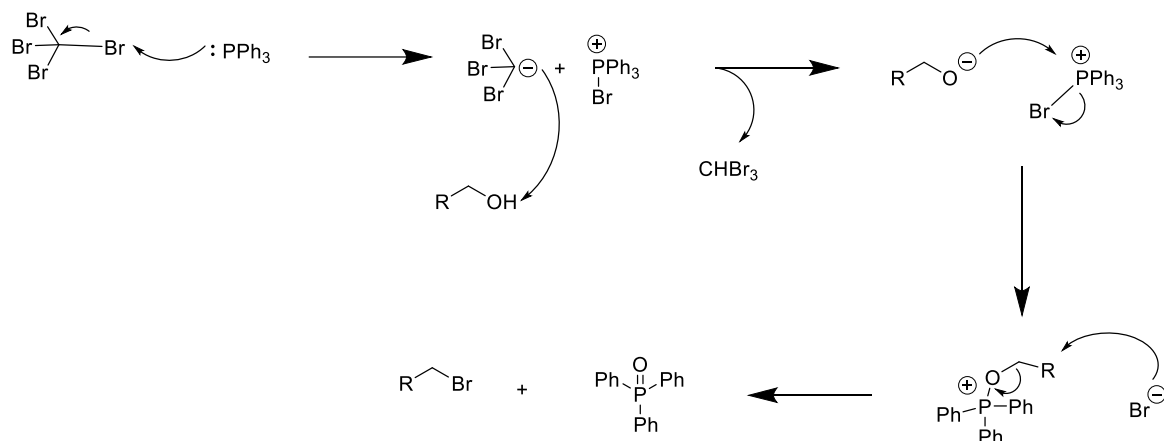


**Scheme 4.32:** Synthesis of dual-analyte NTR-GGT probe **30** based on D-luciferin.

To connect this moiety to OH-CBT, the benzylic alcohol **30** needs to be converted into a suitable leaving group, to allow a nucleophilic substitution between the generated electrophile and OH-CBT (cfr. synthesis of **8**). There are a variety of reactions in which an alcohol can be converted into a suitable leaving groups. Examples include halides (chlorides, bromides, iodides), tosylates, mesylates or triflates. A decision was made to first try tosylation<sup>101</sup> of **30** in DCM with 3 eq. of DIPEA and 2.5 eq. of TsCl. After overnight stirring, no reaction occurred. The decision was then made to generate an alkyl iodide as a leaving group, since primary mesylates and triflates are not stable enough long-term to be purified and stored. A first method that was tried to synthesize iodide was by reacting **30** with  $I_2$ ,  $PPh_3$  and imidazole in DCM<sup>102</sup> overnight at room temperature, however no reaction was observed according to TLC. Then, another variation of iodination was tried by reacting **30** with trimethylsilyl chloride (TMS-Cl)/NaI<sup>103</sup> (both 6 eq.) in ice bath for 30 min. in  $CH_3CN$ . TLC analysis showed that no substrate remained after 30 min., and a spot at  $R_f$  0.5 was observed using hexane/EtOAc 1/1 v/v as eluent. Since the  $R_f$  for alkyl halides should be higher than alcohols, due to the lower polarity of alkyl halides, this was a good sign. Purification with silica gel column chromatography gave 27% yield. The low yields were suspected to be due to the high probability of TMS-Cl being wet, and that TMS-Cl could potentially act as a Lewis acid, which could cleave the tBu-ester bond. The final iodination trial was done with  $P_2O_5/KI$  in  $CH_3CN$ <sup>104</sup> at room temperature for 2 hours. This method gave a yield of 33%, which was considered too low for future scale-up.

Due to the low yields of iodinations, the next step was to try out bromination reactions. Traditionally,  $PBr_3$  is a classic reagent used for this purpose, however due to its inherent danger and toxicity, other methods for brominations were used instead. The first reaction tried out was an Appel halogenation<sup>105,106</sup>, using  $CBr_4$  and  $PPh_3$  in DCM at room temperature for 16 hours. The typically quoted reaction mechanism for this known transformation is shown in **scheme 4.33**: the phosphine attacks the  $CBr_4$ , generating a phosphonium species and tribromomethyl anion, which is stabilized due to the negative inductive effect of the three bromine atoms. This anion can then deprotonate the alcohol, which generates bromoform and a nucleophilic alkoxide species, that can then attack the positive phosphorous center, displacing the bromide. Afterwards, the bromide attacks the carbon center in a nucleophilic substitution reaction, resulting in the

final alkyl bromide, with an inverted stereocenter. This reaction mechanism is also similar for  $\text{CCl}_4$  or  $\text{CI}_4$ , when synthesizing alkyl chlorides or alkyl iodides respectively. A yield of 33% was obtained, prompting the search for an alternative bromination method.



**Scheme 4.33:** Reaction mechanism for the halogenation of alcohols via carbon tetrabromide/triphenyl phosphine.

The second bromination method that was tried involved using NBS and  $\text{PPh}_3$  in DCM at room temperature for 2 hours.<sup>107</sup> This reaction yielded 67% yield, decreasing to 40% yield when stirred for 16 hours at room temperature. Thus, the short stirring time using NBS and  $\text{PPh}_3$  were used afterwards. The reaction mechanism is similar to **scheme 4.33**, but with a slight difference: trace amounts of  $\text{HBr}$  present in NBS catalyze the formation of  $\text{Br}_2$  *in situ*, which can then be attacked by  $\text{PPh}_3$ , yielding the phosphonium bromide intermediate, and undergoing subsequent reactions shown in **scheme 4.33**. Bromide **31** is a versatile intermediate, as it could be used to create potential dual-analyte fluorescent probes, or for creating a potential dual-analyte NTR-GGT probe for furimazine, as described previously in chapter 4.3.1.

**Table 4.34** shows a concise summary of all the conditions tried in converting benzylic alcohol **30** into a suitable leaving group.

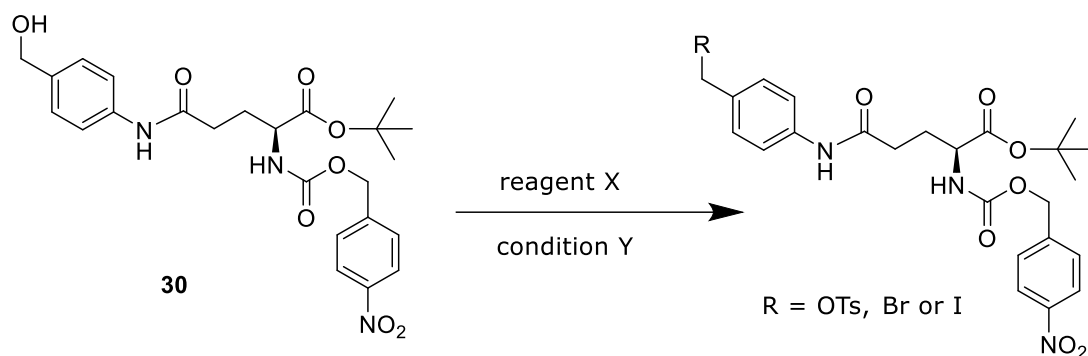


**Table 4.34:** summary of reaction conditions and yields for generating (pseudo)halogens as a leaving group.

| Leaving Group (R) | Reagent   | Conditions |                    |       | Yield       |
|-------------------|---|------------|--------------------|-------|-------------|
|                   |   | Temp.      | Solvent            | Time  |             |
| OTs               | TsCl and DIPEA                                  | RT         | DCM                | 16 h  | No reaction |
| I                 | I <sub>2</sub> , PPh <sub>3</sub> and imidazole | RT         | DCM                | 16 h  | No reaction |
| I                 | TMS-Cl and NaI                                  | 0 °C       | CH <sub>3</sub> CN | 0.5 h | 27%         |
| I                 | P <sub>2</sub> O <sub>5</sub> and KI            | RT         | CH <sub>3</sub> CN | 2 h   | 33%         |
| Br                | CBr <sub>4</sub> and PPh <sub>3</sub>           | RT         | DCM                | 16 h  | 33%         |
| Br                | NBS and PPh <sub>3</sub>                        | RT         | DCM                | 2 h   | 67%         |
| Br                | NBS and PPh <sub>3</sub>                        | RT         | DCM                | 16 h  | 40%         |

Product **32** was then synthesized in 42% yield by reacting OH-CBT with alkyl bromide **32** in CH<sub>3</sub>CN and Cs<sub>2</sub>CO<sub>3</sub>. Then, the condensation reaction with D-Cys/NaHCO<sub>3</sub> was done in DCM/MeOH/water 2/2/1 v/v/v for 10 hours at room temperature. The product was precipitated after addition of 0.5 M H<sub>2</sub>SO<sub>4(aq)</sub> to precipitate a yellow solid **33**. It was decided to use the crude product without further purification, as the NMR showed convincingly a formation of the product with little impurities (<10%). Peaks at 3.74 ppm and 5.29 ppm show the presence of the thiazoline ring. A final deprotection reaction was done with 16% TFA in DCM to yield **34** with a 7% yield.



#### 4.4.3. Summary of dual-analyte probes for NTR and GGT based on D-aminoluciferin and D-luciferin

This study has described the development of two novel dual-analyte probes based on D-luciferin (**34**) or D-aminoluciferin (**29**), where two analyte-responsive moieties are present on the 6'-OH or 6'-NH<sub>2</sub> side, respectively. These probes represent the first innovative dual-analyte probes designed for the selective detection of both NTR and GGT and only second and third instances of dual-analyte bioluminescent probes. The probe's novel design incorporates a sequential mechanism and requires the presence of both analytes for a complete and functional response. This was tested for **29** in bioluminescent *in vitro* studies, which demonstrated the probe's remarkable specificity, with a clear response only when both NTR and GGT were present. Furthermore, the response of **29** exhibited a directly proportional dependence of signal intensity to NTR concentration, (with constant GGT concentrations) and to a lesser extent with increasing GGT concentration (while keeping NTR constant), suggesting NTR-catalysed cleavage to be a key rate determining step in the selected assay conditions

Probe **34** incorporates a design using a self-immolative linker, based on PABA, that can undergo an aza-quinone methide elimination, after reaction with GGT, to yield D-luciferin. The design strategy of **34** can also be incorporated into other probe designs, by using **31** (benzylic bromide moiety containing NTR and GGT responsive groups), such as furimazine (see chapter 4.3.1) or fluorescent probes, giving a whole array of possibilities for future probe designs.

This research has established a groundbreaking approach for dual-analyte detection. Compound **29's** specificity to both analytes and its sequential activation mechanism, offer significant advantages for various biological applications. Future studies could focus on optimizing the probe for *in cellulo* and *in vivo* investigations and exploring its potential in studying redox homeostasis in cancer models. Overall, this work lays the foundation for the development of more sophisticated multi-analyte detection systems with diverse applications in biomedical research.

## 5. Conclusions and Perspectives

This thesis has successfully demonstrated the design, synthesis, and evaluation of novel bioluminescent probes for the detection of various analytes related to redox homeostasis. The growing demand for multi-analyte sensing tools in complex biological systems is addressed by these probes, which hold significant promise, and will expand the toolbox available to biologists for studying intricate biological phenomena in which the interplay of analytes is important.

Compound X, designed for Fe<sup>2+</sup> detection, serves as a valuable case study. It was successfully synthesized and its functionality was established *in vitro* and in lysates, but the same could not be done for H1299 LUC cells, which could be due to challenges with cellular uptake or interaction with cellular components, limiting its effectiveness. *In vitro*, it was seen that **4** showed lower response than OH-CBT with D-Cys, due to the complex reaction kinetics of **4**, with 5 reaction rates in total. The experiments with **4** highlights the crucial role of well-defined reaction kinetics and a strong initial validation of *in vitro* response for successful split-luciferin probes before moving on to complex models such as cells. Furthermore, the influence of metal ions on bioluminescence signal generation was also studied in-depth. We have shown that several biologically relevant metal ions can negatively impact bioluminescence. This study screened a comprehensive and diverse panel of metal ion interferents, highlighting their significant influence on bioluminescence-based high-throughput screening (HTS) assays involving Firefly luciferase, *Renilla* luciferase, and NanoLuc® luciferase. Notably, the observed quenching effects occurred within biologically and environmentally relevant concentration ranges of metal ions, underscoring their substantial impact on HTS campaigns and the subsequent interpretation of screening data. The susceptibility to metal ion-induced quenching varied among the three luciferase systems, with Firefly luciferase exhibiting the highest sensitivity, followed by *Renilla* luciferase, and NanoLuc® luciferase being the most stable. This variability and the differential effects of buffer compositions, preincubation, EDTA, and GSH emphasize the complexity of the underlying mechanisms. These findings have important implications for the design, optimization, and interpretation of bioluminescence-based HTS assays, highlighting the need for rigorous assay validation protocols and potentially incorporating mitigating strategies, such as the use of chelators or

## Chapter 5: Conclusions and Perspectives

alternative luciferase systems, depending on the anticipated metal ion composition of the samples or compound libraries.

Compound **8** and **10**, two probes for NTR detection, were synthesized and can be used to sense NTR in a split-luciferin reaction. Activity of **10** towards NTR *in vitro* was observed, and further HPLC kinetic studies demonstrated the consumption of **10** by NTR, showcasing its promise as an excellent way for sensing NTR using the split-luciferin method.

Compound **19**, one of the first furimazine-based NTR probes, represents a significant advancement despite the challenges associated with its multi-step synthesis. Its activity against NTR and the establishment of a deprotection method of acetylfurimazine to furimazine pave the way for future furimazine-based probes. Additionally, the attachment of a complex electrophile **31** on furimazine offers a valuable starting point for the design of dual-analyte furimazine probes.

The success of **29** and **34** validates the hypothesis derived from structure-activity relationship studies on GGT. Capping the alfa-amine of glutamic acid proved to be an effective strategy for hindering GGT activity, thus achieving a sequential dual-analyte molecule. This paves the way for the development of probes with various cleavable analyte-targeting groups attached to the alfa-amine, alfa-COOH, or even the 4-COOH of firefly luciferin, enabling the creation of multi-analyte probes. Furthermore, the approach presented here can be adapted for the design of fluorescent probes as well.

In conclusion, this thesis has significantly advanced the field of bioluminescent probes for redox homeostasis analysis. The developed strategies offer a powerful platform for the design and synthesis of novel probes with diverse functionalities, enabling researchers to explore complex biological systems with greater depth and precision. Future endeavors can focus on optimizing existing probes for cellular uptake and further exploring the potential of furimazine-based probes and probes with functionalities for multi-analyte detection.

## 6. Materials and Methods

### 6.1. Materials

Chemicals were procured from Sigma-Aldrich (St. Louis, United States), TCI (Zwijndrecht, Belgium), Fluorochem (Hadfield, United Kingdom), Angene (London, United Kingdom), Ambeed (Arlington Heights, United States) and Warchem (Zakręć, Poland). Analytical grade solvents were obtained from Chempur (Piekary, Poland) and POCH (Gliwice, Poland). Deuterated solvents for NMR were purchased from Eurisotop (Saint-Aubin, France) and Sigma-Aldrich (St. Louis, United States). HPLC-grade solvents were obtained from Sigma-Aldrich (St. Louis, United States). All chemicals and solvents were utilized as received unless specified otherwise. Firefly luciferase (QuantiLum® Recombinant Luciferase) and NanoLuc® (RealTime-Glo™ MT Cell Viability Assay) were obtained from Promega (Madison, United States). NTR and GGT enzymes were purchased from Sigma Aldrich (St. Louis, United States). White 96 well plates with flat bottom for *in vitro* studies were procured from GreinerBioOne (Kremsmünster, Austria).

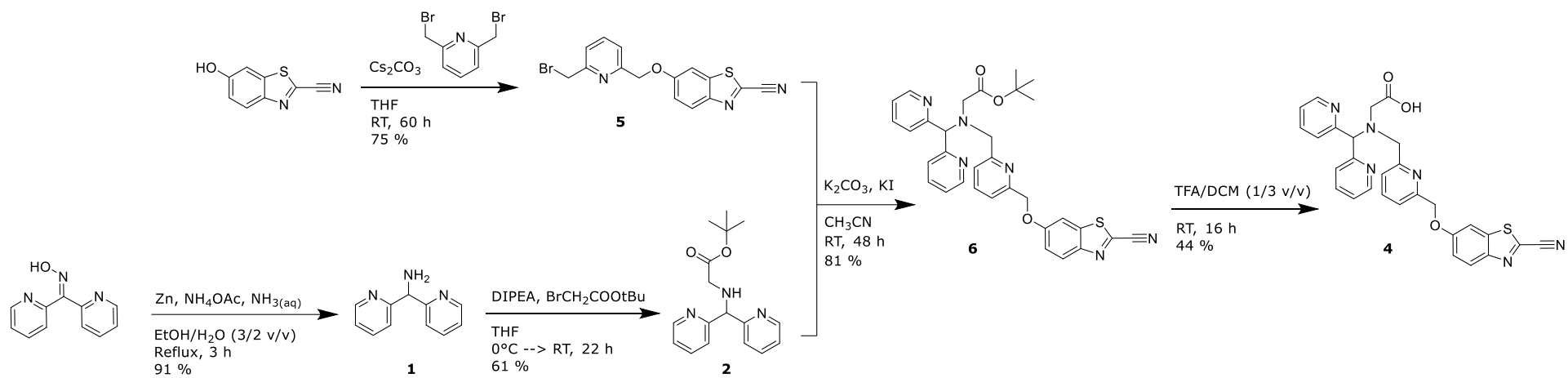
## **6.2. Instruments**

NMR spectra were recorded at the Laboratory of NMR. The  $^1\text{H}$  and  $^{13}\text{C}$  NMR spectra of the compounds, dissolved using  $\text{CDCl}_3$ ,  $\text{CD}_3\text{OD}$  or  $\text{CD}_3\text{CN}$ , were acquired using an AVANCE III Bruker spectrometer with frequencies of 400 MHz, 500 MHz, or, when necessary, 700 MHz. Chemical shifts are presented as  $\delta$  values in parts per million (ppm), referencing residual solvent peaks (DMSO:  $^1\text{H}$  2.50 ppm,  $^{13}\text{C}$  39.52 ppm;  $\text{CDCl}_3$ :  $^1\text{H}$  7.26 ppm,  $^{13}\text{C}$  77.16 ppm;  $\text{CD}_3\text{OD}$ :  $^1\text{H}$  3.31 ppm,  $^{13}\text{C}$  49.00 ppm;  $\text{CD}_3\text{CN}$   $^1\text{H}$  1.94 ppm,  $^{13}\text{C}$  1.32 ppm and 118.26 ppm). NMR spectra were processed using MestReNova Version 9.0.1-13254. Coupling constants are reported in Hertz (Hz), and peak patterns are denoted by abbreviations such as bs (broad singlet), s (singlet), d (doublet), t (triplet), q (quadruplet), dd (doublet of doublets), dt (doublet of triplets), dq (doublet of quartets), td (triplet of doublets), tt (triplet of triplets), m (multiplet).

High-resolution mass spectra were obtained in the Laboratory of Mass Spectrometry (at the European Center for Bioinformatics and Genomics) by Dr. Łukasz Marczak using a Nano/micro LC-MS (OrbiTrap) - Dionex RSLC nano 3000 + Thermo QExactive.

HPLC analyses were carried out at the Institute of Bioorganic Chemistry on a Thermofisher Ultimate 3000 HPLC system equipped with a HPG-3200BX and a UV-VIS detector, using an Atlantis T3 Column, 100Å, 3.0  $\mu\text{m}$ , 2.1 mm X 150 mm with  $\text{CH}_3\text{CN}$  (containing 0.1% TFA) and water (containing 0.1% of TFA) as the eluent.

Luminescence spectra were obtained at the Laboratory of Molecular Assays and Imaging with Biotek Cytation™ 3. The luminescence values obtained are referenced in relative luminescence units (RLU). The bioluminescent intensity was measured at every 1 min. with an integration time of 1 second, unless otherwise specified.

**6.3. Chemistry****6.3.1. Synthesis of 4****Scheme 6.1:** Synthesis of **4**.

### Synthesis of **5**

2-cyano-6-hydroxy-benzothiazole (300 mg, 1.70 mmol, 1 eq.), 2,6-bisbromomethyl pyridine (541 mg, 2.04 mmol, 1.2 eq.) and cesium carbonate (665 mg, 2.04 mmol, 1.2 eq.) were added to a round-bottom flask containing 30 mL THF. The resulting suspension was stirred for 60 hours at room temperature. Afterwards, the reaction mixture was filtered and the filtrate was concentrated in vacuo. The crude mixture was purified using silica gel column chromatography (hexane/EtOAc 8/2 v/v → hexane/EtOAc 6/4 v/v) to yield **5** as a white solid (456 mg, 1.28 mmol, 75%).

TLC (silica, hexane/EtOAc 1/1 v/v): R<sub>f</sub> = 0.8

<sup>1</sup>H NMR (400 MHz, CDCl<sub>3</sub>) δ 8.07 (dd, *J* = 9.1, 2.6 Hz, 1H), 7.76 – 7.70 (m, 1H), 7.45 (s, 2H), 7.42 – 7.37 (m, 1H), 7.35 – 7.28 (m, 1H), 5.28 (d, *J* = 2.4 Hz, 2H), 4.56 (d, *J* = 2.6 Hz, 2H).

<sup>13</sup>C NMR (101 MHz, CDCl<sub>3</sub>) δ 159.09, 156.61, 156.08, 147.22, 138.25, 137.42, 133.84, 126.04, 122.92, 120.91, 118.96, 113.21, 104.61, 71.26, 33.54.

### Synthesis of **1**

2,2-dipyridyl ketoxime (1.21 g, 6.07 mmol, 1 eq.), ammonium acetate (1.74 g, 10.04 mmol) and 21 mL of a 25 % aqueous ammonia solution were added to a round bottom flask. A solvent mixture of 30 mL denatured ethanol and 20 mL water was added and the resulting solution was stirred at room temperature for 30 minutes.

During this time, zinc powder (1.74 g, 26.61 mmol, 4.38 eq.) was added gradually. After completing the addition over 30 min., the resulting suspension was stirred at reflux for 3 hours. Following the completion of the reaction, the solution was cooled down and filtered afterwards. The solution was basified to pH 14 with 5 M NaOH<sub>(aq)</sub>.

The basified solution was added to a separatory funnel and was extracted six times with 30 mL DCM. The organic fractions were combined and washed once with 100 mL brine. The organic fraction was dried with anhydrous magnesium sulfate, the

drying agent was filtered off and the solvent was evaporated to yield **1** as a beige oil (1.02 g, 5.53 mmol, 91%). The product was used without further purification.

$^1\text{H}$  NMR (400 MHz,  $\text{CDCl}_3$ )  $\delta$  8.54 (s, 2H), 7.65 – 7.54 (m, 2H), 7.38 (d,  $J$  = 7.3 Hz, 2H), 7.13 (d,  $J$  = 4.2 Hz, 2H), 5.38 (s, 1H), 3.28 (br s, 2H).

$^{13}\text{C}$  NMR (101 MHz,  $\text{CDCl}_3$ )  $\delta$  162.2, 149.1, 136.7, 122.1, 121.8, 62.0.

### Synthesis of **2**

To a 50 mL anhydrous THF solution of **1** (1.02 g, 5.53 mmol, 1 eq.) cooled in an ice bath was added dropwise a 5 mL THF solution of anhydrous DIPEA (1.35 mL, 7.74 mmol, 1.4 eq.) and tert-butyl bromoacetate (0.98 mL, 6.64 mmol, 1.2 eq.). The resulting solution was stirred for 22 hours in melting ice bath.

THF was removed by evaporation under reduced pressure. The crude mixture was purified by silica gel column chromatography using an isocratic elution system consisting of EtOAc/MeOH/ 25% concentrated  $\text{NH}_3(\text{aq})$  (97/2/1 v/v/v) to yield compound **2** as a yellow oil (1.02 g, 3.43 mmol, 62%).

TLC (neutral alumina, hexane/ethyl acetate 1/1 v/v):  $R_f$  = 0.55

$^1\text{H}$  NMR (400 MHz,  $\text{CDCl}_3$ )  $\delta$  8.56 – 8.43 (m, 2H), 7.56 (t,  $J$  = 7.6 Hz, 2H), 7.39 (d,  $J$  = 7.8 Hz, 2H), 7.12 – 7.03 (m, 2H), 5.10 (s, 1H), 3.61 (br s, 1H), 3.30 (s, 2H), 1.38 (s, 9H).

$^{13}\text{C}$  NMR (101 MHz,  $\text{CDCl}_3$ )  $\delta$  171.24, 160.87, 149.24, 136.71, 122.34, 81.22, 77.16, 68.77, 49.72, 28.11.



### Synthesis of **6**

Compound **2** (157 mg, 0.52 mmol, 1 eq.), compound **5** (230 mg, 0.64 mmol, 1.23 eq.), K<sub>2</sub>CO<sub>3</sub> (718 mg, 5.2 mmol, 10 eq.) and catalytic amounts of KI (17.3 mg, 20 mol %) were added to a round-bottom flask containing 20 mL acetonitrile. The resulting suspension was stirred for 48 hours at room temperature. The solids were filtered off and the solvent was evaporated under reduced pressure. Silica gel column chromatography was used to purify **6** as a beige oil, using an isocratic eluent system of 0.5% Et<sub>3</sub>N in EtOAc (243 mg, 0.42 mmol, 81%).

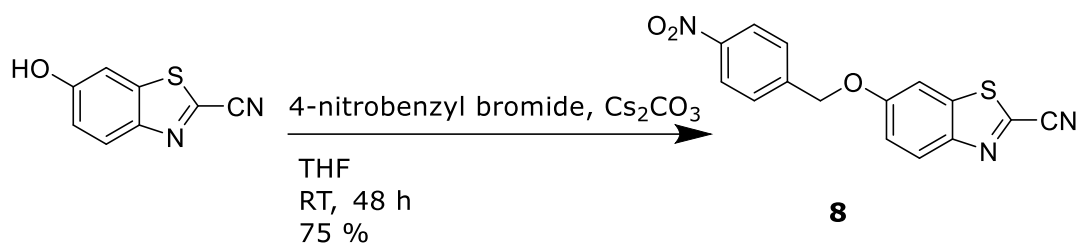
TLC (neutral alumina, hexane/ethyl acetate 1/1 v/v): R<sub>f</sub> = 0.45

<sup>1</sup>H NMR (400 MHz, CDCl<sub>3</sub>) δ 8.56 – 8.46 (m, 2H), 8.08 – 8.04 (m, 1H), 7.79 – 7.59 (m, 6H), 7.51 – 7.39 (m, 1H), 7.37 – 7.22 (m, 2H), 7.17 – 7.08 (m, 2H), 5.57 (s, 1H), 5.24 (s, 2H), 4.05 (s, 2H), 3.38 (s, 2H), 1.39 (s, 9H).

<sup>13</sup>C NMR (101 MHz, CDCl<sub>3</sub>) δ 170.8, 160.1, 159.6, 159.3, 155.2, 149.2, 147.2, 137.6, 137.5, 136.8, 133.8, 126.0, 124.1, 122.5, 122.4, 119.8, 119.0, 113.3, 104.6, 81.0, 72.7, 71.6, 57.7, 52.9, 28.2.

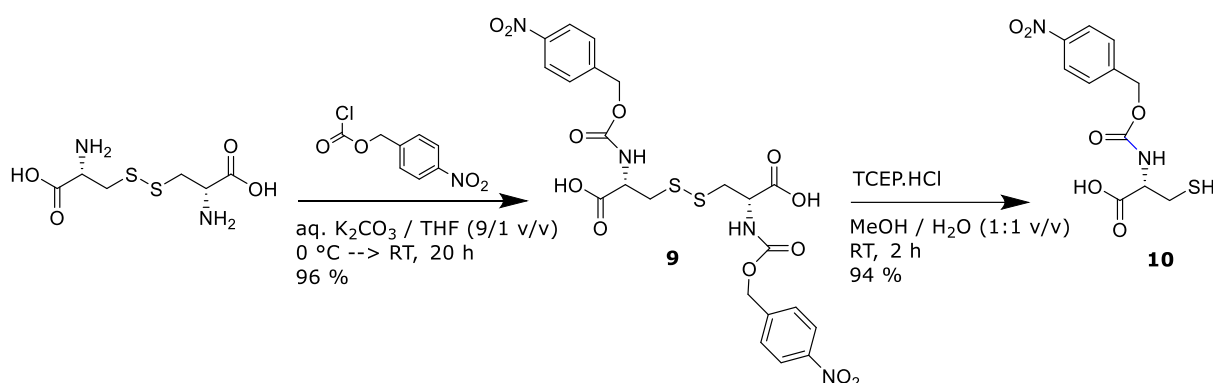
### Synthesis of **4**

Compound **6** (93 mg, 0.16 mmol) was dissolved in a round-bottom flask in a mixture of 1 mL TFA and 3 mL DCM and was stirred for 16 h at room temperature. TFA was neutralized by adding 1.85 mL Et<sub>3</sub>N and the reaction mixture was diluted with 20 mL DCM. The organic layer was washed once with 25 mL water and 25 mL brine. The organic layer was dried with anhydrous magnesium sulfate, the drying agent was filtered off and the organic solvent was evaporated. The crude was purified using preparative TLC using reverse-phase C18 silica as the stationary phase and as eluent acetone/water (2/1 v/v) to yield **4** as a yellow streak (R<sub>f</sub> = 0.6, 37 mg, 0.07 mmol, 44%).

**6.3.2. Synthesis of 8****Scheme 6.2:** Synthesis of **8**.**Synthesis of 8**

6-hydroxy-2-cyanobenzothiazole (300 mg, 1.70 mmol, 1 eq.), 4-nitrobenzyl bromide (441 mg, 2.04 mmol, 1.2 eq.) and cesium carbonate (775 mg, 2.38 mmol, 1.4 eq.) were added to a round-bottom flask containing 30 mL THF. The resulting suspension was stirred for 48 hours at room temperature. The solids were filtered off and the filtrate was concentrated in vacuo. The product was purified with silica gel column chromatography using an eluent system of hexane/EtOAc (9/1 v/v → 7/3 v/v) to yield **8** as a yellow solid (394 mg, 1.27 mmol, 75%).

$^1\text{H}$  NMR (400 MHz, DMSO)  $\delta$  8.28 (d,  $J$  = 8.7 Hz, 2H), 8.19 (d,  $J$  = 9.1 Hz, 1H), 7.98 (d,  $J$  = 2.3 Hz, 1H), 7.76 (d,  $J$  = 8.6 Hz, 2H), 7.45 (dd,  $J$  = 9.1, 2.5 Hz, 1H), 5.42 (s, 2H).

6.3.3. Synthesis of **10****Scheme 6.3:** Synthesis of **10**.Synthesis of **9**

To an ice-cold solution of D-cystine (200 mg, 0.83 mmol, 1 eq.) and potassium carbonate (344 mg, 2.49 mmol, 3 eq.) in water (20 mL) was added dropwise a solution of 4-nitrobenzyl chloroformate (467 mg, 2.16 mmol, 2.6 eq.) in 2 mL THF. The solution was stirred for 20 h in melting ice bath. The pH of the water layer was checked and adjusted to pH 9-10 if necessary. The aqueous layer was washed twice with 20 mL ethyl acetate (this organic layer was discarded). The water layer was then acidified to pH 1-2 and extracted twice with 20 mL ethyl acetate. The combined organic layers were then washed once with 40 mL brine. The organic layer was dried with anhydrous magnesium sulfate, the drying agent was filtered and the solvent was evaporated to yield **9** (478 mg, 0.80 mmol, 96%) as an off-white solid. The product was used without further purification.

TLC (silica, DCM/MeOH/Et<sub>3</sub>N 70/30/1 v/v/v):  $R_f = 0.45$

<sup>1</sup>H NMR (400 MHz, CD<sub>3</sub>CN)  $\delta$  8.18 (d,  $J = 8.4$  Hz, 2H), 7.54 (d,  $J = 8.4$  Hz, 2H), 6.31 (d,  $J = 7.8$  Hz, 1H), 5.20 (s, 2H), 4.50 (dd,  $J = 12.6, 8.2$  Hz, 1H), 3.29 – 3.20 (m, 1H), 3.05 (dd,  $J = 13.7, 8.8$  Hz, 1H).

<sup>13</sup>C NMR (101 MHz, CD<sub>3</sub>CN)  $\delta$  172.05, 156.84, 148.55, 145.56, 128.93, 124.56, 66.09, 54.25, 41.00.

HRMS (ESI) C<sub>22</sub>H<sub>22</sub>N<sub>4</sub>O<sub>12</sub>S<sub>2</sub> [M-H]<sup>-</sup> m/z calc. for 597.06027, found 597.0569

### Synthesis of **10**

To a round-bottom flask containing **9** (110 mg, 0.184 mmol, 1 eq.) and TCEP.HCl (239 mg, 0.84 mmol, 4.6 eq.) was added 5 mL of methanol and 5 mL of water. The clear, colorless solution was stirred for 2 h at room temperature. The methanol was evaporated and 10 mL of water and 20 mL of DCM were added to the solution. The organic layer was separated and the water layer was washed three more times with 20 mL DCM. The combined organic layers were dried with anhydrous magnesium sulfate, the drying agent was filtered off and the solvent was evaporated. After lyophilization, **10** was obtained as a white solid (104 mg, 0.35 mmol, 94%). The product was used without further purification.

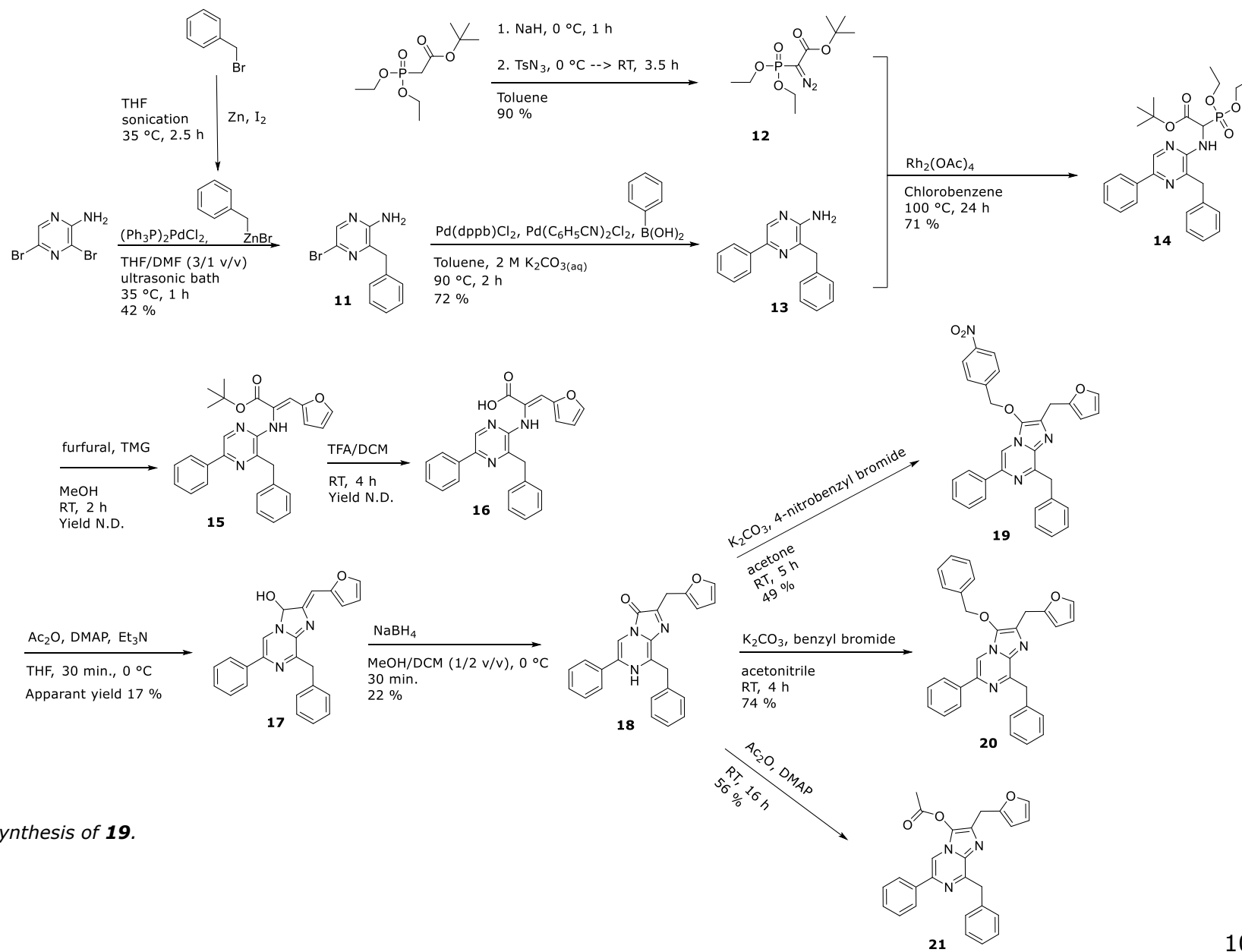
TLC (silica, DCM/MeOH/Et<sub>3</sub>N 70/30/1 v/v/v): R<sub>f</sub> = 0.75

<sup>1</sup>H NMR (400 MHz, CD<sub>3</sub>CN) δ 8.22 (d, *J* = 8.6 Hz, 2H), 7.59 (d, *J* = 8.5 Hz, 2H), 6.17 (s, 1H), 5.21 (d, *J* = 8.1 Hz, 2H), 4.40 (s, 1H), 2.93 (d, *J* = 19.7 Hz, 2H).

<sup>13</sup>C NMR (101 MHz, CD<sub>3</sub>CN) δ 171.68, 156.62, 148.53, 145.59, 128.94, 124.59, 66.03, 56.83, 26.86.

HRMS (ESI) C<sub>11</sub>H<sub>12</sub>N<sub>2</sub>O<sub>6</sub>S [M-H]<sup>-</sup> m/z calc. for 299.03432, found 299.0330

## 6.3.4. Synthesis of 19



Scheme 6.4: Synthesis of 19.

## Synthesis of **11**

All glass ware, syringes and needles were dried in oven at 80 °C for 3 hours prior to use. This synthesis was performed in two parts:

**11.1) Synthesis of benzylzinc bromide:** Zn dust (940 mg, 14.4 mmol, 2.4 eq) was dried in vacuo (0.02 mbar) at 140 °C for 2 h in glass oven. Afterwards, the Zn dust was placed in a dry round-bottom flask, anhydrous THF (15 mL) and iodine crystals (56 mg, 0.22 mmol, 5.5 mol %) were added. The flask was closed off with a septum and flushed with argon. The flask was placed in an ultrasonic bath and sonicated for 30 min. at 35 °C in an argon atmosphere. Benzyl bromide (720 µl, 6 mmol, 1.5 eq.) was added and the reaction was sonicated for an additional 2 h. The benzylzinc bromide was used in the next step without further purification.

**11.2) Negishi coupling:** During the 2 h sonication of the previous reaction, (Ph<sub>3</sub>P)<sub>2</sub>PdCl<sub>2</sub> (140 mg, 0.2 mmol, 5 mol %) and 2-amino-3,5-dibromopyrazine (1012 mg, 4 mmol, 1 eq.) were dried in vacuo (0.02 mbar) for 2 h at 40 °C. After generation of benzylzinc bromide, (Ph<sub>3</sub>P)<sub>2</sub>PdCl<sub>2</sub> and 2-amino-3,5-dibromopyrazine, along with anhydrous DMF (5 mL) were added. The reaction was carried out in ultrasonic bath for 1 hour at 35 °C.

The organic solvents were evaporated and the residue was redissolved in 50 mL ethyl acetate and was washed twice with 50 mL with brine. The combined aqueous layers were then washed three times with 50 mL EtOAc. The organic layers were combined and dried with anhydrous magnesium sulfate, the drying agent was filtered off and the solvent was evaporated under reduced pressure. The product was purified via silica gel column chromatography (DCM → DCM/MeOH 97/3 v/v) to yield **11** as a yellow oil (443 mg, 1.68 mmol, 42%).

TLC (silica, DCM/MeOH 99/1 v/v): R<sub>f</sub> = 0.5

<sup>1</sup>H NMR (400 MHz, CDCl<sub>3</sub>) δ 8.03 (s, 1H), 7.38 – 7.26 (m, 4H), 7.22 (d, J = 7.0 Hz, 2H), 4.38 (br s, 2H), 4.08 (s, 2H).

### Synthesis of **12**

Tert-butyl diethylphosphonoacetate (0.57 mL, 2.4 mmol, 1 eq.) was added dropwise to a stirred solution of NaH (106 mg of 60% dispersion, equal to 63.3 mg pure NaH, 2.6 mmol, 1.1 eq.) in dry toluene (30 mL) at 0 °C over 20 min. The mixture was stirred further for 1 h at 0 °C. Afterwards, tosyl azide solution (30% w/w solution in toluene, 3.7 mL, 4.9 mmol, 2.0 eq.) was added dropwise over 20 min while stirring in ice bath.

Following the addition, the reaction was then carried out for 3 h at room temperature. After the reaction was finished, the precipitate was removed via filtration. The filtrate was evaporated and then redissolved in 60 mL diethyl ether. The ether solution was washed with 30 mL 0.5 M NaOH<sub>(aq.)</sub>, 30 mL water and 30 mL brine. The organic layer was then dried over anhydrous sodium sulfate, the drying agent was filtered off and the solvent was evaporated to yield crude **12** as a yellow oil (545 mg, 2.16 mmol). The crude yield was determined to be 90% and the product was used without further purification. Store argonated in freezer at -20 °C to prevent degradation.

<sup>1</sup>H NMR (400 MHz, CDCl<sub>3</sub>) δ 4.20 – 4.00 (m, 4H), 1.54 – 1.40 (m, 9H), 1.34 – 1.25 (m, 6H).

### Synthesis of **13**

Compound **11** (2.89 g, 10.94 mmol, 1 eq.), Pd(dppb)Cl<sub>2</sub> (500 mg, 0.83 mmol, 7.6 mol %), Pd(C<sub>6</sub>H<sub>5</sub>CN)<sub>2</sub>Cl<sub>2</sub> (500 mg, 1.30 mmol, 11.9 mol %) and 25 mL toluene were added into a round bottom flask. Then, phenylboronic acid (2.93 g, 24.03 mmol, 2.2 eq.) and an aqueous solution of 2 M K<sub>2</sub>CO<sub>3</sub> (1.5 mL) were added. The dark reaction mixture was stirred at 90 °C for 2 h.

Afterwards, the solvent was evaporated and the product was purified via silica gel column chromatography (hexane/EtOAc 2/1 v/v → 1/1 v/v) to yield **13** as a yellow solid (2.05 g, 7.84 mmol, 72 %).

TLC (silica, hexane/EtOAc 1/1 v/v): R<sub>f</sub> = 0.5

$^1\text{H}$  NMR (400 MHz,  $\text{CDCl}_3$ )  $\delta$  8.35 (s, 1H), 7.94 (d,  $J = 7.6$  Hz, 2H), 7.47 (t,  $J = 7.5$  Hz, 2H), 7.42 – 7.30 (m, 3H), 7.28 (d,  $J = 7.7$  Hz, 2H), 4.72 (br s, 2H), 4.22 (s, 2H).

$^{13}\text{C}$  NMR (126 MHz,  $\text{CDCl}_3$ )  $\delta$  151.49, 142.73, 141.33, 137.17, 136.66, 136.50, 129.21, 128.99, 128.72, 128.35, 127.31, 125.92, 77.16, 41.43.

### Synthesis of **14**

Compound **13** (2.34 g, 8.94 mmol, 1 eq.), diazo compound **12** (6.7 g crude, 24.11 mmol, 2.7 eq.),  $\text{Rh}_2(\text{OAc})_4$  (395 mg, 0.89 mmol, 10 mol %) and 40 mL chlorobenzene were added to a round bottom flask and stirred at 100 °C for 24 h. After the reaction was completed, the solvent was evaporated and the product was purified via silica gel column chromatography (Hex/EtOAc 9/1 v/v  $\rightarrow$  2/1 v/v) to yield **14** as a brown-yellow solid (3.25 g, 6.35 mmol, 71%).

TLC (silica, hexane/EtOAc 1/1 v/v):  $R_f = 0.4$

$^1\text{H}$  NMR (400 MHz,  $\text{CDCl}_3$ )  $\delta$  8.41 (s, 1H), 7.94 (d,  $J = 7.3$  Hz, 2H), 7.45 (t,  $J = 7.6$  Hz, 2H), 7.33 (dq,  $J = 15.1, 7.5$  Hz, 5H), 7.22 (t,  $J = 7.0$  Hz, 1H), 5.26 – 5.21 (m, 1H), 5.15 (dd,  $J = 21.3, 8.1$  Hz, 1H), 4.23 (d,  $J = 7.6$  Hz, 2H), 4.15 – 3.84 (m, 4H), 1.44 (s, 9H), 1.26 (t,  $J = 7.1$  Hz, 3H), 1.19 (t,  $J = 7.1$  Hz, 3H).

### Synthesis of **15**

Compound **14** (941 mg, 2 mmol, 1 eq.), furfural (172  $\mu\text{l}$ , 2 mmol, 1 eq.) and MeOH (40 mL) were added into a round bottom flask and placed on magnetic stirrer. To this mixture was added 1,1,3,3-Tetramethylguanidine (0.69 mL, 5.5 mmol, 2.75 eq.). The reaction was carried out for 1.5 h. Afterwards, the reaction mixture was poured into water (100 mL) and extracted three times with EtOAc (150 mL). The combined organic layers were dried over anhydrous  $\text{MgSO}_4$ . The drying agent was filtered off and the solvent was evaporated. The product was used in the next step without further purification.



### Synthesis of **16**

Compound **15** (878 mg, 1.93 mmol) was dissolved in 50 mL DCM in a round bottom flask. To this solution was added 8.2 mL TFA and the reaction mixture was stirred for 4 h at room temperature. The solvents were evaporated and the product was used in the next step without further purification.

### Synthesis of **17**

Compound **16** (299 mg crude, approx. 0.75 mmol) was dissolved in dry THF (17 mL) in an argon atmosphere at 0 °C. Then, in the following order, were added acetic anhydride (0.55 mL, 1.4 mmol, 1.9 eq.), 4-(dimethylamino)pyridine (7 mg, 0.057 mmol, 7.6 mol %) and triethylamine (0.82 mL, 5.9 mmol, 7.9 eq.) were added. The dark red reaction mixture was stirred under argon for 30 min. at 0 °C. The reaction was poured into 100 mL water and extracted three times with 50 mL DCM. The organic layer was dried with anhydrous magnesium sulfate, the drying agent was filtered off and product **17** was purified via silica gel column chromatography using an isocratic elution mixture of pure DCM (50 mg, 0.13 mmol, apparent yield 17 %).

Note: it is not recommended to store this product long-term due its instability, use immediately in the next step for the synthesis of **17**.

TLC (silica, DCM/MeOH 99/1 v/v): R<sub>f</sub> = 0.9

### Synthesis of **18** (furimazine)

Compound **17** (63 mg, 0.16 mmol) was dissolved in DCM (40 mL) and MeOH (20 mL). The mixture was cooled down to 0 °C and sodium borohydride (74 mg, 2 mmol, 12.5 eq.) was added. The reaction was stirred for 30 min in ice bath and protected from light. After 30 min., the reaction mixture was poured into 175 mL 0.1 M HCl<sub>(aq)</sub>. Note: hydrogen gas is being released! The aqueous layer was extracted three times with 30 mL DCM. The product was purified via silica gel column chromatography (DCM → DCM/MeOH 95/5 v/v) to yield furimazine (**18**) as a yellow solid (17 mg, 0.045 mmol, 28%).

TLC (silica, DCM/MeOH 95/5 v/v): R<sub>f</sub> = 0.15

$^1\text{H}$  NMR (400 MHz,  $\text{CDCl}_3$ )  $\delta$  7.40 (s, 2H), 7.31 (m, 12H), 6.27 (s, 1H), 6.18 (s, 1H), 4.40 (d,  $J = 10.2$  Hz, 2H), 4.21 (s, 2H).

### Synthesis of **19**

To a solution of **18** (23 mg, 0.06 mmol, 1 eq.) in 9 mL acetone was added potassium carbonate (25 mg, 0.18 mmol, 3 eq.) and 4-nitrobenzylbromide (39 mg, 0.18 mmol, 3 eq.). The reaction was stirred for 5 h at room temperature. Afterwards, the reaction was poured in to water (30 mL) and the aqueous layer was extracted four times with 20 mL EtOAc. The organic layer was dried with anhydrous magnesium sulfate and the product was purified via silica gel column chromatography (DCM  $\rightarrow$  DCM/MeOH 98/2 v/v) to yield **19** as a yellow-brown oil (15 mg, 0.029 mmol, 49%).

TLC (silica, DCM/MeOH 98/2 v/v):  $R_f = 0.8$

$^1\text{H}$  NMR (400 MHz,  $\text{CDCl}_3$ )  $\delta$  8.25 (d,  $J = 8.5$  Hz, 2H), 7.88 (s, 1H), 7.85 – 7.80 (m, 2H), 7.61 (d,  $J = 7.8$  Hz, 2H), 7.56 (d,  $J = 8.4$  Hz, 2H), 7.44 (t,  $J = 7.2$  Hz, 2H), 7.39 (d,  $J = 7.1$  Hz, 1H), 7.33 – 7.27 (m, 3H), 7.21 (t,  $J = 6.3$  Hz, 1H), 6.32 (d,  $J = 1.6$  Hz, 1H), 6.15 (s, 1H), 5.14 (s, 2H), 4.60 (s, 2H), 4.20 (s, 2H).

$^{13}\text{C}$  NMR (126 MHz,  $\text{CDCl}_3$ )  $\delta$  153.27, 152.22, 148.26, 142.81, 141.64, 139.01, 138.01, 137.06, 136.84, 132.57, 130.53, 129.87, 128.98, 128.74, 128.40, 126.61, 126.32, 124.13, 110.76, 108.91, 106.90, 75.71, 39.47, 27.02.

HRMS (ESI)  $\text{C}_{31}\text{H}_{24}\text{N}_4\text{O}_4$   $[\text{M}+\text{H}]^+$   $m/z$  calc. 517.18701, observed 517.1870

### Synthesis of **20**

Furimazine (**18**) (19 mg, 0.050 mmol, 1 eq.) was dissolved in 5 mL anhydrous acetonitrile. To this solution was added  $\text{K}_2\text{CO}_3$  (33 mg, 0.24 mmol, 4.8 eq.) and benzyl bromide (12  $\mu\text{L}$ , 0.10 mmol, 2 eq.). The reaction was stirred for 16 h at room temperature. Afterwards, 30 mL of water and 30 mL of EtOAc were added. The organic layer was separated and the aqueous layer was then extracted three times with 25 mL EtOAc. The combined organic layers were washed once with 50 mL brine. The organic layer was dried with anhydrous magnesium sulfate, the drying agent was filtered off and the organic layer was evaporated. The product

was purified via silica gel column chromatography (DCM → DCM/MeOH 95/5 v/v) to yield **20** (17.3 mg, 0.037 mmol, 74%) as a dark reddish solid.

TLC (silica, DCM): R<sub>f</sub> = 0.2

<sup>1</sup>H NMR (500 MHz, CDCl<sub>3</sub>) δ 7.69 – 7.66 (m, 2H), 7.64 (s, 1H), 7.50 (d, *J* = 7.3 Hz, 2H), 7.32 (t, *J* = 7.5 Hz, 3H), 7.27 (t, *J* = 2.7 Hz, 3H), 7.24 (dd, *J* = 9.5, 1.6 Hz, 3H), 7.19 (t, *J* = 7.6 Hz, 2H), 7.11 (t, *J* = 7.4 Hz, 1H), 6.24 (dd, *J* = 3.0, 1.9 Hz, 1H), 6.09 – 6.06 (m, 1H), 4.95 (s, 2H), 4.48 (s, 2H), 4.08 (s, 2H).

<sup>13</sup>C NMR (126 MHz, CDCl<sub>3</sub>) δ 152.75, 152.52, 141.55, 138.38, 138.14, 137.46, 136.99, 135.86, 132.51, 130.74, 129.84, 129.32, 129.00, 128.98, 128.78, 128.42, 128.32, 126.48, 126.26, 110.66, 109.28, 106.77, 77.88, 39.34, 26.79.

### Synthesis of **21**

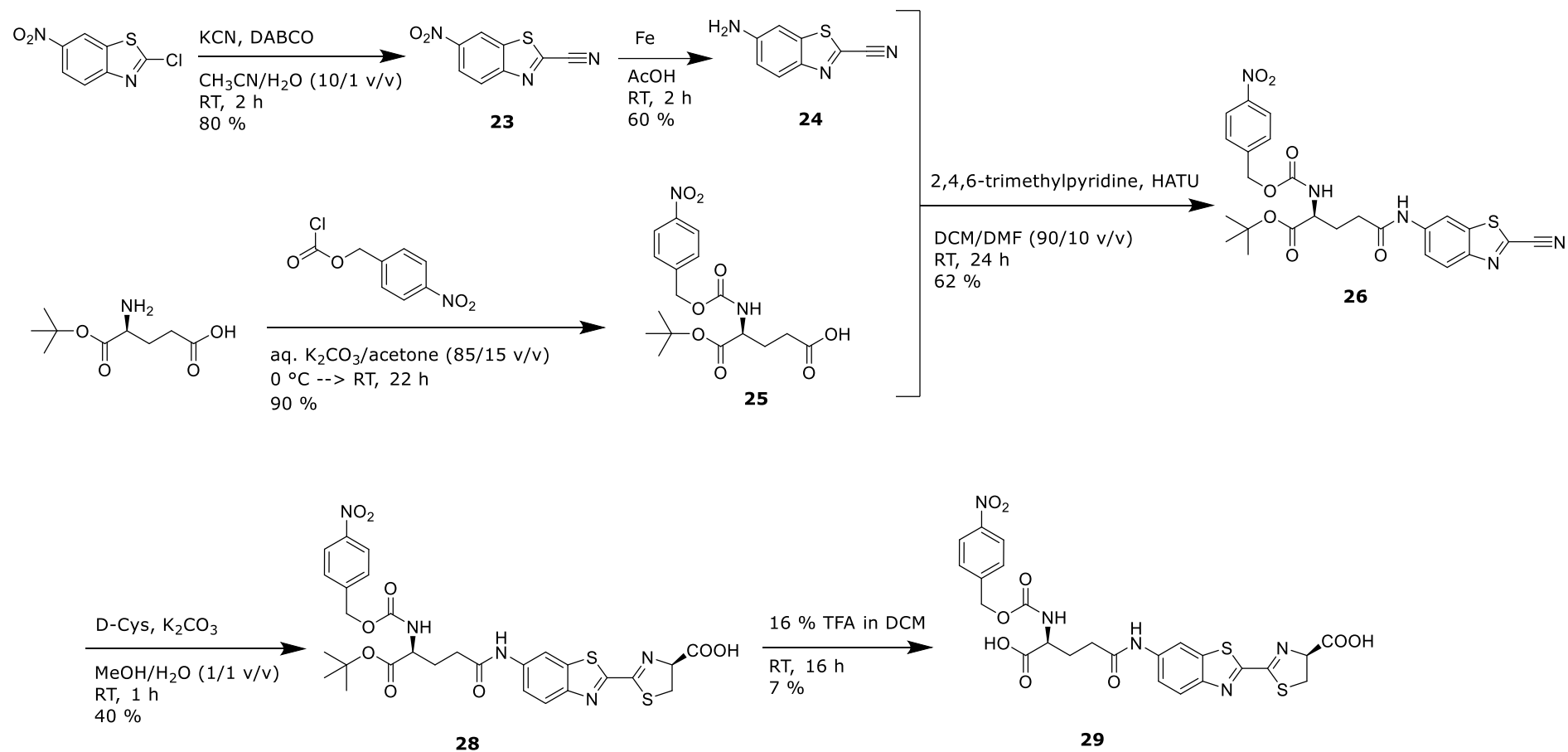
Compound **18** (18 mg, 0.047 mmol, 1 eq.) was dissolved in acetic anhydride (1 mL). Afterwards, DMAP (15.3 mg, 0.125 mmol, 2.66 eq.) was added. The reaction was stirred at room temperature for 16 h under inert atmosphere. The excess of acetic anhydride was removed via evaporation and the product was purified via silica gel column chromatography (DCM → DCM/MeOH 95/5 v/v) to yield **21** (11.1 mg, 0.026 mmol, 56%).

TLC (silica, DCM/MeOH 95/5 v/v): R<sub>f</sub> = 0.6

<sup>1</sup>H NMR (400 MHz, CDCl<sub>3</sub>) δ 7.93 – 7.87 (m, 2H), 7.85 (s, 1H), 7.67 (t, *J* = 8.1 Hz, 2H), 7.50 – 7.38 (m, 4H), 7.36 – 7.28 (m, 3H), 7.22 (t, *J* = 7.4 Hz, 1H), 6.34 (dd, *J* = 3.2, 1.9 Hz, 1H), 6.20 (d, *J* = 2.9 Hz, 1H), 4.73 (s, 2H), 4.32 (s, 2H), 2.35 (s, 3H).

<sup>13</sup>C NMR (126 MHz, CDCl<sub>3</sub>) δ 167.21, 153.07, 151.57, 141.76, 139.23, 137.85, 136.79, 133.61, 132.60, 129.79, 128.97, 128.85, 128.68, 128.39, 126.58, 126.48, 110.57, 108.99, 106.93, 39.42, 27.29, 20.16.

## 6.3.5. Synthesis of 29

**Scheme 6.5:** Synthesis of 29.

### Synthesis of **23**

To a round-bottom flask containing 2-chloro-6-nitrobenzothiazole (3.06 g, 14.26 mmol, 1 eq.) and DABCO (250 mg, 2.23 mmol, 16 mol %) was added 150 mL acetonitrile. To this solution was added dropwise an aqueous solution (15 mL) of KCN (1.25 g, 19.20 mmol, 1.35 eq.). The resulting dark solution was stirred for 2 h at room temperature. The solution was diluted with 300 mL brine and was extracted three times with 150 mL EtOAc. The combined organic layers were then washed once with 200 mL brine and dried afterwards with anhydrous magnesium sulfate. The drying agent was filtered off, the organic layer was evaporated and the crude product was purified using silica gel column chromatography using isocratic elution with CHCl<sub>3</sub> to yield **23** as an off-white solid (2.33 g, 11.37 mmol, 80%).

TLC (silica, CHCl<sub>3</sub>): R<sub>f</sub> = 0.65

<sup>1</sup>H NMR (400 MHz, CDCl<sub>3</sub>) δ 8.95 (d, *J* = 2.1 Hz, 1H), 8.52 (dd, *J* = 9.1, 2.2 Hz, 1H), 8.38 (d, *J* = 9.1 Hz, 1H).

### Synthesis of **24**

To a round-bottom flask containing **23** (3.16 g, 15.40 mmol, 1 eq.) was added 200 mL of glacial acetic acid. Iron powder (17.20 g, 308 mmol, 20 eq.) was added portion-wise to the solution and the resulting suspension was vigorously stirred for 2 h at room temperature. Afterwards, the reaction mixture was filtered through Celite and rinsed with EtOAc. To the filtrate was added 500 mL water and was subsequently washed three times with 250 mL EtOAc. The combined organic layers were then washed once with 1 L saturated bicarbonate (note: careful for pressure build-up due to CO<sub>2</sub> formation!) and dried afterwards with anhydrous magnesium sulfate. The drying agent was filtered off and the organic layer was evaporated. Silica gel column chromatography was performed (hexane/EtOAc 9/1 v/v → 1/1 v/v) to purify **24** as a yellow solid (1.62 g, 9.26 mmol, 60%).

TLC (silica, hexane/EtOAc 1/1 v/v): R<sub>f</sub> = 0.6

<sup>1</sup>H NMR (400 MHz, CDCl<sub>3</sub>) δ 7.95 (d, *J* = 8.9 Hz, 1H), 7.08 (d, *J* = 2.3 Hz, 1H), 6.95 (dd, *J* = 8.8, 2.3 Hz, 1H), 4.12 (br s, 2H).

### Synthesis of **25**

H-Glu-OtBu (2 g, 9.84 mmol, 1 eq.) and K<sub>2</sub>CO<sub>3</sub> (3.4 g, 24.63 mmol, 2.5 eq.) were added to a round-bottom flask and dissolved in 60 mL water. To this clear solution stirring at 0 °C was added dropwise a solution of 4-nitrobenzyl chloroformate (2.8 g, 13.00 mmol, 1.3 eq.) dissolved prior in acetone (10 mL). The reaction was stirred for 1 h at 0 °C and at room temperature for 21 h.

To the aqueous solution was added an additional 20 mL water. The pH of the aqueous layer was measured and adjusted to pH 8-10 if required. The solution was filtered and was washed twice with 50 mL EtOAc (this organic layer was discarded). The aqueous layer was then acidified to pH 1-2 with 3 M HCl<sub>(aq)</sub> and extracted three times with 50 mL EtOAc. The combined organic layers were then washed once with 100 mL brine and was dried afterwards with anhydrous magnesium sulfate. The drying agent was filtered off and the organic layer was evaporated to yield **25** (3.4 g, 8.9 mmol, 90%) as a light yellow oil, which solidifies overnight in the fridge as a waxy substance. The product was used without further purification.

TLC (silica, DCM/MeOH/Et<sub>3</sub>N 90/10/1): R<sub>f</sub> = 0.2

<sup>1</sup>H NMR (400 MHz, CDCl<sub>3</sub>) δ 8.21 (d, *J* = 8.7 Hz, 2H), 7.51 (d, *J* = 8.6 Hz, 2H), 5.52 (d, *J* = 7.8 Hz, 1H), 5.20 (s, 2H), 4.30 (dd, *J* = 12.8, 7.6 Hz, 1H), 2.54 – 2.36 (m, 2H), 2.21 (dt, *J* = 13.2, 7.2 Hz, 1H), 1.97 (td, *J* = 14.4, 7.8 Hz, 1H), 1.47 (s, 9H).

<sup>13</sup>C NMR (101 MHz, CD<sub>3</sub>CN) δ 174.84, 173.76, 157.02, 148.54, 145.70, 128.89, 124.56, 82.61, 65.96, 54.15, 30.40, 28.11, 27.24.

HRMS (ESI) C<sub>17</sub>H<sub>22</sub>N<sub>2</sub>O<sub>8</sub> [M+H]<sup>+</sup> *m/z* calc. 383.14487, observed 383.14

### Synthesis of **26**

To a round-bottom flask containing **25** (360 mg, 0.94 mmol, 1 eq.), HATU (715 mg, 1.88 mmol, 2 eq.) and 2,4,6-trimethylpyridine (0.51 mL, 4.7 mmol, 5 eq.) was added 20 mL DCM. The solution was stirred for 20 min. at room temperature. Afterwards, a DMF solution (2 mL) containing **24** (165 mg, 0.94 mmol, 1 eq.) was added and the resulting yellow solution was stirred for 24 h at room temperature. The reaction mixture was filtered through Celite and rinsed twice with 50 mL DCM. The filtrate was washed once with 70 mL 0.5 M HCl<sub>(aq)</sub>, 70 mL water and 100 mL brine. The organic layer was dried with anhydrous magnesium sulfate, the drying agent was filtered off and the solvent was evaporated. The product was purified with silica gel column chromatography using an eluent system of hexane/EtOAc (8/2 v/v → 6/4 v/v) to yield **26** as a light yellow oil (315 mg, 0.58 mmol, 62%).

TLC (silica, hexane/EtOAc 1/1 v/v): R<sub>f</sub> = 0.15

<sup>1</sup>H NMR (400 MHz, CDCl<sub>3</sub>) δ 8.91 (s, 1H), 8.72 (s, 1H), 8.21 (d, *J* = 8.3 Hz, 2H), 8.11 (d, *J* = 8.9 Hz, 1H), 7.51 (d, *J* = 8.5 Hz, 3H), 5.76 (d, *J* = 7.5 Hz, 1H), 5.25 (d, *J* = 4.9 Hz, 2H), 4.33 – 4.24 (m, 1H), 2.52 (t, *J* = 6.4 Hz, 2H), 2.41 – 2.29 (m, 1H), 1.97 – 1.90 (m, *J* = 9.7 Hz, 1H), 1.47 (s, 9H).

HRMS (ESI) C<sub>25</sub>H<sub>25</sub>N<sub>5</sub>O<sub>7</sub>S [M+H]<sup>+</sup> *m/z* calc. 540.15473, observed 540.1498

### Synthesis of **28**

Compound **26** (248 mg, 0.46 mmol, 1 eq.) was dissolved in 8 mL MeOH in a round-bottom flask. To this solution was added an aqueous solution (8 mL) of D-Cys (278.7 mg, 2.3 mmol, 5 eq.) and K<sub>2</sub>CO<sub>3</sub> (318 mg, 2.3 mmol, 5 eq.). The resulting yellow solution was stirred for 1 h at room temperature in the absence of light. Afterwards, methanol was evaporated and the residue was diluted with 20 mL water. The pH was brought to pH 9-10 with 1 M K<sub>2</sub>CO<sub>3</sub>, if necessary. The aqueous layer was washed twice with 20 mL EtOAc (the combined organic layers were discarded). Then, the aqueous layer was acidified with 3 M HCl<sub>(aq)</sub> until the pH was 1-2, which was then afterwards extracted with 30 mL EtOAc three times. The combined organic layers were dried with anhydrous magnesium sulfate, the drying agent was filtered off and the organic solvent was evaporated. The crude

product was purified with preparative silica TLC using an eluent system of 20% MeOH in DCM ( $R_f \sim 0.3$ ) to yield **28** as a yellow solid (117 mg, 0.182 mmol, 40%).

$^1\text{H}$  NMR (400 MHz, MeOD)  $\delta$  8.45 (s, 1H), 8.14 (d,  $J = 8.6$  Hz, 2H), 7.93 (d,  $J = 8.9$  Hz, 1H), 7.52 (dd,  $J = 15.3, 8.7$  Hz, 3H), 5.26 – 5.06 (m, 3H), 4.18 (dd,  $J = 9.6, 4.7$  Hz, 1H), 3.73 (dd,  $J = 9.3, 2.6$  Hz, 2H), 2.56 (t,  $J = 7.2$  Hz, 2H), 2.32 – 2.22 (m, 1H), 2.12 – 1.99 (m, 1H), 1.47 (s, 9H).

$^{13}\text{C}$  NMR (101 MHz, MeOD)  $\delta$  177.37, 173.41, 172.75, 165.09, 161.95, 158.20, 150.54, 148.76, 145.80, 139.18, 138.12, 128.94, 124.90, 124.47, 120.90, 113.03, 83.25, 83.04, 66.21, 55.97, 37.39, 34.33, 28.24, 24.20.

HRMS (ESI)  $\text{C}_{28}\text{H}_{29}\text{N}_5\text{O}_9\text{S}_2$   $[\text{M}+\text{H}]^+$   $m/z$  calc. 644.14793, observed 644.1422

### Synthesis of **29**

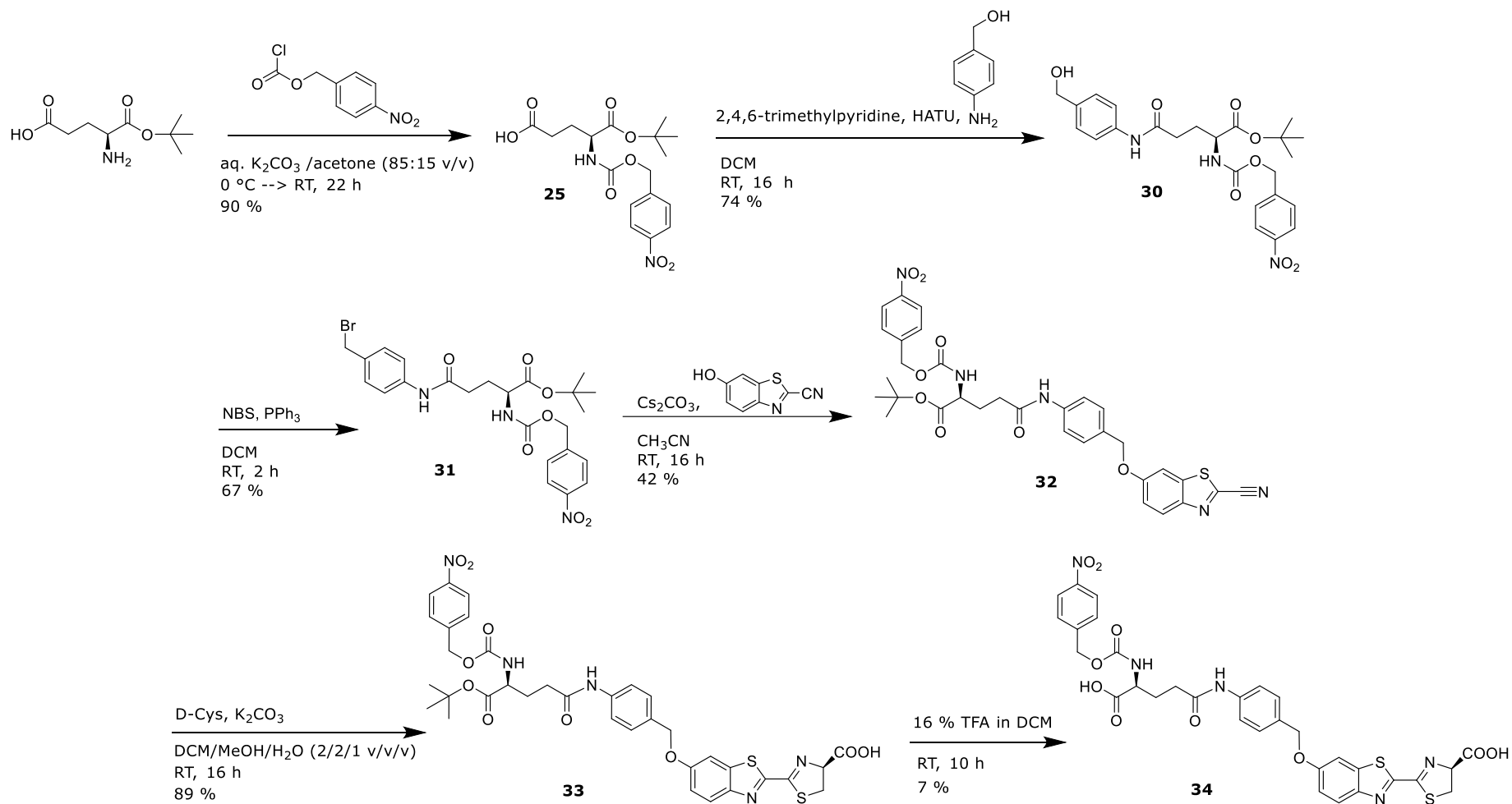
To a round-bottom flask containing **28** (151 mg, 0.235 mmol) was added a mixture of 1 mL TFA and 5 mL DCM. The resulting solution was stirred for 16 h at room temperature. The solvents were evaporated and the crude product was purified with preparative silica TLC using an eluent system of EtOAc/MeOH (1/1 v/v,  $R_f \sim 0.3$ ) to yield **29** (9 mg, 0.015 mmol, 7%) as a yellow solid.

$^1\text{H}$  NMR (400 MHz, MeOD)  $\delta$  8.48 (s, 1H), 8.12 (d,  $J = 8.6$  Hz, 2H), 7.94 (d,  $J = 8.9$  Hz, 1H), 7.58 (d,  $J = 8.8$  Hz, 1H), 7.48 (d,  $J = 8.5$  Hz, 1H), 5.20 (t,  $J = 9.4$  Hz, 1H), 5.09 (dd,  $J = 28.5, 13.9$  Hz, 2H), 4.13 (dd,  $J = 7.5, 4.9$  Hz, 1H), 3.72 (dt,  $J = 15.6, 7.9$  Hz, 2H), 2.50 (t,  $J = 7.2$  Hz, 2H), 2.36 – 2.21 (m, 1H), 2.11 (m, 1H).

HRMS (ESI)  $\text{C}_{24}\text{H}_{21}\text{N}_5\text{O}_9\text{S}_2$   $[\text{M}+\text{H}]^+$   $m/z$  calc. 588.08533, observed 588.0800



## 6.3.6. Synthesis of 34

**Scheme 6.6:** Synthesis of **34**.

### Synthesis of **30**

To a round-bottom flask containing **25** (3.65 g, 9.55 mmol, 1.34 eq) and 2,4,6-trimethylpyridine (4.7 mL, 35.53 mmol, 5 eq.) was added 140 mL DCM. The solution was stirred until clear and to this flask was added HATU (8.0 g, 21.04 mmol, 2.96 eq). The resulting suspension was stirred for 30 min. at room temperature. Afterwards, 4-aminobenzyl alcohol (0.875 g, 7.11 mmol, 1 eq) was added and the yellow reaction mixture was stirred for 16 h at room temperature. The reaction mixture was filtered through Celite and rinsed twice with 40 mL DCM. The filtrate was then washed twice with 100 mL 0.5 M H<sub>2</sub>SO<sub>4(aq)</sub> and once with 100 mL brine. The organic layer was dried with anhydrous magnesium sulfate, the drying agent was filtered off and the organic layer was evaporated under reduced pressure.

The product was purified via silica gel column chromatography (CHCl<sub>3</sub>/Et<sub>3</sub>N 99.5/0.5 v/v → CHCl<sub>3</sub> : MeOH : Et<sub>3</sub>N 97/3/0.5 v/v/v) to yield **30** as a yellow, foamy solid (2.58 g, 5.29 mmol, 74%) when dried on high vacuum.

TLC (silica, CHCl<sub>3</sub>/MeOH/Et<sub>3</sub>N 95/5/1 v/v/v): R<sub>f</sub> = 0.1

<sup>1</sup>H NMR (400 MHz, CDCl<sub>3</sub>) δ 8.15 (d, *J* = 8.5 Hz, 2H), 8.12 (s, 1H), 7.52 (d, *J* = 8.1 Hz, 2H), 7.45 (d, *J* = 8.6 Hz, 2H), 7.29 (d, *J* = 8.2 Hz, 2H), 5.79 (d, *J* = 7.7 Hz, 1H), 5.17 (s, 2H), 4.64 (s, 2H), 4.28 (td, *J* = 9.0, 3.9 Hz, 1H), 2.49 – 2.42 (m, 2H), 2.32 – 2.25 (m, 1H), 2.06 – 1.97 (m, 2H), 1.46 (s, 9H).

<sup>13</sup>C NMR (101 MHz, CDCl<sub>3</sub>) δ 170.96, 170.51, 156.36, 147.75, 143.65, 137.57, 137.02, 128.18, 127.91, 123.88, 120.00, 83.14, 65.67, 65.00, 54.31, 34.01, 29.36, 28.11.

HRMS (ESI) C<sub>24</sub>H<sub>29</sub>N<sub>3</sub>O<sub>8</sub> [M+H]<sup>+</sup> *m/z* calc. 488.20272, observed 488.19

### Synthesis of **31**

Compound **30** (160 mg, 0.33 mmol, 1 eq.) was dissolved in 15 mL DCM in a round-bottom flask. To this solution was added triphenylphosphine (112 mg, 0.43 mmol, 1.3 eq.) and NBS (76 mg, 0.43 mmol, 1.3 eq.). The solution was stirred for 2 hours at room temperature. The solvent was evaporated and the product was purified via silica gel column chromatography ( $\text{CHCl}_3 \rightarrow \text{CHCl}_3/\text{EtOAc}$  9/1 v/v) to yield **31** as an off-white solid (121 mg, 0.22 mmol, 67%).

TLC (silica,  $\text{CHCl}_3/\text{EtOAc}$  1/1 v/v):  $R_f = 0.6$

$^1\text{H}$  NMR (400 MHz,  $\text{CDCl}_3$ )  $\delta$  8.20 (d,  $J = 8.4$  Hz, 2H), 8.13 (s, 1H), 7.56 (d,  $J = 7.8$  Hz, 2H), 7.48 (d,  $J = 8.5$  Hz, 2H), 7.34 (d,  $J = 8.3$  Hz, 2H), 5.70 (d,  $J = 7.7$  Hz, 1H), 5.19 (q,  $J = 13.2$  Hz, 2H), 4.56 (s, 2H), 4.32 – 4.24 (m,  $J = 6.8$  Hz, 1H), 2.49 – 2.42 (m,  $J = 9.9$  Hz, 2H), 2.36 – 2.26 (m, 1H), 2.05 – 1.94 (m,  $J = 16.2$  Hz, 1H), 1.47 (s, 9H).

HRMS (ESI)  $\text{C}_{24}\text{H}_{28}\text{BrN}_3\text{O}_7$   $[\text{M}+\text{H}]^+$   $m/z$  calc. 550.11837, observed 550.11

### Synthesis of **32**

2-cyano-6-hydroxybenzothiazole (140 mg, 0.79 mmol, 1 eq.), **31** (520 mg, 0.94 mmol, 1.19 eq.) and cesium carbonate (470 mg, 1.44 mmol, 1.82 eq.) were added to a round-bottom flask containing 20 mL acetonitrile. The solution was stirred for 16 h at room temperature. The solids were filtered off and the solvent was evaporated under reduced pressure. The product was purified via silica gel column chromatography using hexane/EtOAc (9/1 v/v  $\rightarrow$  1/1 v/v) as eluent to yield **32** as a yellow foamy solid (217 mg, 0.34 mmol, 42 %) when dried under high vacuum.

TLC (silica, hexane/EtOAc 1/1 v/v):  $R_f = 0.15$

$^1\text{H}$  NMR (400 MHz,  $\text{CDCl}_3$ )  $\delta$  8.18 (d,  $J = 8.7$  Hz, 3H), 8.09 (d,  $J = 9.1$  Hz, 1H), 7.61 (d,  $J = 8.2$  Hz, 2H), 7.47 (d,  $J = 8.7$  Hz, 2H), 7.40 (d,  $J = 8.0$  Hz, 3H), 7.30 (dd,  $J = 9.1, 2.5$  Hz, 1H), 5.72 (d,  $J = 7.8$  Hz, 1H), 5.20 (s, 2H), 5.12 (s, 2H), 4.29 (td,  $J = 9.6, 3.9$  Hz, 1H), 2.47 (m, 2H), 2.36 – 2.27 (m, 1H), 2.04 – 1.96 (m, 1H), 1.47 (s, 9H).

$^{13}\text{C}$  NMR (101 MHz,  $\text{CDCl}_3$ )  $\delta$  170.82, 170.51, 159.54, 156.54, 147.80, 147.23, 143.50, 138.30, 137.46, 133.66, 131.60, 128.54, 128.24, 126.09, 123.54, 120.06, 119.15, 113.26, 104.38, 83.26, 70.49, 65.66, 54.06, 34.03, 29.69, 28.12.

HRMS (ESI)  $\text{C}_{32}\text{H}_{31}\text{N}_5\text{O}_8\text{S}$   $[\text{M}+\text{H}]^+$   $m/z$  calc. 646.19659, observed 646.18

### Synthesis of **33**

To a round-bottom flask containing **32** (217 mg, 0.34 mmol, 1 eq.) was added 8 mL DCM and 8 mL MeOH. To this solution was added an aqueous solution of D-Cys (122 mg, 1.02 mmol, 3 eq.) and  $\text{NaHCO}_3$  (85 mg, 1.02 mmol, 3 eq.) in 4 mL water. After stirring for 10 h at room temperature in the absence of light, the organics were evaporated, and the solution was acidified to pH 1-2 with 20 mL 0.5 M aqueous sulfuric acid to yield a yellow precipitate which was collected and dried under vacuum. The yellow solid **33** (224 mg, 0.30 mmol, 89%) was used without further purification in the next step.

TLC (RP-C18 silica,  $\text{CH}_3\text{CN}/\text{H}_2\text{O}$  1/1):  $R_f$  = 0.05

$^1\text{H}$  NMR (400 MHz, MeOD)  $\delta$  8.15 (d,  $J$  = 8.4 Hz, 2H), 7.92 (t,  $J$  = 7.5 Hz, 1H), 7.60 – 7.50 (m, 5H), 7.40 (d,  $J$  = 8.5 Hz, 2H), 7.21 (dd,  $J$  = 9.0, 2.4 Hz, 1H), 5.29 (t,  $J$  = 9.2 Hz, 1H), 5.15 (d,  $J$  = 5.8 Hz, 2H), 5.11 (s, 2H), 4.17 – 4.13 (m, 1H), 3.74 (d,  $J$  = 9.3 Hz, 2H), 2.50 (t,  $J$  = 7.2 Hz, 2H), 2.28 – 2.19 (m, 1H), 2.06 – 2.02 (m, 1H), 1.46 (s, 9H).

$^{13}\text{C}$  NMR (101 MHz, MeOD)  $\delta$  173.13, 172.84, 160.05, 159.83, 158.19, 148.91, 148.84, 145.91, 139.75, 138.94, 133.68, 129.41, 129.10, 125.71, 124.52, 121.18, 118.73, 106.35, 83.01, 71.28, 66.19, 55.92, 47.84, 36.56, 34.15, 30.75, 28.22.

HRMS (ESI)  $\text{C}_{35}\text{H}_{35}\text{N}_5\text{O}_{10}\text{S}_2$   $[\text{M}-\text{H}]^-$   $m/z$  calc. 748.17523, observed 748.1552

### Synthesis of **34**

Compound **33** (45 mg, 0.060 mmol) was dissolved in a mixture of 1 mL TFA and 5 mL DCM and stirred at room temperature for 10 h. The solvent was evaporated and the crude mixture was purified via RP-PLC (CH<sub>3</sub>CN/H<sub>2</sub>O 1/1 v/v, R<sub>f</sub> = 0.15) to yield **34** as light yellow streak (3 mg, 0.0043 mmol, 7%).

TLC (RP-C18 silica, CH<sub>3</sub>CN/H<sub>2</sub>O 1/1 v/v): R<sub>f</sub> = 0.15

<sup>1</sup>H NMR (400 MHz, MeOD) δ 8.17 (d, *J* = 8.6 Hz, 1H), 8.13 (d, *J* = 8.8 Hz, 1H), 7.94 (d, *J* = 9.0 Hz, 1H), 7.64 – 7.50 (m, 5H), 7.41 (d, *J* = 8.5 Hz, 2H), 7.23 (d, *J* = 7.0 Hz, 1H), 5.24 – 5.08 (m, 5H), 4.18 – 4.04 (m, 1H), 3.71 (dt, *J* = 9.5, 3.6 Hz, 2H), 2.49 – 2.37 (m, 2H), 2.32 – 2.20 (m, 1H), 2.13 – 2.00 (m, 1H).

HRMS (ESI) C<sub>31</sub>H<sub>27</sub>N<sub>5</sub>O<sub>10</sub>S<sub>2</sub> [M-H]<sup>-</sup> m/z calc. 692.11264, observed 692.0945

#### **6.4. In vitro bioluminescence studies**

The final volume inside the white 96-well plate for all *in vitro* bioluminescence studies is 100  $\mu$ L total.

##### **6.4.1. *In vitro* procedure for **4****

To a white 96-well plate was added the following volumes (of a specific concentration) in the following order: 1  $\mu$ L of **4** (2 mM in DMSO), 49  $\mu$ L of TRIS-HCl buffer (50 mM, pH 7.5 containing 10 mM MgCl<sub>2</sub> and 0.1 mM EDTA), 20  $\mu$ L of firefly luciferase (100  $\mu$ g/mL in TRIS-HCl buffer), 10  $\mu$ L of ATP (20 mM in TRIS-HCl), 10  $\mu$ L of D-Cys (0.2 mM in TRIS-HCl buffer) and 10  $\mu$ L of FAS (2 mM in water). Bioluminescence intensity was measured for 30 min. at 37 °C, with an interval time of 1 min. and integration time of 1 second.

For positive control, **4** was replaced with OH-CBT (20  $\mu$ M) and for negative control, FAS was replaced with buffer (TRIS-HCl).

Final concentrations of the components: 20  $\mu$ M for **4** or OH-CBT, 20  $\mu$ M D-Cys, 2 mM ATP, 20  $\mu$ g/mL FLuc and 200  $\mu$ M FAS.

##### **6.4.2. *In vitro* procedure for **10****

To a white 96-well plate was added the following volumes (of a specific concentration) in the following order: 1  $\mu$ L of **10** (2 mM in DMSO), 53  $\mu$ L TRIS-HCl buffer (50 mM, pH 7.5 containing 10 mM MgCl<sub>2</sub> and 0.1 mM EDTA), 20  $\mu$ L of firefly luciferase (100  $\mu$ g/mL in TRIS-HCl buffer), 5  $\mu$ L of NTR (100  $\mu$ g/mL in TRIS-HCl buffer), 10  $\mu$ L of NADH solution (5 mM in TRIS-HCl buffer), 10  $\mu$ L of ATP (20 mM in TRIS-HCl) and 1  $\mu$ L of OH-CBT (2 mM in DMSO). Bioluminescence intensity was measured for 30 min. at 37 °C, with an interval time of 1 min. and integration time of 1 second.

For positive control, **10** was replaced with D-Cys (20  $\mu$ M) and for negative control, NTR and NADH were replaced with buffer (TRIS-HCl).

Final concentrations of the components: 20  $\mu$ M for **10** and OH-CBT, 2 mM ATP, 20  $\mu$ g/mL FLuc, 5  $\mu$ g/mL NTR, 0.5 mM NADH.

#### **6.4.3. *In vitro* procedure for **19****

To a white 96-well plate was added the following volumes (of a specific concentration), in the following order: 1  $\mu\text{L}$  of **19** (2 mM in DMSO) 74  $\mu\text{L}$  PBS buffer (pH 7.4), 10  $\mu\text{L}$  of NADH solution (5 mM in PBS buffer), 5  $\mu\text{L}$  of NTR (100  $\mu\text{g}/\text{mL}$  in 50 mM TRIS-HCl buffer pH 7.5 containing 10 mM  $\text{MgCl}_2$  and 0.1 mM EDTA) and 10  $\mu\text{L}$  of NLuc (4  $\mu\text{g}/\text{mL}$  in PBS buffer). Bioluminescence intensity was measured for 60 min. at 37  $^\circ\text{C}$ , with an interval time of 1 min. and integration time of 1 second.

Final concentrations of the components: 20  $\mu\text{M}$  for **19**, 5  $\mu\text{g}/\text{mL}$  NTR, 0.5 mM NADH and 0.4  $\mu\text{g}/\text{mL}$  NLuc.

#### **6.4.4. *In vitro* procedure for **29****

To a white 96-well plate was added the following volumes (of a specific concentration), in the following order: 1  $\mu\text{L}$  of **29** (2 mM in DMSO), 14  $\mu\text{L}$  TRIS-HCl buffer (50 mM, pH 7.5 containing 10 mM  $\text{MgCl}_2$  and 0.1 mM EDTA), 20  $\mu\text{L}$  of firefly luciferase (100  $\mu\text{g}/\text{mL}$  in TRIS-HCl buffer), 50  $\mu\text{L}$  GGT solution (100 U/L in TRIS-HCl), 10  $\mu\text{L}$  of NADH solution (5 mM in TRIS-HCl buffer), 10  $\mu\text{L}$  of ATP (20 mM in TRIS-HCl) and 5  $\mu\text{L}$  NTR (100  $\mu\text{g}/\text{mL}$  in TRIS-HCl buffer). Bioluminescence intensity was measured for 45 min. at 37  $^\circ\text{C}$ , with an interval time of 1 min. and integration time of 1 second.

Final concentrations of the components: 20  $\mu\text{M}$  for **29**, 2 mM ATP, 20  $\mu\text{g}/\text{mL}$  FLuc, 5  $\mu\text{g}/\text{mL}$  NTR, 0.5 mM NADH and 50 U/L GGT.

For negative control, NTR and NADH were replaced with buffer (TRIS-HCl).

## **6.5. HPLC**

### **6.5.1. Kinetic study of **10** and **NTR****

To a 2 mL Eppendorf, was added the following solutions in order: 930  $\mu\text{L}$  of 50 mM TRIS-HCl buffer (pH 7.5, containing 10 mM  $\text{MgCl}_2$  and 0.1 mM EDTA), 10  $\mu\text{L}$  of 20 mM **10** in DMSO, 10  $\mu\text{L}$  of 50 mM NADH solution in TRIS-HCl and 50  $\mu\text{L}$  of 100  $\mu\text{g}/\text{mL}$  NTR solution in TRIS-HCl buffer.

The resulting solution was vortexed at 35  $^\circ\text{C}$ ., and aliquots of 500  $\mu\text{L}$  were taken after 1 h and 4 h. The aliquots were diluted with 500 microliters of LC-grade acetonitrile and filtered through 0.22 micron filter. Sixty microliters of this filtered solution was injected. A gradient elution was used starting with 95%  $\text{H}_2\text{O}$  (+0.1% TFA) and 5%  $\text{CH}_3\text{CN}$  (+0.1% TFA) for 3 min. and then scaling the proportion of  $\text{CH}_3\text{CN}$  (+0.1% TFA) linearly to 95% until 28 min.



## **6.6. Biology**

The following methodology was carried out by the team of prof. Natalia Rozwadowska from the Institute of Human Genetics, Polish Academy of Sciences in Poznań, Poland. The text below is adapted from the MSc. thesis of Michalina Krakowiak, MSc., one of the team members of prof. Rozwadowska.

### **6.6.1. Cell culture**

H1299 LUC cells (expressing firefly luciferase) were cultured at 37 °C in the high CO<sub>2</sub> atmosphere (21% O<sub>2</sub>, 5% CO<sub>2</sub>) in RPMI medium enriched with glutamine (2 mM) and a fetal bovine serum (20% v/v), all with addition of antibiotics (penicillin and streptomycin at 1% v/v concentration in medium). After cell propagation in T25 flasks, when reached 80% confluence, they were washed 2 times with PBS, incubated for 2 min with trypsin (1 mL of 0.05% solution). Followed by addition of complete medium with 20% FBS to inhibit trypsin activity the cells were either lysed (see below) or passaged onto 96-well flat-bottom plates at 50 000 cells/well (black with transparent bottom) for probe testing in live cells.

### **6.6.2. Cell lysate preparation**

Cells were cultured and detached from the flask as above. Concentration of cells in such cell suspension in full RPMI media was calculated by cell counting and 250,000 cells were placed in a Falcon tube (15 mL), centrifuged (300 rcf, 5 min, RT), supernatant discarded, and 0.5 mL of PBS added followed by another centrifugation (300 g, 5 min, 4 °C). Then, after the removal of the supernatant, 110 µL of CCLR lysis buffer (1x concentrated) was added to the pellet and placed on ice, shook on vortex (10-15 s) and centrifuged (10 000 rcf, 2 min, 4 °C). The lysate (50,000 cells in 20 µL) was then transferred to a new tube and used in the assay or stored in the freezer at – 20 °C.

### **6.6.3. Probe testing in lysates**

All the experiments on the plate with the probe has been carried out in 100 µL volumes in each well. Firstly, 20 µL of lysate (50,000 H1299 LUC cells), 1 µL of D-cysteine (100 mM frozen stock in water diluted to 2 mM and then used for addition to the well to final concentration of 20 µM), 10 µL of FAS (freshly prepared 1 mM or 2 mM stock in water was used to then add to the well for a final concentration of 100 µM or 200 µM) and 20 µL of luciferase (from a stock of 100 µg/mL to the

final well concentration of 20  $\mu\text{g}/\text{mL}$ ) were all mixed on the plate in the well. Then 20  $\mu\text{L}$  of substrate buffer containing  $\text{MgSO}_4$  (50 mM for final well concentration of 10 mM) EDTA (5 mM for final well concentration of 1 mM) and Tris-HCl (125 mM for final well concentration of 25 mM) was mixed with 5  $\mu\text{L}$  of OH-CBT or the probe solution (from 2 mM stock solution for a final concentration of 100  $\mu\text{M}$ ) and added to the well. Then, the solution in the well was filled up with miliQ water to 90  $\mu\text{L}$  and ATP was added (20 mM stock solution in miliQ water to the final concentration of 2 mM) to commence the reaction and the plate was immediately placed in the IVIS Imaging System chamber and data collected according to the protocol below.

### **6.6.4. Probe testing in live cells**

For iron(II) exposure experiments in live cells, ferrous ammonium sulfate (FAS) was used. A stock solution (100 mM in miliQ water prepared from solid form of the salt) was prepared freshly every time just before the experiment (to minimize any degradation / oxidation) and added to clear RPMI medium for a final concentration of 100  $\mu\text{M}$  or 200  $\mu\text{M}$ . Such medium was then used to replace a medium in which cells were growing for 24h (on 96-well plate) and the cells were incubated in it for 1h or 24h at 37°C, depending on the experiment (details on the figures). After a dedicated time of incubation, FAS-containing medium was aspirated, cell washed once with PBS and 100  $\mu\text{l}$  of D-Cys solution (100  $\mu\text{M}$ ) in RPMI medium was added to each well, and cells incubated 30 min in 37°C. Then, medium was removed, cells washed once with PBS and 20  $\mu\text{L}$  of substrate buffer containing Tris-HCl (25 mM),  $\text{MgSO}_4$  (10 mM), EDTA (1 mM) and ATP (5 mM) was added. Finally, 80  $\mu\text{L}$  of substrate buffer (Tris-HCl at 25 mM,  $\text{MgSO}_4$  at 10 mM), EDTA at 1 mM and ATP at 5 mM) supplemented with the desired concentration of probe or OH-CBT was added at the same time to all wells using multichannel pipette, plate shook briefly and placed immediately in the IVIS Imaging System chamber for measurements.

### **6.6.5. Bioluminescence recording of cell samples:**

IVIS Imaging System was used for those samples with 5 min exposure/measurement, 6 time points with no time breaks between measurements. The results were analyzed in Living Image Software, Excel, and GraphPad Prism programs.

## 7. Bibliography

1. Kaskova, Z. M., Tsarkova, A. S. & Yampolsky, I. V. 1001 lights: Luciferins, luciferases, their mechanisms of action and applications in chemical analysis, biology and medicine. *Chem. Soc. Rev.* **45**, 6048–6077 (2016).
2. Widder, E. A. Bioluminescence in the ocean: Origins of biological, chemical, and ecological diversity. *Science* **328**, 704-708 (2010).
3. Lee, J. Bioluminescence: the First 3000 Years (Review). *J. Sib. Fed. Univ. Biol.* **1**, 194–205 (2008).
4. Syed, A. J. & Anderson, J. C. Applications of bioluminescence in biotechnology and beyond. *Chem. Soc. Rev.* **50**, 5668–5705 (2021).
5. Prescher, J. A. & Contag, C. H. Guided by the light: visualizing biomolecular processes in living animals with bioluminescence. *Curr. Opin. Chem. Biol.* **14**, 80–89 (2010).
6. Cordeau, P. & Kriz, J. *Real-time imaging after cerebral ischemia: Model systems for visualization of inflammation and neuronal repair. Methods Enzymol.* **506**, 117-133 (2012).
7. Bakhsheshian, J. *et al.* Bioluminescent imaging of drug efflux at the blood-brain barrier mediated by the transporter ABCG2. *Proc. Natl. Acad. Sci. U. S. A.* **110**, 20801–20806 (2013).
8. Zhang, Y., Pullambhatla, M., Laterra, J. & Pomper, M. G. Influence of bioluminescence imaging dynamics by dluciferin uptake and efflux mechanisms. *Mol. Imaging* **11**, 499–506 (2012).
9. Gibbons, A. E., Luker, K. E. & Luker, G. D. Dual reporter bioluminescence imaging with NanoLuc and firefly luciferase. *Methods Mol. Biol.* **1790**, 41–50 (2018).
10. Takakura, H. Molecular design of d-luciferin-based bioluminescence and 1,2-dioxetane-based chemiluminescence substrates for altered output wavelength and detecting various molecules. *Molecules* **26**, 1-21 (2021).
11. Endo, M. & Ozawa, T. Advanced bioluminescence system for in vivo imaging

## Chapter 7: Bibliography

- with brighter and red-shifted light emission. *Int. J. Mol. Sci.* **21**, 1–19 (2020).
12. Virostko, J. & Jansen, E. D. Validation of bioluminescent imaging techniques. *Methods Mol. Biol.* **574**, 15–23 (2009).
  13. Podsiadły, R. *et al.* Recent progress in the synthesis of firefly luciferin derivatives. *Dye. Pigment.* **170**, 107627 (2019).
  14. Shinde, R., Perkins, J. & Contag, C. H. Luciferin derivatives for enhanced in vitro and in vivo bioluminescence assays. *Biochemistry* **45**, 11103–11112 (2006).
  15. Coutant, E. P. & Janin, Y. L. Synthetic Routes to Coelenterazine and Other Imidazo[1,2-a]pyrazin-3-one Luciferins: Essential Tools for Bioluminescence-Based Investigations. *Chem. - A Eur. J.* **21**, 17158–17171 (2015).
  16. Boute, N. *et al.* NanoLuc Luciferase - A multifunctional tool for high throughput antibody screening. *Front. Pharmacol.* **7**, 1–11 (2016).
  17. Gaspar, N. *et al.* Evaluation of NanoLuc substrates for bioluminescence imaging of transferred cells in mice. *J. Photochem. Photobiol. B Biol.* **216**, (2021).
  18. Jiang, T., Du, L. & Li, M. Lighting up bioluminescence with coelenterazine: Strategies and applications. *Photochem. Photobiol. Sci.* **15**, 466–480 (2016).
  19. Fraga, H., Fernandes, D., Fontes, R. & Esteves Da Silva, J. C. G. Coenzyme A affects firefly luciferase luminescence because it acts as a substrate and not as an allosteric effector. *FEBS J.* **272**, 5206–5216 (2005).
  20. Li, J., Chen, L., Du, L. & Li, M. Cage the firefly luciferin! - A strategy for developing bioluminescent probes. *Chem. Soc. Rev.* **42**, 662–676 (2013).
  21. Mcelroy, W. D., Seliger, H. H. & White, E. H. Mechanism of Bioluminescence, Chemi-Luminescence and Enzyme Function in the Oxidation of Firefly Luciferin. *Photochem. Photobiol.* **10**, 153–170 (1969).
  22. Tung, J. K., Berglund, K., Gutekunst, C.-A., Hochgeschwender, U. & Gross,

## Chapter 7: Bibliography

- R. E. Bioluminescence imaging in live cells and animals. *Neurophotonics* **3**, 1-6 (2016).
23. Mezzanotte, L., van 't Root, M., Karatas, H., Goun, E. A. & Löwik, C. W. G. M. In Vivo Molecular Bioluminescence Imaging: New Tools and Applications. *Trends Biotechnol.* **35**, 640–652 (2017).
24. Maria Maddalena Calabretta & Michelini, E. Current advances in the use of bioluminescence assays for drug discovery: an update of the last ten years. *Expert Opin. Drug Discov.* **19**, 85-95 (2024).
25. Breton, B. *et al.* Multiplexing of multicolor bioluminescence resonance energy transfer. *Biophys. J.* **99**, 4037–4046 (2010).
26. Kobayashi, H., Picard, L. P., Schönege, A. M. & Bouvier, M. Bioluminescence resonance energy transfer–based imaging of protein–protein interactions in living cells. *Nat. Protoc.* **14**, 1084–1107 (2019).
27. Westerhausen, S. *et al.* A NanoLuc luciferase-based assay enabling the real-time analysis of protein secretion and injection by bacterial type III secretion systems. *Mol. Microbiol.* **113**, 1240–1254 (2020).
28. Sadikot, R. T. & Blackwell, T. S. Bioluminescence imaging. *Proc. Am. Thorac. Soc.* **2**, 537–540 (2005).
29. de Almeida, P. E., van Rappard, J. R. M. & Wu, J. C. In vivo bioluminescence for tracking cell fate and function. *Am. J. Physiol. - Hear. Circ. Physiol.* **301**, 663–671 (2011).
30. Kim, S. J. & Lee, H. Y. In vivo molecular imaging in preclinical research. *Lab. Anim. Res.* **38**, 1–6 (2022).
31. Rice, B. W., Cable, M. D. & Nelson, M. B. In vivo imaging of light-emitting probes. *J. Biomed. Opt.* **6**, 432-440 (2001).
32. Paley, M. A. & Prescher, J. A. Bioluminescence: A versatile technique for imaging cellular and molecular features. *Medchemcomm* **5**, 255–267 (2014).
33. Badr, C. E. & Tannous, B. A. Bioluminescence imaging: Progress and applications. *Trends Biotechnol.* **29**, 624–633 (2011).

## Chapter 7: Bibliography

34. Anuj K Yadav & Jefferson Chan. Activity-based bioluminescence probes for in vivo sensing applications. *Curr. Opin. Chem. Biol.* **74**, (2023).
35. Prost, M. & Hasserodt, J. "Double gating" – a concept for enzyme-responsive imaging probes aiming at high tissue specificity. *Chem. Commun.* **50**, 14896–14899 (2014).
36. Kolanowski, J. L., Liu, F. & New, E. J. Fluorescent probes for the simultaneous detection of multiple analytes in biology. *Chem. Soc. Rev.* **47**, 195–208 (2018).
37. Wang, C. *et al.* An AND-gate bioluminescent probe for precise tumor imaging. *Chem. Sci.* **14**, 5768–5773 (2023).
38. Van De Bittner, G. C., Bertozzi, C. R. & Chang, C. J. Strategy for dual-analyte luciferin imaging: In vivo bioluminescence detection of hydrogen peroxide and caspase activity in a murine model of acute inflammation. *J. Am. Chem. Soc.* **135**, 1783–1795 (2013).
39. Godinat, A. *et al.* A biocompatible 'split luciferin' reaction and its application for non-invasive bioluminescent imaging of protease activity in living animals. *Curr. Protoc. Chem. Biol.* **6**, 169–189 (2014).
40. Ren, H. *et al.* A biocompatible condensation reaction for the labeling of terminal cysteine residues on proteins. *Angew. Chemie - Int. Ed.* **48**, 9658–9662 (2009).
41. Feng, P. *et al.* Real-Time Bioluminescence Imaging of Nitroreductase in Mouse Model. *Anal. Chem.* **88**, 5610–5614 (2016).
42. Chen, P. *et al.* Bioluminescent Turn-On Probe for Sensing Hypochlorite in Vitro and in Tumors. *Anal. Chem.* **89**, 5693–5696 (2017).
43. Mofford, D. M., Adams, S. T., Reddy, G. S. K. K., Reddy, G. R. & Miller, S. C. Luciferin Amides Enable in Vivo Bioluminescence Detection of Endogenous Fatty Acid Amide Hydrolase Activity. *J. Am. Chem. Soc.* **137**, 8684–8687 (2015).
44. Zheng, Z. *et al.* Hydrazide d-luciferin for in vitro selective detection and intratumoral imaging of Cu<sup>2+</sup>. *Biosens. Bioelectron.* **83**, 200–204 (2016).

## Chapter 7: Bibliography

45. Heffern, M. C. *et al.* In vivo bioluminescence imaging reveals copper deficiency in a murine model of nonalcoholic fatty liver disease. *Proc. Natl. Acad. Sci. U. S. A.* **113**, 14219–14224 (2016).
46. Aron, A. T. *et al.* In vivo bioluminescence imaging of labile iron accumulation in a murine model of *Acinetobacter baumannii* infection. *Proc. Natl. Acad. Sci. U. S. A.* **114**, 12669–12674 (2017).
47. Li, J. Bin *et al.* A Bioluminescent Probe for Imaging Endogenous Peroxynitrite in Living Cells and Mice. *Anal. Chem.* **90**, 4167–4173 (2018).
48. Lin, Y. *et al.* Bioluminescence probe for  $\gamma$ -glutamyl transpeptidase detection in vivo. *Bioorganic Med. Chem.* **26**, 134–140 (2018).
49. Zhou, W. *et al.* New bioluminogenic substrates for monoamine oxidase assays. *J. Am. Chem. Soc.* **128**, 3122–3123 (2006).
50. Monsees, T., Miska, W. & Geiger, R. Synthesis and Characterization of a Bioluminogenic Substrate for alpha-Chymotrypsin. *Anal. Biochem.* **221**, 239–334 (1994).
51. Ke, B. *et al.* In Vivo Bioluminescence Imaging of Cobalt Accumulation in a Mouse Model. *Anal. Chem.* **90**, 4946–4950 (2018).
52. Scabini, M. *et al.* In vivo imaging of early stage apoptosis by measuring real-time caspase-3/7 activation. *Apoptosis* **16**, 198–207 (2011).
53. Li, S. *et al.* Specific Imaging of Tyrosinase in Vivo with 3-Hydroxybenzyl Caged D -Luciferins. *Anal. Chem.* **90**, 9296–9300 (2018).
54. Zhou, W. *et al.* Electrophilic aromatic substituted luciferins as bioluminescent probes for glutathione S-transferase assays. *Chem. Commun.* 4620–4622 (2006).
55. Yang, L. *et al.*  $\beta$ -Glucuronidase-Activated Bioluminescence Probe for In Vivo Tumor Imaging. *Anal. Chem.* **95**, 14165–14168 (2023).
56. Meisenheimer, P., Walker, J. R. & Wenhui, Z. Dual protected pro-coelenterazine substrates. *EP3510035B1* (2017).
57. Zullo, A., Guida, R., Sciarrillo, R. & Mancini, F. P. Redox Homeostasis in Cardiovascular Disease: The Role of Mitochondrial Sirtuins. *Front.*

## Chapter 7: Bibliography

- Endocrinol. (Lausanne)*. **13**, 1–8 (2022).
58. Li, Y., Zhang, X., Wang, Z., Li, B. & Zhu, H. Modulation of redox homeostasis: A strategy to overcome cancer drug resistance. *Front. Pharmacol.* **14**, 1–16 (2023).
  59. Azarova, I., Polonikov, A. & Klyosova, E. Molecular Genetics of Abnormal Redox Homeostasis in Type 2 Diabetes Mellitus. *Int. J. Mol. Sci.* **24**, (2023).
  60. Dutta, R. K. *et al.* Catalase deficiency facilitates the shuttling of free fatty acid to brown adipose tissue through lipolysis mediated by ROS during sustained fasting. *Cell Biosci.* **11**, 1–14 (2021).
  61. Ferreira-Cravo, M., Moreira, D. C. & Hermes-Lima, M. Glutathione Depletion Disrupts Redox Homeostasis in an Anoxia-Tolerant Invertebrate. *Antioxidants* **12**, 1–14 (2023).
  62. Le Gal, K., Schmidt, E. E. & Sayin, V. I. Cellular redox homeostasis. *Antioxidants* **10**, 1–7 (2021).
  63. Mitrić, A. & Castellano, I. Targeting gamma-glutamyl transpeptidase: A pleiotropic enzyme involved in glutathione metabolism and in the control of redox homeostasis. *Free Radic. Biol. Med.* **208**, 672–683 (2023).
  64. Galaris, D., Barbouti, A. & Pantopoulos, K. Iron homeostasis and oxidative stress: An intimate relationship. *Biochim. Biophys. Acta - Mol. Cell Res.* **1866**, 118535 (2019).
  65. Chen, Z., Han, F., Du, Y., Shi, H. & Zhou, W. Hypoxic microenvironment in cancer: molecular mechanisms and therapeutic interventions. *Signal Transduct. Target. Ther.* **8**, (2023).
  66. Koleini, N., Shapiro, J. S., Geier, J. & Ardehali, H. Ironing out mechanisms of iron homeostasis and disorders of iron deficiency. *J. Clin. Invest.* **131**, 1–11 (2021).
  67. Hong, T. C. *et al.* Relationship between serum gamma-glutamyl transferase level and colorectal adenoma. *PLoS One* **15**, 1–8 (2020).
  68. Hanigan, M. H. *Gamma-glutamyl transpeptidase: Redox regulation and drug resistance.* *Adv. Cancer Res.* **122**, 103–141 (Elsevier Inc., 2014).



## Chapter 7: Bibliography

69. Feng, P. *et al.* In vivo bioluminescence imaging of labile iron pools in a murine model of sepsis with a highly selective probe. *Talanta* **203**, 29–33 (2019).
70. Stanley, L. A. Drug Metabolism. *Pharmacognosy: Fundamentals, Applications and Strategy* (Elsevier Inc., 2017).
71. Gutkina, E. A., Rubtsova, T. B. & Shteinman, A. A. Synthesis and catalytic activity of the Fe(II) and Fe(III) complexes with a new polydentate ligand containing an amide donor. *Kinet. Catal.* **44**, 106–111 (2003).
72. Chen, K. T., Nguyen, K., Ieritano, C., Gao, F. & Seimbille, Y. A flexible synthesis of <sup>68</sup>Ga-labeled carbonic anhydrase IX (CAIX)-targeted molecules via CBT/1,2-aminothiols click reaction. *Molecules* **24**, 1–13 (2019).
73. Lee, R. T., Denburg, J. L. & McElroy, W. D. Substrate-binding properties of firefly luciferase. II. ATP-binding site. *Arch. Biochem. Biophys.* **141**, 38–52 (1970).
74. Mitchell, P. & Moyle, J. Metal complexing by TRIS buffer. *Nat. Publ. Gr.* **216**, 615–616 (1967).
75. Mundra, S., Tits, J., Wieland, E. & Angst, U. M. Aerobic and anaerobic oxidation of ferrous ions in near-neutral solutions. *Chemosphere* **335**, 138955 (2023).
76. Orino, K., Kamura, S., Natsuhori, M., Yamamoto, S. & Watanabe, K. Two pathways of iron uptake in bovine spleen apoferritin dependent on iron concentration. *BioMetals* **15**, 59–63 (2002).
77. Karan, S. *et al.* Hypoxia-Directed and Self-Immolative Theranostic Agent: Imaging and Treatment of Cancer and Bacterial Infections. *J. Med. Chem.* **66**, 14175–14187 (2023).
78. Liu, F., Zhang, H., Li, K., Xie, Y. & Li, Z. A novel nir fluorescent probe for highly selective detection of nitroreductase and hypoxic-tumor-cell imaging. *Molecules* **26**, 1–8 (2021).
79. Zhai, B. *et al.* A two-photon fluorescent probe for nitroreductase imaging in living cells, tissues and zebrafish under hypoxia conditions. *Analyst* **142**, 1545–1553 (2017).

## Chapter 7: Bibliography

80. Guo, T. *et al.* A highly sensitive long-wavelength fluorescence probe for nitroreductase and hypoxia: Selective detection and quantification. *Chem. Commun.* **49**, 10820–10822 (2013).
81. Prost, M., Canaple, L., Samarut, J. & Hasserodt, J. Tagging live cells that express specific peptidase activity with solid-state fluorescence. *ChemBioChem* **15**, 1413–1417 (2014).
82. Gravel, C., Lapierre, D., Labelle, J. & Keillor, J. W. Acyl transfer from carboxylate, carbonate, and thiocarbonate esters to enzymatic and nonenzymatic thiolates. *Can. J. Chem.* **85**, 164–174 (2007).
83. Shakhmin, A. *et al.* Three Efficient Methods for Preparation of Coelenterazine Analogues. *Chem. - A Eur. J.* **22**, 10369–10375 (2016).
84. Yan, C., Du, L. & Li, M. Novel NanoLuc-type substrates with various C-6 substitutions. *Bioorganic Med. Chem. Lett.* **30**, 127085 (2020).
85. Yuan, M. L., Jiang, T. Y., Du, L. P. & Li, M. Y. Luminescence of coelenterazine derivatives with C-8 extended electronic conjugation. *Chinese Chem. Lett.* **27**, 550–554 (2016).
86. Shiraki, C., Saito, H., Takahashi, K., Urakawa, C. & Tadashi Hirata. Preparation of Amino(diethoxyphosphoryl)acetic Esters. Catalytic Hydrogenation of Diazo Compounds to Amines. *Synthesis* **5**, 299–401 (1988).
87. Coutant, E. P. *et al.* Gram-scale synthesis of luciferins derived from coelenterazine and original insights into their bioluminescence properties. *Org. Biomol. Chem.* **17**, 3709–3713 (2019).
88. Yang, X., Li, Z., Jiang, T., Du, L. & Li, M. A coelenterazine-type bioluminescent probe for nitroreductase imaging. *Org. Biomol. Chem.* **16**, 146–151 (2017).
89. Shi, X. *et al.* An Efficient Probe for Bacterial Nitroreductase Imaging and Detection Based on NanoLuc-Furimazine Bioluminescent Pair. *Chinese J. Chem.* **42**, 1373–1380 (2024).
90. Lin, Y. *et al.* Bioluminescence probe for  $\gamma$ -glutamyl transpeptidase detection in vivo. *Bioorg. Med. Chem.* **26**, 134–140 (2018).

## Chapter 7: Bibliography

91. Keillor, J. W., Castonguay, R. & Lherbet, C. Gamma-glutamyl transpeptidase substrate specificity and catalytic mechanism. *Methods Enzymol.* **401**, 449–467 (2005).
92. Wang, P. *et al.* Site-specific immobilization of biomolecules by a biocompatible reaction between terminal cysteine and 2-cyanobenzothiazole. *Chem. Commun.* **49**, 8644–8646 (2013).
93. Hauser, J. R. *et al.* Economical and scalable synthesis of 6-amino-2-cyanobenzothiazole. *Beilstein J. Org. Chem.* **12**, 2019–2025 (2016).
94. Kovács, A. K. *et al.* Synthesis of N-peptide-6-amino-D-luciferin conjugates. *Front. Chem.* **6**, 1–11 (2018).
95. Hu, X. *et al.* CBT-Cys click reaction for optical bioimaging in vivo. *View* **4**, 1–9 (2023).
96. Rao, J. *et al.* Exploring condensation reaction between aromatic nitriles and amino thiols to form nanoparticles in cells for imaging the activity of protease and glycosidase. *Angew. Chem. Int. Ed. Engl.* **59**, 3272–3279 (2019).
97. Alouane, A., Labruère, R., Le Saux, T., Schmidt, F. & Jullien, L. Self-immolative spacers: Kinetic aspects, structure-property relationships, and applications. *Angew. Chemie - Int. Ed.* **54**, 7492–7509 (2015).
98. Thorn-Seshold, O., Vargas-Sanchez, M., McKeon, S. & Hasserodt, J. A robust, high-sensitivity stealth probe for peptidases. *Chem. Commun.* **48**, 6253–6255 (2012).
99. Gonzaga, R. V. *et al.* Perspectives About Self-Immolative Drug Delivery Systems. *J. Pharm. Sci.* **109**, 3262–3281 (2020).
100. Gavriel, A. G., Sambrook, M. R., Russell, A. T. & Hayes, W. Recent advances in self-immolative linkers and their applications in polymeric reporting systems. *Polym. Chem.* **13**, 3188–3269 (2022).
101. Dobbs, A. P. *et al.* A detailed investigation of the aza-prins reaction. *Org. Biomol. Chem.* **8**, 1064–1080 (2010).

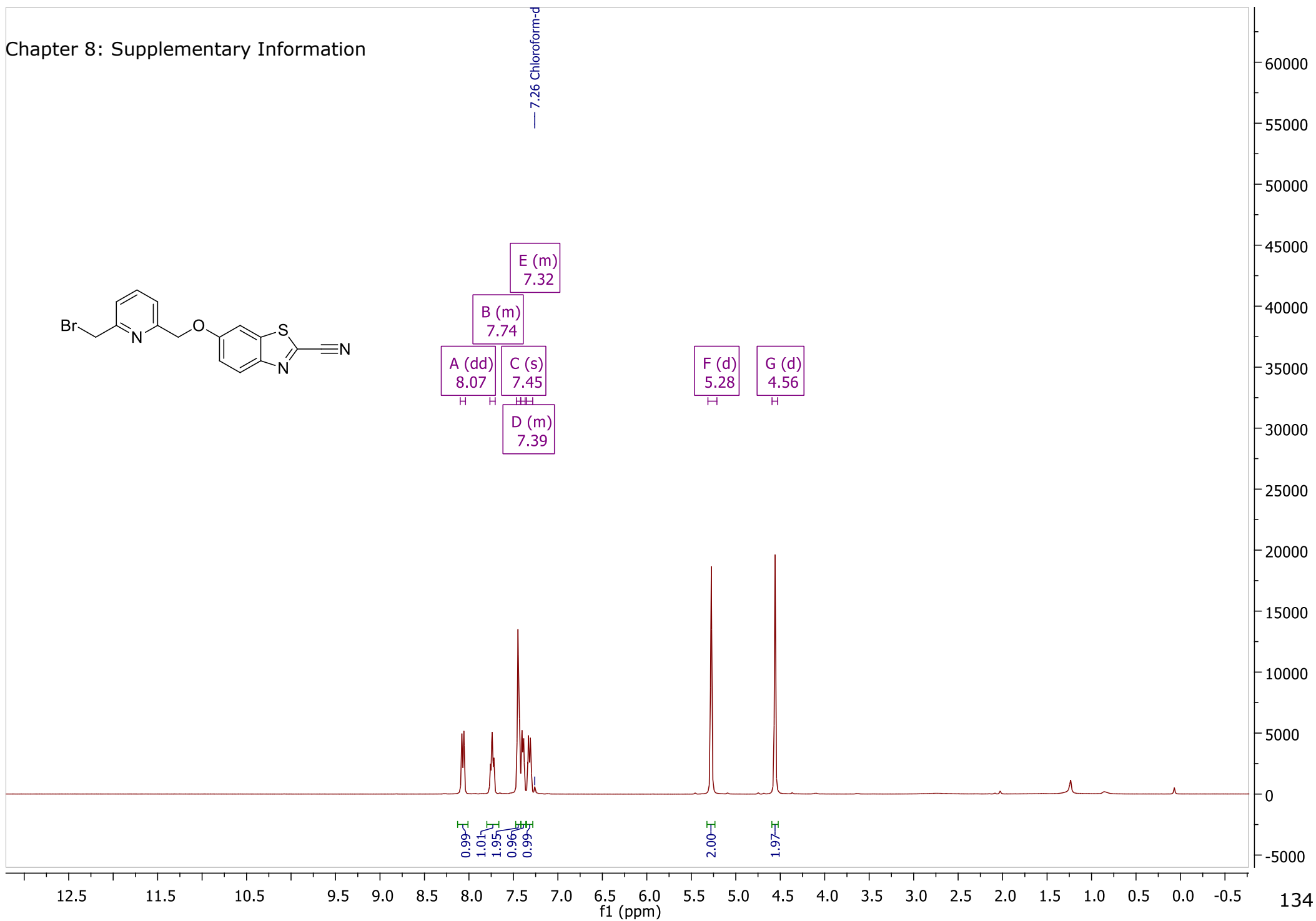
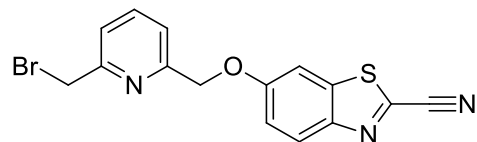
## Chapter 7: Bibliography

102. Anilkumar, G., Nambu, H. & Kita, Y. A simple and efficient iodination of alcohols on polymer-supported triphenylphosphine. *Org. Process Res. Dev.* **6**, 190–191 (2002).
103. Olah, G. A., Narang, S. C., Gupta, B. G. B. & Malhotra, R. Synthetic methods and reactions. 62. Transformations with chlorotrimethylsilane/sodium iodide, a convenient in situ iodotrimethylsilane reagent. *J. Org. Chem.* **44**, 1247–1251 (1979).
104. Khazdooz, L., Zarei, A., Aghaei, H., Azizi, G. & Gheisari, M. M. An efficient and selective method for the iodination and bromination of alcohols under mild conditions. *Tetrahedron Lett.* **57**, 168–171 (2016).
105. Appel, R. Tertiary Phosphane/Tetrachloromethane, a Versatile Reagent for Chlorination, Dehydration, and P-N Linkage. *Angew. Chem. int. Ed. Engl.* **14**, 801–811 (1975).
106. Fuenzalida, N. M. D. R., Alme, E., Lundevall, F. J. & Bjørsvik, H. R. An environmentally benign and high-rate Appel type reaction. *React. Chem. Eng.* **7**, 1650–1659 (2022).
107. Ponpipom, M. M. & Hanessian, S. A method for the selective bromination of primary alcohol groups. *Carbohydr. Res.* **18**, 342–344 (1971).

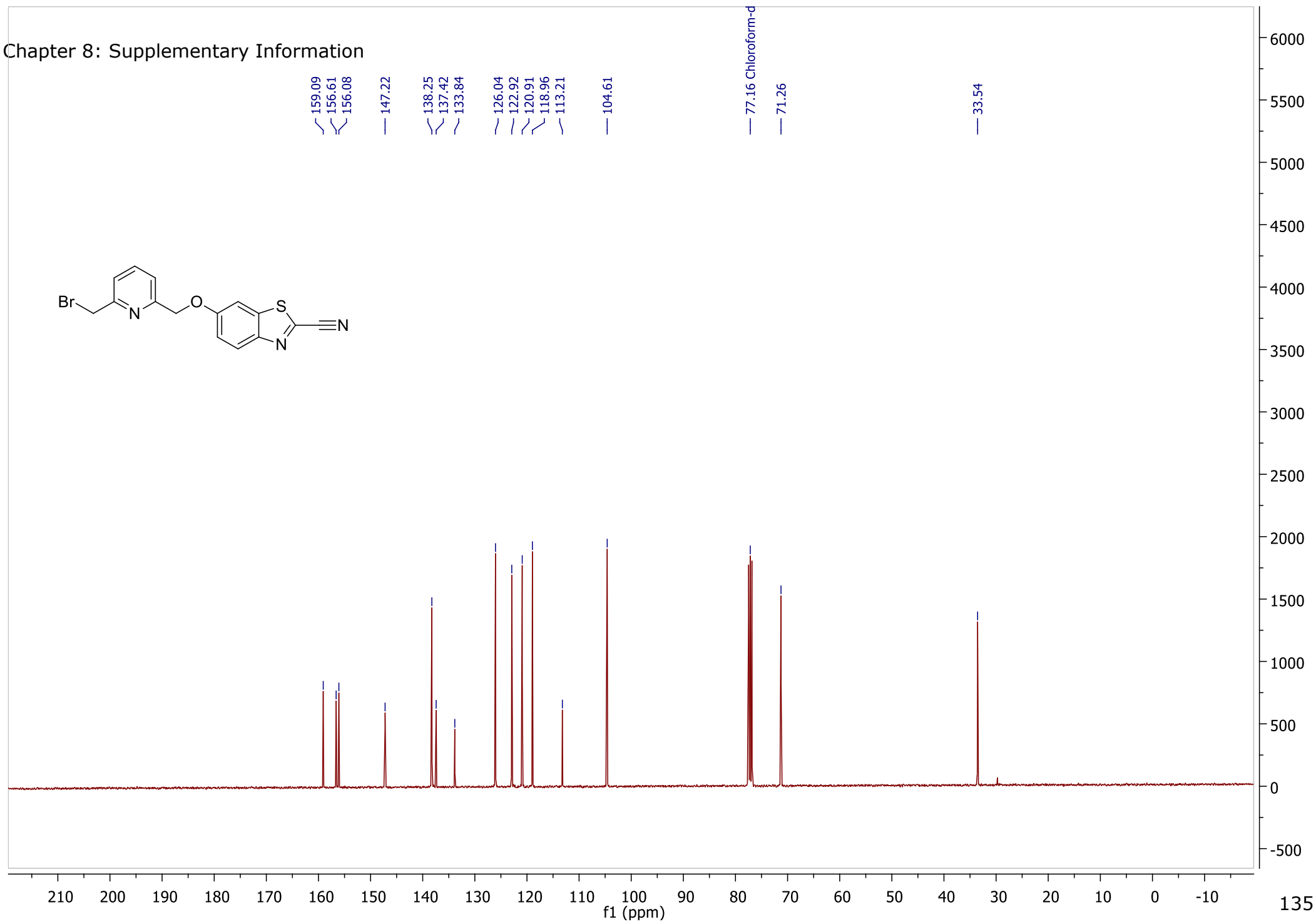
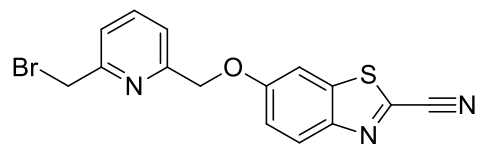
## **8. Supplementary Information**

The accompanying supplementary information provides a comprehensive collection of spectroscopic data (NMR and MS) for all compounds synthesized as detailed in the methodology section of chapter 6. The data is presented in the same order as the corresponding compound descriptions within chapter 6, to facilitate easy cross-referencing.

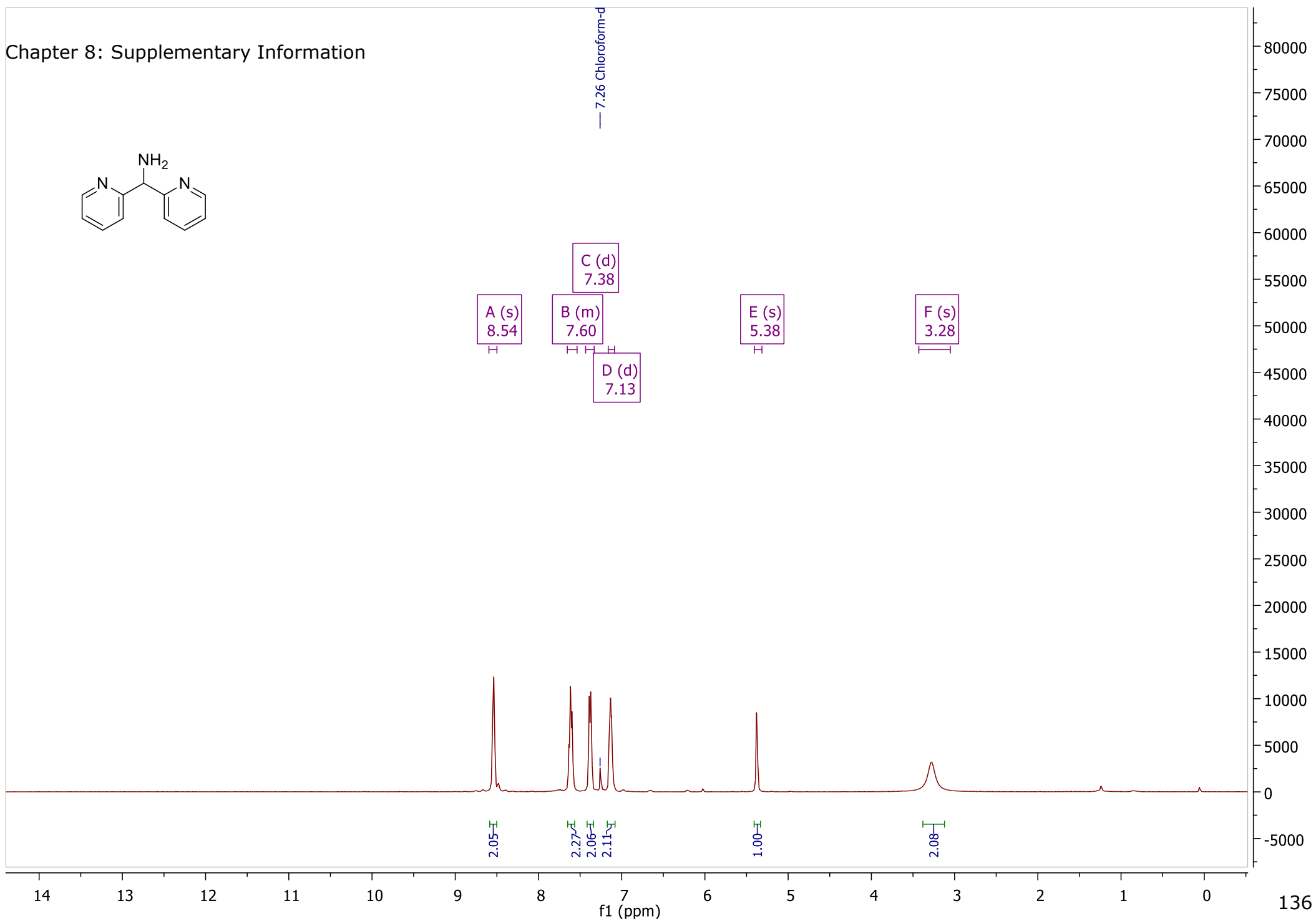
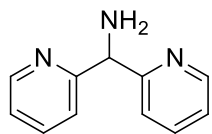
Chapter 8: Supplementary Information



Chapter 8: Supplementary Information

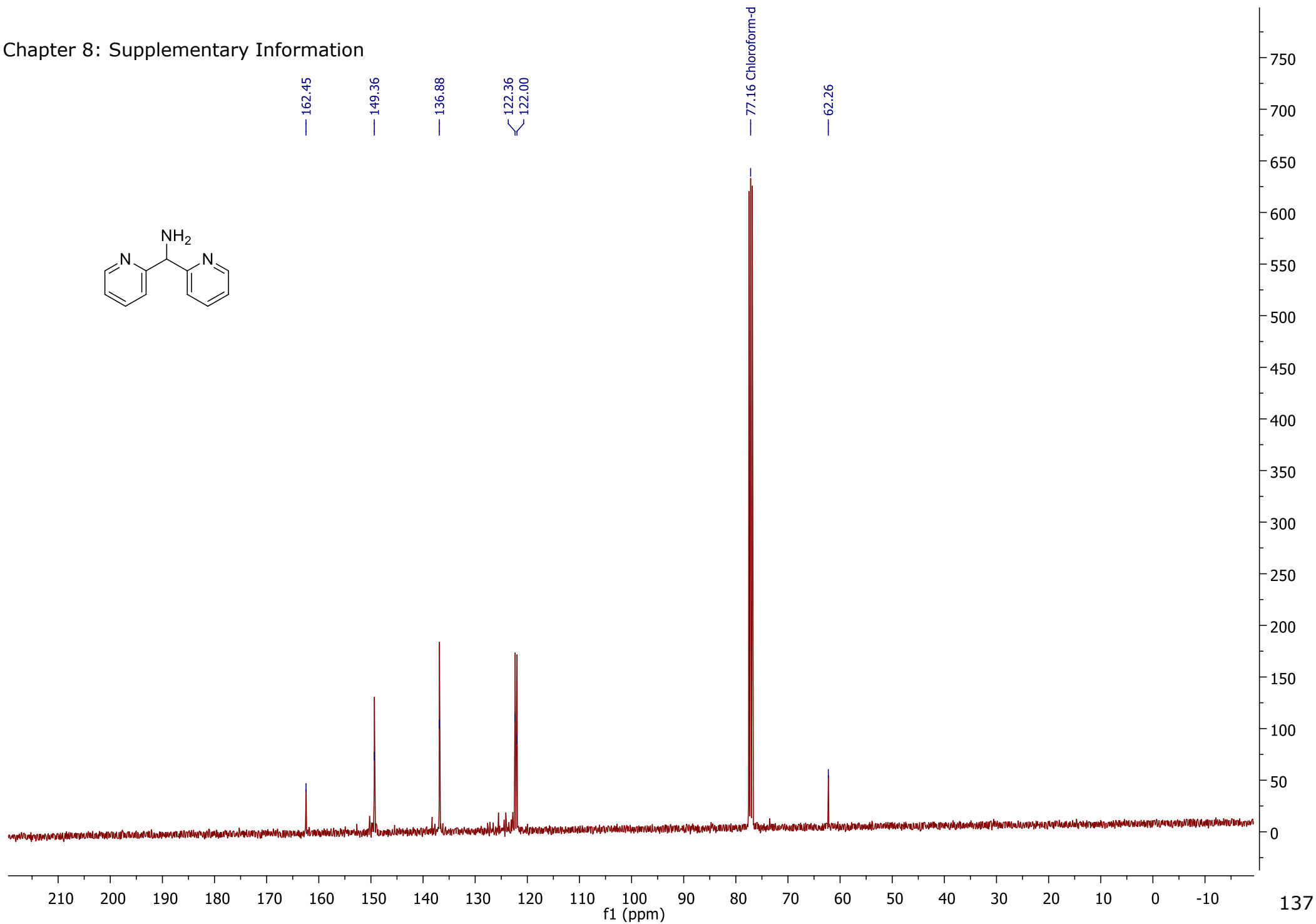
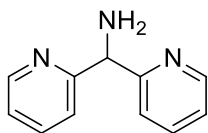


Chapter 8: Supplementary Information

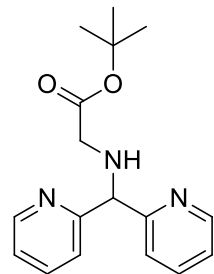




Chapter 8: Supplementary Information



Chapter 8: Supplementary Information



7.26 Chloroform-d

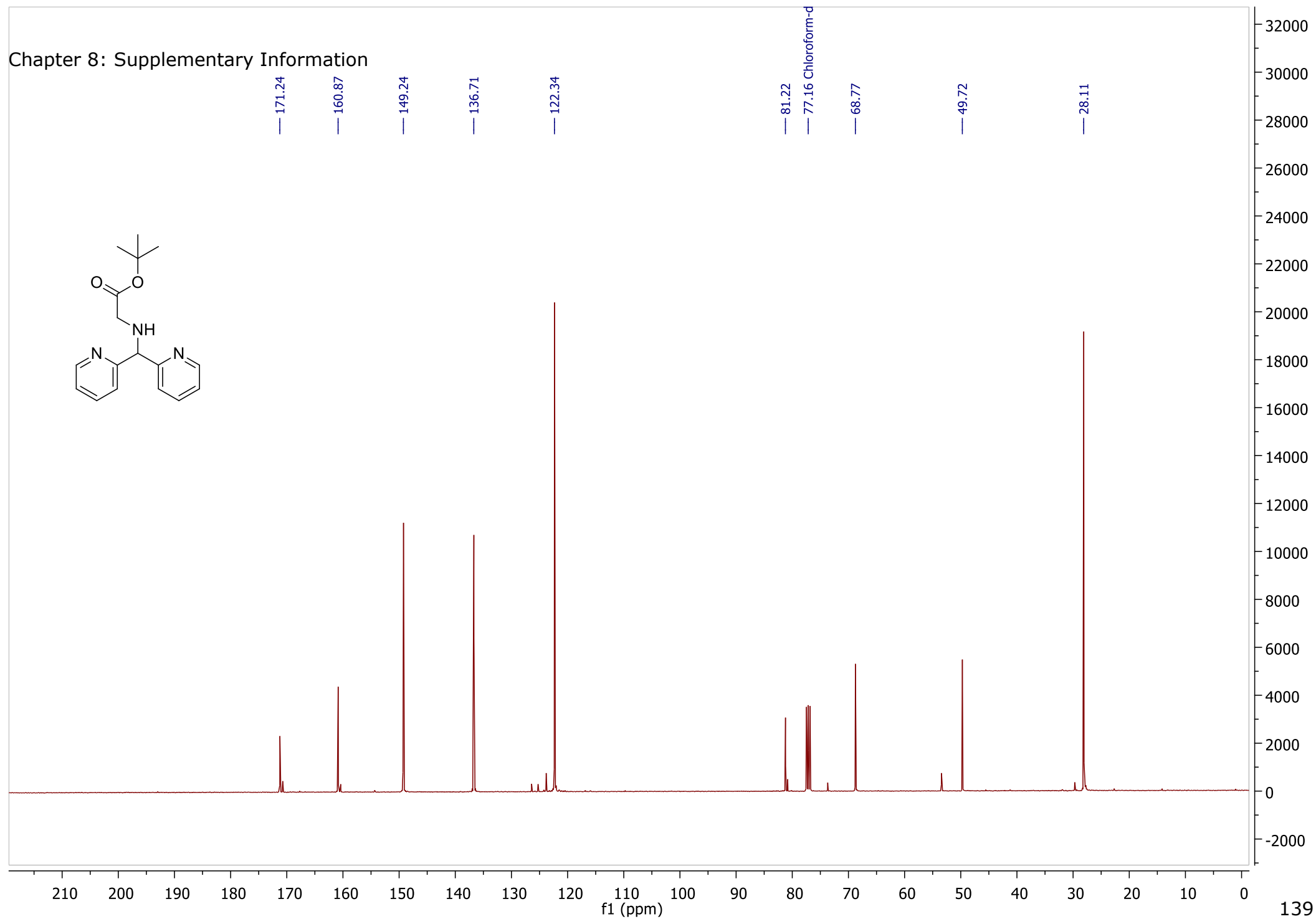
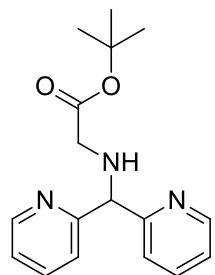
A (m) 8.50  
B (t) 7.56  
C (d) 7.39  
D (m) 7.09  
E (s) 5.10  
F (s) 3.61  
G (s) 3.30  
H (s) 1.38

2.06  
2.19  
1.97  
2.18  
1.00  
1.10  
2.07  
9.27

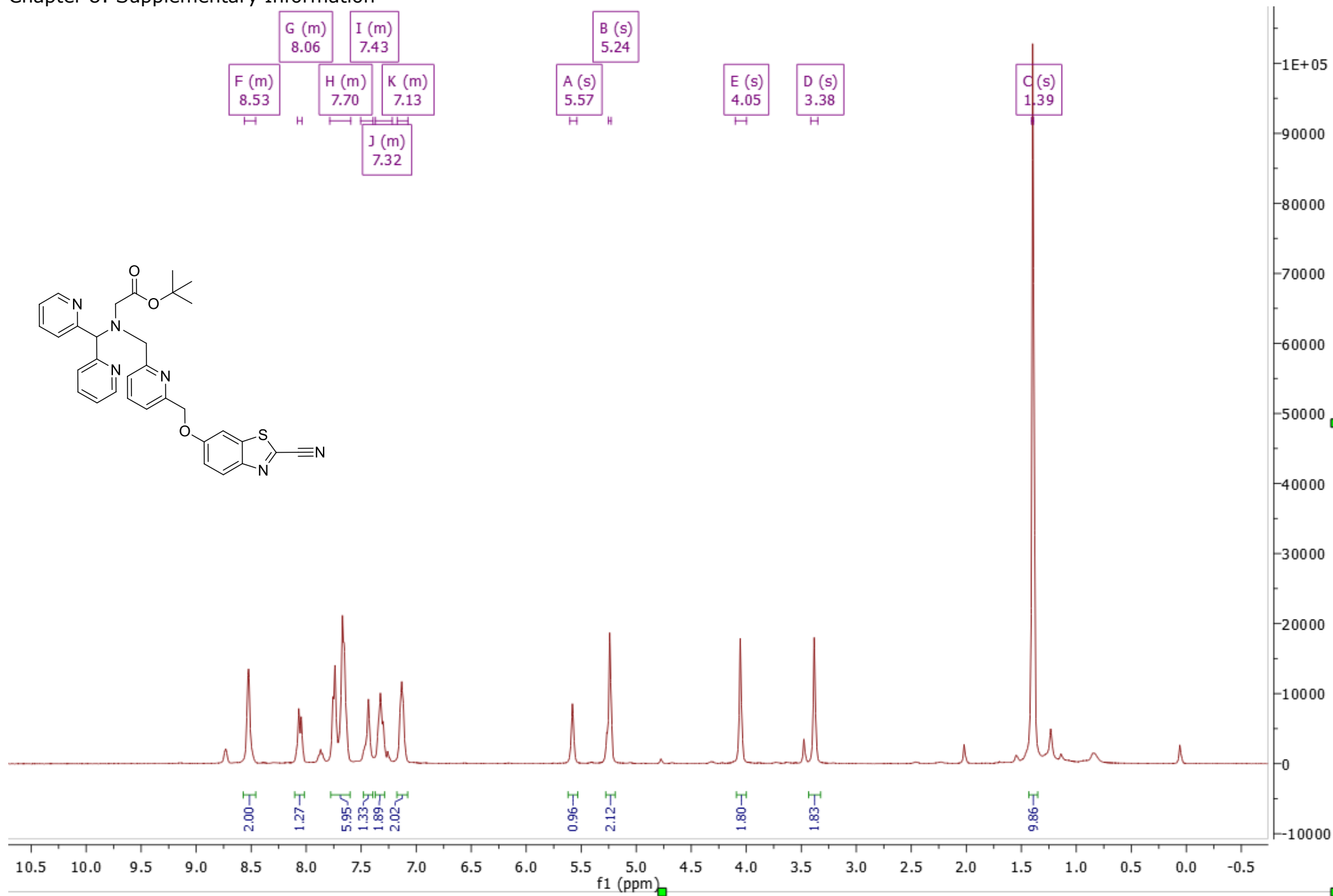
11.0 10.5 10.0 9.5 9.0 8.5 8.0 7.5 7.0 6.5 6.0 5.5 5.0 4.5 4.0 3.5 3.0 2.5 2.0 1.5 1.0 0.5 0.0

f1 (ppm)

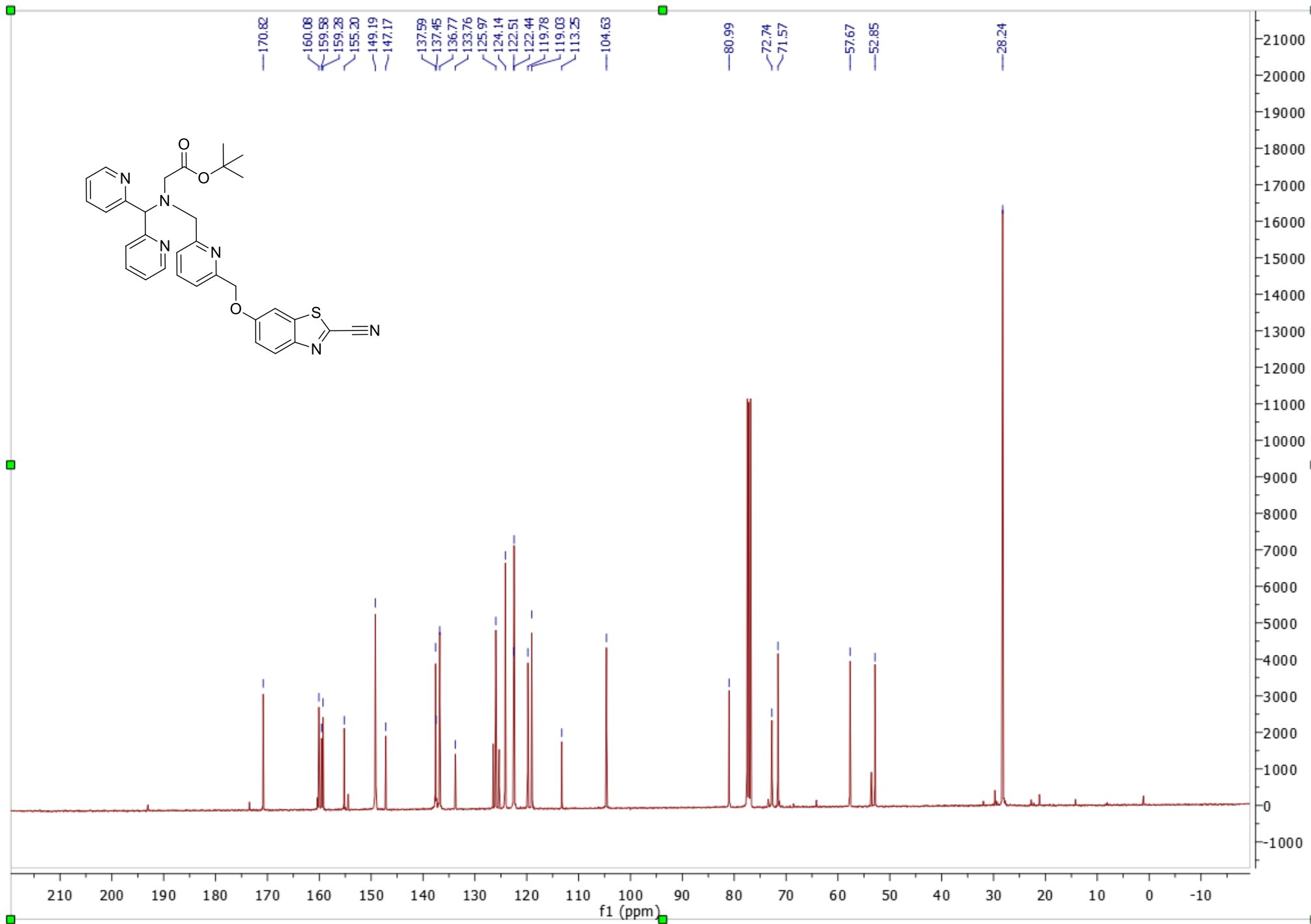
Chapter 8: Supplementary Information



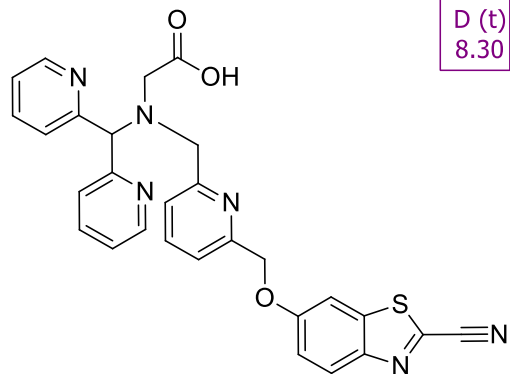
Chapter 8: Supplementary Information



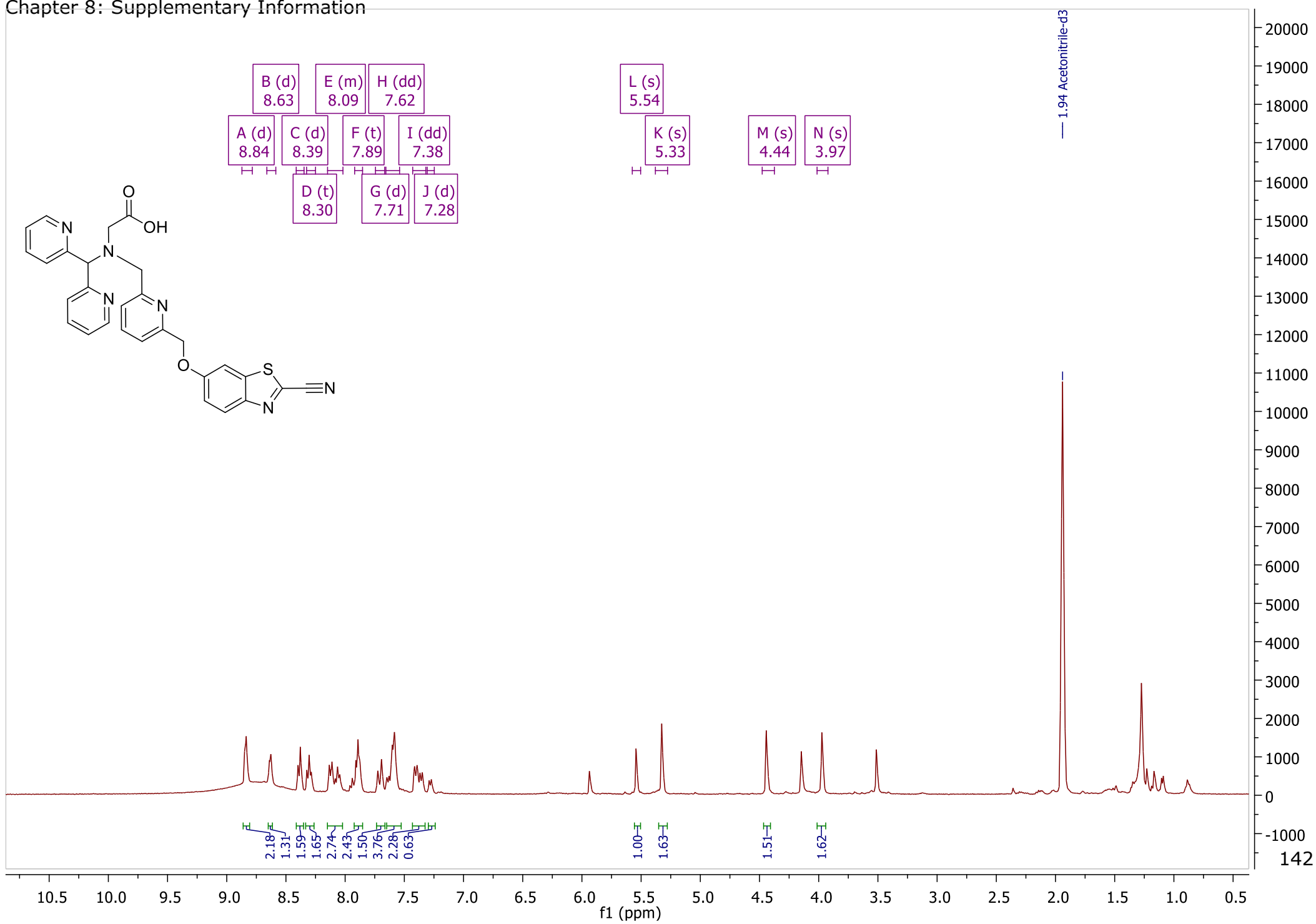
Chapter 8: Supplementary Information



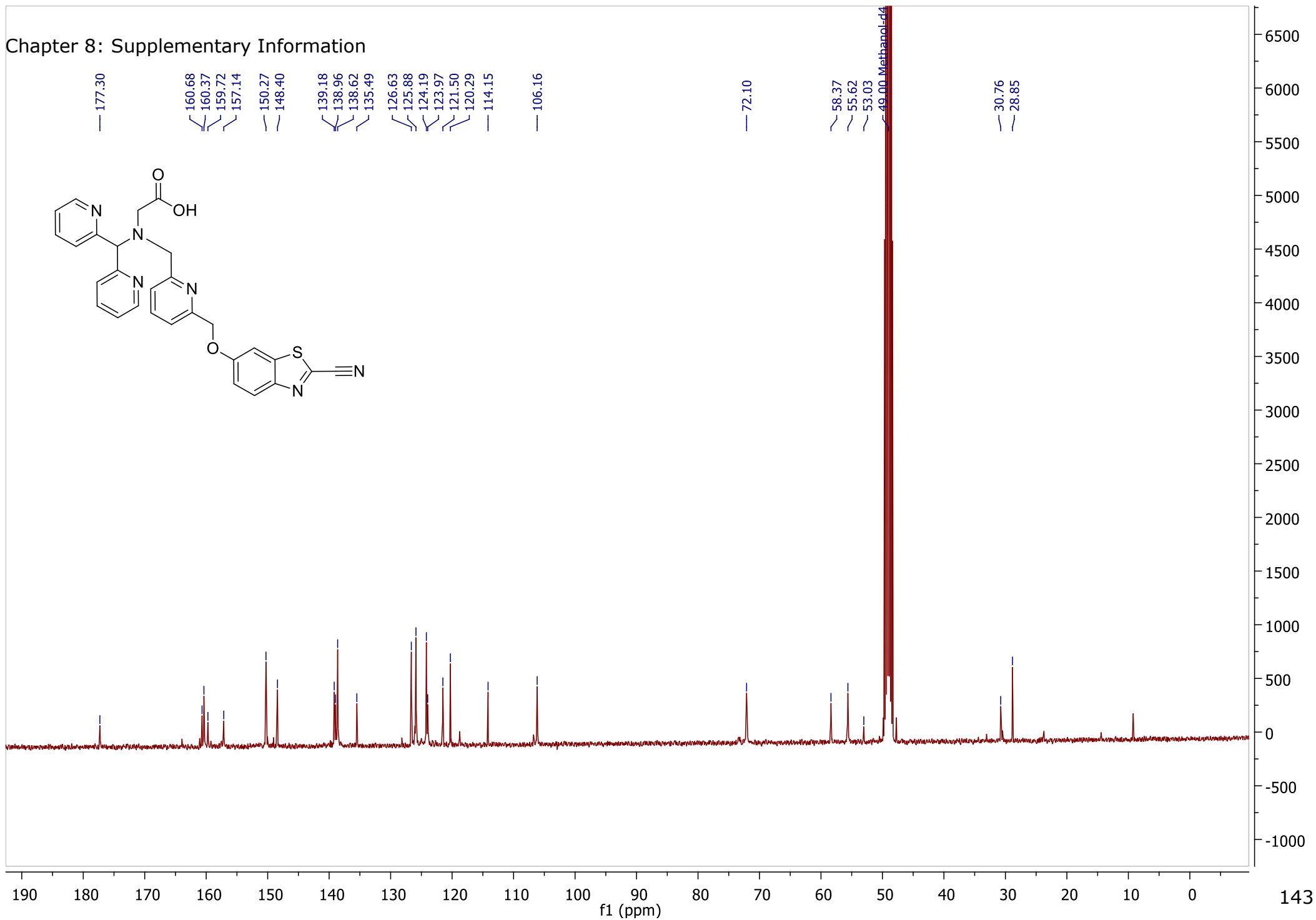
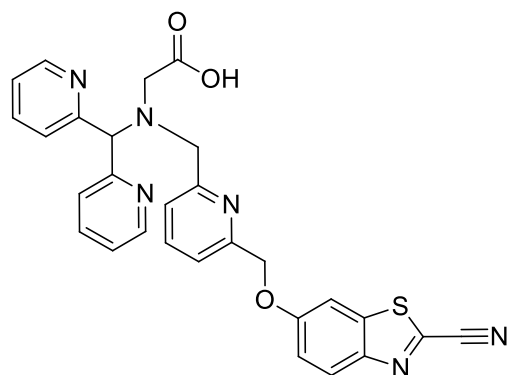
Chapter 8: Supplementary Information



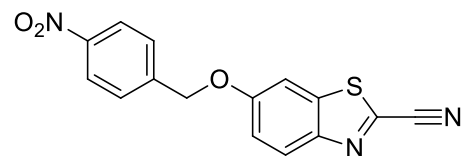
|               |               |               |               |               |               |               |                |                |               |               |               |               |               |
|---------------|---------------|---------------|---------------|---------------|---------------|---------------|----------------|----------------|---------------|---------------|---------------|---------------|---------------|
| A (d)<br>8.84 | B (d)<br>8.63 | C (d)<br>8.39 | D (t)<br>8.30 | E (m)<br>8.09 | F (t)<br>7.89 | G (d)<br>7.71 | H (dd)<br>7.62 | I (dd)<br>7.38 | J (d)<br>7.28 | K (s)<br>5.33 | L (s)<br>5.54 | M (s)<br>4.44 | N (s)<br>3.97 |
|---------------|---------------|---------------|---------------|---------------|---------------|---------------|----------------|----------------|---------------|---------------|---------------|---------------|---------------|



Chapter 8: Supplementary Information



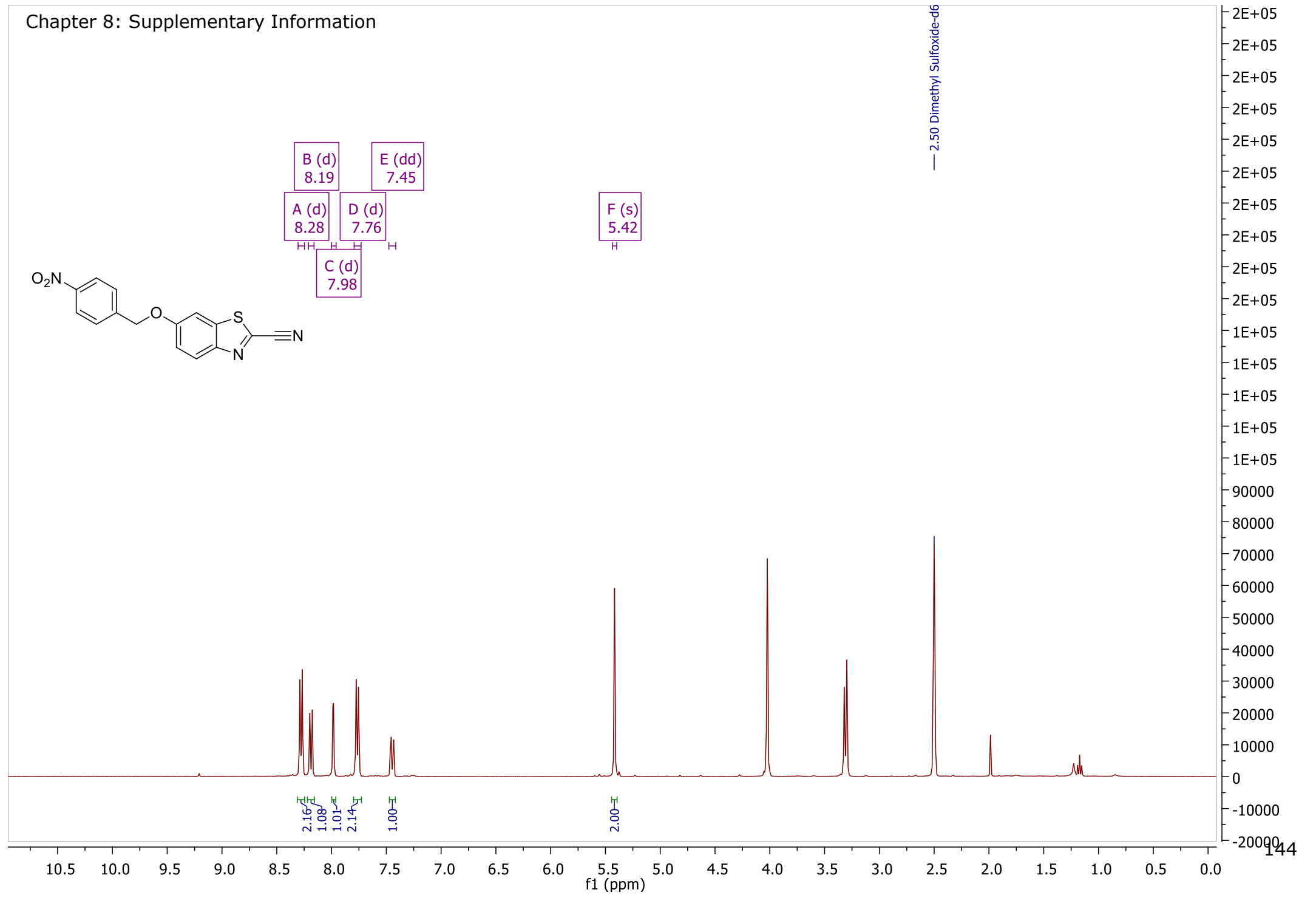
Chapter 8: Supplementary Information



B (d) 8.19  
A (d) 8.28  
C (d) 7.98  
D (d) 7.76  
E (dd) 7.45

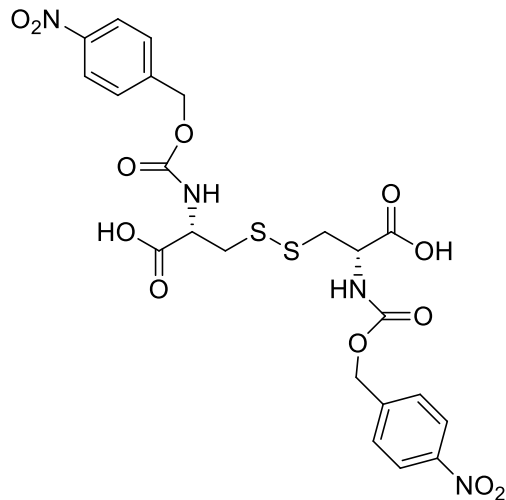
F (s) 5.42

— 2.50 Dimethyl Sulfoxide-d6





Chapter 8: Supplementary Information



B (d)  
8.18  
H

C (d)  
7.54  
H

D (d)  
6.31  
H

A (s)  
5.20  
H

E (dd)  
4.50  
H

F (m)  
3.26  
H H

G (dd)  
3.05

— 1.94 Acetonitrile-d3

2.00

2.08

0.84

2.10

1.07

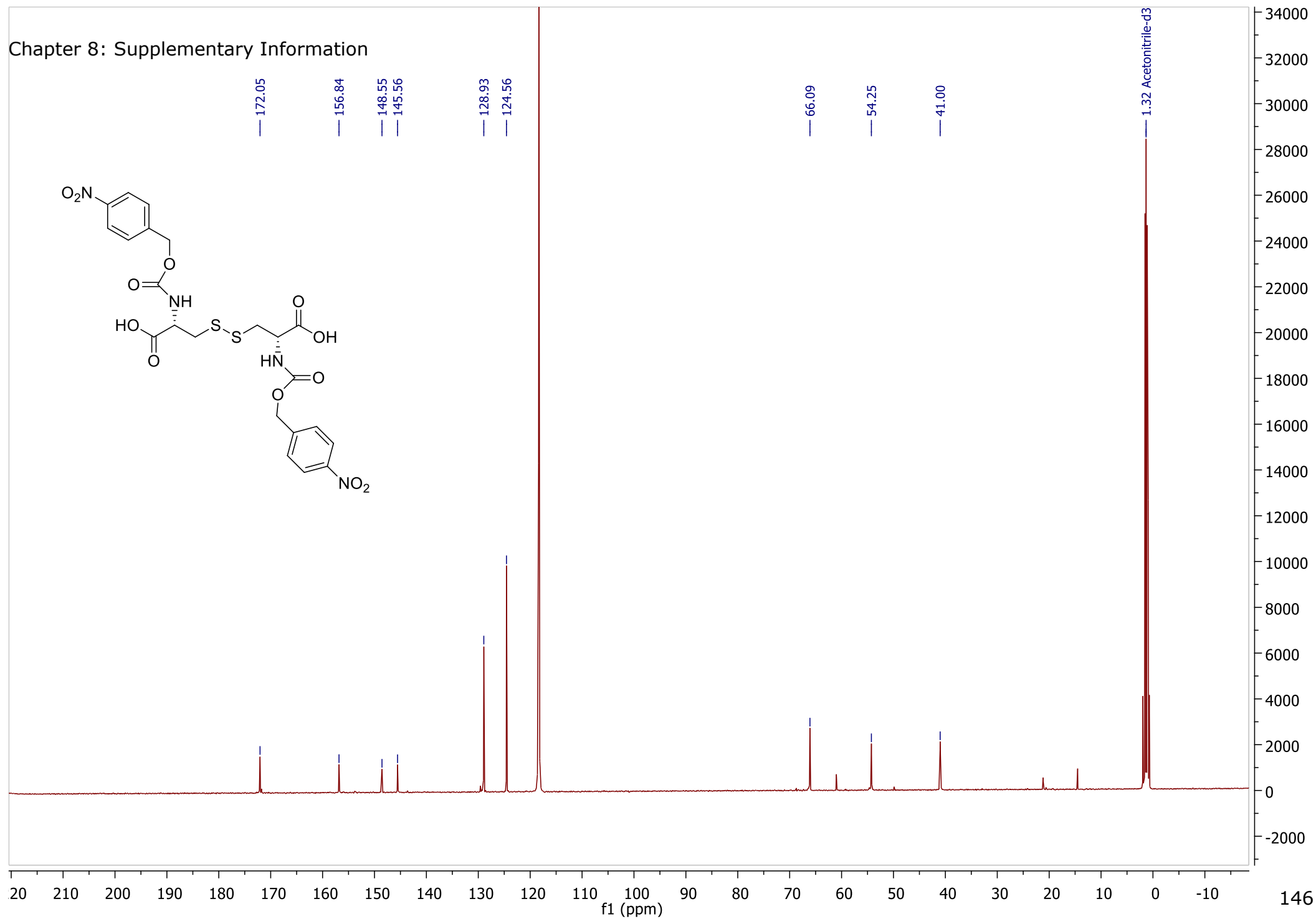
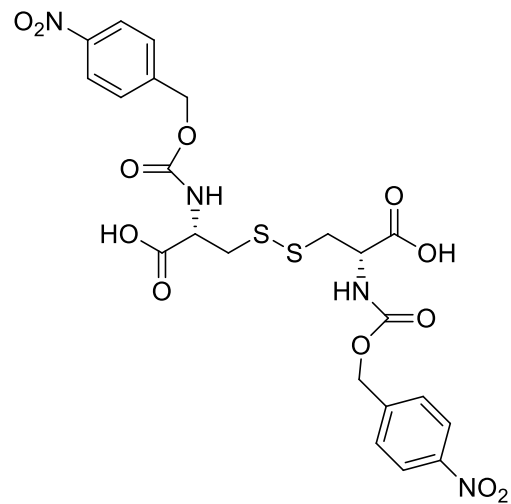
1.33

1.10

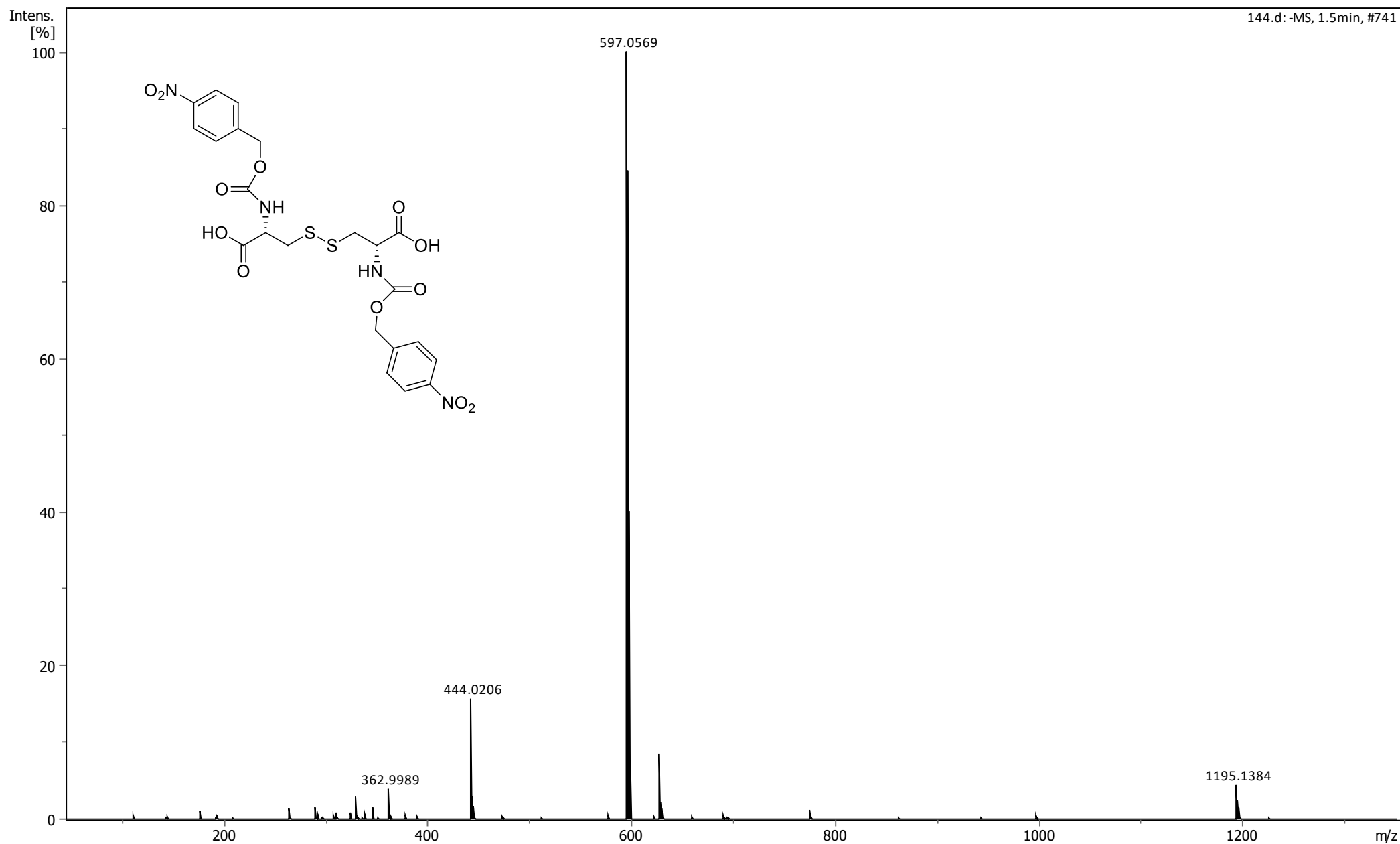
12.0 11.5 11.0 10.5 10.0 9.5 9.0 8.5 8.0 7.5 7.0 6.5 6.0 5.5 5.0 4.5 4.0 3.5 3.0 2.5 2.0 1.5 1.0 0.5 0.0

f1 (ppm)

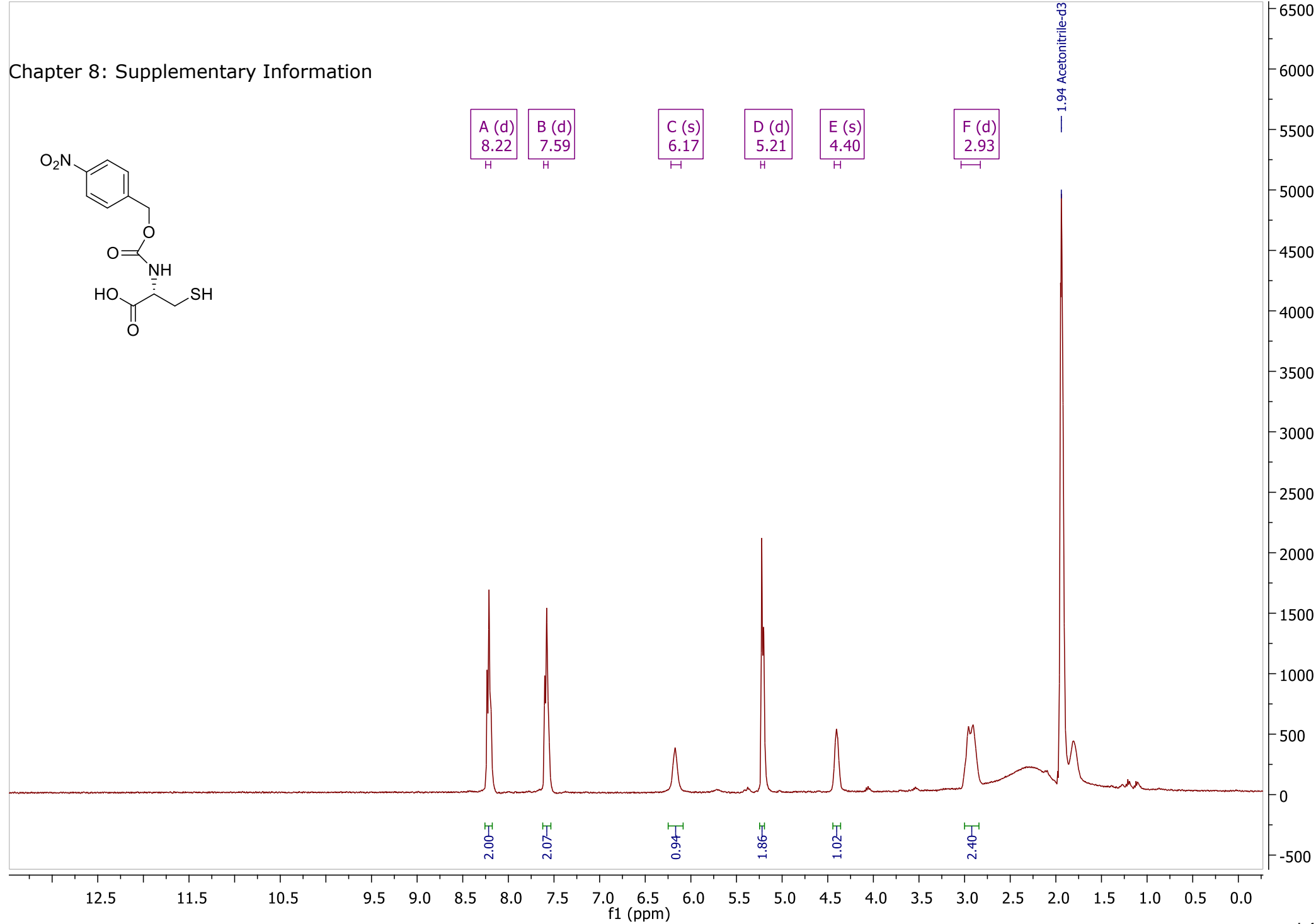
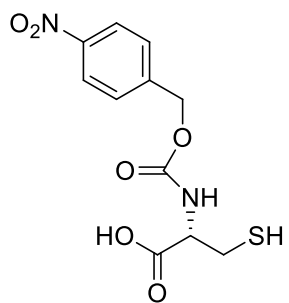
Chapter 8: Supplementary Information



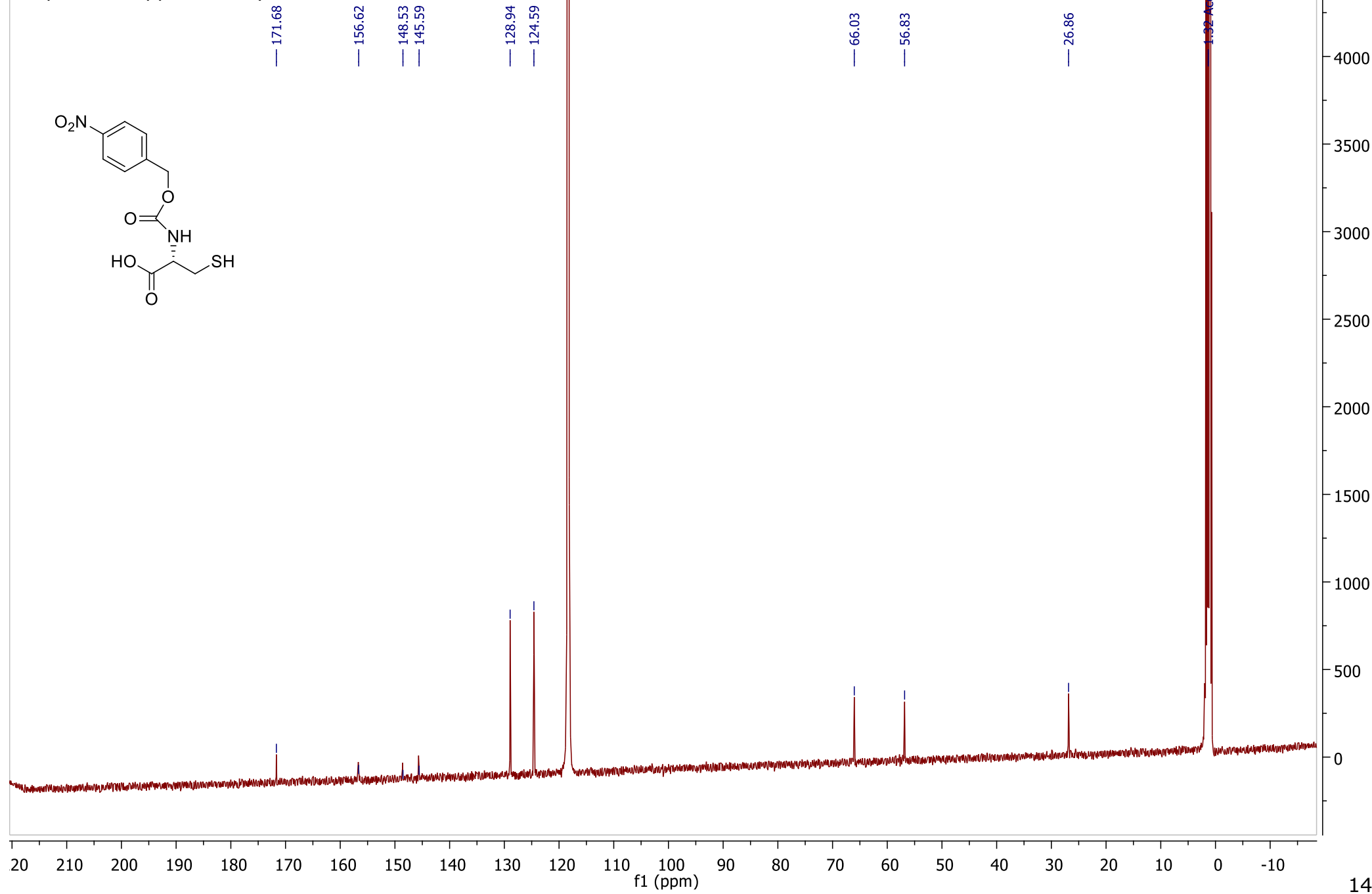
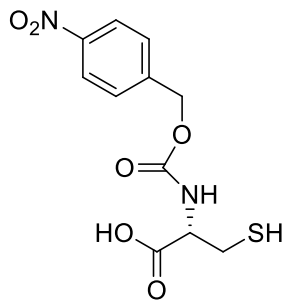
Chapter 8: Supplementary Information



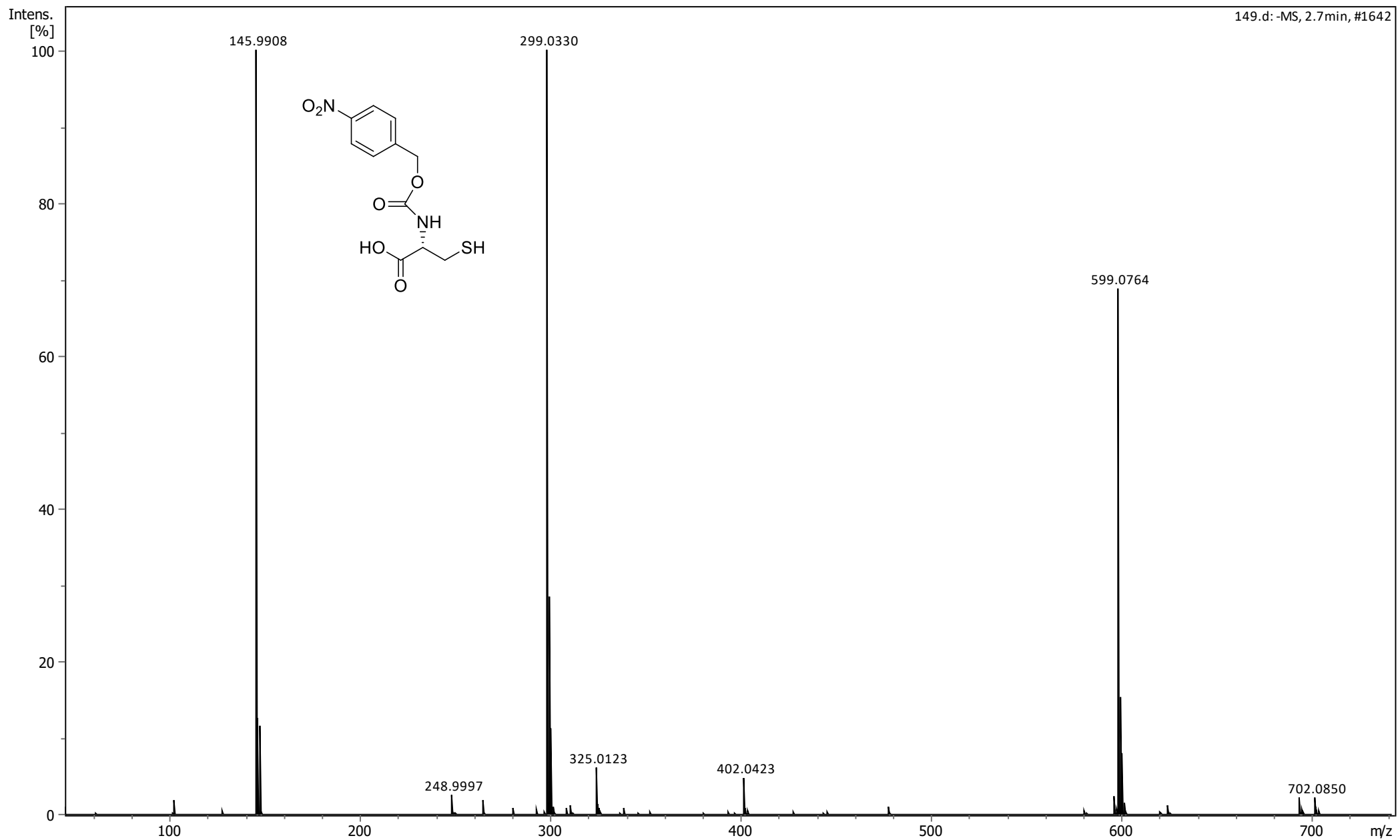
Chapter 8: Supplementary Information



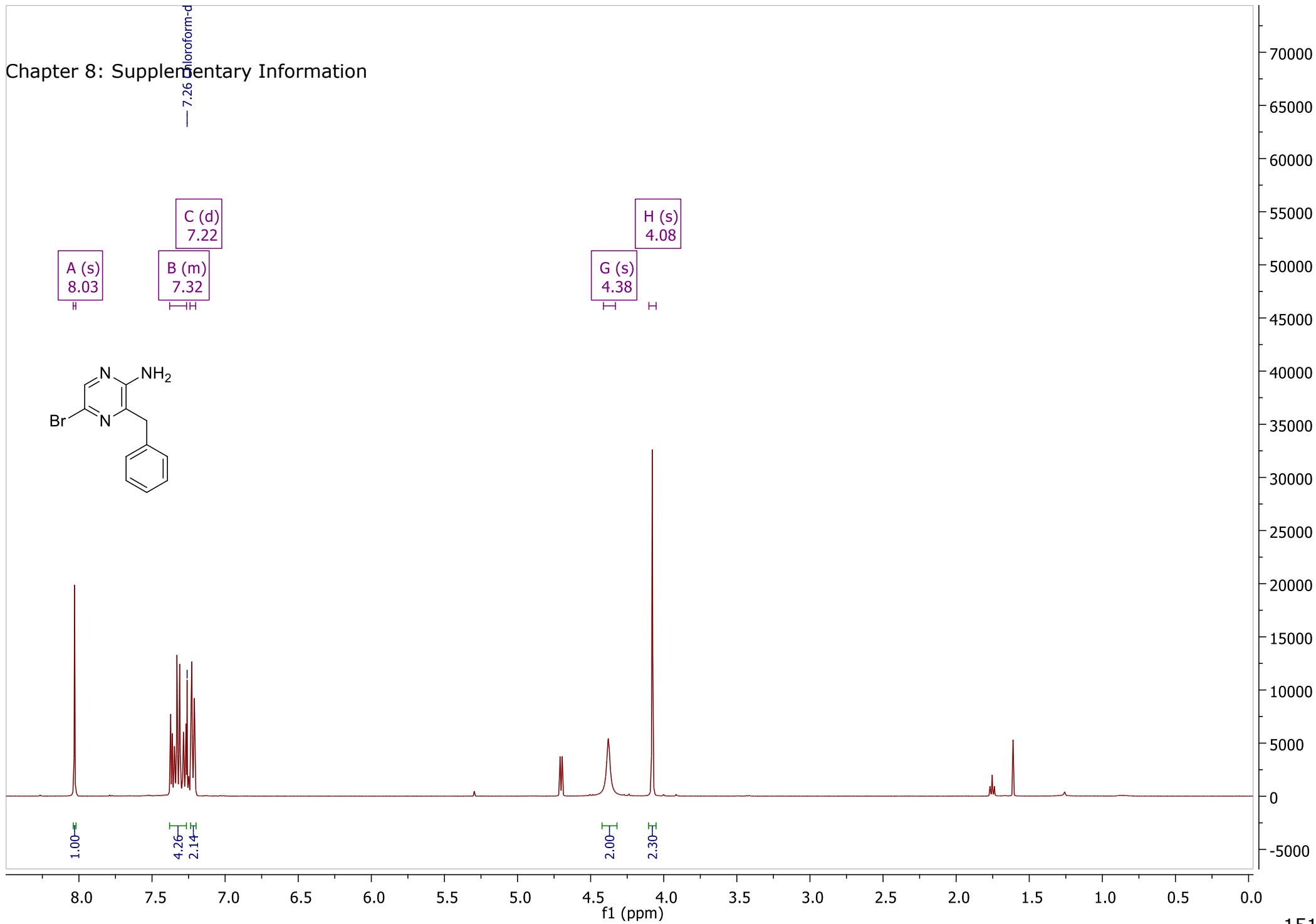
Chapter 8: Supplementary Information



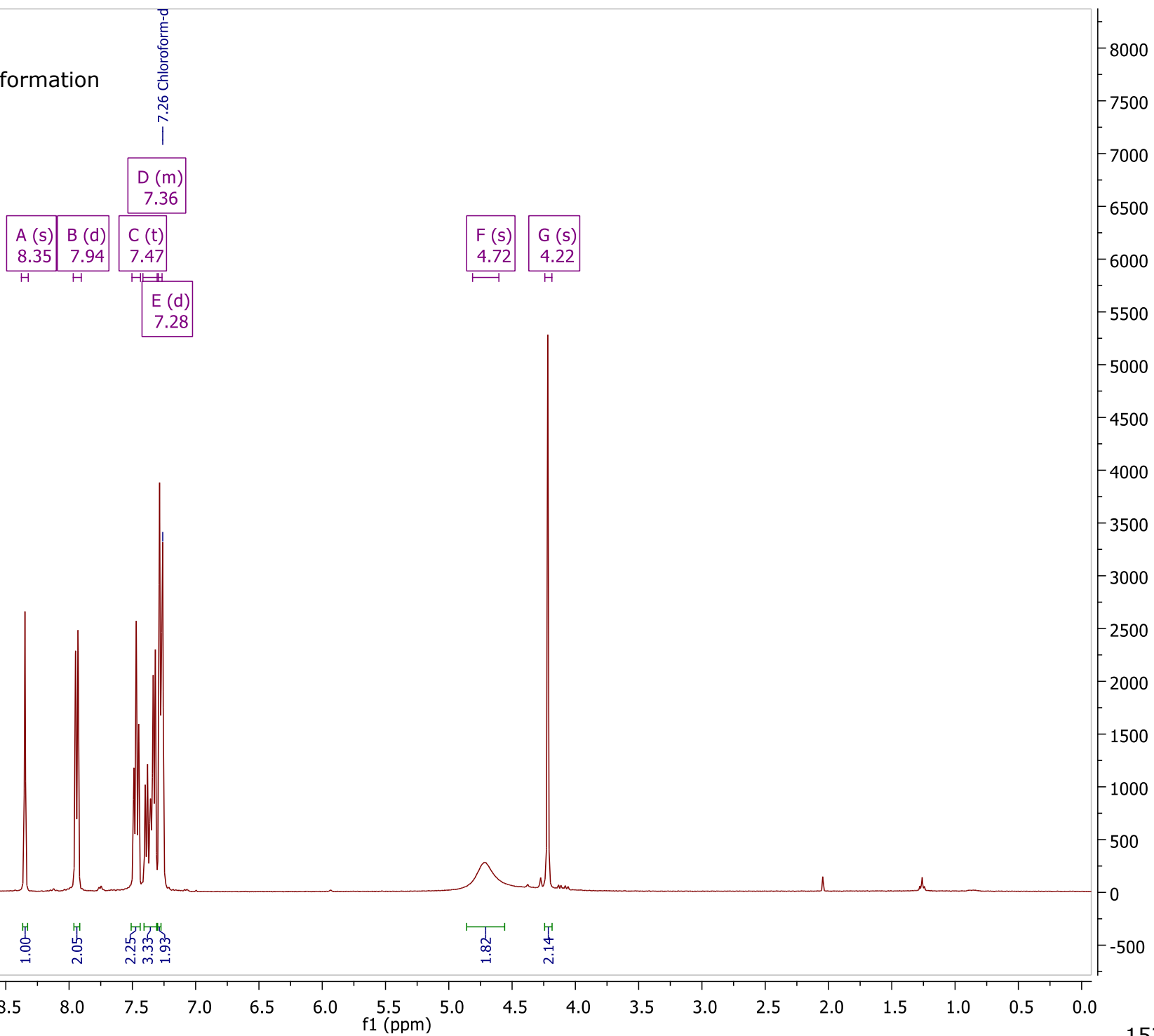
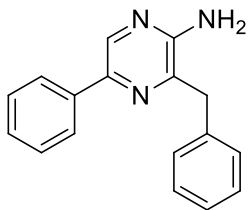
Chapter 8: Supplementary Information



Chapter 8: Supplementary Information

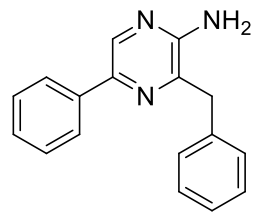


Chapter 8: Supplementary Information





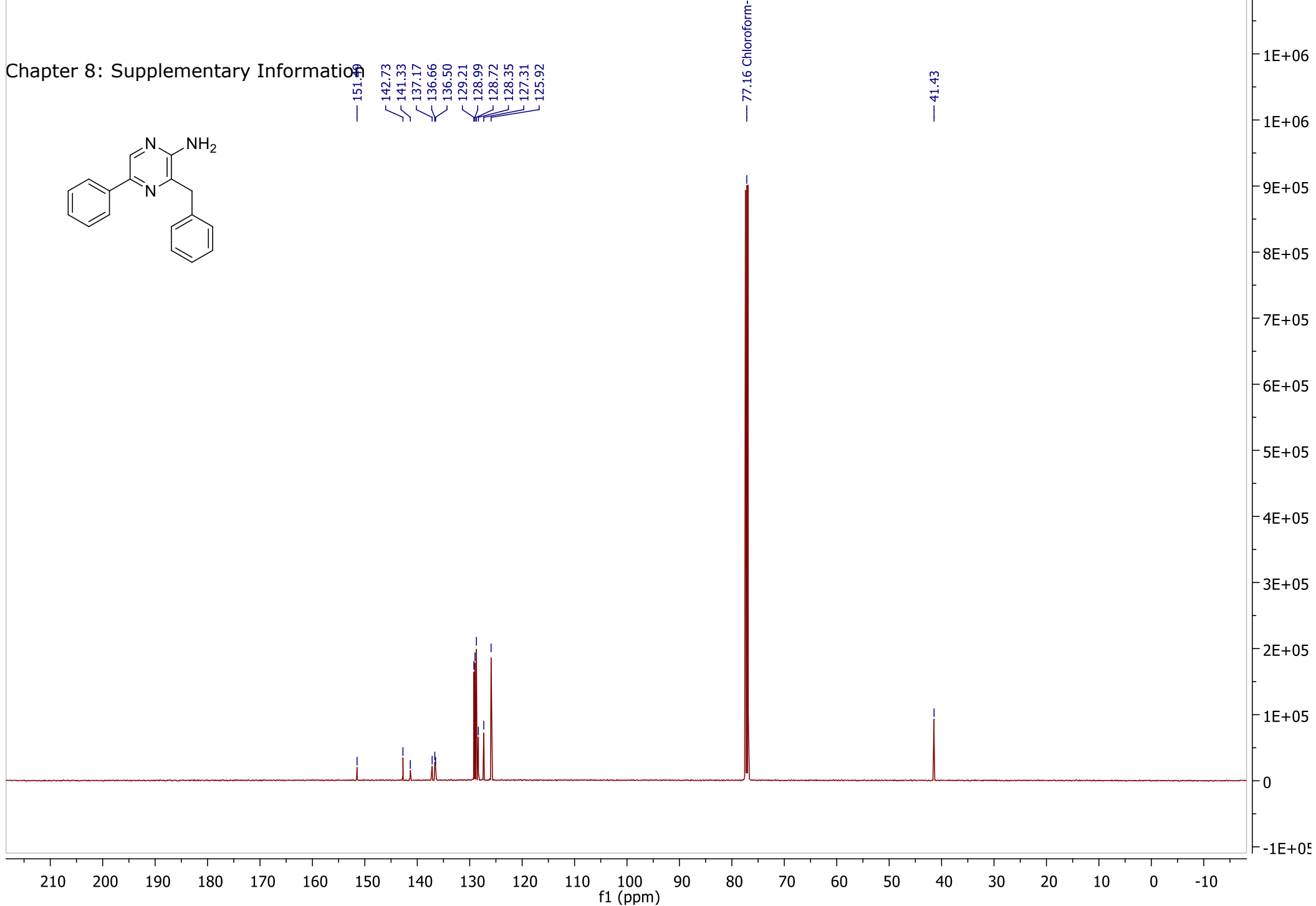
Chapter 8: Supplementary Information



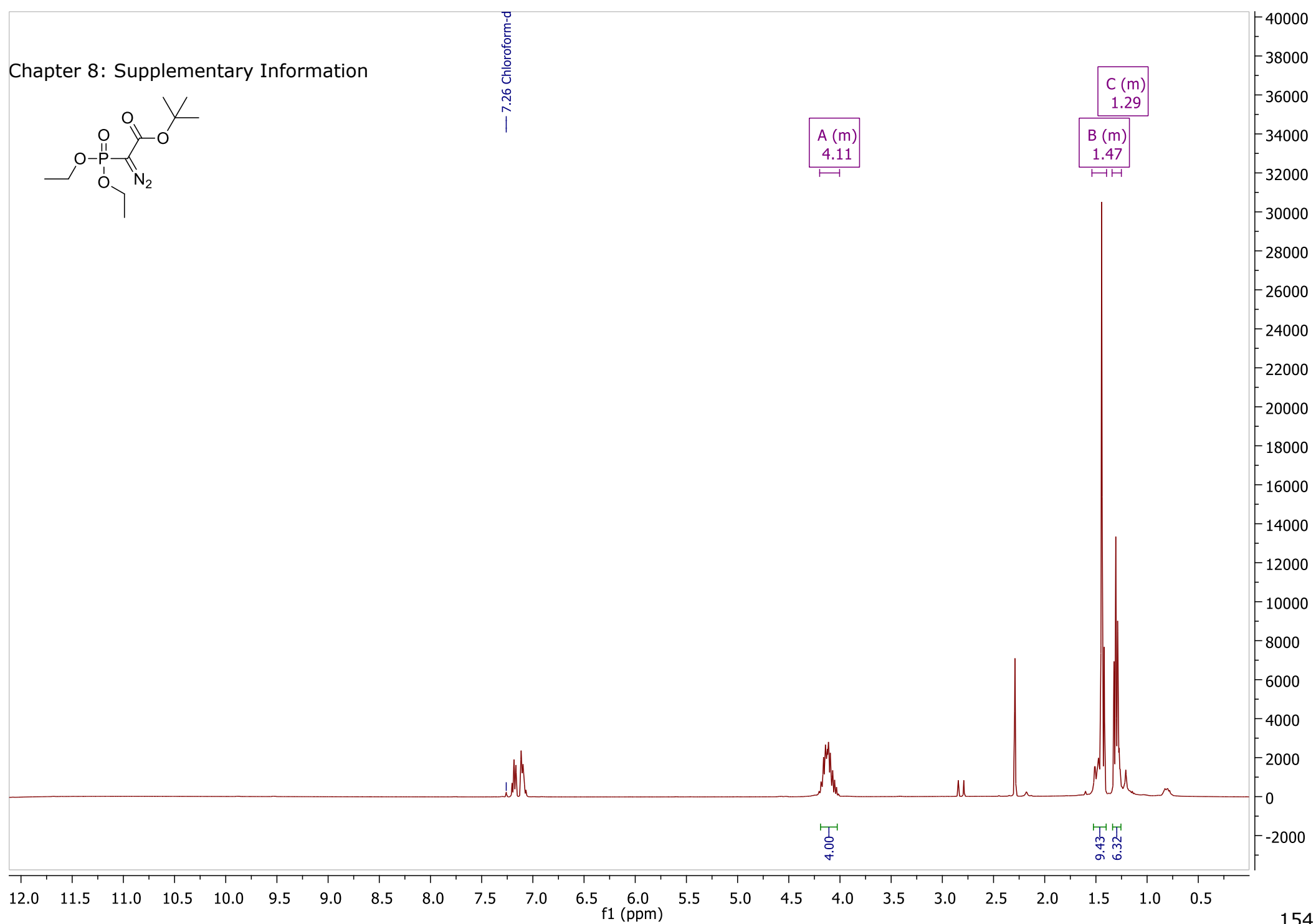
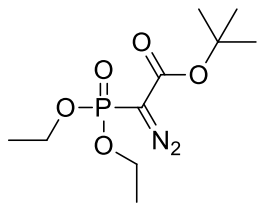
151.99  
142.73  
141.33  
137.17  
136.66  
136.50  
129.21  
128.99  
128.72  
128.35  
127.31  
125.92

77.16 Chloroform

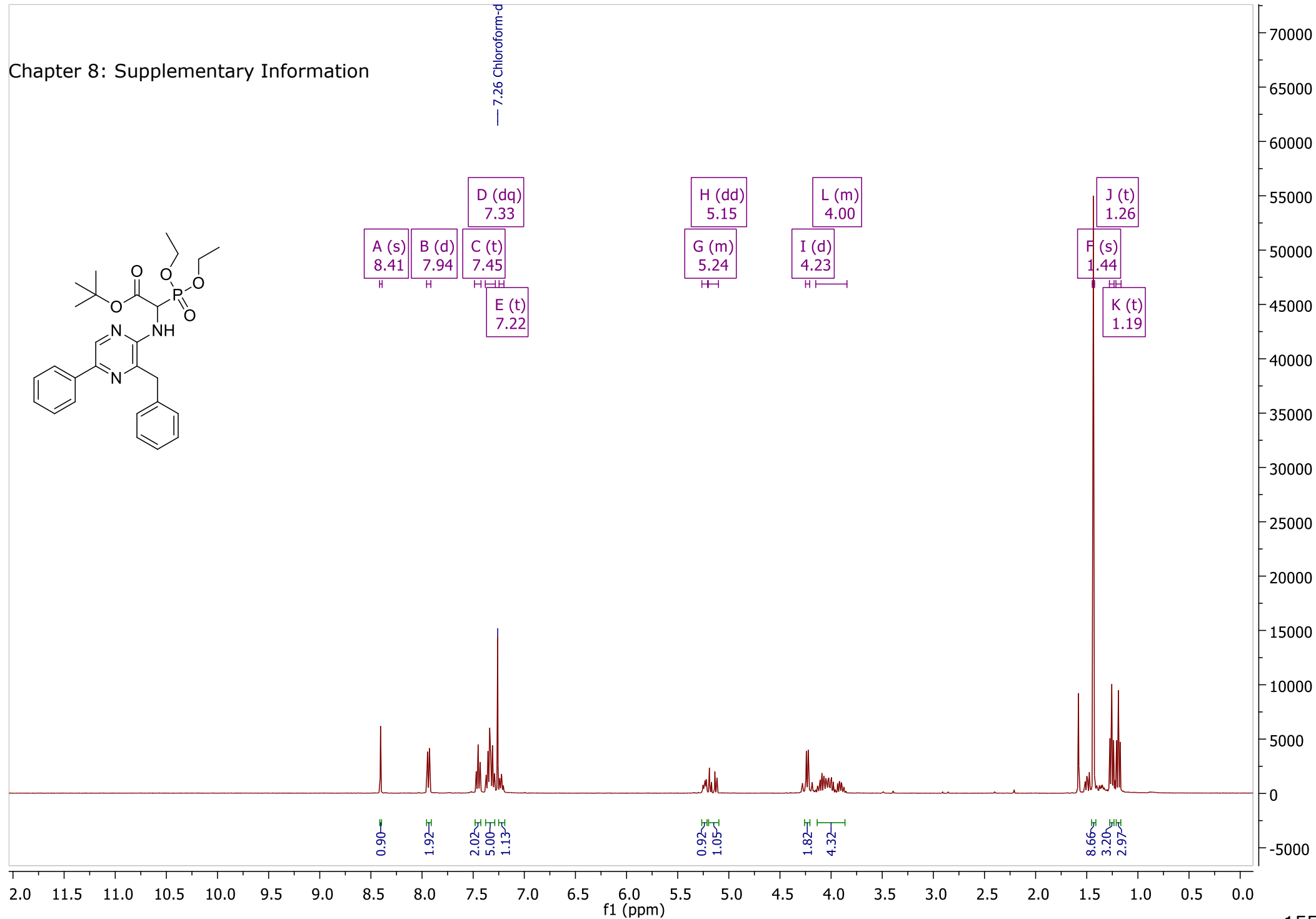
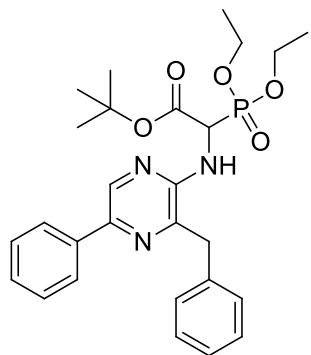
41.43



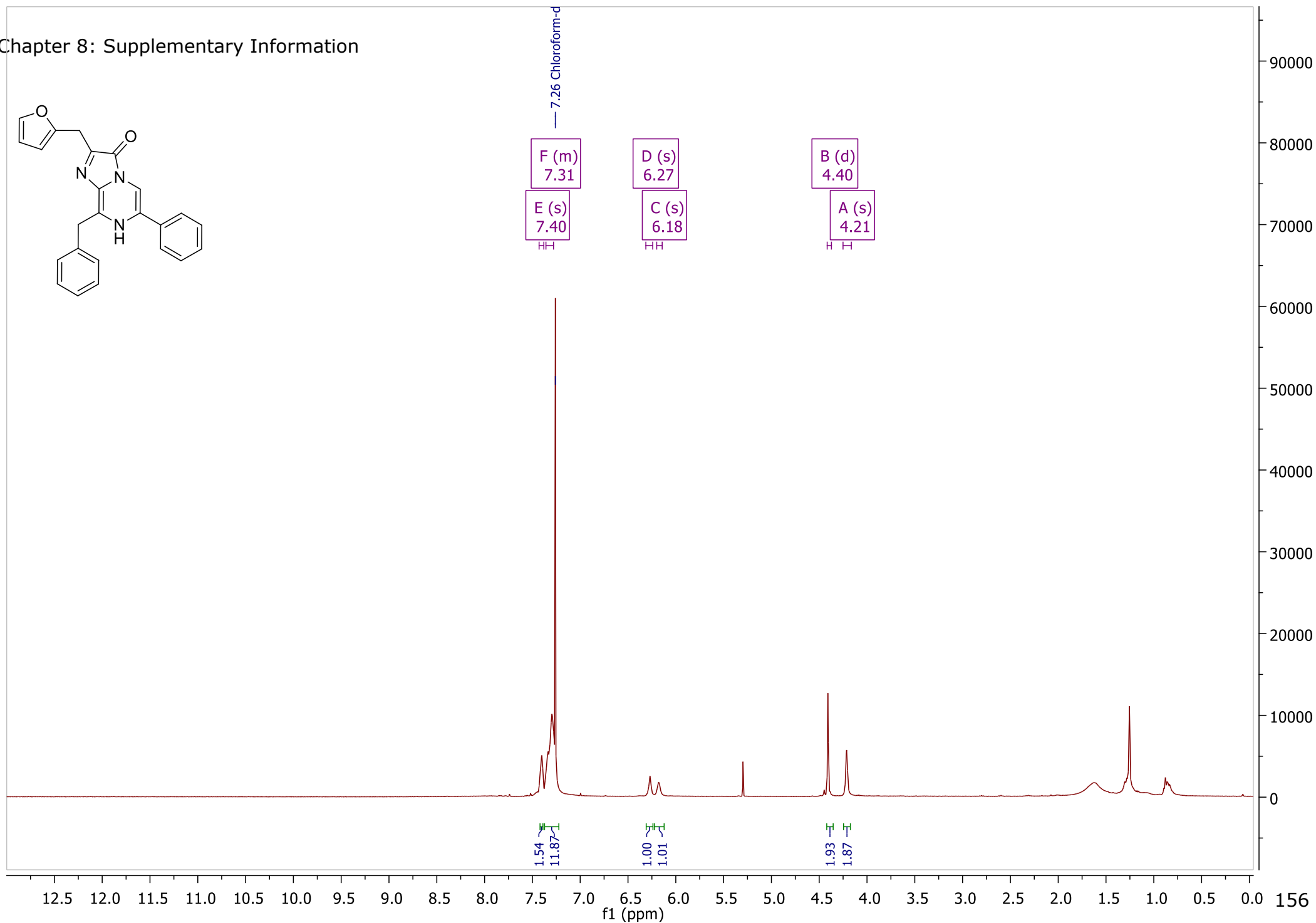
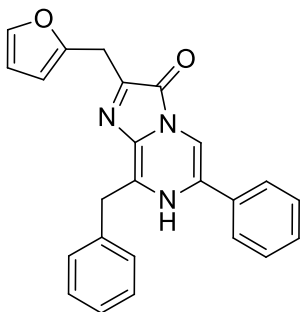
Chapter 8: Supplementary Information



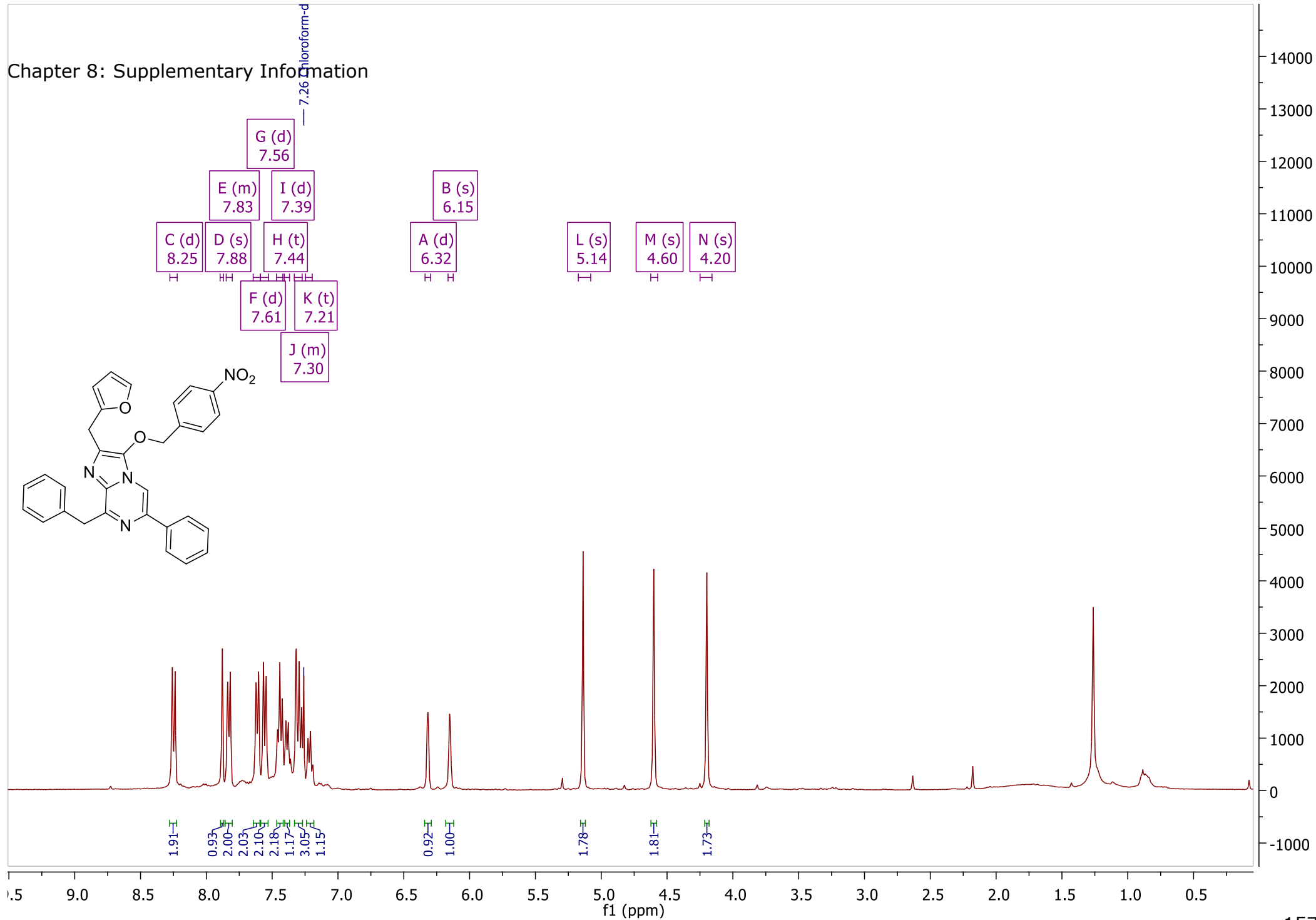
Chapter 8: Supplementary Information



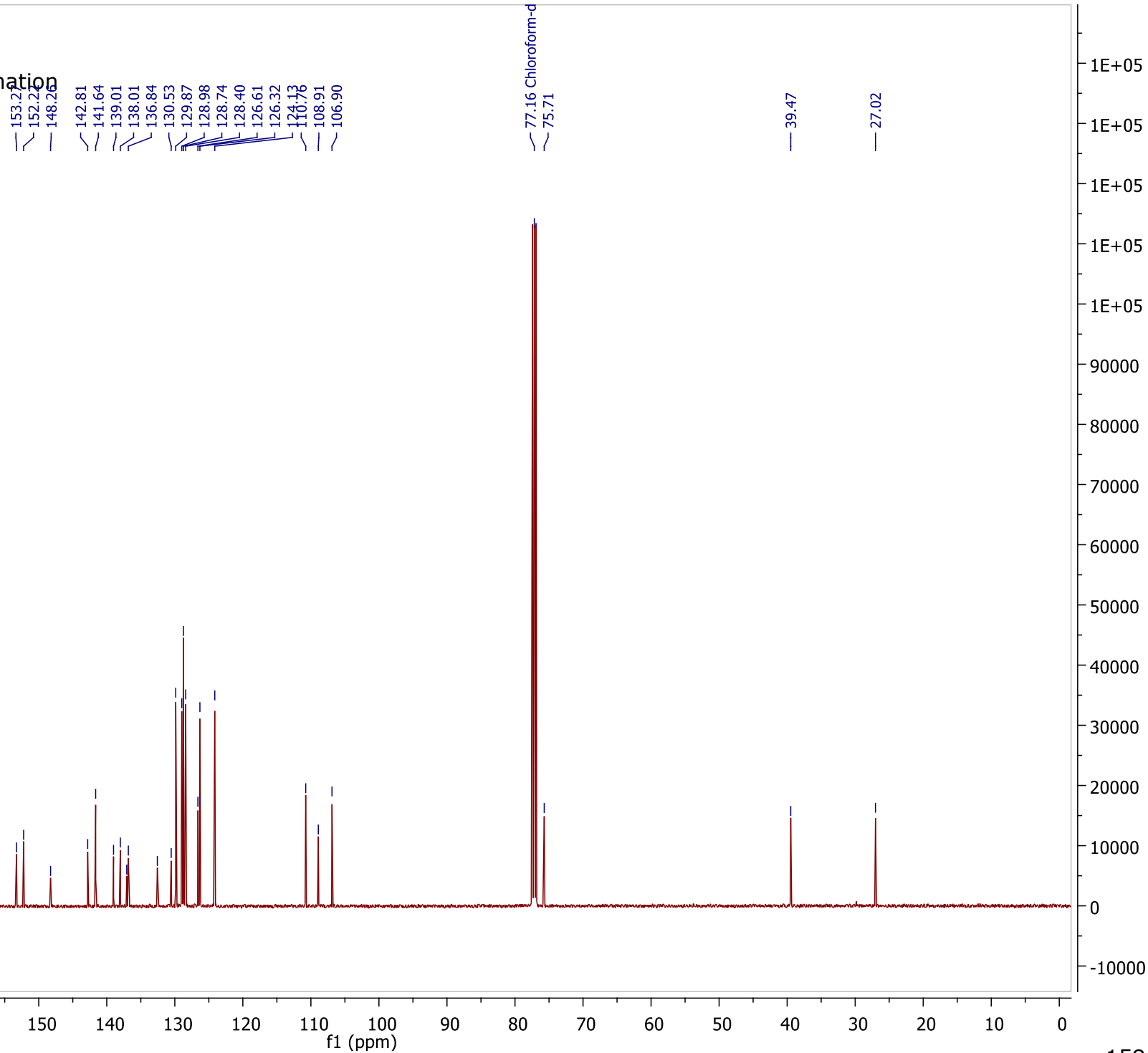
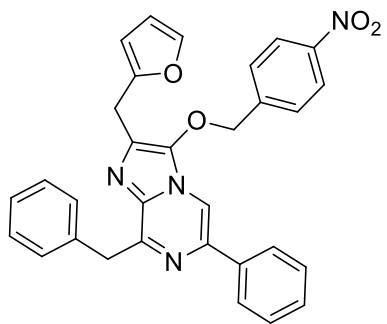
Chapter 8: Supplementary Information



Chapter 8: Supplementary Information



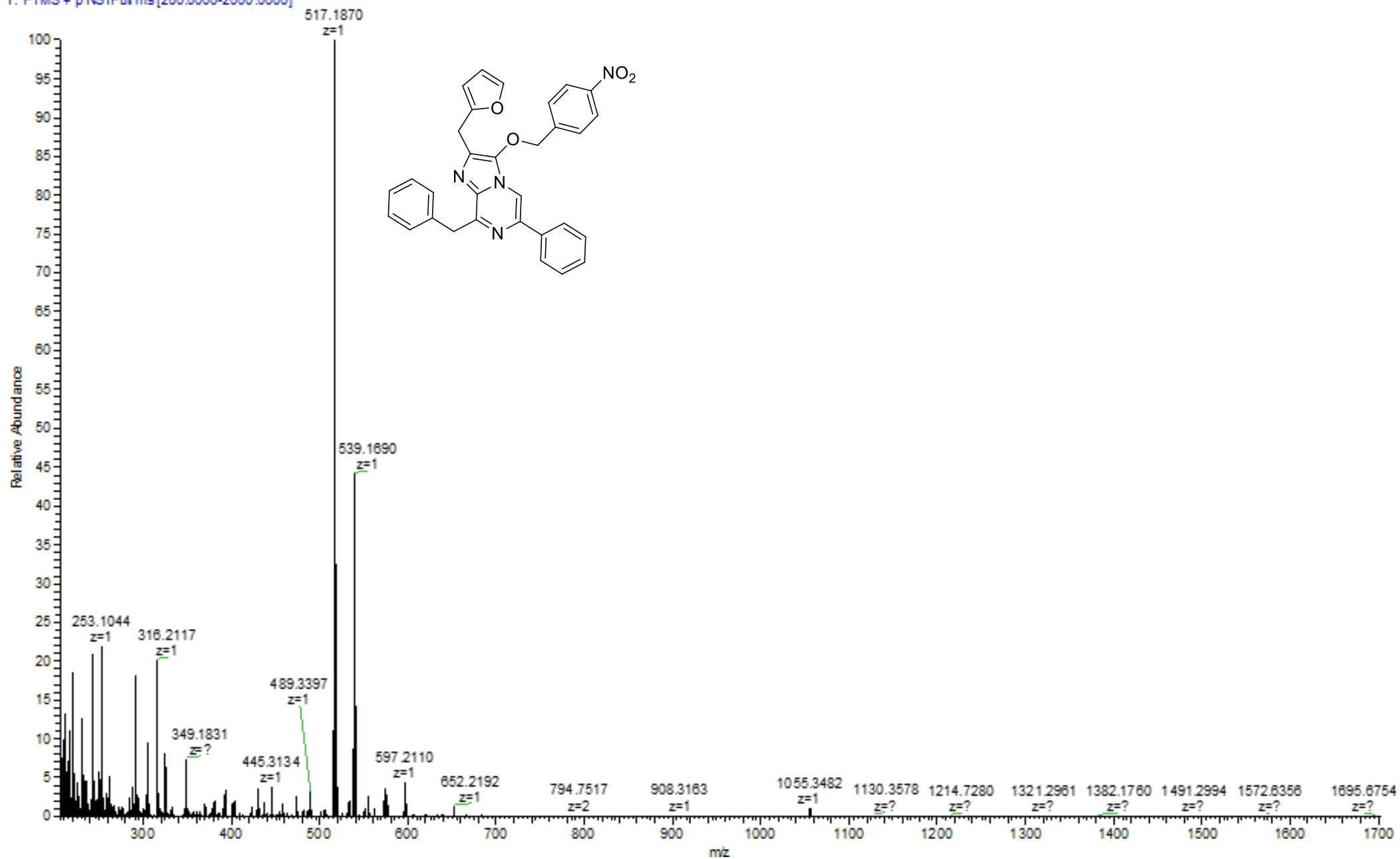
Chapter 8: Supplementary Information



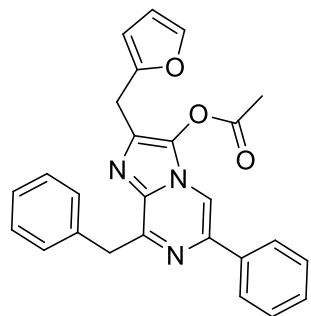
# Chapter 8: Supplementary Information

62 #50-81 RT: 0.44-0.53 AV: 12 NL: 1.85E5

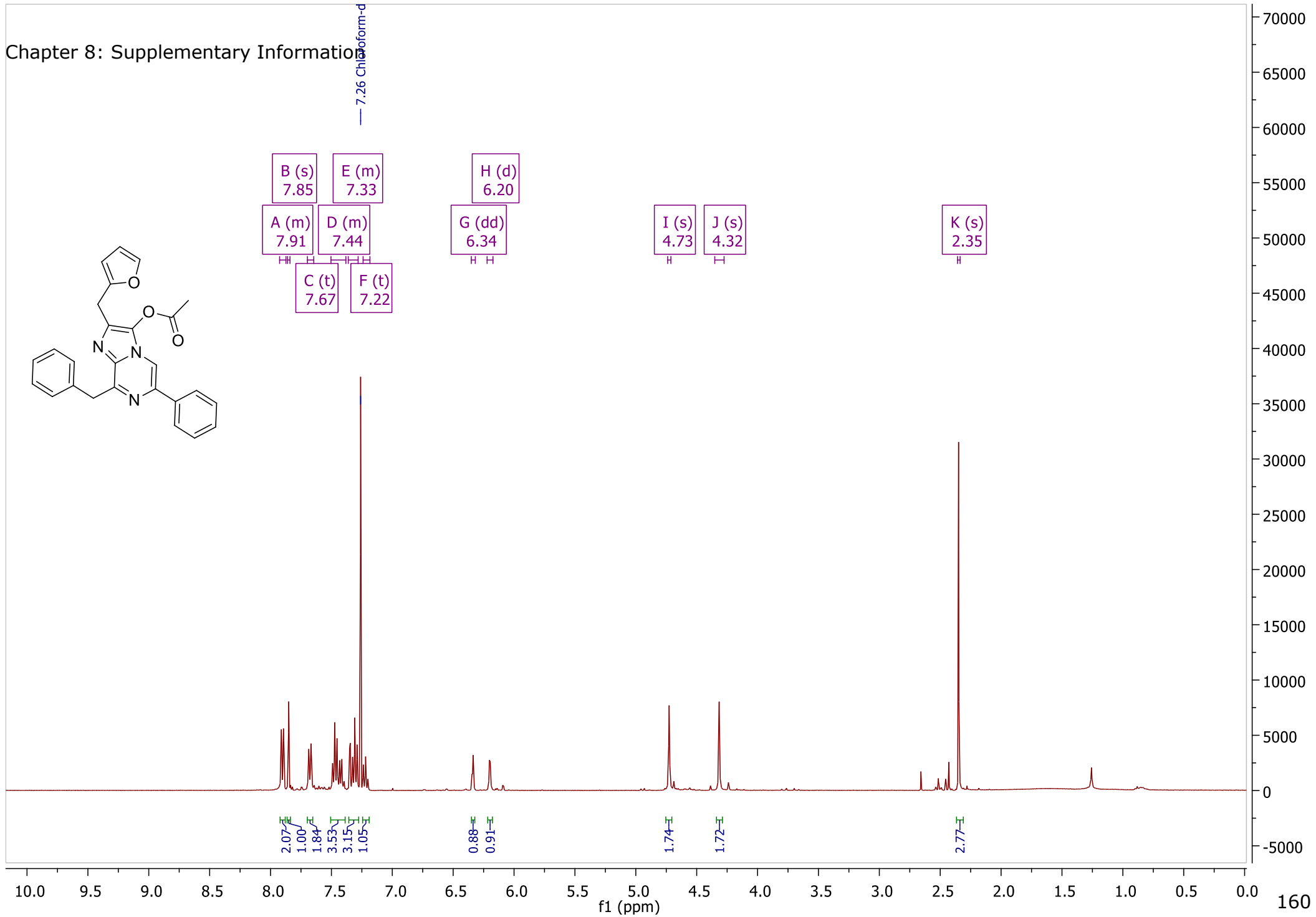
T: FTMS + p NSIFull.ms[200.0000-2000.0000]



7.26 Chloroform-d

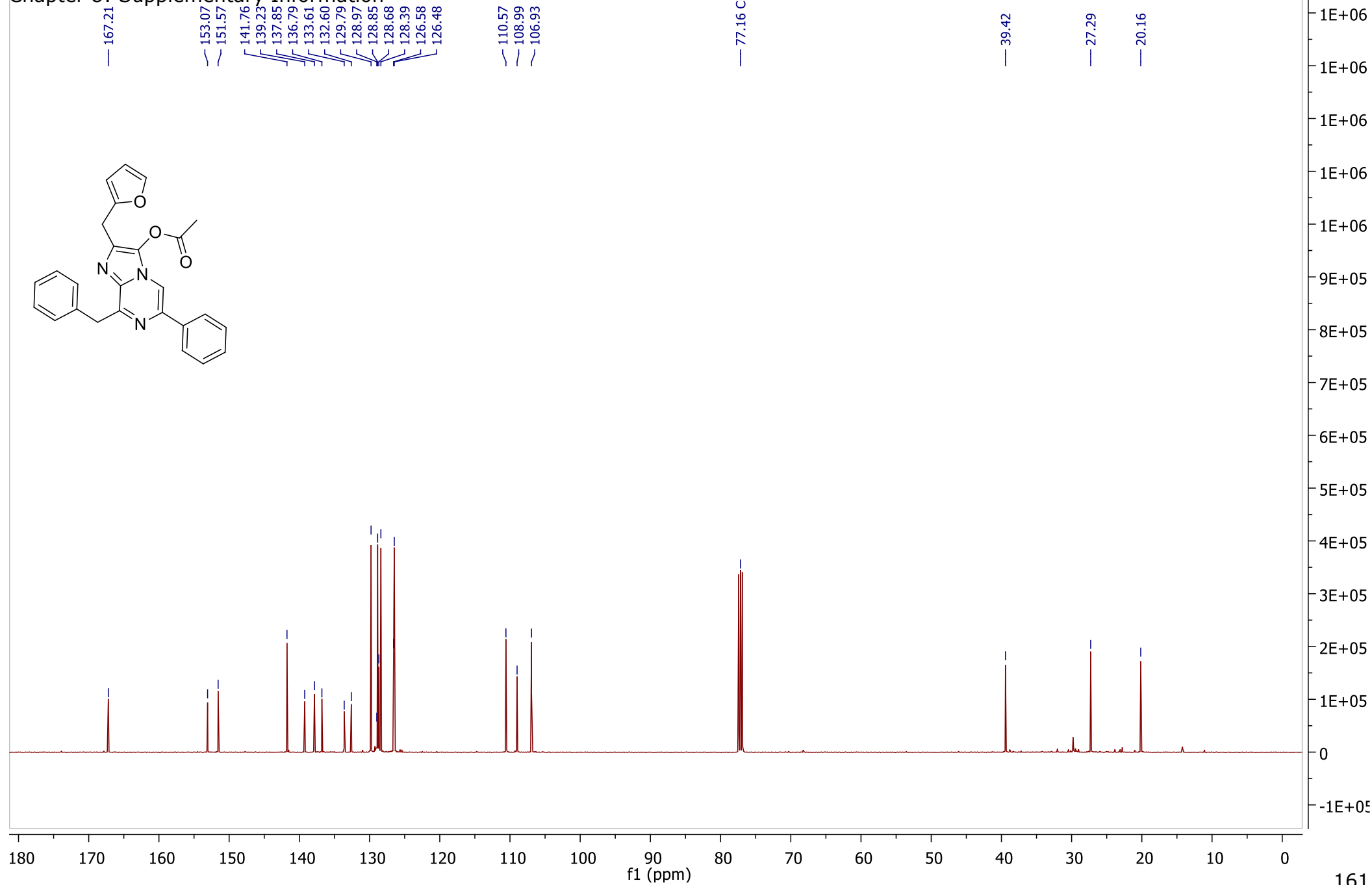
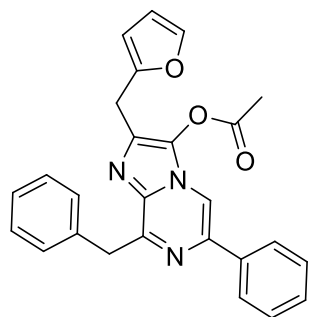


|               |               |                |               |               |               |
|---------------|---------------|----------------|---------------|---------------|---------------|
| B (s)<br>7.85 | E (m)<br>7.33 | H (d)<br>6.20  | I (s)<br>4.73 | J (s)<br>4.32 | K (s)<br>2.35 |
| A (m)<br>7.91 | D (m)<br>7.44 | G (dd)<br>6.34 |               |               |               |
|               | C (t)<br>7.67 |                |               |               |               |
|               | F (t)<br>7.22 |                |               |               |               |

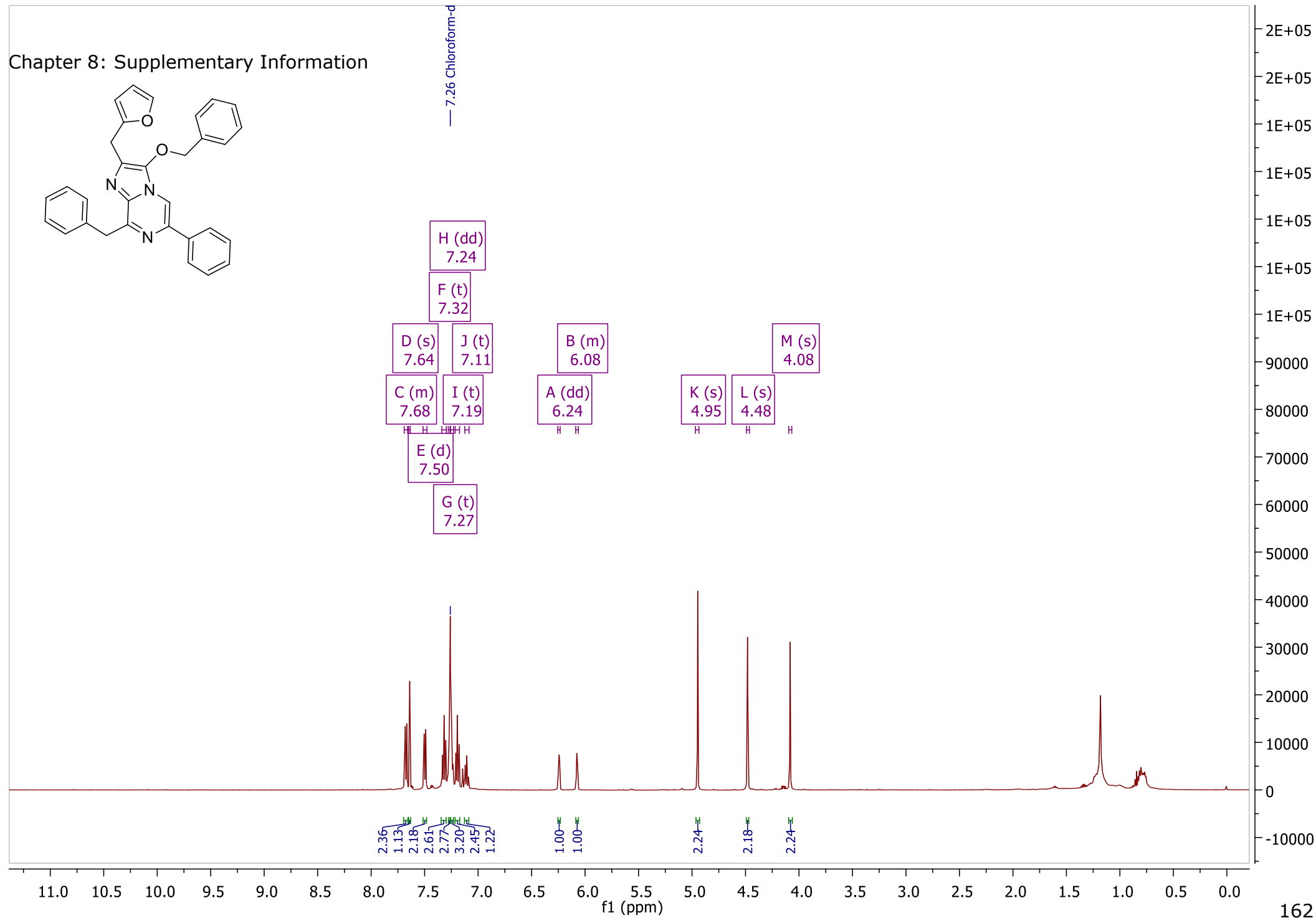
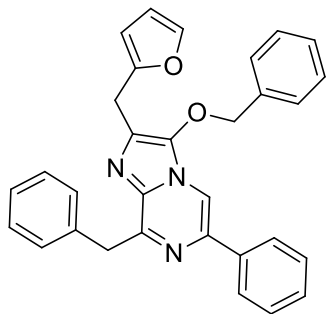




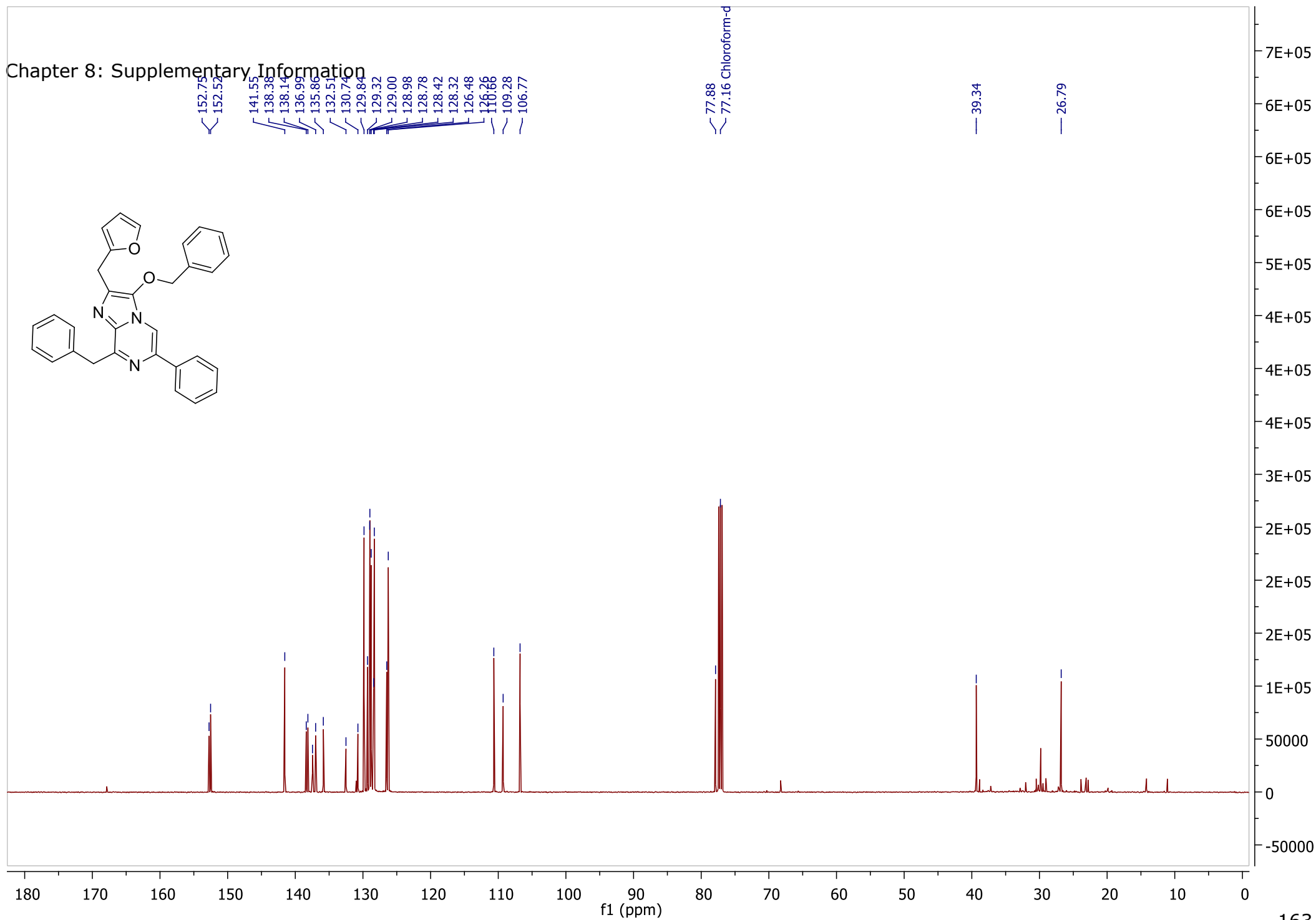
# Chapter 8: Supplementary Information



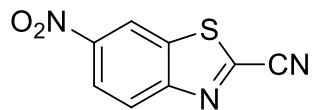
Chapter 8: Supplementary Information



Chapter 8: Supplementary Information



Chapter 8: Supplementary Information

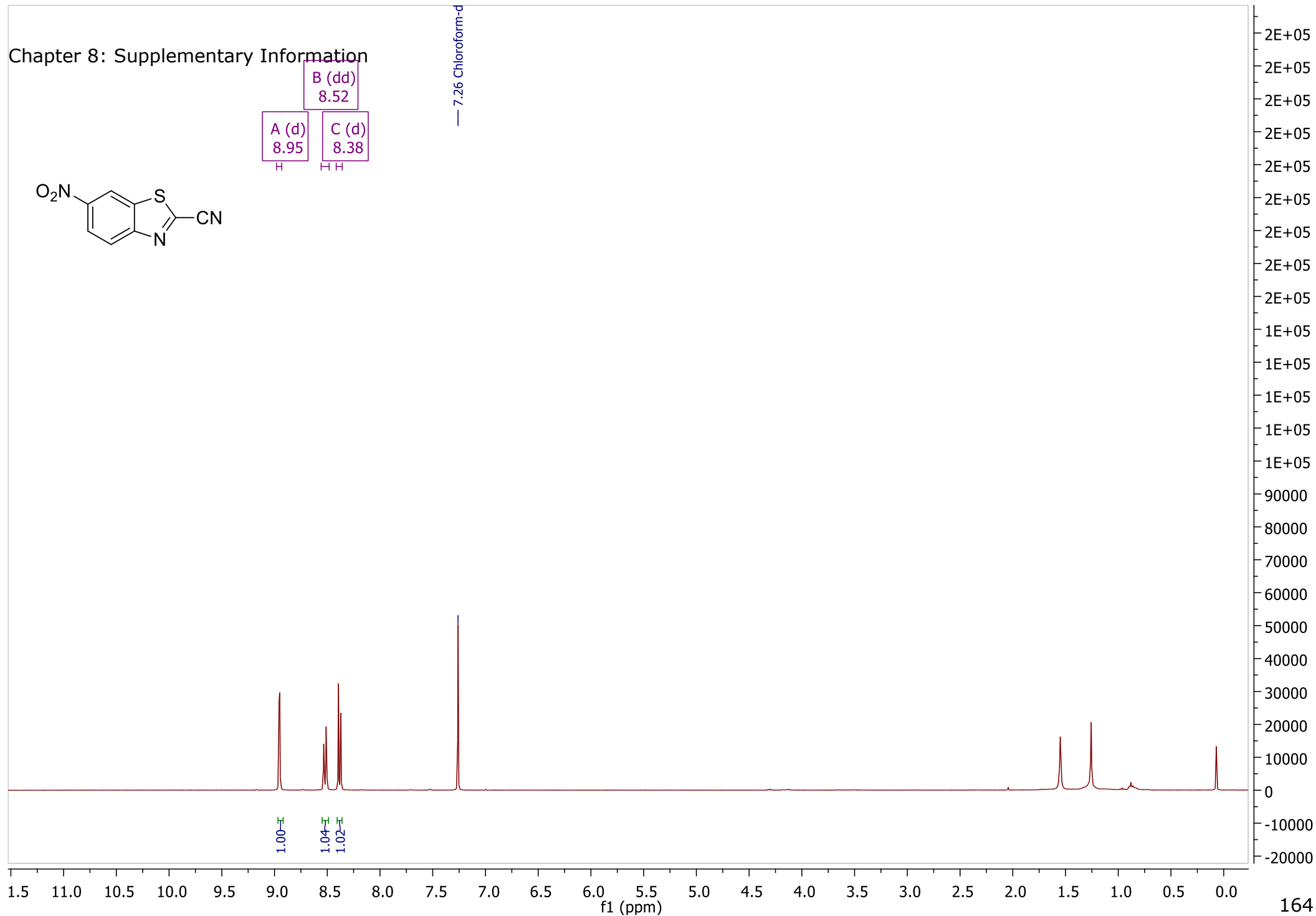


A (d)  
8.95  
H

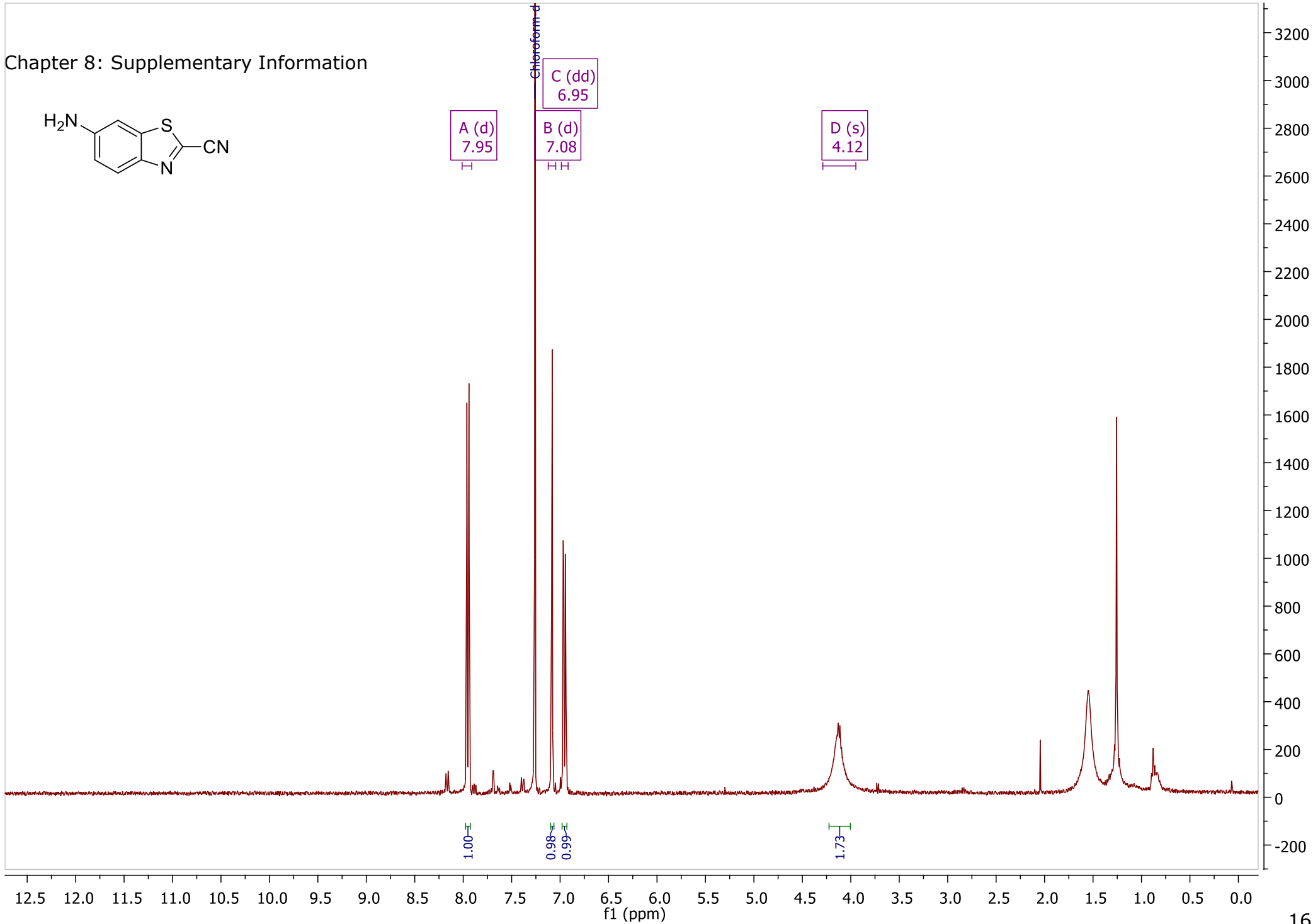
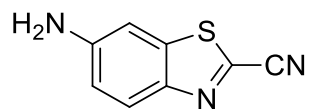
B (dd)  
8.52

C (d)  
8.38  
H H

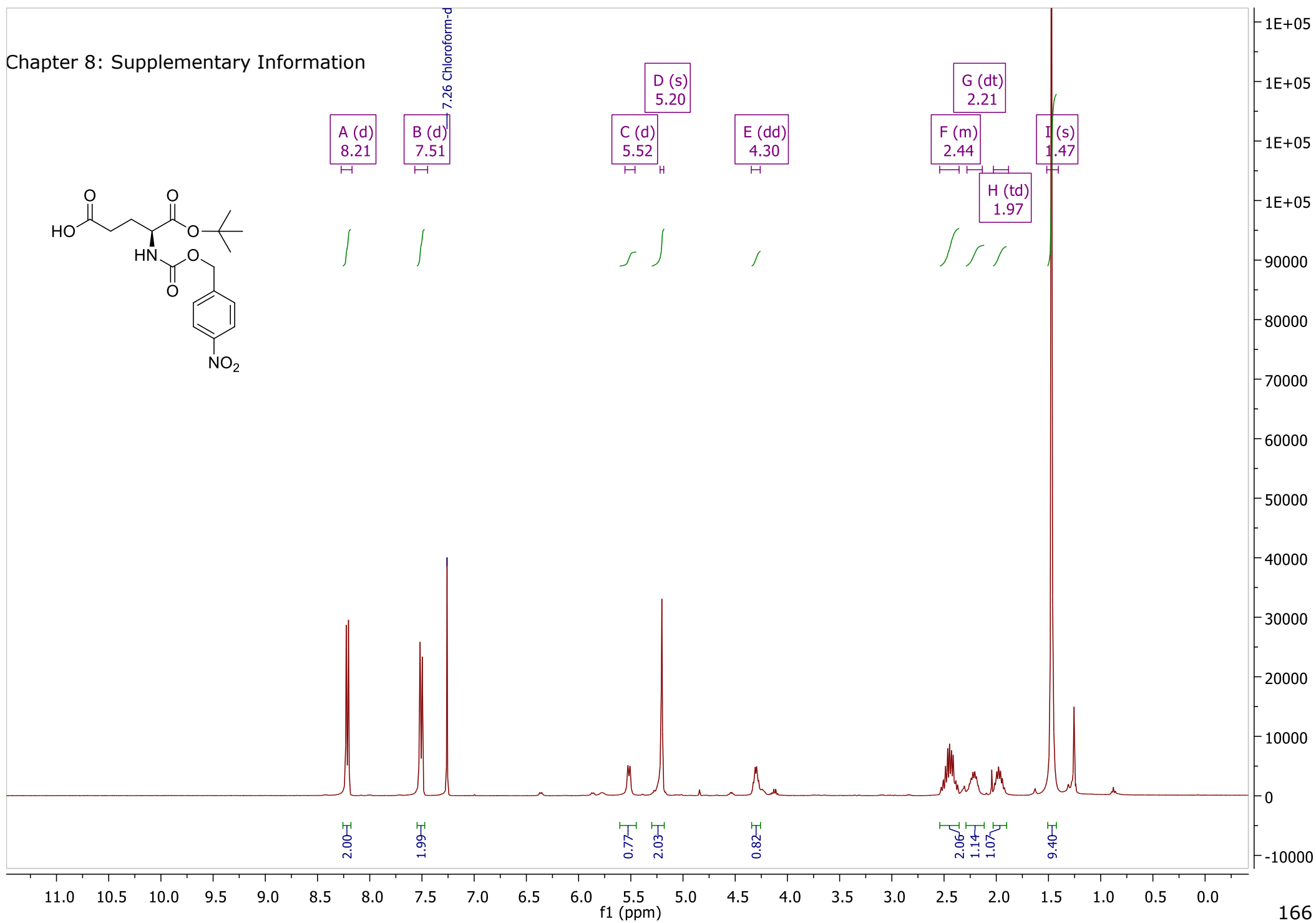
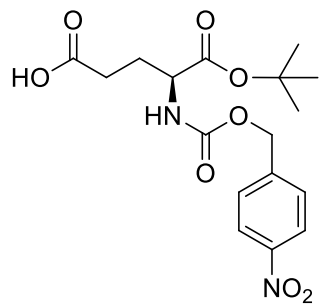
— 7.26 Chloroform-d



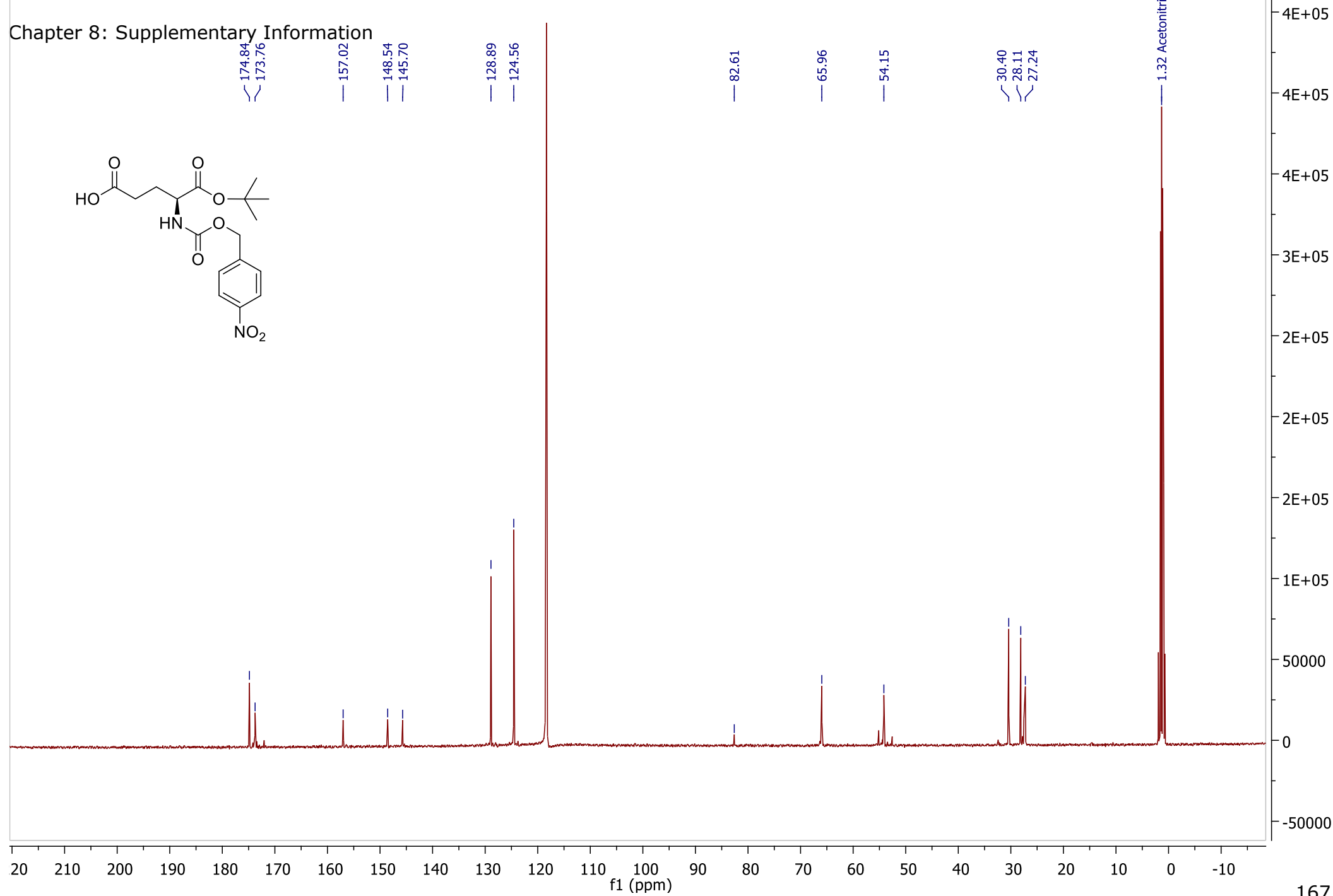
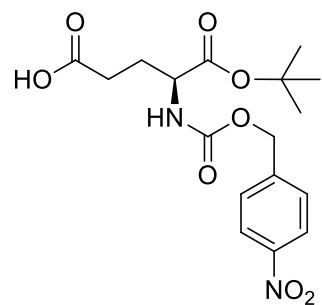
Chapter 8: Supplementary Information



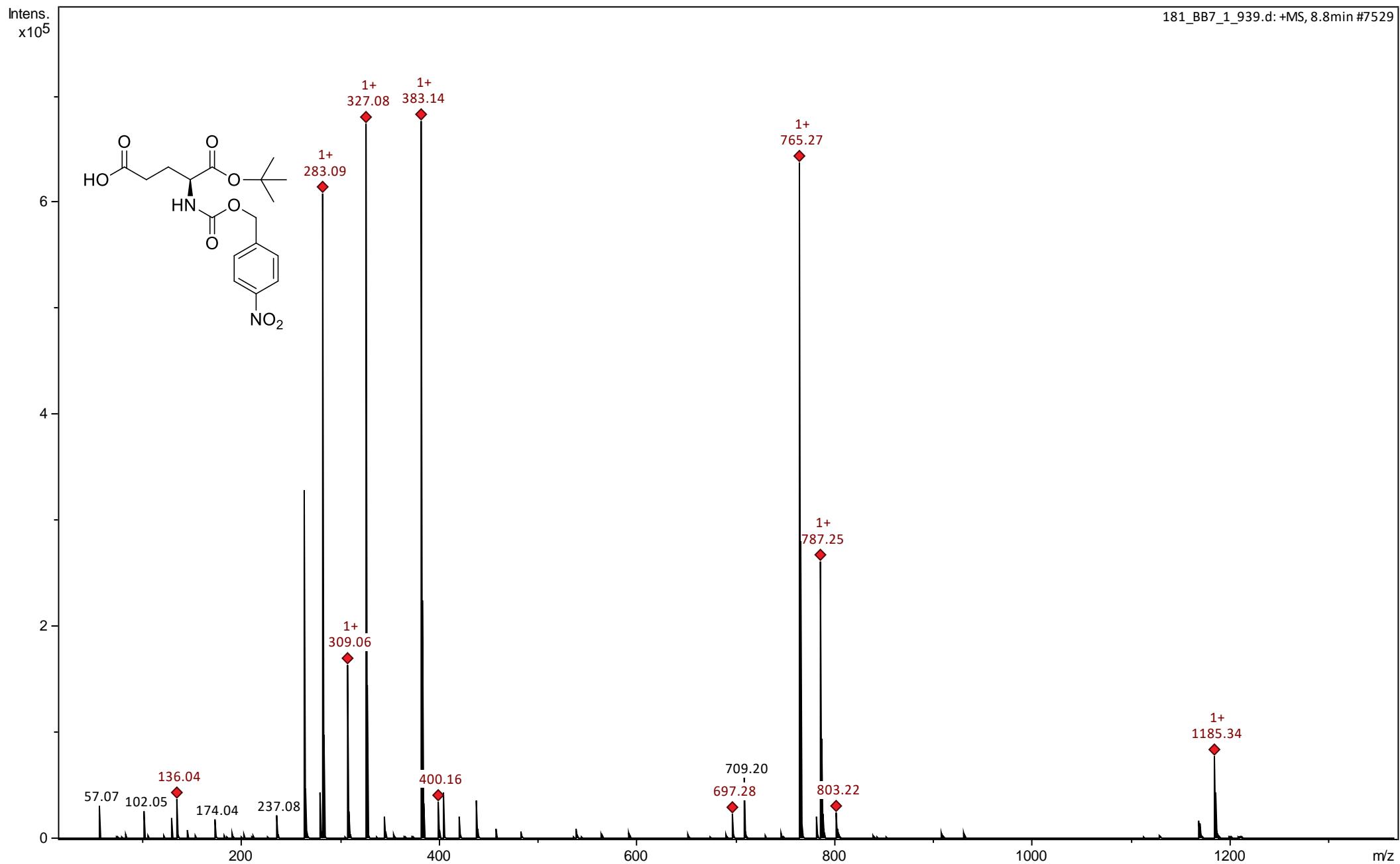
Chapter 8: Supplementary Information



Chapter 8: Supplementary Information

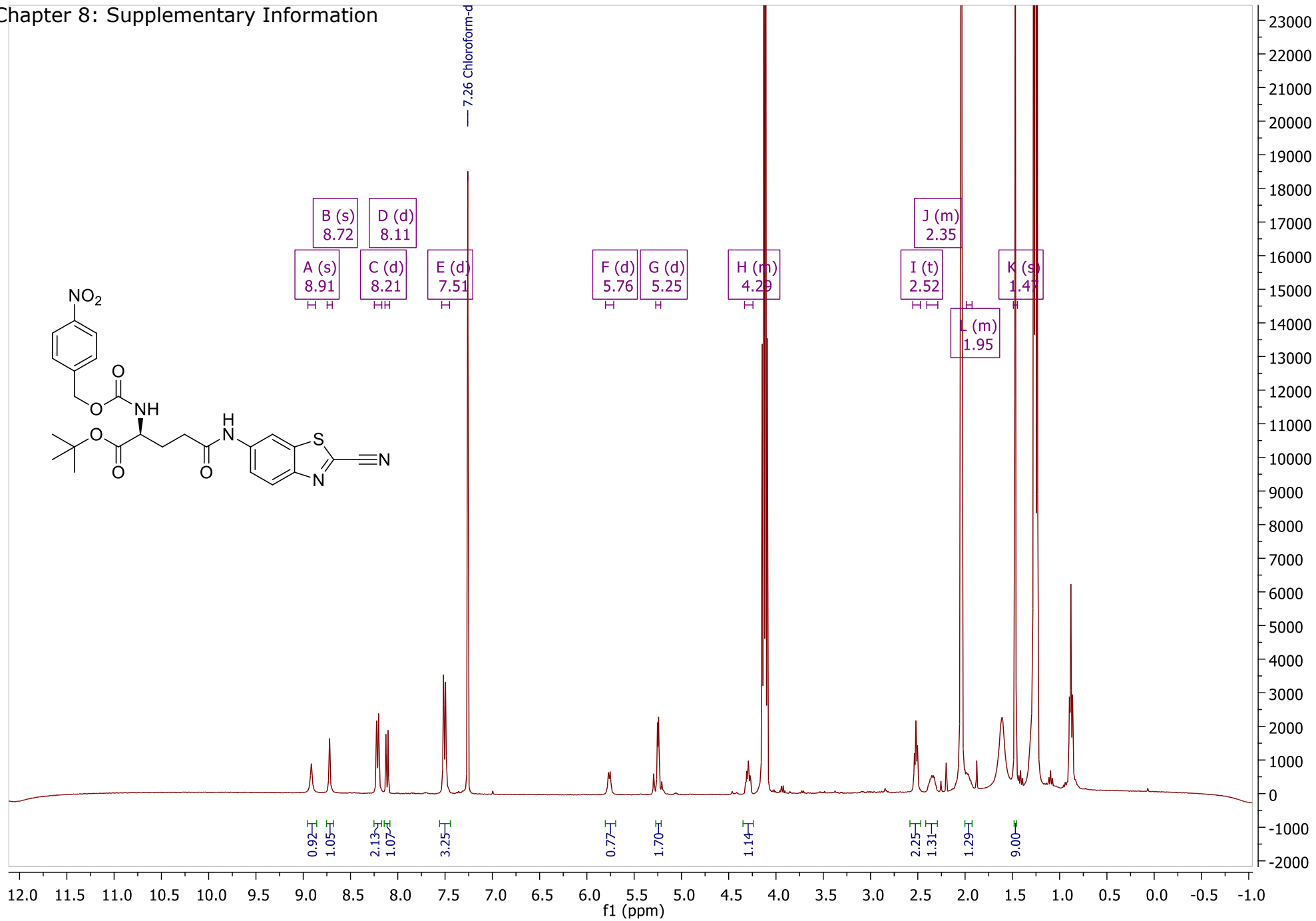


Chapter 8: Supplementary Information

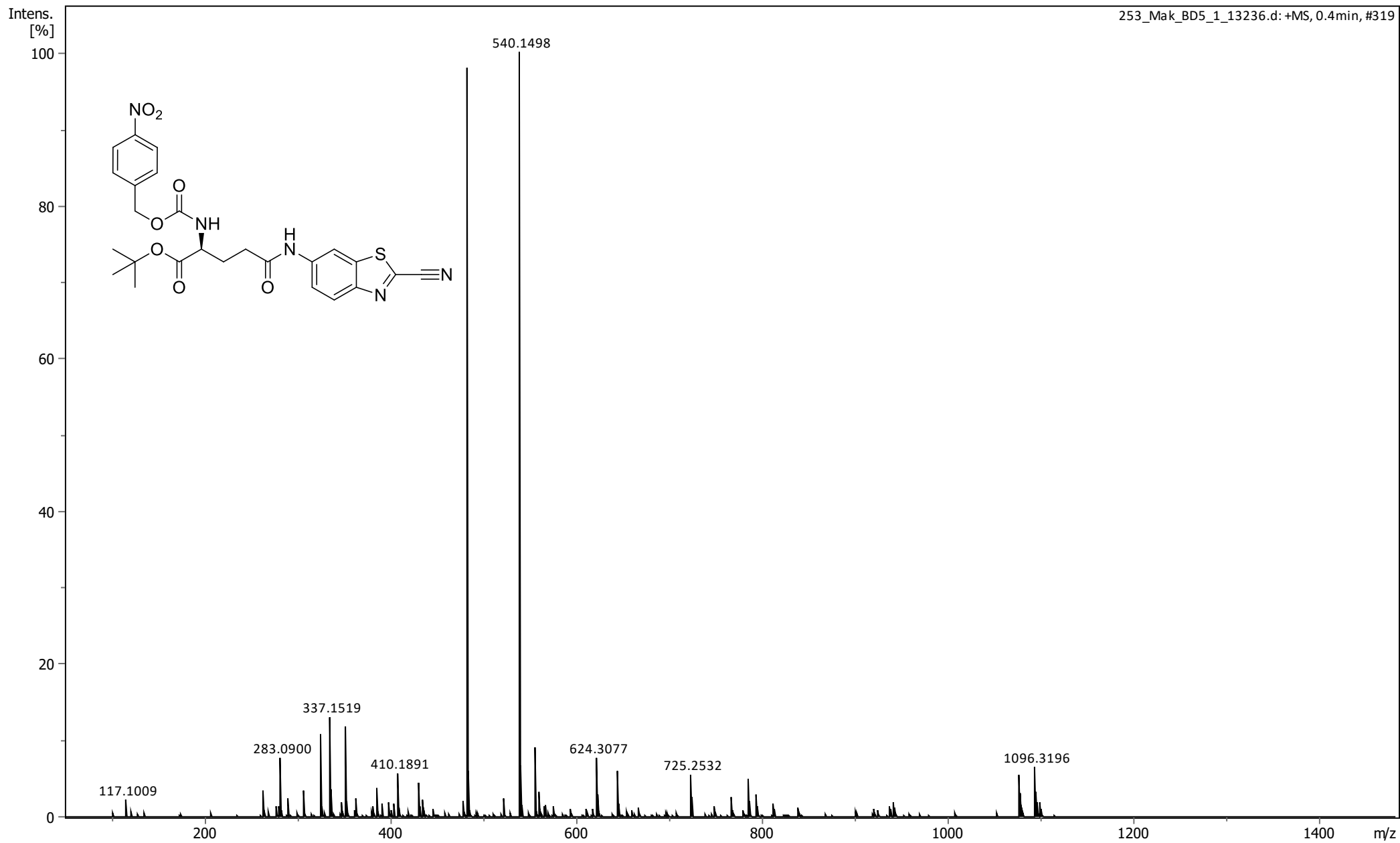




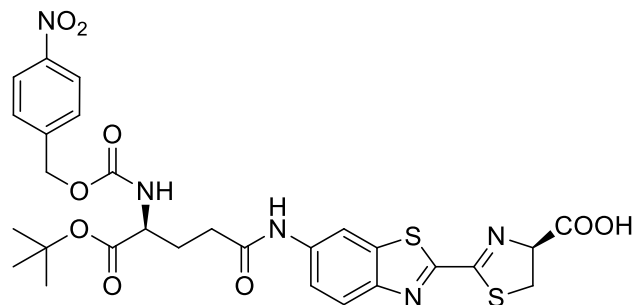
Chapter 8: Supplementary Information



Chapter 8: Supplementary Information



Chapter 8: Supplementary Information



|               |               |               |                |
|---------------|---------------|---------------|----------------|
| A (s)<br>8.45 | B (d)<br>8.14 | C (d)<br>7.93 | D (dd)<br>7.52 |
| H             | H             | H             | H              |

E (m)  
5.17

F (dd)  
4.18

G (dd)  
3.73

3.31 Methanol-d4

H (t)  
2.56

I (m)  
2.27

J (m)  
2.06

K (s)  
1.47

0.76  
1.92  
0.92

2.91

3.10

0.86

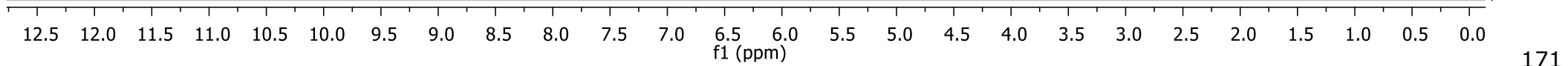
1.88

2.00

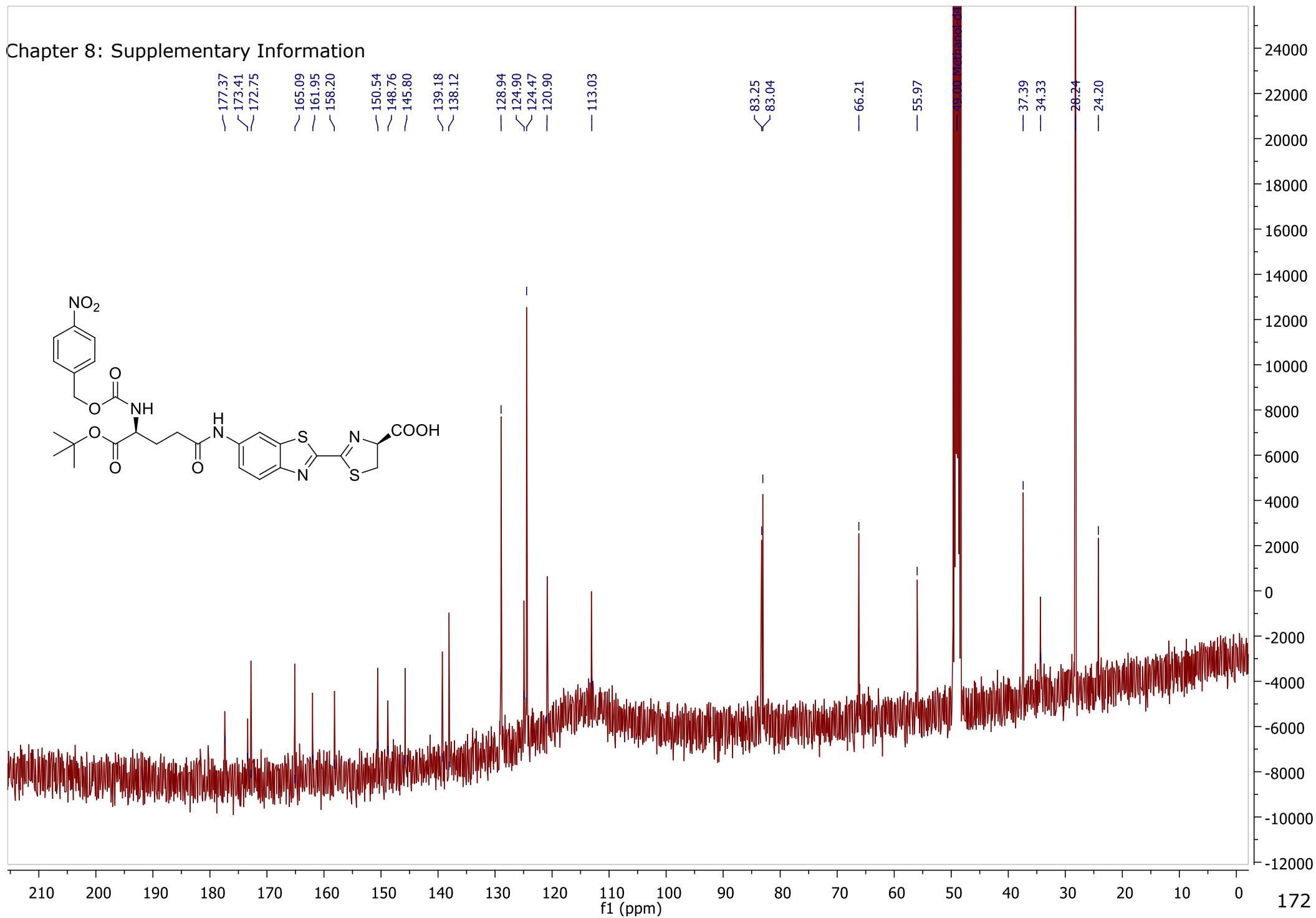
1.10

1.13

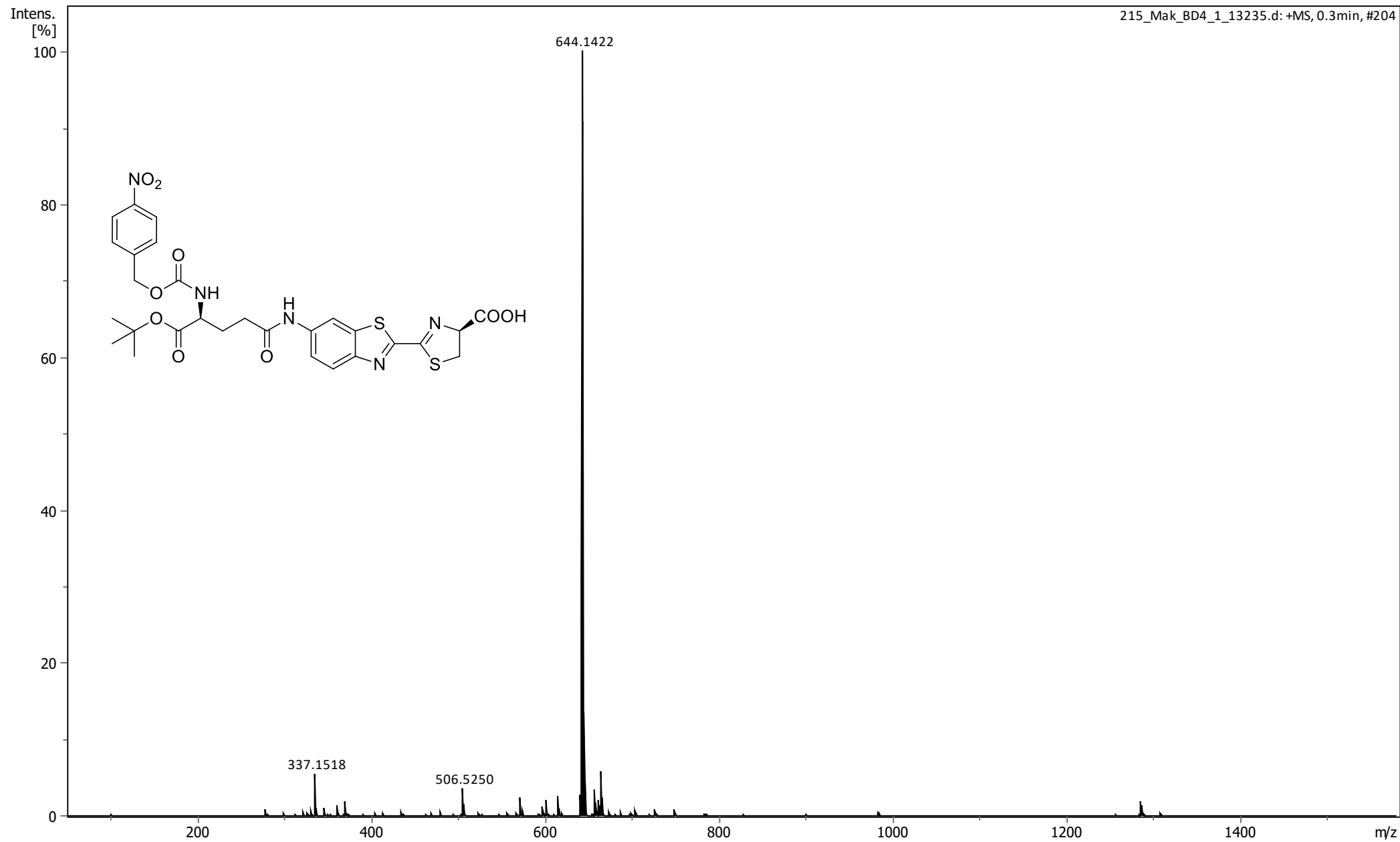
9.06



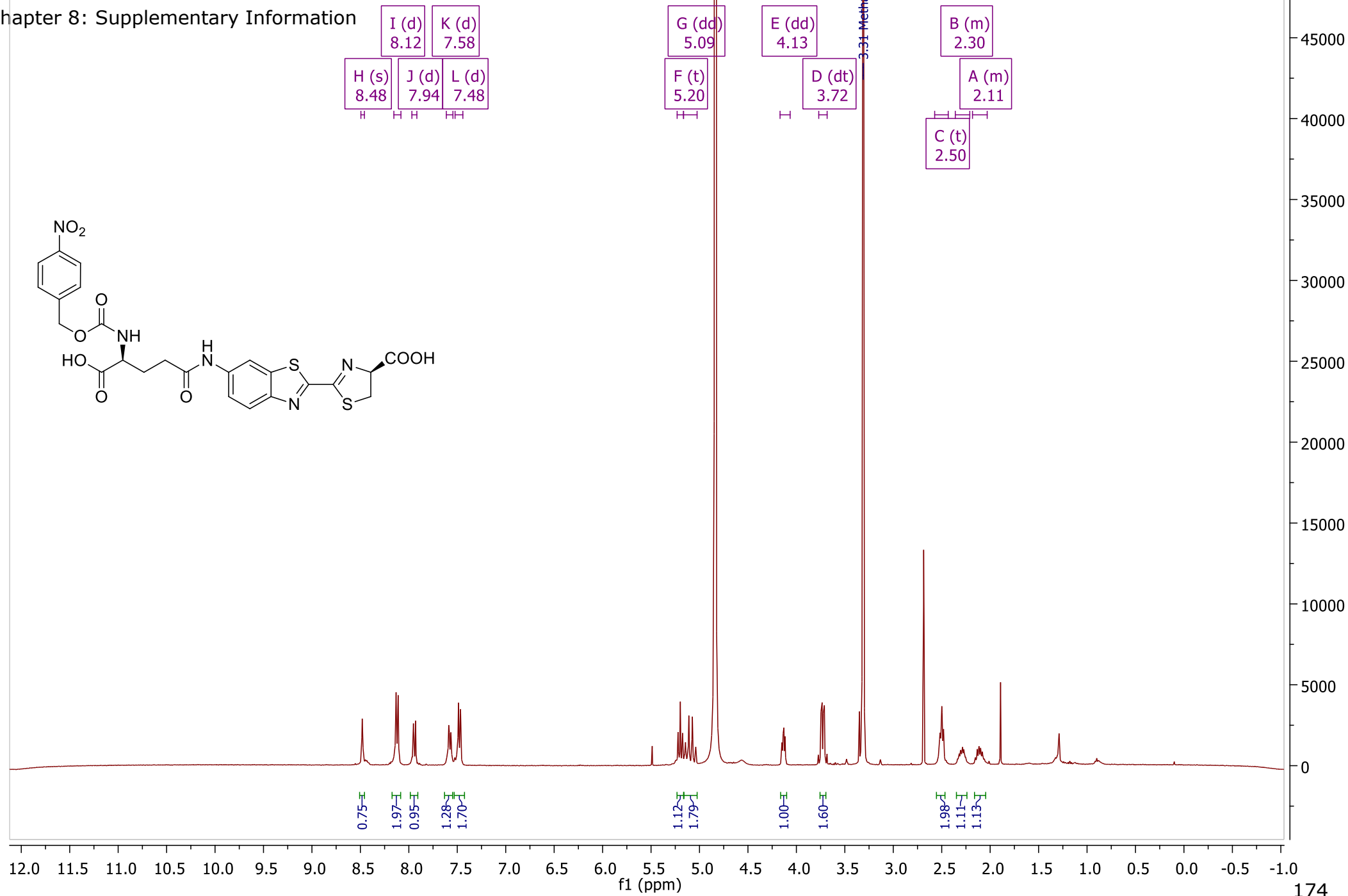
# Chapter 8: Supplementary Information



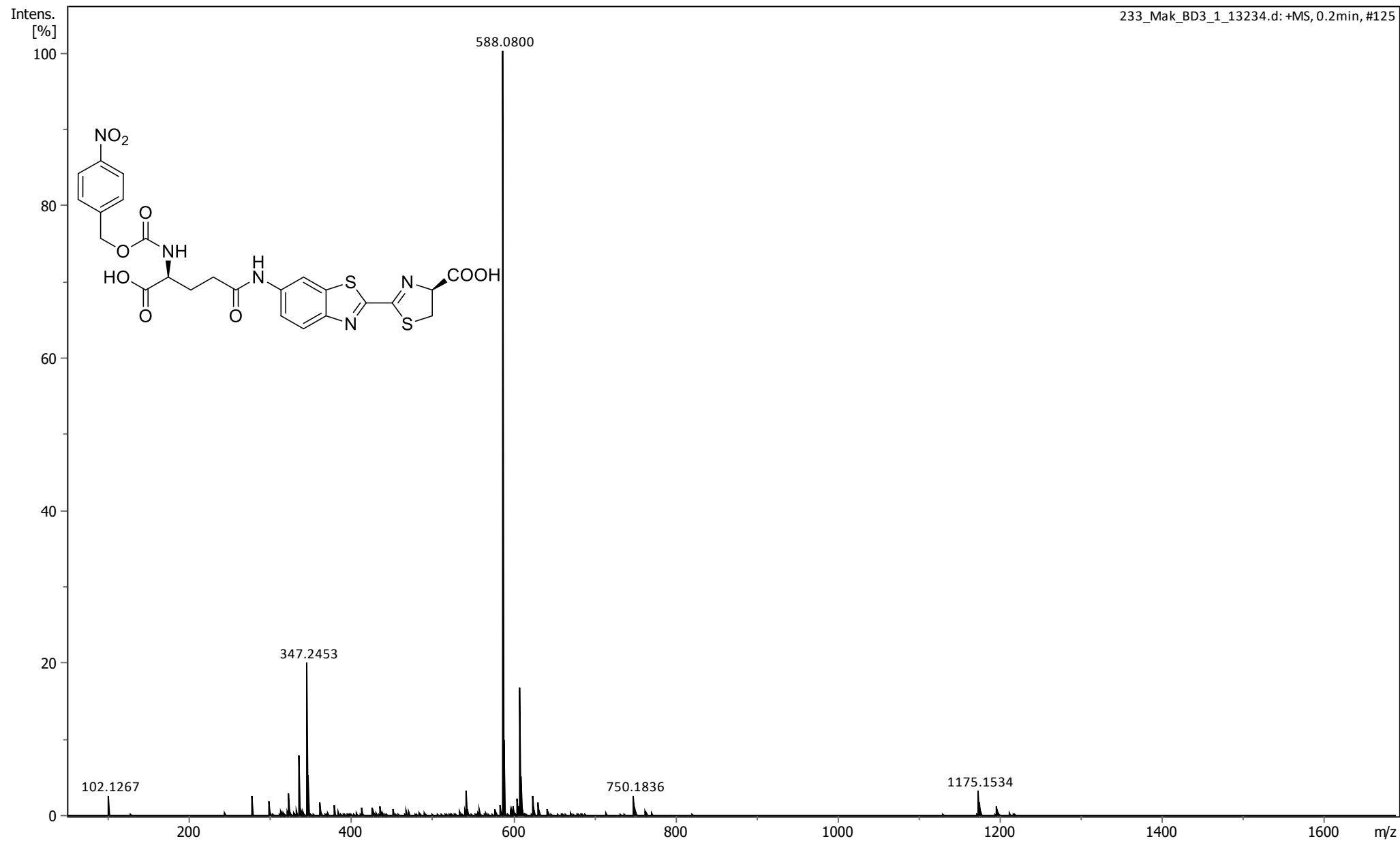
Chapter 8: Supplementary Information

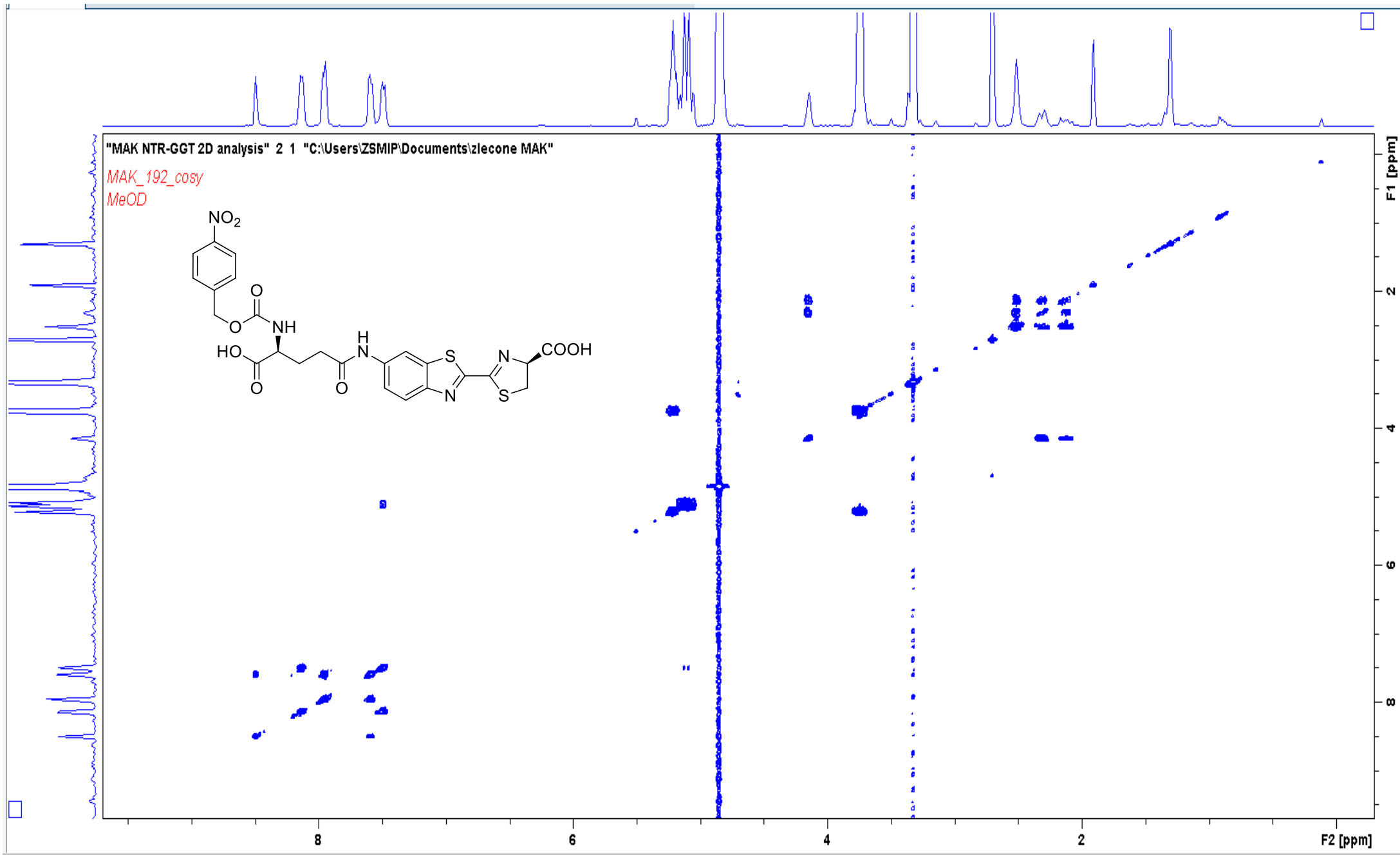


Chapter 8: Supplementary Information



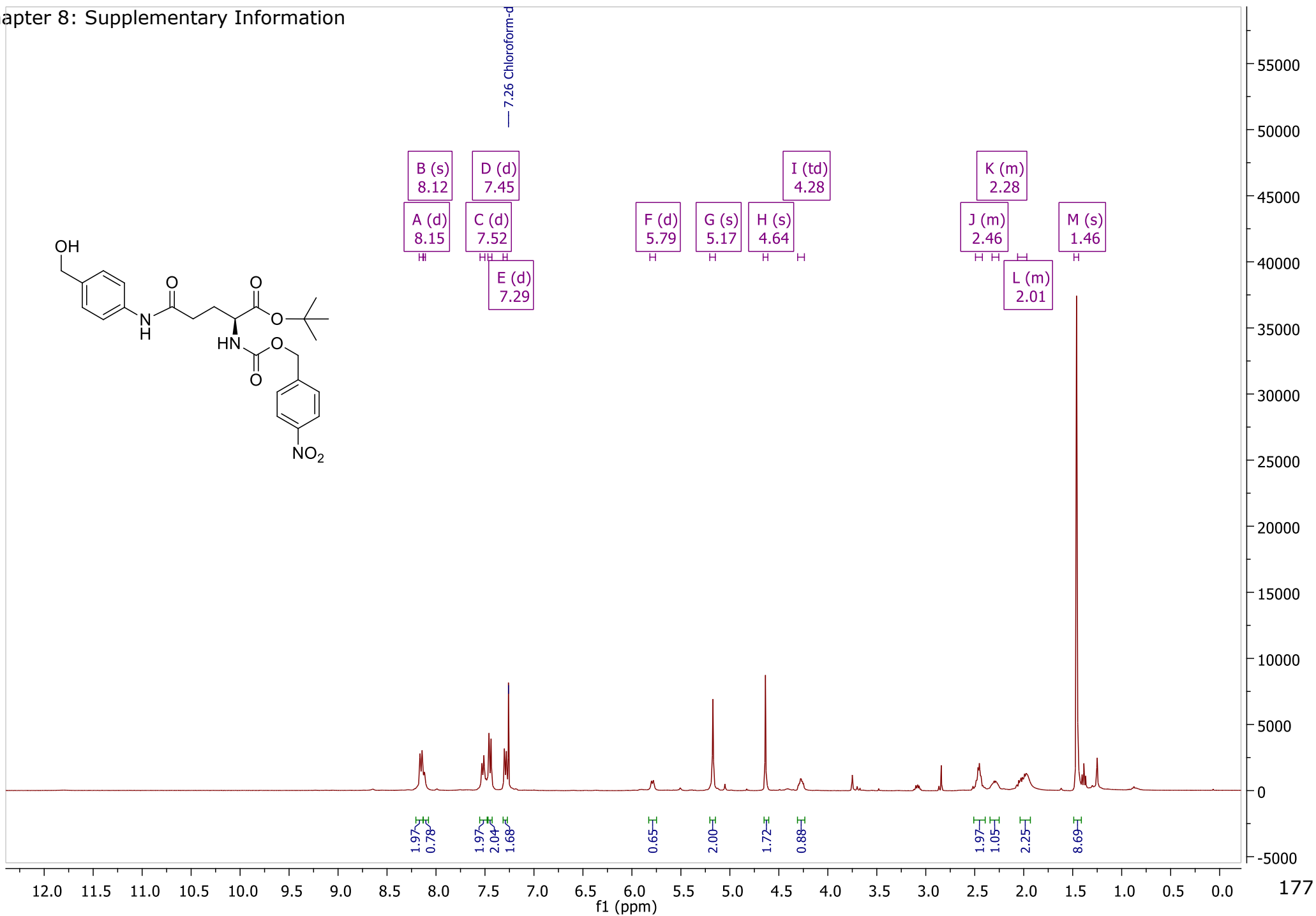
# Chapter 8: Supplementary Information



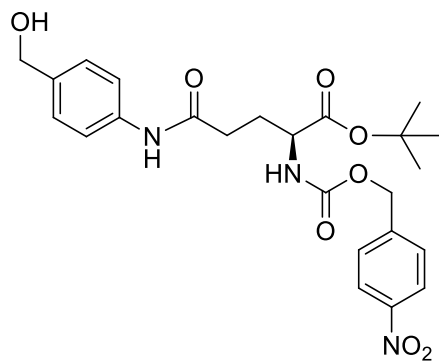




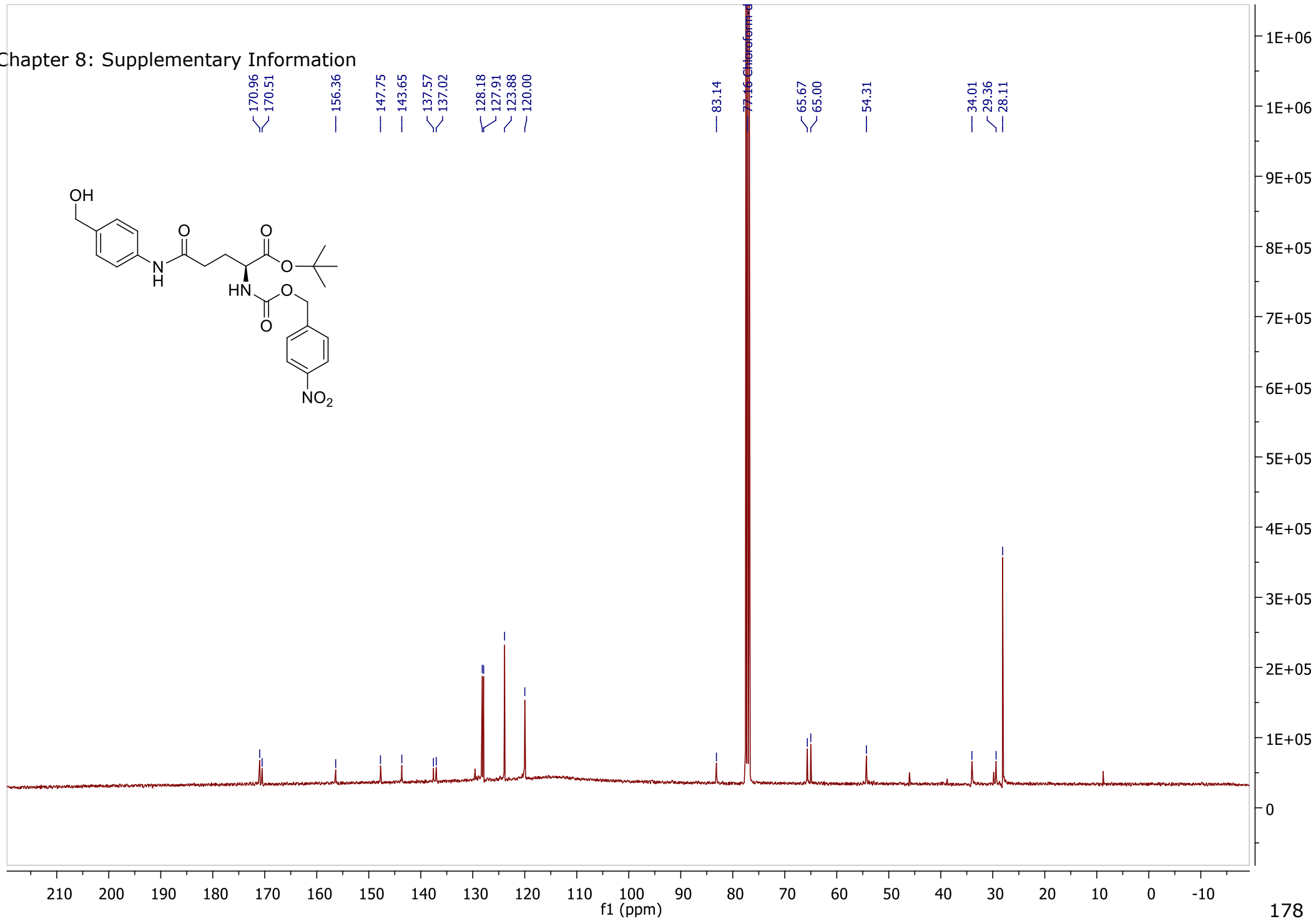
Chapter 8: Supplementary Information



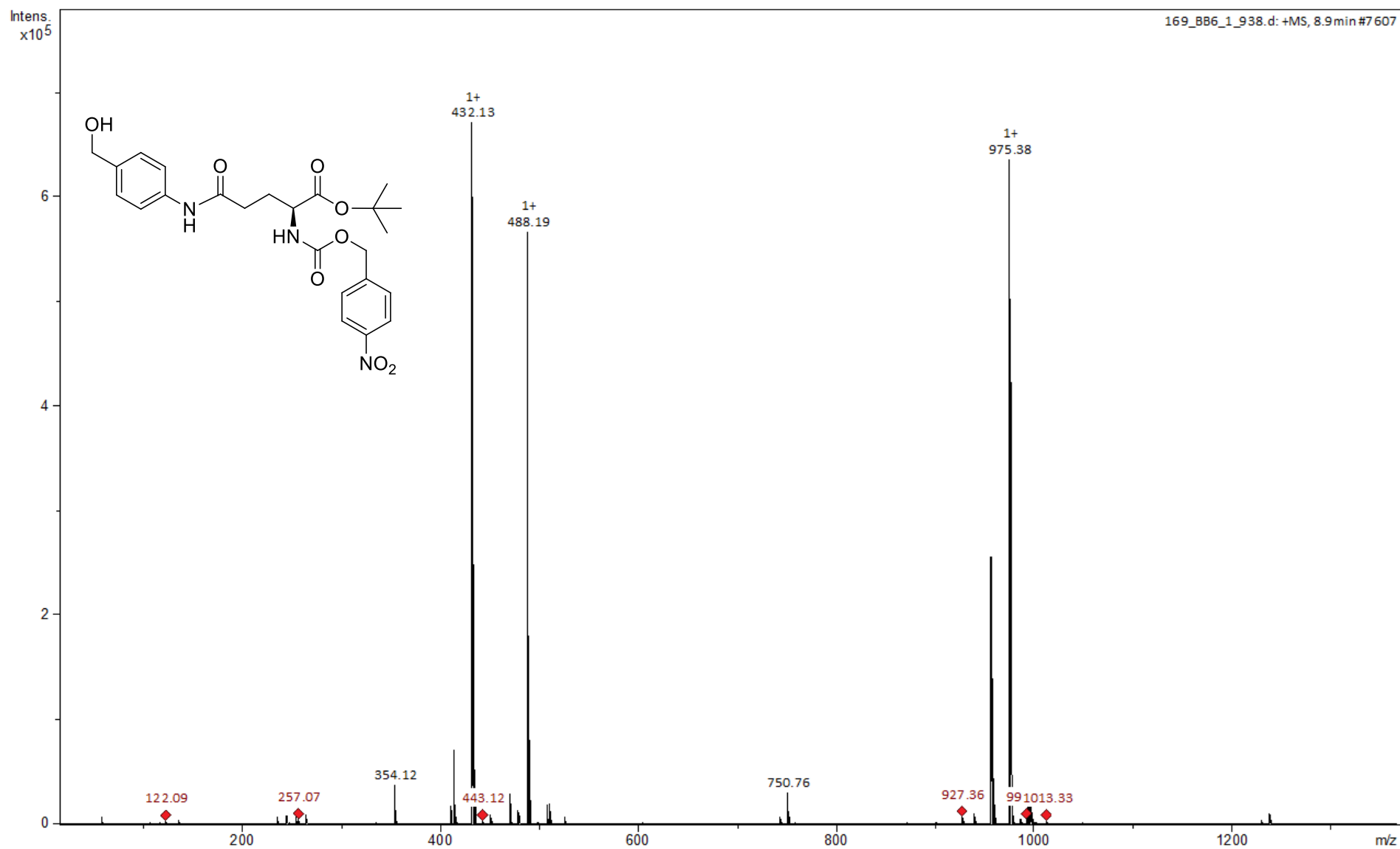
Chapter 8: Supplementary Information



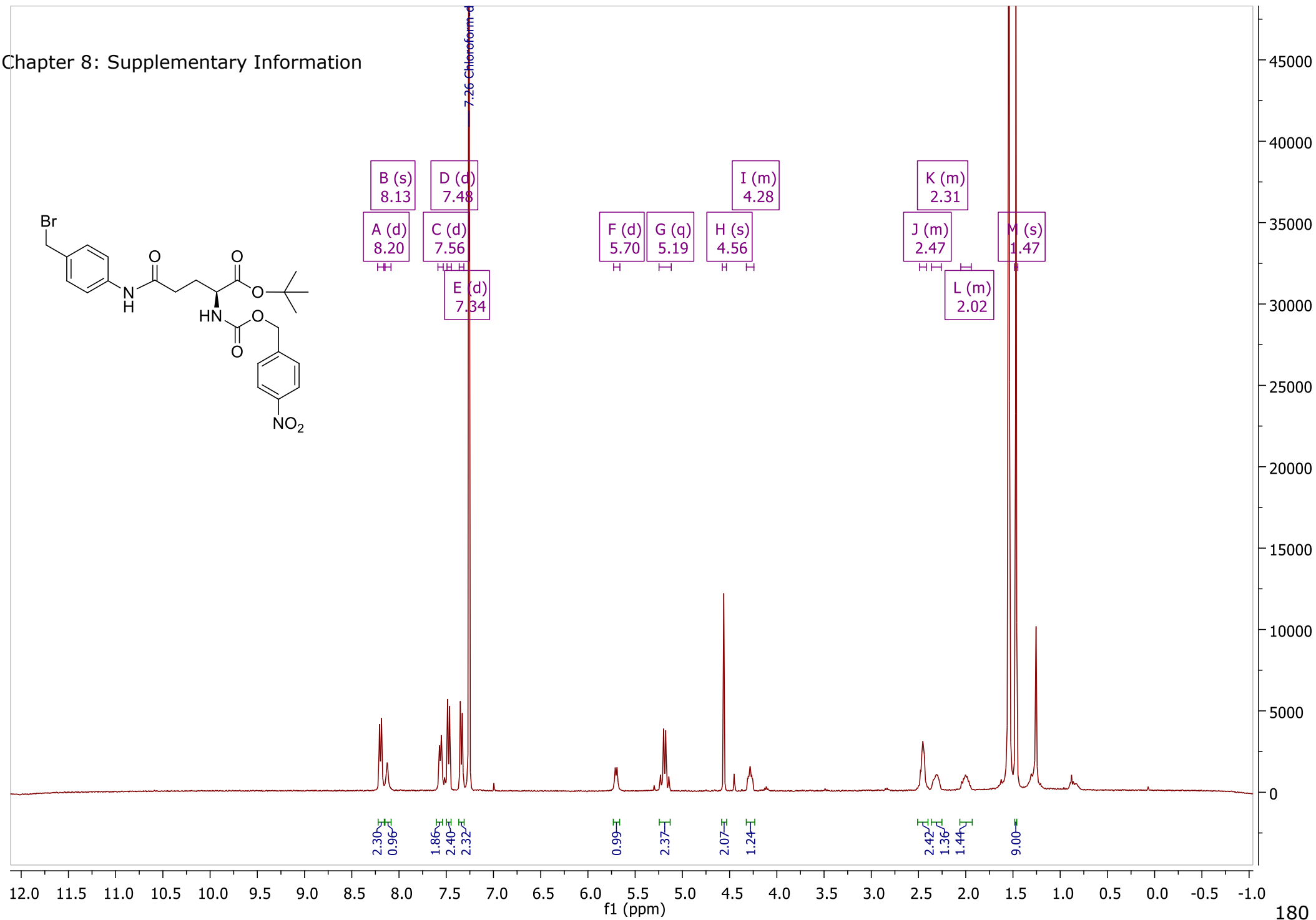
- 170.96
- 170.51
- 156.36
- 147.75
- 143.65
- 137.57
- 137.02
- 128.18
- 127.91
- 123.88
- 120.00
- 83.14
- 77.16 (CDCl<sub>3</sub>)
- 65.67
- 65.00
- 54.31
- 34.01
- 29.36
- 28.11



Chapter 8: Supplementary Information

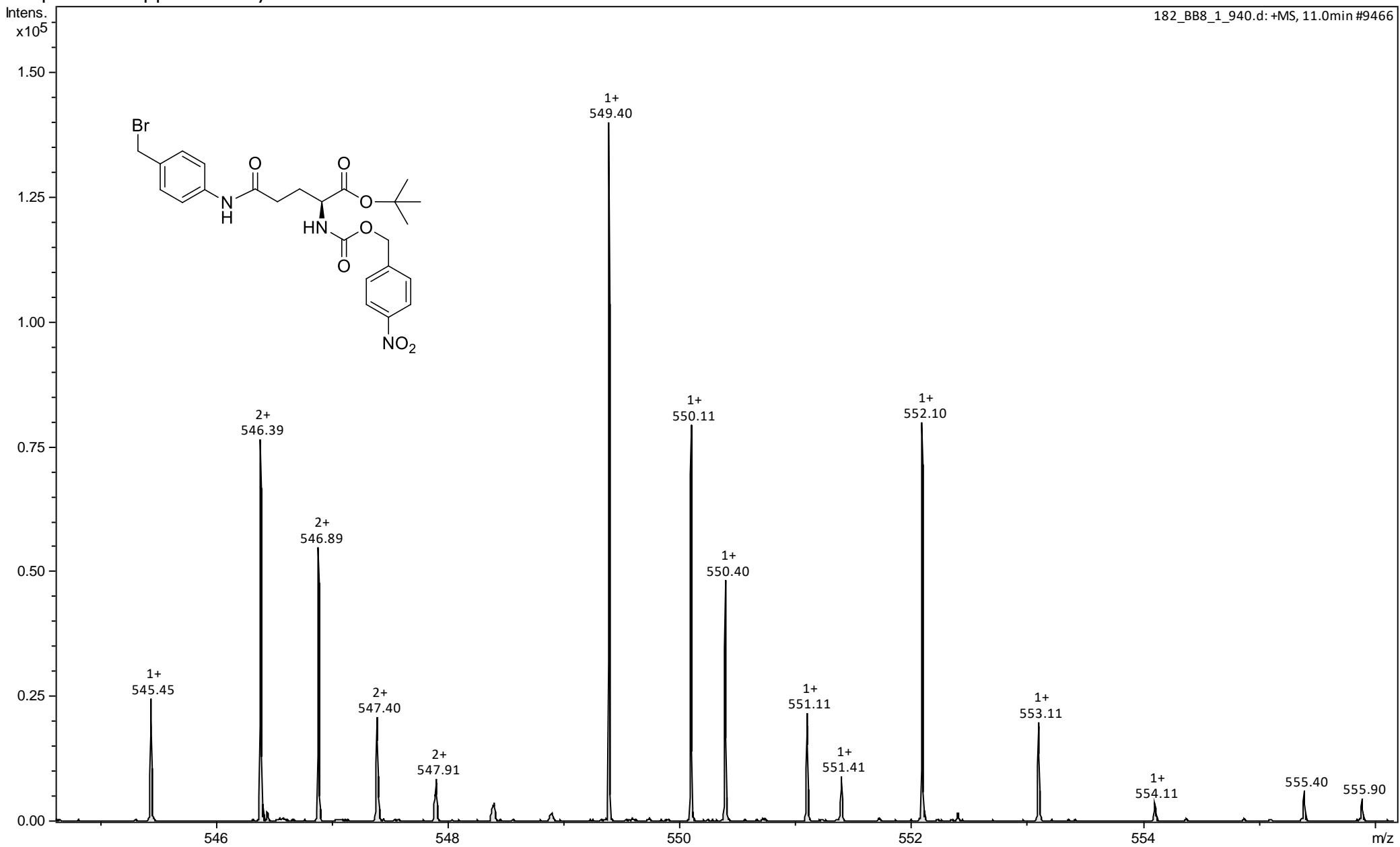


Chapter 8: Supplementary Information

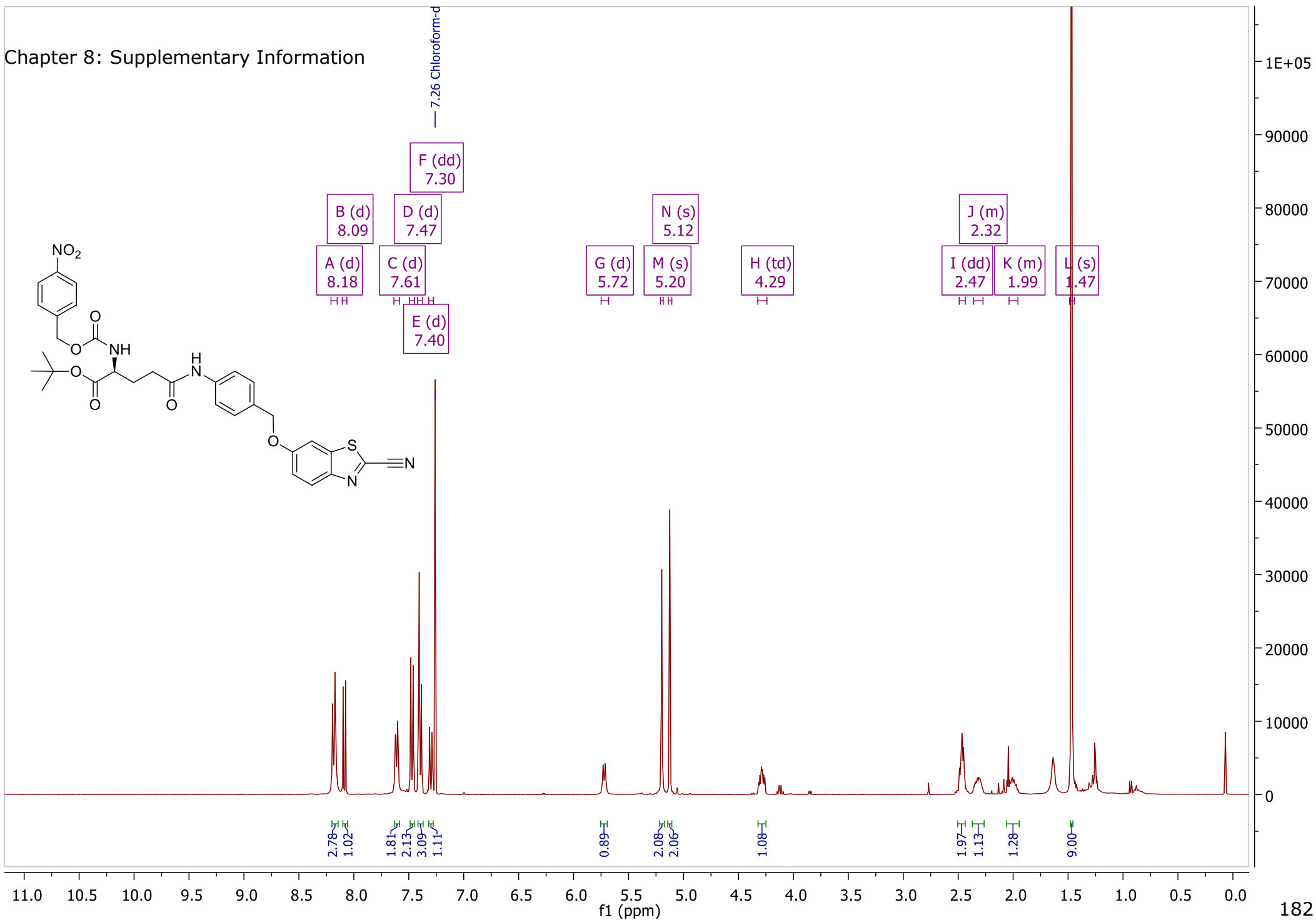


Chapter 8: Supplementary Information

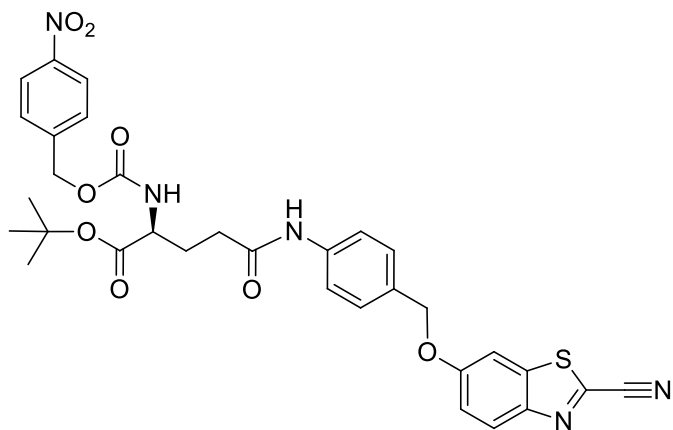
182\_BB8\_1\_940.d: +MS, 11.0min #9466



Chapter 8: Supplementary Information



Chapter 8: Supplementary Information



170.82  
170.51

159.54  
156.54

147.80  
147.23

143.50  
138.30

137.46  
133.66

131.60  
128.54

128.24  
126.09

123.54  
120.06

119.15  
113.26

104.38

83.26

77.16 Chloroform-d

70.49  
65.66

54.06

34.03  
29.69

28.12

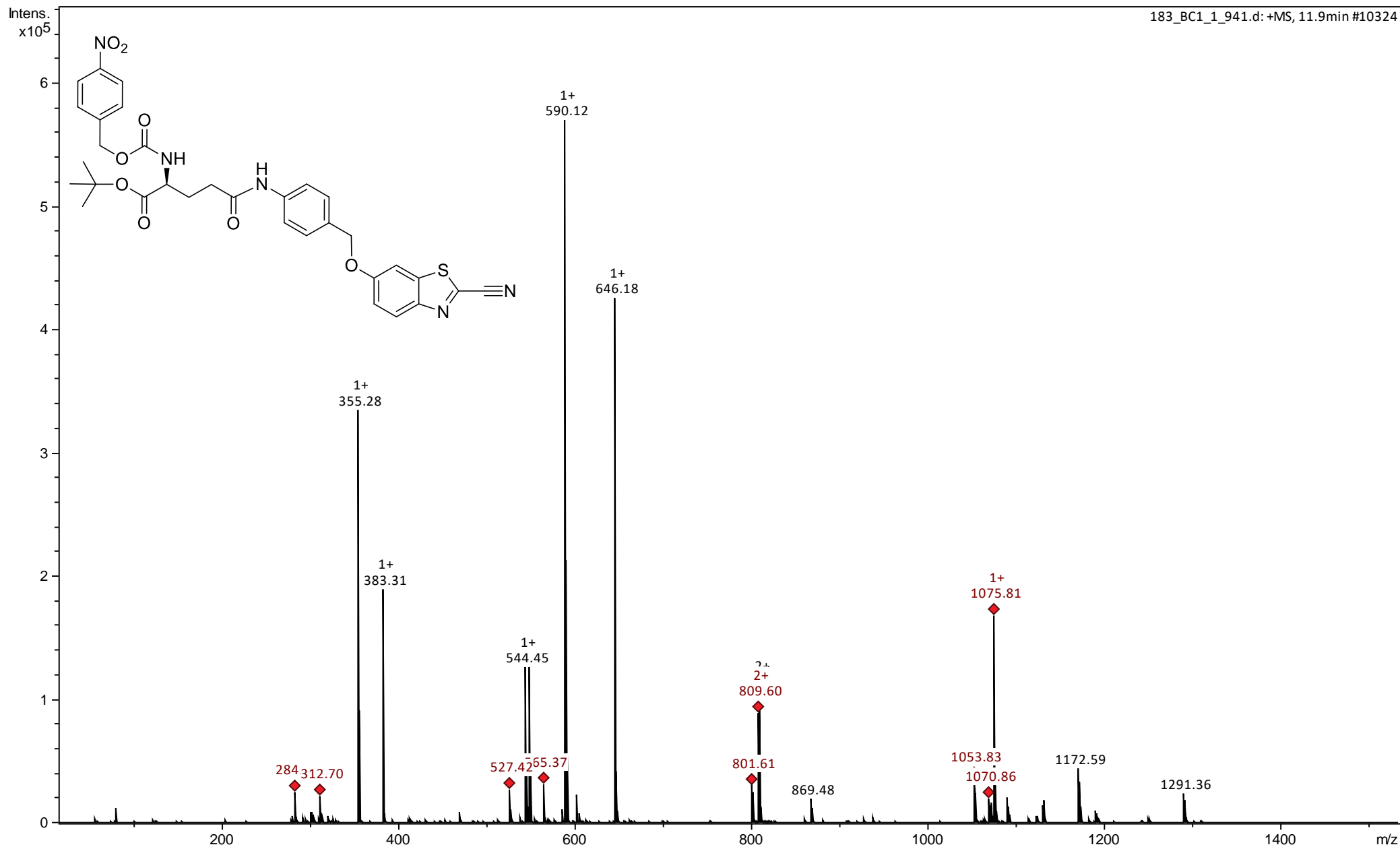
210 200 190 180 170 160 150 140 130 120 110 100 90 80 70 60 50 40 30 20 10 0 -10

f1 (ppm)

183

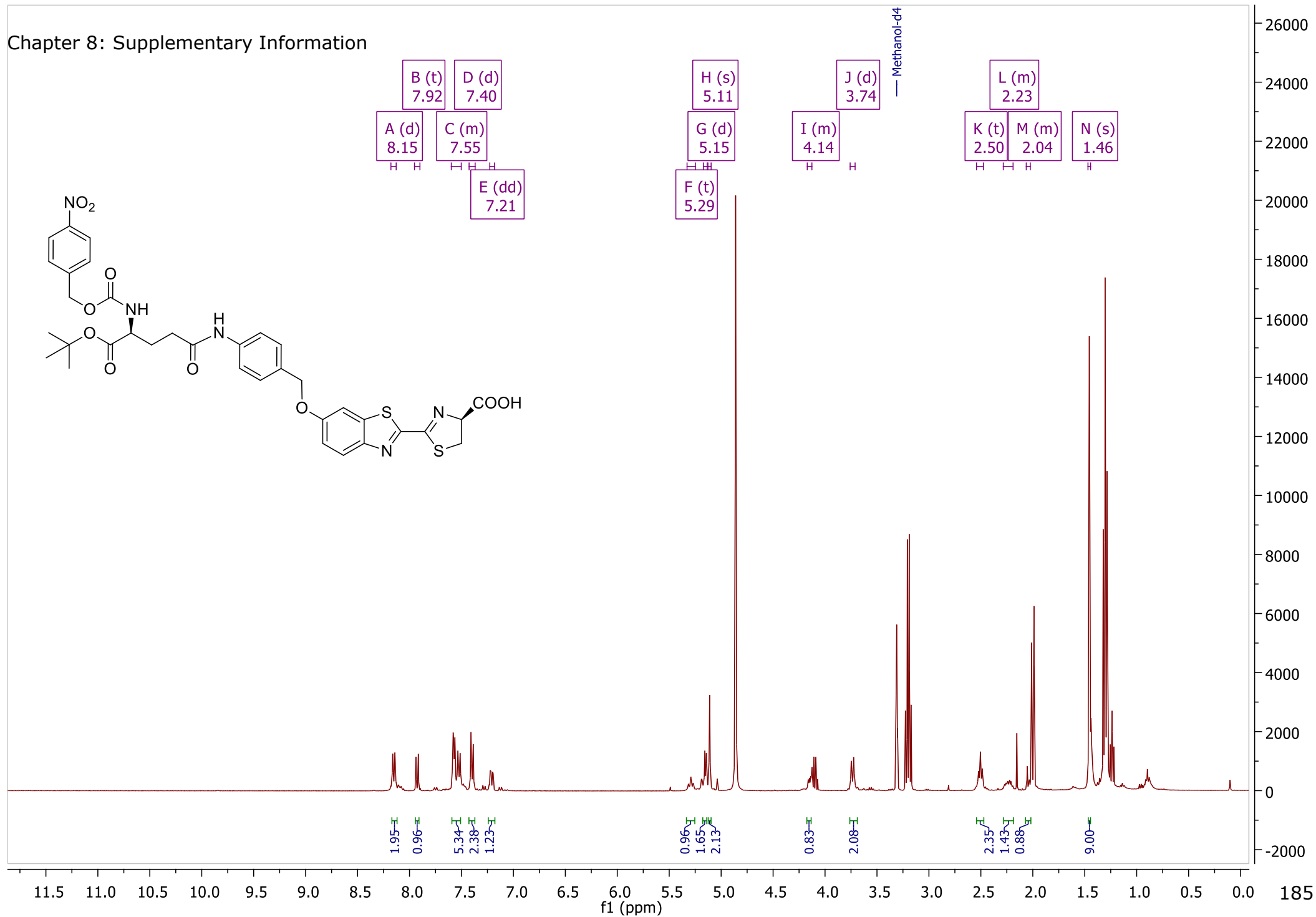
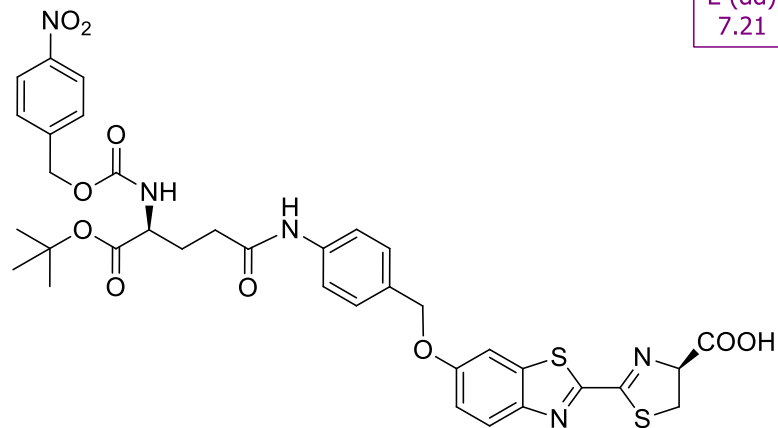
4E+05  
4E+05  
4E+05  
3E+05  
2E+05  
2E+05  
2E+05  
1E+05  
50000  
0  
-50000  
-1E+05

Chapter 8: Supplementary Information

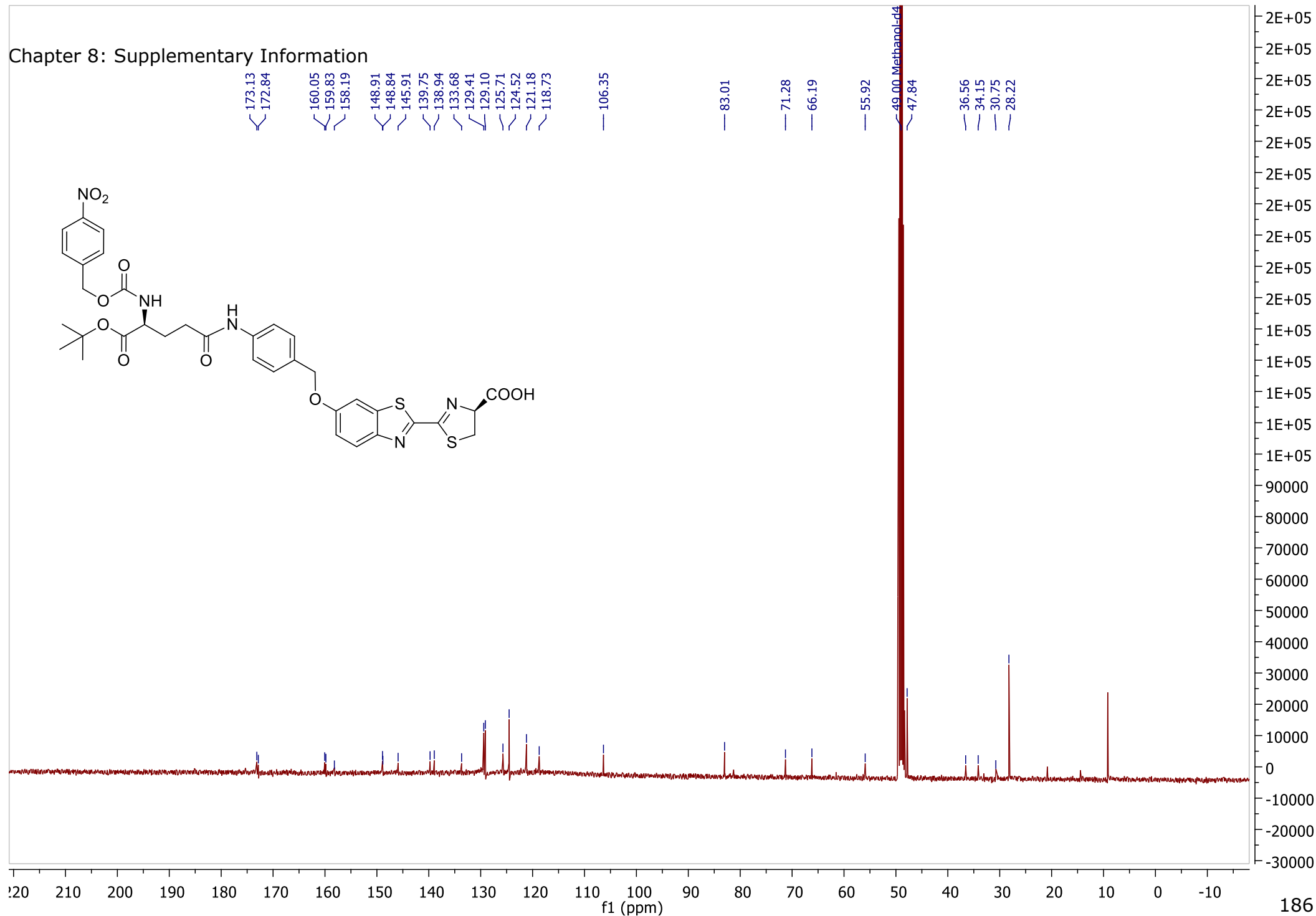
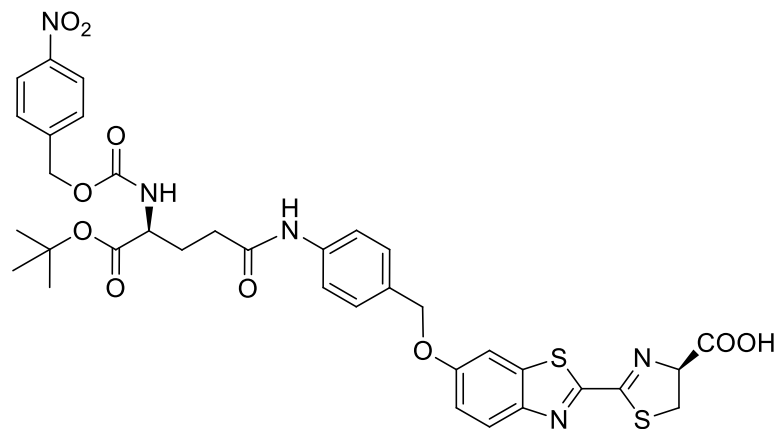




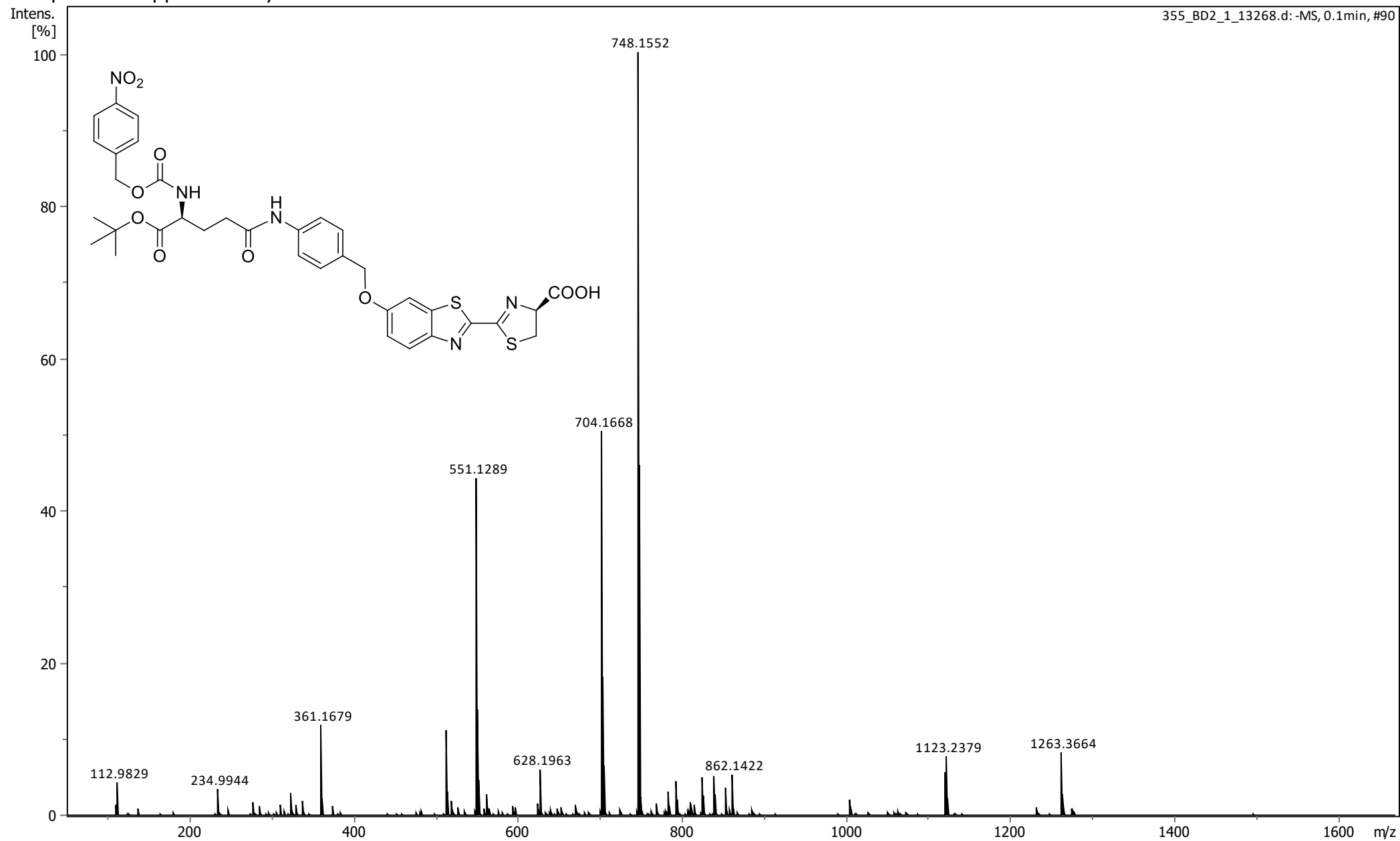
Chapter 8: Supplementary Information



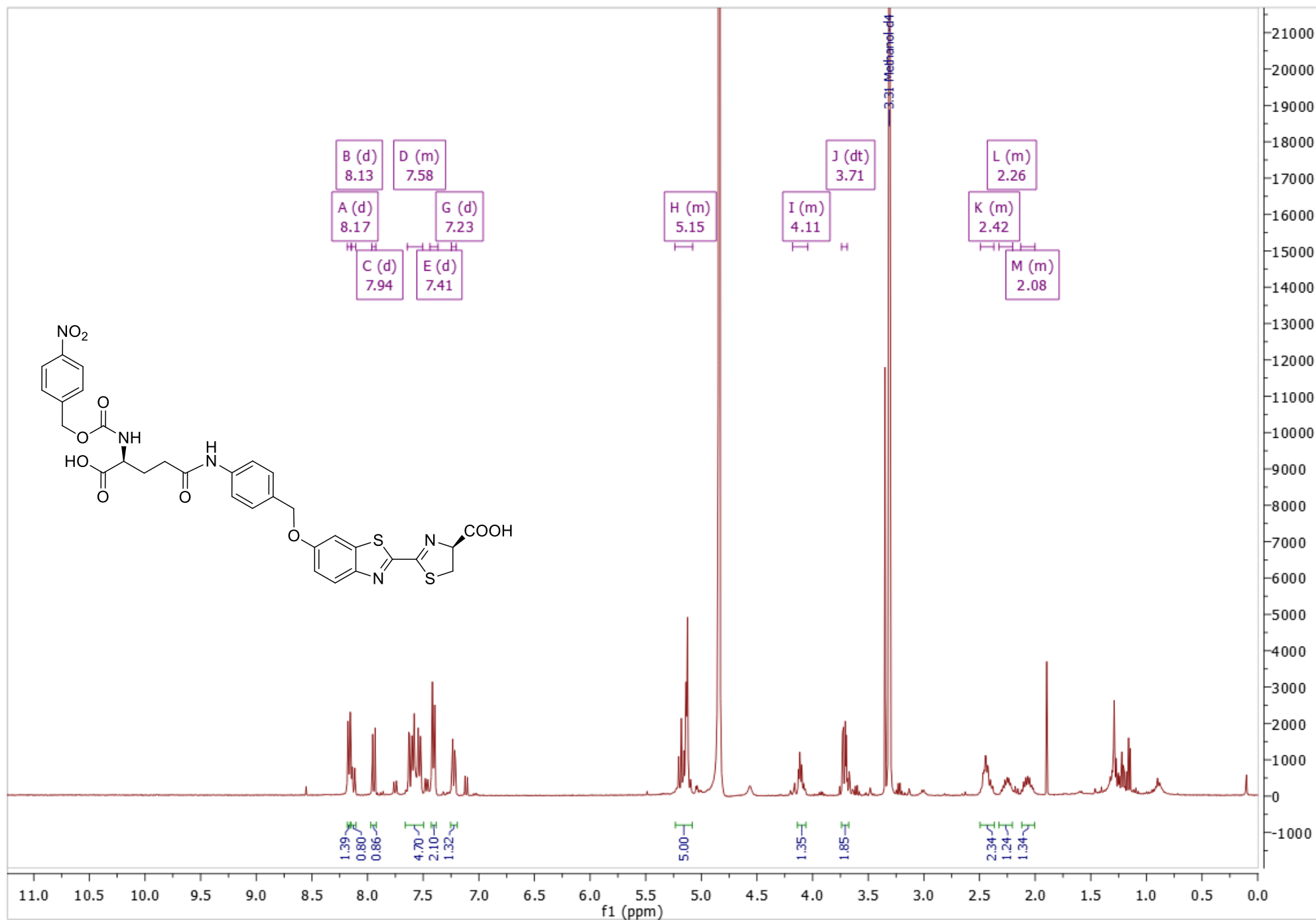
Chapter 8: Supplementary Information



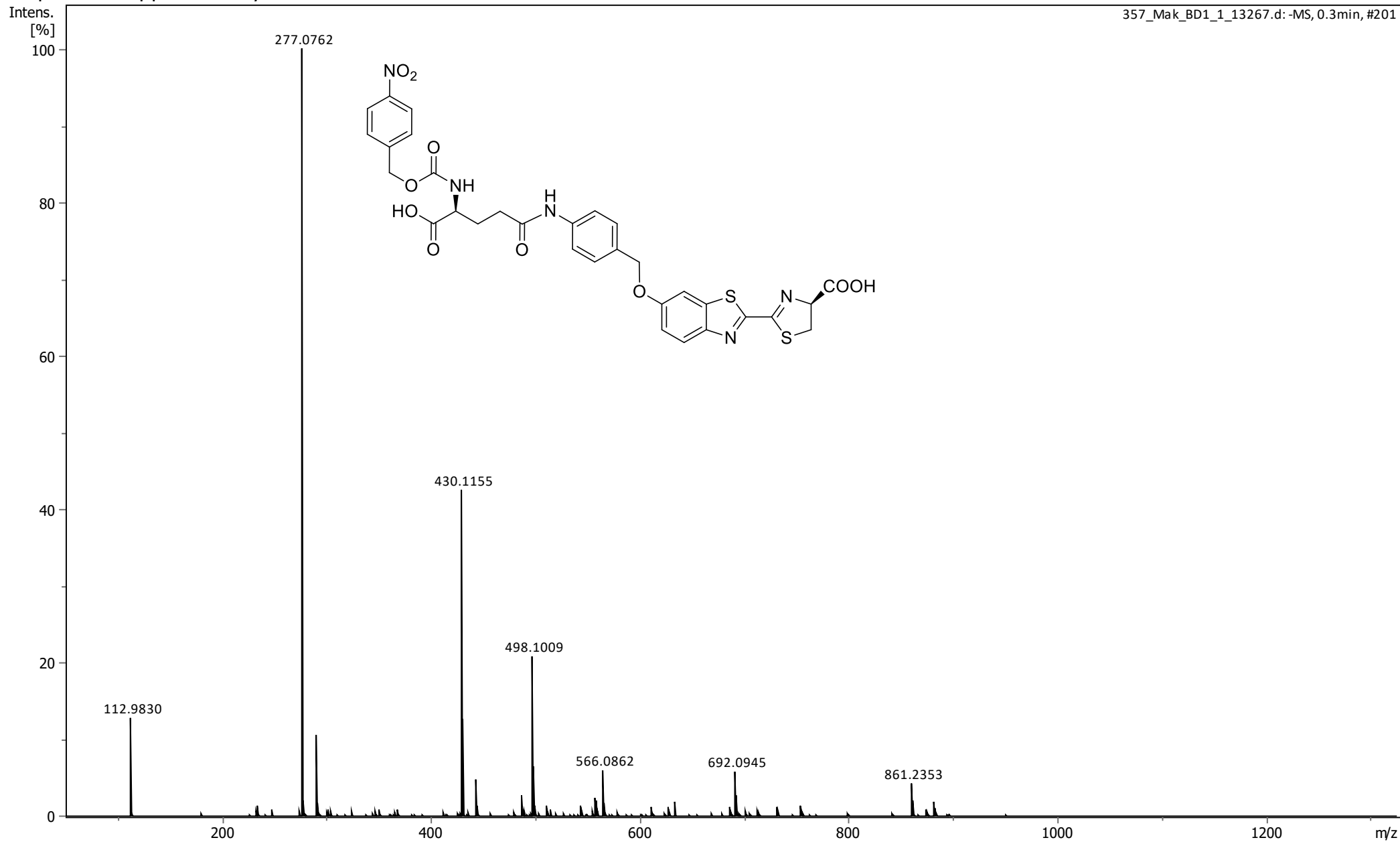
# Chapter 8: Supplementary Information



Chapter 8: Supplementary Information



Chapter 8: Supplementary Information



## 9. List of Publications

- Manuscript in review (2024): Frontiers in Chemistry  
Interference of Metal Ions on Bioluminescent Signal of Firefly, Renilla and Nano-Luciferases in High-Throughput Screening Assays. Francesca Canyelles i Font, Krzysztof Żukowski, **Masroor A. Khan**, Dorota Kwiatek, Jacek L. Kolanowski.
- Review article (2024): Postępy Biochemii  
Multi-analyte responsive luminescent probes for the detection of biochemical targets in cell models. Anna Wychowaniec, Francesca Canyelles i Font, **Masroor A. Khan**, Michał Gładysz, Dorota Kwiatek, Jacek Ł. Kolanowski. [https://doi.org/10.18388/pb.2021\\_538](https://doi.org/10.18388/pb.2021_538)
- Publication (2019): Antibiotics  
Nautiyal M, Gadakh B, De Graef S, Pang L, **Khan M**, Xun Y, Rozenski J, Van Aerschot A. Synthesis and Biological Evaluation of Lipophilic Nucleoside Analogues as Inhibitors of Aminoacyl-tRNA Synthetases. <https://doi.org/10.3390/antibiotics8040180>